Age as a modulator of ionising radiation-induced cardiovascular disease



Christopher Whiteman

Oriel College

University of Oxford

A thesis submitted for the degree of

Doctor of Philosophy

Hilary 2024

Abstract

Cardiovascular disease (CVD), in particular atherosclerosis, remains the most common underlying cause of mortality worldwide. The link between ionising radiation (IR) and CVD has been well established; however, current evidence on whether age influences IR-induced CVD is limited. Furthermore, with links between CVD and senescence having been established, along with the potential of IR to induce senescence, it is plausible that IR-induced senescence may contribute to CVD development. In this thesis, I firstly demonstrate the novel use of the Ldl receptor knockout mouse ($Ldlr^{-/-}$) model for investigation into IR-CVD. Secondly, I report that age does mediate the development of IR-CVD in two separate mouse models, the ApoE receptor knockout and $Ldlr^{-/-}$ models, with older mice developing IR-CVD. Thirdly, using human coronary artery endothelial cells (HCAECs) from donors ranging 17-55 years, I report IR-induced increases in adhesion and permeability, phenotypes that are pro-atherogenic. Notably, I report a correlation between SA-β-Gal activity and increasing HCAEC adhesion, along with the ability to ameliorate these effects by targeting senescence with rapamycin, supporting the hypothesis of IR-induced senescence promoting CVD. Finally, I present molecular profiles of the gene and protein changes associated with age, IR exposure, the modulation of IR-induced changes by age, and the effects of rapamycin on IR-induced changes. My findings provide evidence for age as a modulator of the effects of IR from animal models to functional *in vitro* assays, and down to human cell molecular expression profiles. Furthermore, the multi-omics performed provide a unique reference for ageing HCAECs.

Acknowledgements

Thank you to my family. Notably, my mum, Linda Whiteman. Throughout what you would call my “rollercoaster journey”, you have inspired, encouraged, and provided all the love and support needed to allow me to find the path that has led me to writing this thesis. My dad and step-mum, Bob Whiteman and Claire Beaumont, who have also provided the love and support needed to get to this point, along with providing the annual BBQ which served as an excellent *viva* preparation ground. To modify a quote by Tyrion Lannister, “I drink and now know quite a bit, about not a lot”.

Thank you to my supervisory team, Lynne Cox for your guidance over the years, and to Ken Raj, Sylwia Kabacik, and Donna Lowe for their support and training, all of which has helped me to develop into the scientist I am today. An important thank you to the UKHSA for providing the studentship which allowed me to carry out this DPhil.

Thank you to my friends for making the “Oxford experience” one to remember. To Gareth and Lizzie for keeping me caffeinated, stocked-up on cakes, and providing me with some form of social interaction during the final stages of writing. To members of the cox lab, past and present, for your encouragement throughout the years. A special mention to the “squad”, Sean, Michael, and Ray, for providing the occasional escape from reality.

Finally, a very big thank you to not Miss-nor-Mrs-but-Doctor Natasha Oughton for keeping me sane, motivating me, and above all, inspiring me.

Contents

Abstract ..... **ii**

Acknowledgements ..... **iii**

Contents ..... **iv**

List of figures ..... **xii**

List of tables ..... **xv**

Common abbreviations ..... **xvi**

1 Introduction **1**

1.1 Cardiovascular disease 1

1.2 Atherosclerosis and its pathogenesis 2

1.2.1 Arterial structure and physiology 2

1.2.2 What is atherosclerosis? 3

1.2.3 Steps in atherogenesis 4

1.2.4 Current treatments for atherosclerosis 8

1.3 The DNA damage response pathway 10

1.3.1 Single-strand break repair pathways 10

1.3.2 Double-strand break pair pathways 11

1.4 Ionising radiation 14

1.4.1 The link between ionising radiation and cardiovascular disease 18

1.5 Cellular senescence 20

1.5.1 Physiological and pathological roles of cell senescence 20

1.5.2 Key features and markers of senescent cells 23

1.5.2.1 Cell cycle arrest 24
1.5.2.2 Changes in morphology 27
1.5.2.3 Nuclear structure and chromatin reorganisation 28
1.5.2.4 Failure of Autophagy 29
1.5.2.5 Lysosomal activity 31
1.5.2.6 Endoplasmic reticulum stress in senescence 33
1.5.2.7 Senescence-associated secretory phenotype 34
1.5.3 Types of Senescence 37
1.5.3.1 Replicative senescence 37
1.5.3.2 Mitochondrial dysfunction-associated senescence 39
1.5.3.3 DNA damage-induced senescence 43
1.5.3.4 Oncogene-induced senescence (OIS) 44
1.5.3.5 Senescence in response to pathogens 45
1.5.3.6 Paracrine senescence (bystander senescence) 46
1.5.3.7 Stress-induced premature senescence 47
1.5.4 Therapeutic targeting of senescent cells 49
1.5.5 Potential role of senescence cells in atherogenesis 53
1.5.6 Targeting vascular senescence 54
1.6 Aims of the thesis 56
2 Materials and methods 58
2.1 Mouse studies 58
2.1.1 Mouse husbandry 58
2.1.2 LDL receptor knockout mouse X-ray dose pilot study 58

2.1.3 Investigation into the effect of age at the time of IR exposure and the development of CVD in Ldlr$^{-/-}$ mice 59
2.1.4 Oil red O plaque staining and quantification 59
2.2 Cell culture 61
2.2.1 Cell maintenance 61
2.2.2 Simulated flow conditions 63
2.3 X-ray exposures 64
2.4 In vitro assays 65
2.4.1 Adhesion assay 65
2.4.2 Permeability assay 66
2.4.3 Senescence-associated β-Galactosidase assay 67
2.5 Pro-inflammatory cytokine secretion analysis 68
2.6 RNA extraction 69
2.7 Western blotting 70
2.8 Immunofluorescence cell staining 71
2.9 Antibodies used for Western blotting and immunofluorescence 71
2.10 Nanopore sequencing 72
2.11 Proteomics 75
2.12 Bioinformatics 76
2.12.1 Differential gene expression analysis pipeline 76
2.12.2 Differential protein analysis pipeline 76
2.13 Drug compounds 77
2.14 Statistical analysis 77
3 Identification of an X-ray dose for investigating IR-CVD in Ldlr$^{-/-}$ mice 78

3.1 Introduction 78

3.2 Chapter aims 79

3.3 Results 79

3.3.1 Identification of a suitable X-ray dose for IR-CVD investigation in Ldlr$^{-/-}$ mice 79

3.4 Discussion 87

4 Analysis of age-modulated X-ray-induced cardiovascular disease in Ldlr$^{-/-}$ and ApoE$^{-/-}$ mice 89

4.1 Introduction 89

4.2 Chapter aims 91

4.3 Results 91

4.3.1 ApoE$^{-/-}$ mouse aortic plaque quantification after X-ray exposure at varying ages 91

4.3.1.1 Introduction 91

4.3.1.2 ApoE$^{-/-}$ mice develop IR-CVD after exposure at 22 weeks of age 92

4.3.1.3 Older male ApoE$^{-/-}$ mice are more susceptible to IR-induced plaque development 94

4.3.2 Ldlr$^{-/-}$ mouse aortic plaque analysis after X-ray exposure 97

4.3.2.1 Age modulates X-ray-induced atherosclerosis within Ldlr$^{-/-}$ mice 98

4.3.2.2 Female Ldlr$^{-/-}$ mice are more susceptible to IR-induced aortic plaque formation 100

4.3.2.3 Analysis of Ldlr$^{-/-}$ mouse circulating cytokines after X-ray 102

4.4 Discussion 109

4.4.1 Age modulated IR-CVD in ApoE$^{-/-}$ and Ldlr$^{-/-}$ mice 109

5 Investigation into the atherogenic effect of X-irradiation on human coronary artery endothelial cells from donors of varying age 112

5.1 Introduction 112

5.2 Chapter aims 114

5.3 Results 114

5.3.1 Characterisation of HCAEC 114

5.3.2 Effect of age on *in vitro* HCAEC atherogenic phenotypes 120

5.3.2.1 Establishing the HCAEC permeability assay 120

5.3.2.2 Establishing the HCAEC adhesion assay 123

5.3.2.3 Effects of age on HCAEC monolayer permeability 125

5.3.2.4 Effects of donor age on HCAEC adhesion to monocytes 127

5.3.2.5 Effect of HCAEC age on the SA-β-Gal activity 129

5.3.3 X-ray dose investigation for HCAEC 132

5.3.4 The atherogenic response of HCAEC to IR from younger donors 133

5.3.4.1 X-ray induced increases in adhesion to HCAEC from young donors 134

5.3.4.2 X-ray-induced increases in permeability of HCAEC monolayers from young donors.....135

5.3.4.3 Increases in SA-β-Gal activity in HCAECs from young donors after X-ray exposure.....137

5.3.5 The atherogenic response of HCAEC from middle-aged donors to IR 138

5.3.5.1 X-ray induced increases in adhesion of HL-60 cells to HCAEC from middle-aged donors 139

5.3.5.2 X-ray-induced increases in permeability of HCAEC monolayers from middle-aged donors.....140

5.3.5.3 Changes in SA-β-Gal activity in HCAECs from middle-aged donors after X-ray exposure 142
5.3.6 Comparison of IR-induced atherogenic response in HCAEC from young and middle-aged donors.....144
5.3.6.1 Age modulation of IR-induced adhesion in HCAEC.....145
5.3.6.2 Age modulation of IR-induced permeability of HCAEC 148
5.3.6.3 Age modulation of IR-induced SA-β-Gal activity in HCAEC 151
5.3.6.4 Correlation between HCAEC senescence and atherogenic phenotypes ...154
5.3.7 Optimising drugs for targeting senescence in HCAEC 156
5.3.7.1 ABT-263 senolytic dose investigation 156
5.3.7.2 Rapamycin senomorphic dose investigation 159
5.3.8 Targeting senescence to prevent IR-induced atherogenic phenotypes in HCAECs.....167
5.3.9 Targeting senescence to prevent IR-induced HL-60 adhesion in HCAEC from young and middle-aged donors.....168
5.3.10 Targeting senescence to prevent X-ray-induced permeability of HCAEC monolayers 172
5.3.10.1 Efficacy of targeting HCAEC senescence with rapamycin and ABT-263...176
5.3.11 The effect of rapamycin treatment on X-ray-induced SASP 179
5.4 Discussion 185
5.4.1 Characterising HCAEC for CVD investigations 186
5.4.2 IR and CVD phenotypes in HCAECs.....187
6 Comparative transcriptomics of HCAECs..... 192

6.1 Introduction 192
6.1.1 Oxford Nanopore sequencing 192
6.2 Chapter aims 193
6.3 Results 194
6.3.1 Age difference in the transcriptome of HCAECs 194
6.3.2 Age differences in IR-induced differential gene expression in HCAEC 205
6.3.3 Modulation of IR-induced CVD related gene expression with rapamycin 217
6.4 Discussion 226
6.4.1 Differences in HCAECs gene expression between young and middle-aged donors 227
6.4.2 Age-modulation of IR-induced gene expression in HCAECs 228
6.4.3 Limitations 229
7 Comparative proteomics of HCAECs 231
7.1 Introduction 231
7.1.1 LC-MS/MS overview 232
7.2 Aims 233
7.3 Results 234
7.3.1 Differences in protein expression in HCAECs with age 234
7.3.1.1 GO pathways associated with HCAEC proteome changes with age 239
7.3.2 Age modulation of IR-induced protein changes in HCAECs 241
7.3.3 Rapamycin alleviates IR-induced CVD-related protein expression in HCAEC .248
7.3.4 Comparison between HCAEC differential gene and protein expression 254
7.4 Discussion 259

7.4.1 Differences in HCAEC protein expression with age.....259

7.4.2 Age-modulation of IR-induced changes in protein expression within HCAECs

.....260

7.4.3 Rapamycin modulation of IR-induced changes in the proteome.....261

8 Discussion..... 263

8.1 Summary.....263

8.1.1 Disparity between age affects in mice and cells 264

8.2 Future work 266

9 References..... 268

10 Supplementary material..... 345

List of figures

Figure 1.1 Structure of an artery and location of plaque development. 3
Figure 1.2 Schematic overview of atherogenesis. 7
Figure 1.3 Hallmarks of senescence. 24
Figure 2.1 Mount for the camera to image the aortas. 61
Figure 3.1. Representative images of Ldlr$^{-/-}$ Oil red O stained plaques. 81
Figure 3.2. Comparison of plaque coverage after different X-ray doses in male and female Ldlr$^{-/-}$ mice. 83
Figure 3.3. X-ray dose and plaque development in Ldlr$^{-/-}$ mice. 84
Figure 3.4. Mass of Ldlr$^{-/-}$ mice throught the experimental period after X-ray exposure. 86
Figure 4.1. ApoE$^{-/-}$ aortic plaque coverage after X-ray exposure at 6-weeks and 22-weeks of age. 93
Figure 4.2. Plaque coverage in the aortas of ApoE$^{-/-}$ male and female mice after X-ray exposure. 95
Figure 4.3. Comparison of plaque development between male and female ApoE$^{-/-}$ mice. 97
Figure 4.4. Quantification of Ldlr$^{-/-}$ mouse aortic plaque coverage after X-ray exposure. 99
Figure 4.5 Quantification of plaque coverage after X-ray exposure at varying ages within male and female Ldlr-/- mice. 101
Figure 4.6. Circulating cytokines from Ldlr$^{-/-}$ mouse whole blood after X-ray exposure. 108
Figure 5.1 Phase contrast images of HCAEC cultured in vitro. 116
Figure 5.2 HCAEC morphology under static and flow conditions. 117
Figure 5.3 Immunofluorescence comparison of HCAEC morphology under static and flow culture conditions. 119
Figure 5.4 Establishing the *in vitro* permeability assay in HCAECs. 122
Figure 5.5 HCAEC adhesion to monocytes. 124
Figure 5.6 Permeability of HCAEC monolayers from donors of varying ages. 126
Figure 5.7 Measure of age-related HCAEC adhesion to monocytes. 128

Figure 5.8 SA-β-Gal activity comparison between HCAEC from donors of varying age. 131
Figure 5.9 HCAEC SA-$\boldsymbol{\beta}$-gal activity after X-ray exposure. 133
Figure 5.10 X-ray induced increases in HL-60 adhesion to HCAEC from young donors. 135
Figure 5.11 X-ray induced increases in the permeability of HCAEC monolayers from young donors. 136
Figure 5.12 X-ray induced increases in SA-β-gal activity of HCAEC from young donors. 138
Figure 5.13 X-ray induced increases in HL-60 adhesion to HCAEC from middle-aged donors. 140
Figure 5.14 X-ray induced increases in the permeability of HCAEC monolayers from middle-aged donors. 142
Figure 5.15 X-ray induced increases in SA-β-gal activity of HCAEC from middle-aged donors. 144
Figure 5.16 Adhesion of HL-60 to HCAECs from young and middle-aged donors after X-ray exposure. 146
Figure 5.17 Age modulation of IR-induced HCAEC adhesion. 147
Figure 5.18 Permeability of HCAEC monolayers from young and middle-aged donors. 149
Figure 5.19 Age modulation of IR-induced HCAEC monolayer permeability. 150
Figure 5.20 SA-β-gal activity in HCAECs from young and middle-aged donors after X-ray exposure. 152
Figure 5.21 SA-β-gal activity in HCAECs from all donors after X-ray exposure. 154
Figure 5.22 Correlation between fold-change in senescence and permeability and adhesion of HL-60s in HCAEC. 155
Figure 5.23 ABT-263 dose investigation in HCAEC exposed to X-rays. 158
Figure 5.24 Rapamycin dose investigation in HCAEC exposed to X-rays. 160
Figure 5.25 The expression of senescence-associated proteins with X-ray exposure and rapamycin treatment. 164
Figure 5.26 Adhesion of HL-60 cells to HCAEC from donors of different ages after X-ray exposure and treatment with rapamycin or ABT-263. 171

Figure 5.27 Permeability of HCAEC monolayers after X-ray exposure and treatment with rapamycin or ABT-263. 175
Figure 5.28 SA-β-gal activity in HCAEC from donors of different ages after X-ray exposure and treatment with rapamycin or ABT-263. 178
Figure 5.29 Secreted cytokines from HCAEC exposed to X-ray with or without rapamycin. 184
Figure 6.1 Differential gene expression analysis of young and middle-aged HCAEC. .199
Figure 6.2 GO pathways of differentially expressed genes in HCAEC from middle-aged donors. 204
Figure 6.3 GO analysis of age-mediated, X-ray-induced differential gene expression in HCAECs. 210
Figure 6.4 Differential expression of genes related to GO pathways within irradiated HCAEC. 216
Figure 6.5 Modulation of IR-induced differential gene expression in HCAECs. 218
Figure 6.6 modulation of IR-induced expression of genes associated with adhesion, cellular junctions, and senescence in HCAECs with rapamycin. 226
Figure 7.1 Differentially expressed proteins in HCAEC from middle-aged donors compared to young. 238
Figure 7.2 GO pathways associated with the differently expressed proteins in the HCAEC from middle-aged donors. 240
Figure 7.3 Differential IR-induced protein expression in HCAECs from young and middle-aged donors. 247
Figure 7.4 The effect of rapamycin on IR-induced protein expression in HCAECs 253

List of tables

Table 1.1 Average radiation doses received during diagnostic medical procedures.....16

Table 2.1 Donor information for HCAEC cell lines used in this thesis.....64

Table 2.2 Antibodies used in Western blotting and immunofluorescence.....72

Common abbreviations

Abbreviation	Meaning
AMP	adenosine monophosphate
AMPK	AMP activated protein kinase
ApoE$^{-/-}$	ApoE receptor knockout mouse
ATV	atorvastatin
CAT T-cells	chimeric antigen receptor T-cells
CCF	cytoplasmic chromatin fragment
CDK	cyclin-dependent kinase
CDKIs	cyclin dependant kinase inhibitors
CTG	cell tracker green
CtIP	C-terminal binding protein interacting protein
CVD	Cardiovascular disease
D+Q	dasatinib and quercetin
DDIS	DNA damage-induced senescence
DDR	DNA damage response
DE	differential expression
DNA-PKcs	DNA-protein kinase catalytic subunit
DSB	double-strand break
EC	endothelial cell

Abbreviation	Meaning
ECM	extracellular matrix
ED	endothelial dysfunction
ER	endoplasmic reticulum
ERAD	ER-associated protein degradation
FAKs	focal adhesion kinases
FDG	fluorescein di-β-D-galactopryanoside
FDR	false discovery rate
FDR	false discovery rate
GM	genetically modified
GSNOR	S-nitrosoglutathione reductase
Gy	Gray
HCAEC	Human coronary artery endothelial cell
HDF	Human lung diploid fibroblast
HMEC	Human mammary epithelial cell
HR	Homologous recombination
HUVEC	Human umbilical vein endothelial cell
ICRP	International Commission on Radiological Protection
IR	Ionising radiation
IR-CVD	Ionising radiation-induced CVD

Abbreviation	Meaning
JNK/SAPK	c-Jun N-terminal kinase/stress-activated protein kinase
LDL	Low-density lipoprotein
$Ldlr^{-/-}$	Ldl receptor knockout mouse
M-CSF	macrophage colony-stimulating factor
MCP-1	monocyte chemoattractant protein 1
MDC1	mediator of DNA damage checkpoint 1
MI	myocardial infarction
MMP	matrix metalloproteinase
mTOR	mammalian target of rapamycin
ORO	Oil red O
ROS	Reactive Oxygen Species
RT	Room temperature
SA-β-Gal	Senescence-associated β-Galactosidase
SASP	Senescence associated secretory phenotype
SIPS	Stress-induced premature senescence
VMSC	Vascular Smooth muscle cell
WT	Wild type

1 Introduction

1.1 Cardiovascular disease

Cardiovascular disease (CVD) is the leading cause of mortality worldwide (Roth *et al.*, 2018), with the World Health Organisation estimating that roughly 31% of all deaths are attributable to the disease (World Health Organization, 2018). While CVD encompasses many conditions, atherosclerotic CVD is the main subset contributing to the high mortality statistics (Ference *et al.*, 2017). Atherosclerosis is a plaque build-up within the wall of arteries supplying organs such as the brain and heart. In addition to the significant impact on the patient's quality and length of life, the disease is an economic burden, with estimates that CVD costs more than €169 billion per year in the European Union alone (Gray, Petersen and Rayner, 2006).

Several environmental and behavioural risk factors are associated with an increased likelihood of developing CVD (Lippi *et al.*, 2007). Examples of modifiable risk factors include smoking (Messner and Bernhard, 2014), high alcohol consumption (Piano, 2017) and obesity (Poirier *et al.*, 2006). While there is potential to mitigate such factors through education and lifestyle changes, other risk factors, such as age (currently the best predictor of CVD) (Izzo *et al.*, 2018), cannot be mitigated through lifestyle modifications alone (Little *et al.*, 2012c). Additional risk factors include exposure to therapeutic ionising radiation (Baker, Moulder and Hopewell, 2011; Finch, Shamsa and Lee, 2014; Mitchell *et al.*, 2021), used, for example, in cancer treatment (Herrmann,

2020), where the increased risk of CVD must be balanced against the risk of not treating the tumour.

1.2 Atherosclerosis and its pathogenesis

1.2.1 Arterial structure and physiology

Arteries carry predominantly oxygenated blood from the heart (with the exception being the pulmonary artery, which delivers deoxygenated blood to the lungs) and need to be structured in a way that allows them to both compensate for and manage the pressure changes during the pulse wave, as well as support the movement of nutrients to the supplied tissues. An artery consists of three main layers, the tunica intima (the endothelium, the innermost layer in direct contact with the blood), the tunica media (the middle layer), and the tunica adventitia (outermost layer).

The tunica intima comprises a single layer of endothelial cells (Ecs) and includes an internal elastic lamina on the medial side, which provides elasticity to the artery, assisting with the ability of vessels to remain intact while expanding (Galley and Webster, 2004). The tunica media is comprised of a collagen matrix and vascular smooth muscle cells (VSMC), which are responsible for the contractile ability of the vessel (Ross and Glomset, 1973). The tunica adventitia comprises connective tissues to maintain the position of the vessel within the surrounding tissues. In larger arteries, within this layer are vasa vasorum (vessels of vessels), which allow for the supply of

nutrients to the adventitia (Levick, 2003; Gonçalves *et al.*, 2021) (Figure 1.1). Atherosclerosis develops in the subendothelial space between the tunica intima and media, which can reduce the size of the arterial lumen (Mazzone *et al.*, 1993).

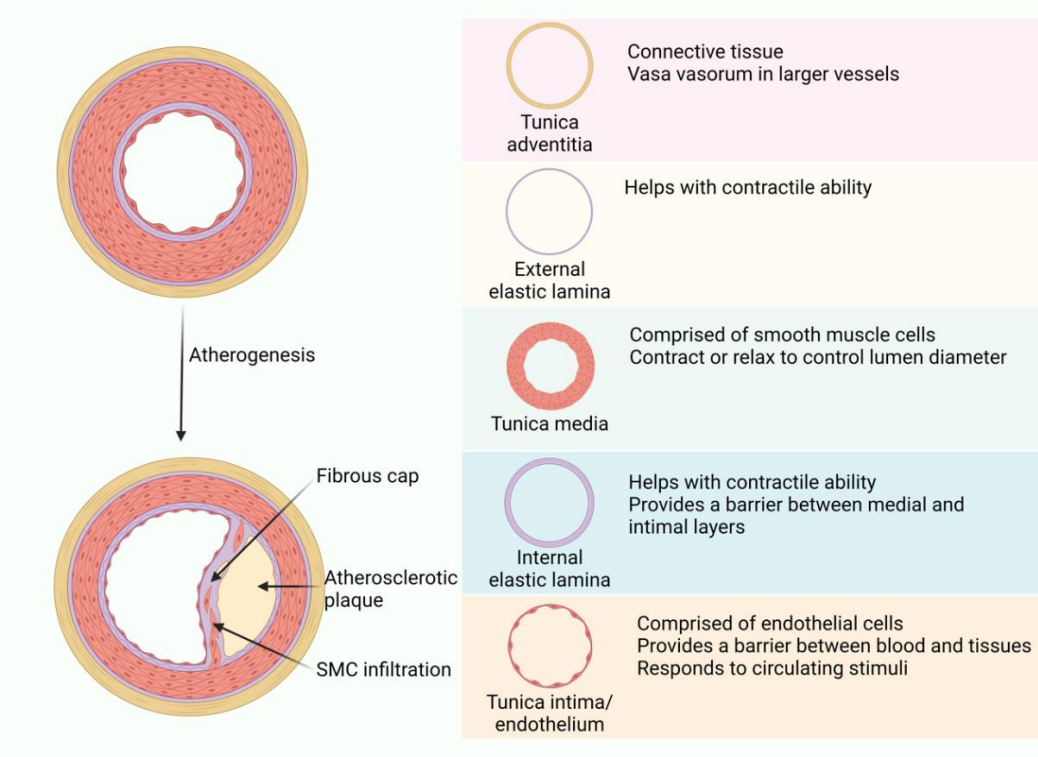


Figure 1.1 Structure of an artery and location of plaque development.

The outermost layer of an artery, the tunica adventitia, is formed mainly of connective tissue, with vasa vasorum present in larger vessels. Following this, an external elastic lamina helps facilitate the vessels ability to contract and relax. The middle layer (tunica media) comprises vascular smooth muscle cells that respond to stimuli from endothelial cells (ECs) to contract or relax, facilitating the shrinking or widening of the arterial lumen. An internal elastic lamina then follows, providing further structural support. The innermost layer, the tunica intima or endothelium, comprises ECs, which form the primary barrier between the circulating blood in the lumen of the vessel and the rest of the artery.

1.2.2 What is atherosclerosis?

Atherosclerosis is predominantly a disease of an inflammatory nature, which is characterised by the accumulation of lipids and immune cells within large arteries

(Lusis, 2000). It can take decades to manifest, with the majority of people with atherosclerosis being asymptomatic (McNamara, 1971). However, if the plaque burden increases, it can encroach into the luminal space (Figure 1.1), reducing or preventing blood from flowing through the vessel, leading to inadequate oxygenation and tissue ischaemia (Palasubramaniam, Wang and Peter, 2019). In terms of cardiac arteries, mild to moderate occlusion can lead to conditions such as angina pectoris (Cairns *et al.*, 1985)(Gray, Petersen and Rayner, 2006), while in more severe cases, ischaemia can result in damage to the affected tissue, causing myocardial infarction (MI; heart attack) when coronary arteries are occluded; stroke can result when cerebral arteries are affected (Cairns *et al.*, 1985; Toth, 2008; Roth *et al.*, 2018).

1.2.3 Steps in atherogenesis

Atherosclerotic plaque development occurs within the subendothelial space (Mazzone *et al.*, 1993; Skålén *et al.*, 2002a) (Figure 1.1B). The initial stages involve damage to the endothelial layer, which affects its ability to maintain a functional barrier and to respond appropriately to vasoactive stimuli, a state known as endothelial dysfunction (ED). This damage can be caused by stressors such as reactive oxygen species (ROS) or chronic high blood pressure. During ED, the activation of ECs causes their characteristics to shift towards a pro-inflammatory phenotype. The expression of surface proteins changes, leading to increased presentation of adhesion molecules (Bochkov *et al.*, 2002). The consistency of the extracellular matrix alters in the early stages of atherosclerosis: proteoglycans initially form the main component, however, as the disease progresses, collagens become more prominent, with decreases in elastin fibres, glycoproteins, and

proteoglycans (Duca *et al.*, 2016; Blokland *et al.*, 2020). Importantly, uncontrolled degradation of elastin and collagen increases the trans-endothelial migration of leukocytes, VSMC migration, and vascular cell death. As elastin fibres stabilise collagen, its degradation increases the likelihood of plaque rupture (Singh, Rai and Agrawal, 2022).

Furthermore, these changes cause the endothelium to be more susceptible to the retention of LDL through both easier migration to the subendothelial space due to degradation of the elastic lamina, and the binding of LDL to collagen (Jimi *et al.*, 1994; Kwon *et al.*, 2008). These changes can also lead to a decrease in the elasticity of the vessel, affecting the vessel's ability to expand in response to the pulse wave. This increases blood pressure and subsequently increases the damage to the endothelium, further exacerbating the development of atherosclerosis (Heagerty *et al.*, 1993; Libby and Theroux, 2005; Kwon *et al.*, 2008). The LDLs retained within the subendothelial space are exposed to enzymes and ROS, resulting in the peroxidation of fatty acid residues within phospholipids, generating proinflammatory lipids such as lysophosphatidylcholine (Figure 1.2). The combination of these factors causes further activation of local Ecs, increasing the presentation of cell surface adhesion molecules such as E-selectin and VCAM-1 (Gharavi *et al.*, 2007).

Human blood flowing through the vessels contains erythrocytes, platelets, and white blood cells, including adaptive immune B and T cells and eosinophils, basophils, monocytes, and immature dendritic cells (Murphy and Weaver, 2016). The presentation of the selectin adhesion molecules (e.g. E-selectin) results in prolonged

contact of circulating monocytes with the vascular lining, leading to the local transient adhesion and rolling of monocytes along the area of affected endothelium, while VCAM-1 and ICAM-1 presentation increases binding affinity for the monocytes (Figure 1.2). This binding, along with the release of chemotactic cytokines CCL2, CCL5, CXCL10, and CXC_3CL1 from activated endothelial cells, facilitates the migration of monocytes into the intimal space (Zernecke, Shagdarsuren and Weber, 2008a; Weber and Noels, 2011), where these monocytes differentiate into macrophages in response to growth factors such as granulocyte-macrophage colony-stimulating factor (GM-CSF) and macrophage colony-stimulating factor (M-CSF) (Williams, Fisher and Greaves, 2012). These macrophages engulf the modified LDLs in the intimal space and become foam cells, forming the "fatty streak" associated with early atherosclerosis (Figure 1.2). This is not necessarily clinically significant and can even be found in infants within the first six months of life, most often fully resolving (Napoli *et al.*, 1997). However, in adults, these fatty streaks often remain unresolved, and lipid deposits begin to accumulate with the foam cells. With further infiltration of monocyte-derived macrophages and dendric cells and the death of foam cells, necrotic, lipid-rich cores begin to manifest (Kolodgie *et al.*, 2003). Growth factors released from adjacent Ecs and infiltrated immune cells stimulate medial smooth muscle cell (SMC) infiltration into the intima, forming a fibrous cap covering the atherosclerotic plaque (Figure 1.2). In this state, the plaque is usually stable, often remaining asymptomatic unless there is significant encroachment into the luminal space (Bentzon *et al.*, 2014). If the fibrous cap becomes damaged and ruptures, it can lead to the activation of platelets, development of a blood clot and occlusion of the artery, which can result in a stroke or MI.

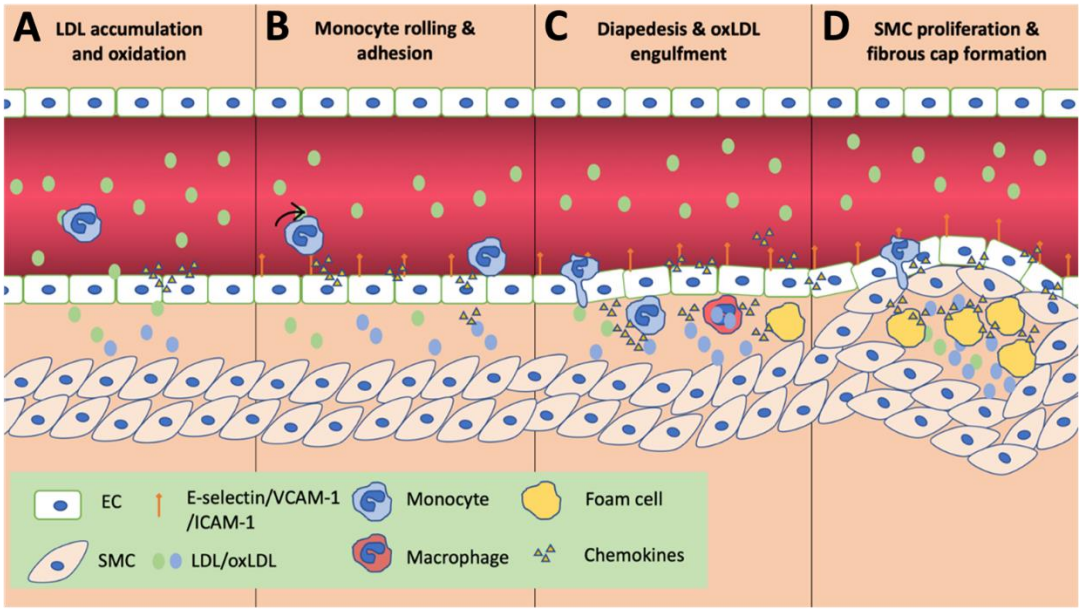


Figure 1.2 Schematic overview of atherogenesis.

A) The initial stages involve the accumulation of lipids, predominantly LDLs, within the subendothelial space, where they can become oxidised. **B)** Damage to the endothelial layer increases the permeability of the layer to these circulating lipids within the blood. The damage and oxidised lipids lead to EC activation, resulting in the presentation of adhesion molecules such as E-selectin, VCAM-1, and ICAM-1, along with the secretion of chemoattractants. This combination promotes the adhesion and rolling of circulating monocytes, which enables easier movement of the monocytes into the subendothelial space (diapedesis). **C)** The monocytes differentiate into macrophages, engulfing the lipids and forming foam cells. **D)** This cycle continues, with the increasing accumulation of foam cells leading to activation and movement of local vascular smooth muscle cells (VSMCs), forming a fibrous cap over the lipid core of the plaque. This final stage is where the main encroachment into the luminal space occurs.

Characteristic phenotypic changes are seen in Ecs during the development of atherosclerosis. In atheroprone areas, the Ecs develop an inflammatory secretory phenotype, dysregulation of cytoskeletal protein expression and organisation, and changes in junctional protein expression (Sima, Stancu and Simionescu, 2009). Interestingly, such phenotypic changes are also observed as cells become senescent

(see section 1.5.2 below), suggesting that senescence may contribute to atherogenesis. This is explored below and throughout the experimental chapters of this thesis.

1.2.4 Current treatments for atherosclerosis

Current treatments for atherosclerosis target the atherogenic pathologies mentioned previously, with primary prevention targeting cholesterol lowering. Statins (e.g. pravastatin, simvastatin) are a typical class of drugs prescribed to reduce the circulating LDL levels. They are competitive inhibitors of 3-hydroxy-3methyl-glutaryl-coenzyme A (HMG-CoA) reductase (HMGCR), which catalyses the conversion of HMG-CoA to mevalonic acid. This is the rate-limiting step in the production of cholesterol, reducing the *de novo* production within cells. This reduction increases the expression of LDL receptors, increasing the uptake of LDL from the circulation for degradation, primarily in the liver (Brown and Goldstein, 1986). The rationale behind this treatment is to decrease circulating LDLs to reduce the ability of lipids to accumulate in areas with damaged endothelium, preventing disease progression (Goldstein and Brown, 1984).

It is apparent that some statins (e.g., atorvastatin (ATV)) also have an immunomodulatory effect, for example, incubation of primary lung mast cells with certain statins inhibits the IgE-mediated release of histamine (Krauth *et al.*, 2006). Furthermore, studies have shown that lovastatin can impair the NF-KB and c-Jun N-terminal kinase/stress-activated protein kinase (JNK/SAPK) pathways, along with inhibition of TNF-α mediated E-selectin expression in human Ecs, resulting in decreased adhesion molecule presentation (Nübel *et al.*, 2004). A meta-analysis of randomised trials of statin therapy demonstrates decreased vascular mortality with statin treatment

compared to placebo. The Scandinavian Simvastatin Survival Study (4S), with a cohort of 4444 patients who had angina or experienced an MI, demonstrated a 4% reduction in mortality with simvastatin treatment compared to placebo control over 5.4 years (12% mortality in placebo, 8% in treatment groups) (Scandinavian Simvastatin Survival Study Group, 1994). In a more recent meta-analysis of 28 randomised control trials (RCTs), it was found that statins produce a 21% and 24% proportional reduction in risk of a first major vascular event and risk of vascular mortality per 1 mmol/L reduction in LDL, respectively (Armitage *et al.*, 2019).

While statins are used as primary and secondary interventions, other therapeutics are used to combat arising pathologies associated with CVD and atherosclerosis. For example, antiplatelet drugs (e.g. aspirin and clopidogrel) are also used to reduce thrombus formation should a rupture occur, with these becoming a standard treatment during and after procedures such as percutaneous coronary interventions (PCIs) (Cairns *et al.*, 1985; Pettersen *et al.*, 2012; Chiarito *et al.*, 2020). PCIs are typically carried out after an ischaemic event has occurred; they allow the placing of a stent less-invasively by accessing the coronary arteries, typically through the femoral artery, widening the narrowed section and restoring blood flow to the ischaemic region (Holmes *et al.*, 2002).

A randomised, double-blind trial has demonstrated that using rapamycin-eluting stents reduced failure of the stent by 12.4% (Moses *et al.*, 2003). Another therapeutic avenue using anti-inflammatory drugs has been investigated in randomised clinical trials. An example is the use of IL-1ß-targeting monoclonal antibody, canakinumab, which

demonstrated a significant reduction in non-fatal MI, non-fatal stroke, or cardiovascular death in those who had previously experienced an MI, compared to placebo. However, it is important to note that this resulted In a higher incidence of fatal infection than placebo (Ridker *et al.*, 2017).

1.3 The DNA damage response pathway

The DNA damage response (DDR) pathway involves sensors, transducers, and downstream effector kinases that drive phosphorylation events (Huang and Zhou, 2020) and allow cells to respond appropriately to damage by initiating transient cell cycle arrest and repair, apoptosis, or cell senescence. DNA damage can be caused by intrinsic (e.g., oxidative stress) and extrinsic stressors (e.g., UV radiation, ionising radiation), leading to single-strand breaks, nucleotide lesions, double-strand breaks (DSBs), or inter-strand crosslinks, with the type of DNA damage influencing the repair mechanism employed, described in the following subsections.

1.3.1 Single-strand break repair pathways

Upon formation of single-strand breaks, RPA and its partner, ATR-interacting protein (ATRIP), coat exposed ssDNA and facilitate the recruitment of ATR. To function, ATR needs the presence of ssDNA-double-stranded DNA junctions, as well as activator proteins, such as topoisomerase II-binding protein-1 (TOPBP1) and Ewing tumour-associated antigen 1 (ETAA1) (Feng *et al.*, 2016). The checkpoint clamp complex RAD9-RAD1-HUS1 (9-1-1) recognises these junctions and, along with the MRN complex

(MRE11-RAD50-NSB1), recruits TOPBP1 through binding to the C-terminal domain of RAD9 (Delacroix *et al.*, 2007). Once it is bound, TOPBP1 activates ATR in an ATRIP-dependent manner (Carney *et al.*, 1998a; Mordes *et al.*, 2008). The formation of the ATR-ATRIP complex enables the phosphorylation of CHK1, which further phosphorylates CDC25 phosphatases, dephosphorylating CDK1 and CDK2, resulting in a halt in the cell cycle (Leung-Pineda, Ryan and Piwnica-Worms, 2006). ATR also phosphorylates other targets, such as Rad17, p53, and Brca1, inhibiting DNA replication and promoting repair (Zou and Elledge, 2003).

1.3.2 Double-strand break pair pathways

In the event of DSBs, two main repair pathways are employed: non-homologous end joining (NHEJ) and homologous recombination (HR). The pathway chosen by the cell is influenced by two main factors: the cell-cycle stage and the complexity of the break. NHEJ is an error-prone repair pathway that functions throughout the cell cycle and is preferred when a simple repair is needed and DNA ends can simply be ligated back together (Roth and Wilson, 1985). Furthermore, NHEJ has Ku/LIG4-dependent and independent pathways. The Ku/LIG4 dependent pathway involves the rapid binding of the Ku heterodimer (Ku70 and Ku80) to the exposed dsDNA, which activates DNA-protein kinase catalytic subunit (DNA-PKcs), which helps to stabilise the DSB ends through a series of phosphorylation reactions, preventing endogenous nucleases from degrading the exposed DNA (Ranjha, Howard and Cejka, 2018). DNA-PKcs also autophosphorylates on the ABCDE cluster to provide access for processing enzymes such as ARTEMIS, which modifies the DNA ends to ensure they can be ligated by XRCC4/

DNA ligase 4 (Goodarzi *et al.*, 2006). The secondary pathway independent of Ku/LIG4 involves the binding of PARP1 to the DSB, mediating the initial accumulation of the MRN complex in a γH2AX and mediator of DNA damage checkpoint 1 (MDC1) dependent manner (Wang *et al.*, 2003; Kuhfittig-Kulle *et al.*, 2007). MRN and PARP1 recruit ATM, increasing activation of the γH2AX cascade and stabilising DDR elements (Lee et al., 2010). This then enables the ligation of the DNA strands by XRCC1 and DNA ligase 3 (Della-Maria *et al.*, 2011).

In contrast to NHEJ, HR uses a sister chromatid to provide a template, making it error-free (Resnick, 1976). However, it is only active during the S phase and G2 phase of the cell cycle i.e., following S-phase DNA replication synthesis, thus providing the homologous template. Initially, the DSB is recognised by the MRN complex (MRE11-RAD50-Nbs1). RAD50 interacts with the MRE11 and associates with the DNA of the DSB. Importantly for HR, MRE11 contains exonuclease and endonuclease activities required for the initial steps of DNA end resection (Anand *et al.*, 2016). NSB1 interacts with MRE11 and associates with ATM via its C-terminal domain (Qiu and Huang, 2021), promoting its recruitment to DSB and activation. Furthermore, upon IR exposure, the inactive dimers of ATM become phosphorylated at Ser1981, forming active monomeric units, and activating the signalling cascade (Kastan and Bakkenist, 2003). Mutations in NBS1 and MRE11 lead to Nijmegen breakage syndrome and ataxia-telangiectasia-like disorder, respectively, which lead to increased radiosensitivity and loss of damage-induced checkpoints (Carney *et al.*, 1998b; Stewart *et al.*, 1999). ATM-regulated end resection is further facilitated by the association of BRCA1 and its phosphorylation of the C-terminal binding protein interacting protein (CtIP) (Anand *et al.*, 2016). After this

initial resection, EXO1 or DNA2 continue progressing the resection in conjunction with WRN or BLM helicases (Nimonkar *et al.*, 2011). Following end resection, RPA accumulates on the 3' end of single-stranded DNA, promoting the recruitment of BRCA2 and RAD51. The interaction between RAD51 and the BRCA2 C-terminus is regulated by the CDK-dependent phosphorylation of BRCA2, providing some control over when HR occurs in the cell cycle (Esashi *et al.*, 2005). RAD51 is a recombinase that mediates the strand inversion of the sister DNA template and therefore is important in the function of HR (Ceccaldi, Rondinelli and D'Andrea, 2016).

Further signalling cascades are activated by the phosphorylation target of p53 by MRN and ATM. One consequence is increased expression of cyclin-dependent kinase inhibitor, $p21^{Cip1}$ (Lashgari *et al.*, 2018; Jiang and Wang, 2019). This inhibits CDK2, which is responsible for progression through the G1/S phase of the cell cycle, resulting in the arrest of the cell cycle at G1/S (Maddika *et al.*, 2008). In addition, ATM phosphorylates CHK2, leading to the arrest of the cell cycle in G2/M. p53 and $p21^{Cip1}$ downstream signalling are discussed in section 1.5.2.1. The main role of the DDR pathway is to repair damaged DNA, or where irreparable damage has occurred, to prevent further cell division, as cells harbouring unrepaired DNA damage may undergo neoplastic transformation. Hence if the damage is not repaired, a cell will either undergo apoptosis or enter into senescence (Lehmann *et al.*, 2007).

1.4 Ionising radiation

To investigate the connections between ionising radiation (IR), senescence, and the development of atherosclerosis, an understanding of what IR is and how it interacts with biological tissue is needed. This section summarises IR from a biological point of view.

IR is a form of radiation with sufficient energy to eject one or more electrons from the atoms it interacts with (Brenner and Hall, 2007). It can be in particulate or electromagnetic form, depending on its source. X-rays and γ-rays are examples of electromagnetic radiation, with examples of particulate radiations being electron, heavy charged ion, and proton. Most particulate radiations are directly ionising, directly causing biological damage. In contrast, electromagnetic radiations indirectly ionise by exciting a secondary electron from the material they interact with, which then causes biological damage (IAEA, 2010). Both electromagnetic and particulate radiations are used diagnostically and therapeutically, with electron beam therapy commonly used for radiotherapy and proton beam therapy becoming more readily available as the technology advances (Levin *et al.*, 2005; Thompson *et al.*, 2018).

There are many sources of IR: natural sources (radon gas), medical procedures (computed tomography scans, radiotherapy), occupational (nuclear powerplant workers, aircrew, astronauts), accidental (nuclear disasters), and war (atomic and nuclear bombs) (International Commission on Radiological Protection (ICRP), 2007). Hence, it is important to understand acute and long-term effects of exposure to IR.

X-rays are the most common medical exposure for the general population, with most people in the Western world experiencing them either for diagnostic reasons or for procedures such as percutaneous coronary intervention. The most common exposure is intraoral use in dentistry (Watson *et al.*, 2005). The doses received for medical diagnostic reasons vary depending on the part of the body and the reason for the exposure; these are summarised in Table 1.

For therapeutic purposes, heavy-charged ion therapy is used for cancer treatment and is another component of space radiation. Interestingly, the interaction of heavy ion radiation with the retina causes astronauts to experience flashes of light in their vision while in space (Hall and Giacia, 2006). Neutron radiation is a result of fission, and is highly abundant in nuclear reactors, although the dose received by those working at these sites is very low (UNSCEAR, 2008).

Table 1.1 Average radiation doses received during diagnostic medical procedures. Adapted from (Brenner and Hall, 2007)

Medical exposure	Organ exposed	Organ dose (mGy)
Chest radiography	Lungs, Heart	0.01-0.15
Dental radiography	Brain	0.005
Mammography	Breast	3
Abdominal CT	Stomach	10
Barium enema	Colon	15
Neonatal abdominal CT	Stomach	20
Radiotherapy		2,000 – 16,000

Within a biological system, IR can cause both direct and indirect damage. For example, if X-rays were to ionise an atom near to DNA, the fast electron released could interact with DNA and cause a strand break. Indirectly, this fast electron could interact with water, causing the creation of free radicals which can also lead to DNA strand breaks. Alongside potential for DNA damage, IR also indirectly leads to activation of various inflammatory cytokine pathways, which can also have a detrimental effect (Kiang and Olabisi, 2019). Radiosensitivity of tissues is variable, with those that contain highly proliferative cells (e.g. hair follicles, bone marrow, small intestine) being the most sensitive and those containing cells which proliferate more slowly (e.g. kidneys, liver)

the least sensitive (Hall and Giacia, 2006). This is important when considering the risk versus benefit of medical exposures. Furthermore, reproductive tissues are also highly sensitive to radiation exposures, so patients about to undergo radiotherapy may undergo extraction and preservation of sperm or egg.

The biological dose of radiation is mainly expressed in Grays (Gy), which is a measure of how much energy is absorbed by the tissue in Joule/Kg. Importantly, the damage caused by 1 Gy of neutrons is greater than 1 Gy of X-ray. This is due to the linear energy transfer (LET) of radiation: the amount of energy transferred to the exposed material per unit distance along the photon's or wave's path. This is because charged particles such as neutrons deposit more energy per unit length along their track compared to X-rays. A comparison between different types of radiation is done by measuring the biological response to the specific IR type ratioed over the response to the same dose of γ-rays, known as relative biological effectiveness (RBE) (IAEA, 2010).

The Sievert (Sv) is used to compare doses of different types of radiation and is a measure of absorbed dose with RBE considered. For example, 1 Gy of X-rays and γ-rays is equal to 1 Sv, whereas with proton radiation, 1 Gy of proton radiation would be equal to 2 Sv. Typically, for every 1 Gy of exposure to X-rays, there are 1000 single-strand breaks (SSBs) and 40 DSBs (Murshed, 2019). These single and DSBs lead to the activation of the DDR, discussed above (section 1.2.2) (De Rozieres *et al.*, 2000; Takagi *et al.*, 2005). This damage leads to cells arresting the cell cycle for repair, or entering into apoptosis or senescence if the damage is not repairable. Considerations of dose response should also be made for those with conditions such as ataxia-telangiectasia, which increases the

sensitivity of the patient due to a reduced ability to repair radiation induced cellular damage (Plowman *et al.*, 1990).

The effect of exposure to IR is thought to be dose dependent. If the dose received exceeds a threshold value, acute effects will likely be observed. However, at doses below this level, there are likely to be statistically detectible changes in disease risk after an extended period. The long-term dose effects present many challenges to assess, as epidemiological evidence, particularly from follow-up studies on survivors of nuclear disasters, is often used, which is open to extrinsic factors due to the lifestyle of the participants (Ivanov *et al.*, 2000; Little *et al.*, 2023).

1.4.1 The link between ionising radiation and cardiovascular disease

While the evidence supports the link between IR and CVD, little is known about the mechanisms behind it. Evidence includes increased risk of developing CVD in patients who have undergone radiotherapy for head and neck cancers, which exposes the coronary vasculature, likely having a direct pro-atherogenic effect (Bradshaw *et al.*, 2016; da Silva, 2019). Furthermore, the incidence of CVD is higher among astronauts who have travelled outside the Earths atmosphere, and therefore been exposed to higher doses of cosmic radiation, compared to astronauts who have not left low Earth orbit or those who have not flown any missions (Boerma, 2015). While correlation exists, it is important to also consider changes a microgravity environment would have on the cardiovascular system (e.g., changes in cardiac output and stokes volume, and

endothelial dysfunction due to suppressed cellular proliferation) (Baran *et al.*, 2022). With increasing potential for both experimental and commercial space travel, understanding the pathogenesis of IR-induced CVD is significant for those involved.

Another major form of exposure of vasculature to IR is medical procedures. Roughly 50% of those who receive treatment for cancers receive radiotherapy. Of those cured, 40% received radiotherapy at some point, indicating its vital role in treatment (Ringborg *et al.*, 2003; Parker, 2012). In 2012, over 14 million new cancer cases were reported, with a significant proportion of these being in the lung or breast, with treatment causing the most exposure of coronary vasculature to IR (Atun *et al.*, 2015). This likely means that over 7 million people, when only accounting for the new cases, received RT that year. Furthermore, a meta-analysis of breast cancer treatment demonstrated women who received left breast cancer RT have an increased CVD mortality incidence compared to those who received RT for right breast cancer (Cheng *et al.*, 2017).

The connection between the exposure of vasculature to IR and the accelerated development of CVD, specifically atherosclerosis, has been known for some time. The Life Span Cohort Study (LSS), which followed the survivors of the Hiroshima and Nagasaki atomic bombs, demonstrated an increased likelihood of death by stroke or heart disease after exposure to >0.5 Gy and >0 Gy, respectively. Mortality due to CVD or stroke was equal to that of cancers, indicating that non-mutagenic causes of disease after exposure are equally important, yet still overlooked (Shimizu *et al.*, 2010). The data from the LSS was statistically modelled by Little *et al.*, who showed that those

exposed at a younger age had an increased risk of mortality related to CVD events than those of an older age at the time of exposure (Little *et al.*, 2012a).

Studies have demonstrated that the exposure of the coronary vasculature to IR increases the expression of VCAM-1 and ICAM-1, which would increase immune cell recruitment to the area, suggesting this would increase the pathogenesis of atherosclerosis (Philipp *et al.*, 2017a). It has also been demonstrated that IR can increase the serum levels of TNF-α, IL-1α and IL-6, all of which contribute to inflammatory signalling and increased adhesion molecule expression (Azimzadeh *et al.*, 2015). Importantly, IR is associated with the development of senescence.

1.5 Cellular senescence

1.5.1 Physiological and pathological roles of cell senescence

Senescence is a state of permanent cell-cycle arrest while remaining metabolically active, which has been observed in vertebrates to serve several physiologically essential roles throughout the life course. In mammals, formation of the foetal placenta and efficient embedding into the endometrium, including vascularisation through invasion of the spiral arteries, requires senescence, while senescence of the decidual (maternal) placenta is thought to contribute to the onset of labour (Cox and Redman, 2017). Senescent cells are detectable during embryogenesis at sites of tissue remodelling, e.g., in the developing limb and kidney; their appearance follows a specific time course, suggesting programmed senescence is necessary for development (Storer *et al.*, 2013;

Gorgoulis *et al.*, 2019). Furthermore, acute cell senescence is associated with improved wound healing, with Hiebert *et al*. demonstrating faster wound closure and decreased scar tissue formation in mice with Nrf2-mediated fibroblast senescence (Hiebert *et al.*, 2018). Senescence also serves as a tumour suppressor mechanism that prevents the propagation of potentially neoplastic cells, e.g., those with damaged DNA (te Poele *et al.*, 2002). Such cells are then cleared by the action of the immune system, mainly through recruitment and engulfment by macrophages attracted to the sites of senescence through cytokine and chemokine signalling (see 1.5.2.7 below 'SASP'). Clearance of senescent cells by the immune system has been well documented in the axolotl, where preventing senescence or depletion of macrophages prevents limb regeneration (Yun, Davaapil and Brockes, 2015; Walters *et al.*, 2023). Hence, the acute onset of cell senescence with subsequent clearance is physiologically vital in both development and in the adult organism.

However, with ageing (at least in vertebrates), the percentage of senescent cells increases, with accumulation linked to age-related diseases (Ohtani *et al.*, 2004; Coppé *et al.*, 2014), such as atherosclerosis (Childs *et al.*, 2016a), liver stenosis (Ogrodnik *et al.*, 2017), osteoarthritis (Philipot *et al.*, 2014), diabetes (Thompson *et al.*, 2019), idiopathic pulmonary fibrosis (Barnes, Baker and Donnelly, 2019), osteoporosis (Kou *et al.*, 2023), age-related cataract (Huang *et al.*, 2022), cardiac dysfunction (Shi *et al.*, 2022), and neurodegeneration (Rivellini *et al.*, 2022). Accumulation of senescent cells has also been linked to age-related physical dysfunction, demonstrated by introducing senescent cells into young mice and evidenced by diminished grip strength, decreased maximal speed, and reduced hanging endurance (Xu *et al.*, 2018), characteristics often

observed in the natural ageing processes. Moreover, these outcomes were similarly identified when replicating the experiment with older mice. Notably, a significant decrease in percentage survival compared to implantation control mice was observed, supporting the role senescence may play in ageing and mortality. Furthermore, within this study, the authors demonstrated significant improvement in both physical dysfunction and lifespan when senescent cells within the mice were targeted with a senolytic combination of dasatinib + quercetin (D + Q). Strengthening these findings, a recent study used an immunological approach to remove senescent cells, improving age-related physical dysfunction. This was achieved using chimeric antigen receptor T-cells (CAR T-cells) designed to target natural killer group 2 member D (NKG2D) ligands MICA/B and ULBP1-6, which are highly expressed in senescent cells (Sagiv *et al.*, 2016; Yang *et al.*, 2023). These findings compellingly underscore the contributory role of senescent cells in driving age-related pathology.

It is hypothesised that cellular senescence contributes to age-related pathologies by reducing the associated tissue'' replicative capacity and causing tissue dysfunction. Furthermore, inflammageing, an age-related phenomenon of chronic low-grade inflammation, is linked to immunosenescence, which is relevant as many age-related diseases have an inflammatory component (Ferrucci and Fabbri, 2018). Recently, a study using a mouse model of immune senescence (Vav-iCre$^{+/-}$; Ercc1$^{-/fl}$) demonstrated an induction of senescence in non-lymphoid organs, such as the aorta, liver, and kidney. This was accompanied by increased tissue damage markers, such as amylase levels, indicating pancreatic dysfunction and the presence of albumin in urine, which suggests kidney dysfunction (Yousefzadeh et al., 2021). This data suggests that

immune senescence may drive organ senescence and may correlate with dysfunction, which can contribute to the development of age-related pathologies. As discussed here, the evidence suggests that senescence can be either beneficial or detrimental, depending on its context.

1.5.2 Key features and markers of senescent cells

To study senescence, the ability to confirm the presence of senescent cells both *in vitro* and *in* vivo is paramount. Currently, there is not one conclusive marker of senescence, but rather, it is necessary to combine several different markers to increase confidence in senescence detection. Many of these markers are associated with the mechanisms of induction and maintenance of the senescent state, most of these characteristics being distinguishable from the original cell type. These can include cell cycle arrest, changes in morphology, changes in nuclear structure and chromatin reorganisation, failure of autophagy, changes in lysosomal activity, mitochondrial dysfunction, and a SASP (Figure 1.3; Hernandez-Segura, Nehme and Demaria, 2018).

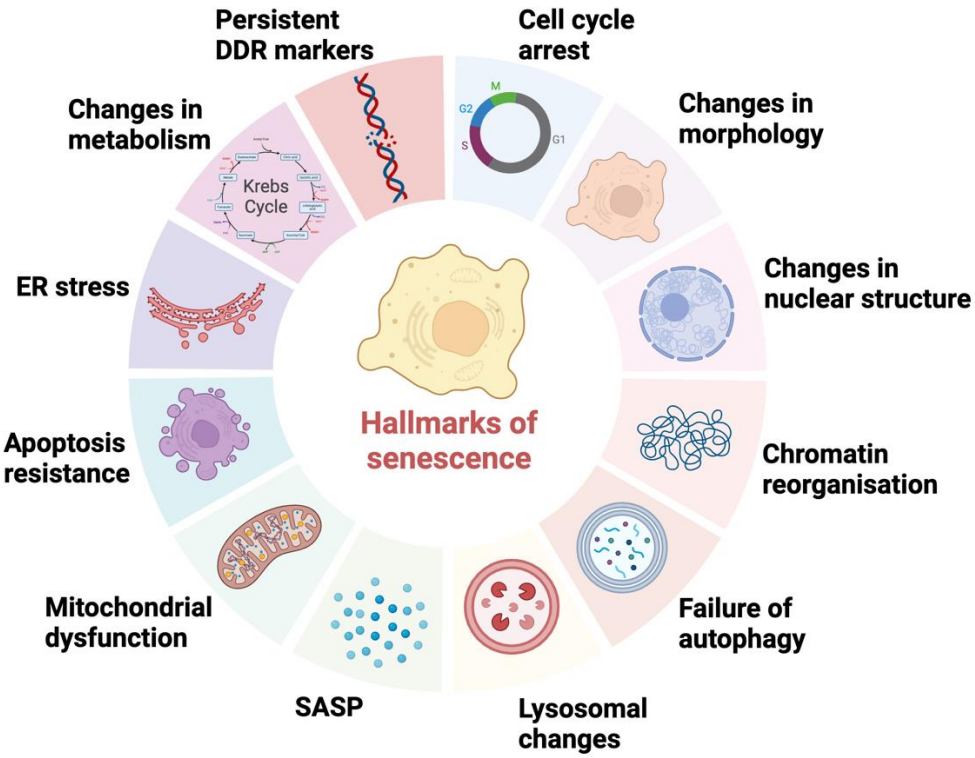


Figure 1.3 Hallmarks of senescence.

Cells which are senescent can display some or all of the hallmarks of senescence, such as cell cycle arrest, changes in morphology, changes in nuclear structure, chromatin reorganisation, failure of autophagy, lysosomal changes, a senescence associated secretory phenotype (SASP), mitochondrial dysfunction, resistance to apoptosis, ER stress, changes in metabolism, and persistent DNA damage response (DDR) markers (created with biorender.com).

1.5.2.1 Cell cycle arrest

A universal feature of senescence is an irreversible halt to the cell division cycle, as first described by Hayflick and Moorhead in 1961 (Hayflick and Moorhead, 1961). Mechanistic drivers of cell cycle arrest in senescence are, therefore, valuable markers,

as they are likely to indicate cells that have exited the cell division cycle; their central role has been confirmed experimentally since premature induction of senescence was observed after cells were transfected with cyclin dependant kinase inhibitors (CDKIs) (McConnell *et al.*, 1998). Of these, the cyclin kinase inhibitors CDKN1A and CDKN2A ($p21^{WAF1/Cip1}$ and $p16^{INK4a}$, respectively; referred to henceforth as p21 and p16) are widely used (Alcorta *et al.*, 1996). p16 allosterically modulates cyclin-dependent kinase (CDK) 4/6 enzymes, inhibiting their binding to D-type cyclin, thus preventing their activation (Pavletich, 1999; Moore *et al.*, 2002) and blocking progression from G1 to S phase of the cell cycle (Cdk4/6 is required to phosphorylate tumour suppressor protein Rb and releases bound transcription factor E2F necessary for expression of many S phase genes). $p14^{ARF}$ is encoded within the same locus as p16, though in an alternative reading frame–- hence ARF, and inhibits the function of MDM2 and E3 ubiquitin ligase that negatively regulates p53 (Pavletich, 1999). Therefore, increased ARF leads to an increase in active p53, a transcription factor that increases the expression of several genes, such as those related to cell cycle checkpoints (e.g., p21), DDR pathways (e.g., GADD45), apoptosis (e.g., Bax), and senescence (e.g., p21) (Hollander *et al.*, 1993; Cory and Adams, 1998; Collins and Sedivy, 2003).

In addition to p16, p21 also inhibits the CDK4/6 – cyclin D complex, along with CDK2 – cyclin E, further inhibiting the phosphorylation of Rb, which is required for progression through the cell cycle. Furthermore, a study by Yosef *et al.* has demonstrated that the knockdown of p21 *in vitro* reduces the viability of DNA damage-induced senescent cells, further confirming this in a p21 knockout mouse model, where liver senescent stellate cells were reduced along with less fibrosis and collagen production (Yosef *et al.*, 2017).

This data demonstrates the critical role of p21 in the induction and maintenance of senescence.

Upregulation of p21 occurs in response to various stressors, such as DNA damage, due to p53-induced transcription. This upregulation, along with the transcription of many other genes, such as GADD45A, prevents the cell from progressing through the cell cycle, providing the cell with the opportunity to repair the damaged DNA, enter into apoptosis, or enter into senescence (Appella and Anderson, 2001). Interestingly, mutations within TP53 (the gene encoding p53) are the most prevalent in all major cancer types, apart from malignant melanoma, further suggesting the importance of senescence in preventing tumorigenesis (Mendiratta *et al.*, 2021). Given p5''s role in initiating cell cycle arrest and activating transcription of genes involved in DNA repair, along with its mutational prevalence in cancers, its importance cannot be understated.

In addition to these aspects, senescent cells have up-regulated pro-survival pathways (e.g., BCL-2/BCL-X_L, p53/p21/serpine), making them apoptosis-resistant (Kirkland and Tchkonia, 2017). This has been demonstrated experimentally with a study targeting these anti-apoptotic pathways in preadipocytes and HUVECS using drugs or siRNA, demonstrating reduced senescent cell viability (Zhu *et al.*, 2015). While p53 and CDKIs are valuable markers for senescent cell detection, it is essential to remember that p53 and CDKIs are expressed during the normal cell cycle and in cell states other than senescence, so when used as senescence markers, they must be analysed in combination with other features (see below).

1.5.2.2 Changes in morphology

Senescent cells often have a distinct morphology and a significant increase in overall size (at least *in vitro*). Adherent cells in culture appear flatter and larger in surface area, though spatial constraints within 3-dimensional tissues may prevent the development of this phenotype *in vivo* (Biran *et al.*, 2017). The failure of cell proliferation coupled with dysregulated mammalian target of rapamycin (mTOR) signalling leads to increased biomass and cell size through stimulation of translation (e.g., through activator phosphorylation S6 kinase and inhibitory phosphorylation of translation inhibitor 4EPB1) and inactivation of autophagy (via phosphorylation of ULK1) (Blagosklonny, 2012; Leontieva *et al.*, 2012; Leontieva and Blagosklonny, 2016). High mTOR activity insensitive to usual proliferation signals (e.g., serum stimulation) can indicate senescence when used together with several other markers. Additionally, the stabilisation of filamentous actin into prominent stress fibres with connections to the cellular substrate through focal adhesion kinases (FAKs) may be responsible (which involves mTOR signalling) for changes in cell morphology (Chen *et al.*, 2000; Dalle Pezze *et al.*, 2014; Moujaber *et al.*, 2019; Rabanal-Ruiz *et al.*, 2021). Indeed, reduction in mTORC2 signalling through pan-mTOR inhibitor AZD8055 leads to markedly fewer stress fibres and a significant decrease in the size of peri-senescent dermal fibroblasts (Walters, Deneka-Hannemann and Cox, 2016).

Interestingly, recent studies suggest that an increase in cell size can induce senescence-like changes in the proteome in non-senescent cells, making these cells more prone to senescence induction (Lanz *et al.*, 2022a). A hypothesis is that cells that have undergone

more replication cycles may be larger due to biosynthesis and the cell cycle only being loosely coupled, meaning where a cell may be held at points during the cell cycle, production of proteins may continue at the same rate, affecting proteostasis (Lengefeld *et al.*, 2021; Lanz *et al.*, 2022b). These studies suggest that aged cells may be more prone to stress-induced senescence due to an age-related increase in size and, therefore, an altered proteome. These changes are also reflected on the cell surface, with an increased presentation of some cell surface proteins, such as adhesion molecules (Mun and Boo, 2010).

1.5.2.3 Nuclear structure and chromatin reorganisation

Along with overall cell size and shape changes, senescent cells usually display an enlarged nucleus and prominent nucleoli (Zhao and Darzynkiewicz, 2013). Moreover, the nuclear membrane begins to lose its integrity, thought to be largely due to a reduction in nuclear membrane lamin protein, lamin B1. Therefore, the detection of reduced lamin B1 suggests that the cell may be in a senescent state, hence why it is a marker commonly used in conjunction with others to confirm senescence (Freund *et al.*, 2012). Additionally, chromatin within senescent cells appears generally decompacted, with senescence-associated distension of satellites (SADS) reported as an early marker of chromatic decompaction, providing another marker to strengthen senescence detection (Swanson *et al.*, 2013).

As persistent (un-repaired) DNA damage is a feature of senescent cells (Fumagalli et al., 2012; Galbiati, Beauséjour and d'Adda di Fagagna, 2017), DNA damage response markers such as γH2AX (phosphor-Ser-139 of histone H2A) and co-localisation with

53BP1 (especially at telomeres; TIRFS) are also used to delineate senescent cells (Collins *et al.*, 2020).

Changes in the chromatin landscape are also observed, with the condensing of chromatin and formation of heterochromatin foci known as senescence-associated heterochromatin foci (SAHF) (Narita *et al.*, 2003). This is accompanied by major shifts in global genomic CpG methylation patterns in cells that have entered senescence as a response to oncogene activation (Kowalski *et al.*, 2013). It is interesting that subsets of genomic CpG methylation patterns can be used to determine the biological age of cells and tissues and even predict all-cause mortality (GRIM-AGE algorithm) (Lu *et al.*, 2019). Such methylation changes can empirically measure biological ageing, acting as epigenetic clocks. However, it is unclear how far such biological clocks can be used to read out senescence – indeed, we have demonstrated that epigenetic ageing measured using the Skin&blood clock algorithm, which determines an estimated age from the methylation states of 391 CpG sites (Horvath *et al.*, 2018), is distinct from cellular senescence, as the clock 'ticks' in non-senescing hTERT immortalised human umbilical vein endothelial cells (HUVECs) (Kabacik *et al.*, 2022a). However, if specific patterns of CpG methylation states can be detected in senescent cells, this could be a novel method of detecting senescent cells.

1.5.2.4 Failure of Autophagy

Autophagy is a homeostatic system within cells that facilitates the degradation of intracellular components via autophagosome engulfment and transportation to lysosomes (Kourtis and Tavernarakis, 2009). Failure of macroautophagy (a subset of

autophagy pathways, hereafter autophagy) is thought to be responsible for the observed increase in granular accumulations in the cytosol (termed juxta-nuclear Q bodies, or JUNQ) (Miller *et al.*, 2015) that are common in senescent cells. Indeed, it is suggested that a failure of autophagy can drive senescence through the accumulation of damaged proteins (Fujii *et al.*, 2012). Furthermore, failure of autophagy is thought, at least in part, to be responsible for the increased mitochondrial biomass accompanied by elevated mitochondrial ROS, which is indicative of mitochondrial dysfunction (such dysfunctional mitochondria would normally be cleared by mitophagy) (Passos *et al.*, 2007; Walters, Deneka-Hannemann and Cox, 2016).

Autophagy is regulated by the nutrient-sensing mTORC1 pathway; increased mTOR activity leads to phosphorylation of the autophagy-initiating kinase ULK1, ATG13, and lysosomally located TFEB, which results in decreased autophagy, therefore, decreased removal of cellular waste such as misfolded proteins (Kim *et al.*, 2011). In fact, studies have demonstrated that in models of cigarette-induced senescence in human bronchial epithelial cells, the anti-senescence ability of SIRT6 (a histone 3 deacetylase involved in the regulation of genes such as those involved in the DDR and telomere maintenance) was diminished by knockdown of ATG5 and LC3B (components required for the formation of the autophagosome, required for autophagy), suggesting that IGF/insulin-Akt-mTOR signalling, at least in part, regulates senescence-associated autophagy dysfunction (Takasaka *et al.*, 2014).

1.5.2.5 Lysosomal activity

Lysosomes are membrane-bound organelles responsible for degrading and recycling large molecules (e.g., proteins) into smaller components which can then be reused by the cell (Bainton, 1981). The delivery of these molecules to the lysosome is carried out through autophagy, a process that can be disrupted by senescence (previously discussed in section 1.5.2.4). Lysosomes contain a number of enzymes, such as hydrolases, proteases, nucleases, glycosidases, peptidases, sulfatases, and lipases, which are active at an acidic pH, meaning lysosomes maintain a luminal pH of roughly 4.5 (Bainton, 1981; Appelqvist *et al.*, 2013).

One of the hallmarks of senescence is the presence of lysosomes that have altered characteristics. When a cell becomes senescent, the number of lysosomes and their mass increases, along with a relative upregulation of lysosomal proteins and deacidification of the lumen (Kurz *et al.*, 2000). One possible explanation for this phenomenon is that during senescence, mTOR activity increases, which in turn activates the transcription factor EB (TFEB). TFEB is responsible for initiating the transcription of genes that are necessary for the formation of lysosomes and autophagy. This process, in turn, leads to an increase in lysosomal biogenesis, which may contribute to the observed effects (Curnock *et al.*, 2023). Furthermore, decreases in V-type ATPase proton pump (V-ATPase) activity on the membrane of lysosomes is thought to be the main driving force behind the deacidification of the lumen (D. Shi *et al.*, 2020). It is hypothesised that the decreased availability of ATP due to mitochondrial dysfunction in senescence results in a reduction in V-ATPase activity. This has been demonstrated in

experiments conducted with senescent HUVECs receiving exogenous ATP, which restored lysosomal pH to original levels (Mai *et al.*, 2019). These characteristics, specifically, the pH of lysosomes within senescent cells, have been utilised with an assay that detects beta-galactosidase (β-gal) activity at pH 6 (compared to pH 4.5 within non-senescent cells), termed the senescence-associated β-galactosidase assay (SA-β-Gal). This has subsequently become one of the most frequently used markers for detecting senescent cells (Kurz *et al.*, 2000; Lee *et al.*, 2006). In addition to this, experiments investigating potential mechanisms behind the increase in SA-β-Gal activity, using primary human fibroblasts, demonstrated increased GLB1 expression (which encodes lysosomal β-galactosidase) during senescence, which may also provide another mechanism for increased β-galactosidase activity (Lee *et al.*, 2006). Quantitative assays for SA-β-Gal often use the chromogenic substrate, X-gal, which forms a blue precipitate when cleaved by β-gal that can be visually observed within cells (Dimri *et al.*, 1995; Debacq-Chainiaux *et al.*, 2009; Storer *et al.*, 2013). A modification of this technique uses substrates that become hydrolysed to form fluorescent products, such as fluorescein di-ß-D-galactopryanoside (FDG) (Hofmann and Sernetz, 1983; Yang and Hu, 2004).

While SA-β-Gal activity is a useful tool for indicating if cells may be senescent, caution needs to be taken depending on the cell line being investigated. Indeed, some non-senescent cells, such as activated macrophage bone osteoclasts, give false positive readouts because of their high lysosomal activity and other cell types can appear positive for SA-β-Gal when confluent (Dimri *et al.*, 1995; Gary and Kindell, 2005). Interestingly, experiments utilising primary human fibroblasts from donors who had autosomal recessive G_{M1}-gangliosidosis (therefore, defective lysosomal β-

galactosidase), in conjunction with knockdown of GLB1 (using small hairpin interfering RNA) within otherwise normal cells, demonstrated that induction of senescence was still possible without SA-β-Gal activity (Lee *et al.*, 2006). Hence, additional indicators should always be used.

1.5.2.6 Endoplasmic reticulum stress in senescence

The endoplasmic reticulum (ER) is an organelle responsible for managing protein folding, posttranslational modifications, and inducing disulphide bonds (Braakman and Bulleid, 2011). The ER also helps regulate calcium levels, produces lipids, and contributes to apoptosis (Pinton *et al.*, 2008). Concerning senescence, the ER processes the majority of proteins that are intended for secretion, many of which form the components of the SASP (Pluquet, Pourtier and Abbadie, 2015).

ER stress can be caused by intrinsic and extrinsic sources, such as oxidative stress, viral infection, nutrient deprivation, and accumulation of misfolded proteins (Schröder and Kaufman, 2005; Coleman and Haller, 2019). As a response to this, the ER-associated protein degradation (ERAD) pathway can become activated. The ERAD pathway exports the unfolded proteins from the ER to the cytoplasm, which can then be degraded by the ubiquitin-proteome system (Hwang and Qi, 2018). Another response is the activation of the unfolded protein response (UPR) pathway, which involves the activation of transcription factors (e.g., ATF4) which regulate genes required for protein chaperones (which play important roles including the folding of proteins and sensing of misfolded proteins, e.g., BiP/GRP78) along with components of the ERAD pathway. This is

accompanied by attenuation of protein synthesis to prevent the increasing accumulation of proteins (Graner, Lillehei and Katsanis, 2015).

There is evidence that ER stress can be both an inducer of senescence and activated during senescence, although with the inducers of ER stress and senescence being similar, untangling the synergy between them is challenging (Carroll *et al.*, 2017; Zhan *et al.*, 2022). Indeed, an early study demonstrated that HRAS oncogene-induced senescence resulted in enlarged and vacuolised ER, independent of p53 and p16 pathways, suggesting ER stress may be an initial driver of senescence (Denoyelle *et al.*, 2006). Supporting this, a study using HCAEC demonstrated that prevention of high glucose-mediated maladaptive UPR (using activated protein C), prevented upregulation of senescence markers (p21 and p16), suggesting that diabetes-induced senescence may be driven by the induction of ER stress and subsequent UPR activation (Fatima *et al.*, 2022). Ultimately, the UPR pathway can lead to the induction of cell death or senescence (Pluquet, Pourtier and Abbadie, 2015). One hypothesis for ER stress during senescence is the increased demand for protein synthesis to accommodate the SASP (Druelle *et al.*, 2016). While this is likely true for senescence induction through means such as OIS, it is likely that other methods of induction, such as ROS, may induce ER stress and senescence concurrently.

1.5.2.7 Senescence-associated secretory phenotype

As the name suggests, the senescence-associated secretory phenotype (SASP) is a complex mixture of cytokines, chemokines, and matrix metalloproteinases (MMPs) that senescence cells secret. The detection of secretory molecules found in the SASP is often

used as a contributory indicator of senescence (Coppé *et al.*, 2008; Basisty *et al.*, 2020). Of the huge range and number of SASP factors, IL-6 is secreted by almost all senescent cell types under almost all conditions of senescence induction and is therefore thought to represent a canonical SASP factor – indeed, it has been used in drug screens for discovery of anti-senescence therapeutics (Birch and Gil, 2020; Moaddel *et al.*, 2022) and SASP suppressors (Freund *et al.*, 2012; Rolt, Nair and Cox, 2019; Wyld *et al.*, 2020).

The SASP is potentially one of the most detrimental consequences of cellular senescence. The specific factors and their relative abundance vary by original cell type and senescence inducer (Rodier *et al.*, 2009; Özcan *et al.*, 2016). Proteomics analysis of the secretome of cells induced to undergo senescence through oncogene activation indicates thousands of factors in the SASP; a comparison of different SASP inducers for fibroblasts and epithelial cell types with the SASP atlas indicates increased secretion of 332-704 soluble proteins and decreased production of 8-37 proteins by epithelial cells undergoing senescence, depending upon the method of senescence induction (Basisty *et al.*, 2020). Within the SASP are multiple pro-inflammatory cytokines (e.g., IL-1, IL-6), chemokines (e.g., MCP-1), proteases (e.g., MMPs), and growth factors (e.g., VEGF, TGFβ). This hints towards the complexity of senescence and its effect on the neighbouring environment.

One potential mechanism implicated in the induction of the SASP is the presence of nuclear chromatin fragments within the cytosol of senescent cells, referred to as cytoplasmic chromatin fragments (CCFs). CCFs are thought to be caused by the nucleus to cytoplasmic 'blebbing' of chromatin, confirmed by the presence of H3K9me3 and

H3K27me3 heterochromatin markers within the CCFs. Furthermore, these fragments are usually positive for the DNA damage marker, γH2AX (Adams *et al.*, 2013). The blebbing process has been linked to the degradation of nuclear laminins, which reduces the integrity of the nuclear envelope (Adams *et al.*, 2013; Dou *et al.*, 2015). The mechanism by which CCFs activate a SASP-like phenotype is through their detection by cyclic GMP-AMP synthase (cGAS), resulting in the activation of stimulator of interferon genes (STING) via a second messenger and subsequent production of inflammatory cytokines (Glück *et al.*, 2017). This provides an exciting avenue for potential anti-SASP therapeutics (Dou *et al.*, 2017). The complete mechanism behind the SASP is unknown, and the cGAS-STING pathway is likely to be one of many contributors.

The formation of CCFs has also been linked to mitochondrial dysfunction, specifically to the downregulation of mitochondrial oxidative phosphorylation genes. This leads to an increase in mitochondrial ROS production, activating the c-Jun N-terminal kinase (JNK) pathway and increasing p53 expression (Liebert *et al.*, 2006). This has been further connected to 53BP1, which is not detected with CCFs but is usually associated with γH2AX. 53BP1 inhibits DSB resection, with experiments demonstrating an increased CCF presence in cells with 53BP1 knocked down (Vizioli *et al.*, 2020). These experiments demonstrated a reduction of most SASP markers down to levels seen in proliferative cells, with markers of cell cycle arrest still present. The variability in activation of SASP expression makes it challenging to study the root cause, hinting towards the complexity of the senescence phenotype.

1.5.3 Types of Senescence

The initial inducer of senescence directly impacts senescence-associated phenotypes and, subsequently, the effect of that senescent cell on its local environment (Dierick *et al.*, 2002). There are both intrinsic and extrinsic drivers of senescence. Whether it is programmed is still a matter of considerable debate and dissent, though developmental senescence appears to follow a temporal programme (Storer *et al.*, 2013; Cox and Redman, 2017), stochastic senescence occurring in response to local or systemic changes in the cell's environment may not be programmed. Different inducers lead to related but different types of cell senescence, as outlined below. While these are discussed separately, many have overlapping mechanisms and are jointly involved.

1.5.3.1 Replicative senescence

The onset of replicative senescence (RS) is observed after multiple cell divisions. It is driven predominantly by telomere attrition, which results in the activation of the DNA damage response (DDR) pathway (discussed in section 1.3) at a point known as the Hayflick limit (Hayflick, 1965; Nassrally *et al.*, 2019). Telomeres comprise tandem DNA repeats, usually 5'-TTAGGG-3' in mammals (Barnes *et al.*, 2022), at the end of eukaryotic chromosomes and are important for chromosome stability (Bailey and Murnane, 2006). Single-stranded 3' overhangs at chromosome ends are folded into a displacement D loop that then further forms a larger T (telomere) loop bound to the shelterin complex of proteins, which prevents the telomeric ends from being recognised as DSBs by DDR pathways (Griffith *et al.*, 1999; Nikitina and Woodcock, 2004). Unlike in stem cells and germ cells, which maintain their telomeres through the action of telomerase (a self-

templated reverse transcriptase) (Lupatov and Yarygin, 2022), somatic cells have little or no telomerase activity and so telomeres shorten (known as telomere attrition) during every round of DNA replication because of the end replication problem (Chan and Blackburn, 2002; Collins and Mitchell, 2002) – both the inability to prime DNA synthesis on the lagging strand near the end of linear chromosomes (Levy *et al.*, 1992) and a consequence of resection of the leading strand to form the telomeric overhang (Wu, Takai and de Lange, 2012). Once the telomere has reached a critically short length, the protective loops and shelterin protein complex can no longer form, leading to exposure of telomeric 3' ends. This is detected as a DNA DSB resulting in the recruitment of ATM and subsequent phosphorylation of CHK2, a protein kinase that phosphorylates p53 (Harris and Levine, 2005).

The DDR activated by the exposed telomeric ends increases the expression of p21 and $p16^{INK4a}$/RB, causing cell cycle arrest and induction of senescence or apoptosis (Jacobs and de Lange, 2004). Early evidence of the link between telomere attrition and replicative senescence comes from experiments that demonstrated an increase in the replicative lifespan of cells *in vitro* after transfection with constructs encoding telomerase, compared to control cells (Bodnar *et al.*, 1998), suggesting that at least *in vitro*, telomere attrition is the driver of replicative senescence. However, the role of telomere attrition in replicative senescence is cell-type dependent – for example, cardiomyocytes enter replicative senescence even with only limited telomere attrition (Ball and Levine, 2005); notably, rodent cells have far longer telomeres than human cells (humans ~5 – 15 Kb, mice ~50 Kb), with suggestions that a faster rate of telomere attrition is related to a shorter lifespan (OKUDA, 2002; Whittemore *et al.*, 2019). More

recent evidence using antibody staining against DNA lesions suggests that it is not only telomere length but also telomere integrity that is important in the cell fate decision to enter senescence, accumulation of 8-oxo-G within the G-rich telomere may provide an early warning of genomic damage, hence telomeres have been termed 'the canary in the coal mine' for cell senescence onset (Barnes *et al.*, 2022). Transfection with telomerase (h-tert) is now commonly conducted in cell culture to generate immortalised cell lines and avoid entry into replicative senescence (Condon *et al.*, 2002; Smith, Coller and Roberts, 2003; Geserick *et al.*, 2006; Mazzucchelli *et al.*, 2008). However, such Tert-immortalised cells can still undergo senescence, suggesting additional factors can lead to senescence. Whether this is a form of RS or induced by accumulation of other senescence inducers has yet to be fully determined.

1.5.3.2 Mitochondrial dysfunction-associated senescence

Mitochondrial dysfunction, characterised by a reduced respiratory capacity per mitochondria leading to a decreased mitochondrial membrane potential, precipitates a cascade of events culminating in the accumulation of reactive oxygen species (ROS), altered NAD+/NADH ratios, and the activation key cellular pathways involving AMPK and p53. This convergence results in cell cycle arrest and the onset of senescence, a phenomenon termed mitochondrial dysfunction-associated senescence (MiDAS) (Wiley et al., 2016). The relationship between mitochondrial dysfunction and senescence resembles a reciprocal interdependence, akin to the proverbial "chicken or egg" scenario. Both mitochondrial dysfunction's ability to induce senescence and

senescence's propensity to exacerbate mitochondrial dysfunction form a cycle of mutual reinforcement. As ageing progresses, both mitochondrial dysfunction and senescent cell burden accumulate, contributing to tissue ageing and the emergence of age-related diseases (Herbst *et al.*, 2007; H. Lee *et al.*, 2010).

There are many ways in which mitochondrial dysfunction can be induced, including reduced intracellular NAD^+/NADH ratio, mitochondrial Ca^{2+} overload, mitochondrial DNA (mtDNA) mutations, the ratio of mitochondrial biogenesis and mitophagy, and mTOR nutrient signalling (modified by SIRT3 and SIRT5) (Miwa *et al.*, 2022). In chronological ageing, there is a reduction in the NAD^+/NADH ratio, which correlates with increased CD38 activity (an NADase). This results in increased metabolism of NAD^+, reducing its availability for use with mitochondrial enzymes, such as SIRT3. This is hypothesised to be one of the driving forces being increasing mitochondrial dysfunction with age (Camacho-Pereira *et al.*, 2016). As many other cellular processes use NAD^+, its reduced availability will affect other pathways involved in senescence induction, therefore, reduced NAD^+-induced MiDAS may be one of many inducers of age-related senescence.

Ca^{2+} overload-induced mitochondrial dysfunction is thought to occur due to the role of mitochondria in maintaining cytosolic Ca^{2+} homeostasis. This is achieved via protein channels located in their inner and outer membranes (e.g., voltage-dependent anion channel 1 on the outer membrane and mitochondrial Ca^{2+} uniporter on the inner membrane); therefore, if there is an increase in cytosolic Ca^{2+}, high levels can

accumulate within the mitochondria, leading to mitochondrial dysfunction (e.g., through Ca^{2+}-enhanced cytochrome C dissociation) (Bravo-Sagua *et al.*, 2017).

In addition, the accumulation of mtDNA mutations or reduced capacity of repair mechanisms can lower the expression of the components required for the electron transport chain. This damage can occur through stressors, such as increased NO leading to guanine deamination (Grishko *et al.*, 1999) and errors in mtDNA replication (Pinto and Moraes, 2015). The impact of mtDNA damage has been demonstrated in mice expressing a proofreading-deficient version of the mitochondrial DNA polymerase γ (POLG), which results in the accumulation of mtDNA mutations, which have been shown to cause a premature ageing phenotype (Kujoth *et al.*, 2005). Later studies then demonstrated that these mice also have an increased accumulation of senescent cells within their inguinal adipose tissue, linking mtDNA damage with the induction of senescence (Wiley *et al.*, 2016). Interestingly, these senescent phenotypes had a differing SASP profile compared to most other inducers, with no induction of IL-1α, IL-1β, IL-6, and IL-8.

The ratio of mitochondrial biogenesis and mitophagy can affect the overall functionality of the mitochondrial network, and subsequent pathways involving the mitochondria. Studies in S-nitrosoglutathione reductase (GSNOR) deficient mice have shown that excessive S-nitrosylation of parkin (which, with PINK1, is involved in the mitophagy pathway) results in decreased mitochondrial fission, which is usually a prerequisite for mitophagy, leading to reduced clearance of dysfunctional mitochondria. This can result in the cell entering into apoptosis or senescence (Rizza *et al.*, 2018).

mTOR nutrient signalling controls many homeostatic pathways within the cell. Nutrient sensing involves the insulin/IGF-1 and mTOR signalling pathways, with high levels of cellular nutrients leading to inhibition of anabolic processes and autophagy. AMPK and sirtuins are activated in nutrient-deprived conditions, increasing mitochondrial biogenesis and autophagy. When this signalling becomes dysregulated, it can lead to unwarranted expression of mTORC1, resulting in reduced mitophagy and increased accumulation of damaged mitochondria (Bartolomé *et al.*, 2017). This is often evident in the morphology of mitochondria in senescent cells. Indeed, both *in vitro* and *in vivo*, the mitochondria of senescent cells often display an increase in size and mass (H. Lee *et al.*, 2010).

In addition to directly causing DNA damage, ROS may trigger retrograde mitochondrial-nuclear signalling through a TGF-beta pathway, reinforcing senescence induction and maintenance, along with activation of the DDR pathway (Lin *et al.*, 1998; Passos *et al.*, 2007; Wiley *et al.*, 2016). Interestingly, studies pharmacologically removing mitochondria from senescent cells *in vitro* attenuated their proinflammatory phenotype, although the cells remained non-proliferative (Correia-Melo *et al.*, 2016). Intriguingly, while mitochondrial dysfunction in proliferative cells may lead to apoptosis, senescent cells appear to be resistant to apoptosis, which appears to be mediated, at least in part, by mitochondrial anti-apoptotic protein, Bcl-2 (Yosef *et al.*, 2016). This has proved a pharmacological target for inducing apoptosis within senescent cells (see section 1.5.4).

As elucidated by the multifaceted mechanisms, the intricate relationship between mitochondrial dysfunction and senescence underscores their pivotal roles in cellular ageing and age-related pathologies. Understanding the reciprocal interactions between these phenomena holds significant promise for advancing therapeutic strategies and furthering insights into age-related diseases.

1.5.3.3 DNA damage-induced senescence

DNA damage-induced senescence (DDIS) can occur when SSBs or DSBs are induced through exposure to ionising radiation (Adams *et al.*, 2006; Geisel *et al.*, 2012; Borrego-Soto, Ortiz-López and Rojas-Martínez, 2015), UV radiation (Malkova *et al.*, 2021), chemotherapeutic drugs (Hsu, Altschuler and Wu, 2019), ROS (Zingoni *et al.*, 2015), and other genotoxic agents (von Koschembahr *et al.*, 2020). After detection, the cell initiates a series of DNA repair pathways, such as NHEJ and HR, and modulates cell cycle progression to prevent the propagation of aberrant DNA. This process is predominantly mediated by the PIKKs ATM and ATR (discussed in section 1.3 DNA damage response). If prolonged DNA damage signalling occurs due to defective repair machinery or a large amount of damage, the cell will enter into apoptosis or senescence (Hernandez-Segura, Nehme and Demaria, 2018). This is mediated by p53-trans-activated p21 expression, together with p16 elevation, which can lead to the onset and maintenance of the senescent state. Furthermore, the DDR causes the degradation of G9a/GLP methyltransferase, leading to a global reduction in H3K9 demethylation, including at

the promoters for IL-6 and IL-8. This increases the expression of these cytokines, which are common in the SASP (Takahashi *et al.*, 2012).

Interestingly, a study of ionising radiation-induced senescence in human aortic endothelial cells demonstrated that increasing DNA damage repair by homologous recombination (HR) using metformin (which promotes BARD-1 mediated repair) suppresses the induction of senescence (Park *et al.*, 2022). This study showed that metformin-treated cells had a quicker reduction in44hermos44o-ATM foci than control cells. This suggests that the quality of DNA repair and the activated DDR pathways dictate whether a cell enters into senescence after acquiring DNA damage.

1.5.3.4 Oncogene-induced senescence (OIS)

OIS is a senescence state driven by oncogenes (e.g., RAS, BRAF), which is usually preceded by hyperproliferation, which would otherwise result in tumorigenesis (Braig and Schmitt, 2006). The initial observation of OIS was the expression of oncogenic RAS within human fibroblasts (Serrano *et al.*, 1997). Subsequent studies have demonstrated a link between OIS and mitochondrial dysfunction, with oncogenic RAS inducing an increase in mitochondrial mass and superoxide production before the initiation of senescence, indicating how linked many of the senescence induction pathways may be (Moiseeva *et al.*, 2009).

The importance of OIS has been highlighted in studies investigating melanomas, where mutant BRAF-expressing ($BRAF^{V600E}$) cells within nevi (moles) displayed markers of senescence (e.g., SA-β-Gal, SAHF) and remained in growth-arrested states (Michaloglou *et al.*, 2005). Furthermore, loss of IGFB7 (an integral part of the senescence or apoptosis

induction pathways) within nevi appears to be an important step in melanoma progression (Wajapeyee *et al.*, 2008). More recently, a study revealed lower expression levels of MZF1 (a regulator of $p16^{INK4A}$ and OIS) in tumorigenic K-ras mutated cells associated with pancreatic cancer (Wu *et al.*, 2021). These studies reveal the important role OIS plays in preventing tumorigenesis.

1.5.3.5 Senescence in response to pathogens

Viral-induced senescence (VIS) has been detected in response to lentivirus, adeno-associated viruses, vesicular stomatitis, and alphacoronavirus NL63 in human lung carcinoma cells and non-malignant epithelial cells (Lee *et al.*, 2021). Many of the senescence-associated phenotypes (pro-inflammatory cytokines within the cytokine storm, neutrophil extracellular traps, matrix metalloproteinases) were observed in patients with SARS-COV-2, with other markers such as upregulation of p16 and p21 detected in pharyngeal and lung tissue from patients who died with PCR positive COVID-19 (Lee *et al.*, 2021). This was further evidenced with single-cell RNA-seq, which demonstrated the same upregulation of senescence markers such as p16 and components of SASP. Furthermore, this study also detected senescent-like changes in macrophages, suggesting that paracrine senescence may play a role in COVID-19 progression (Chua *et al.*, 2020). Building upon these findings, researchers investigated the treatment of SARS-COV-2 with senolytics (Navitoclax, D+Q) in 2 different hamster models and one severe mouse model (Syrian golden hamster, Roborovski dwarf hamster, and K18-hACE2 GM mice). They demonstrated decreased severity of SARS-COV-2-related inflammatory cytokines, and decreased mortality (either due to weight

loss prevention, which prevented animals from falling below ethical standards, or reduced symptom severity) with D+Q or fisetin treatment resulting in 100% 6-day survival compared to 60% in the solvent control group (Lee *et al.*, 2021). Furthermore, it was demonstrated in the murine model that infection with the influenza virus leads to the development of senescent cells within the lung (Schulz *et al.*, 2023). These results suggest that pathogen-induced senescence may contribute to prolonged symptoms after clearing the virus.

1.5.3.6 Paracrine senescence (bystander senescence)

Senescence can be induced locally or systemically by exposure to the SASP or certain SASP factors. For instance, high levels of IL-6 have been shown to induce senescence in normal human fibroblasts through STAT3 signalling (Kojima *et al.*, 2012, 2013). Furthermore, studies using a 4-hydroxytamoxifen-induced OIS line of IMR90 fibroblast (IMR90-ER:RAS or IMR90-MEK:ER) demonstrated that when co-cultured with normal IMR90 cells, the induction of senescence within the OIS inducible IMR90 cells led to a halt in the proliferation of the normal IMR90 cells along with upregulation of markers of senescence (e.g., CDKIs, SA-β-Gal), suggesting that either through the SASP or through direct cell-cell signalling, the senescent cells were instructing their neighbours to enter into senescence (Acosta *et al.*, 2013). This was also observed when co-culturing with human mammary epithelial cells (HMECs), demonstrating that this effect is also present between cell types. To identify whether it was the SASP-inducing paracrine senescent phenotypes, the authors performed the study again within transwell plates, ensuring no contact between the senescent and non-senescent cells. This led to the

same induction of senescence, supporting the theory that paracrine senescence is mediated, at least in part, by the SASP.

This was also supported *in vivo*, with evidence of senescence cell clustering within the liver of 9-month-old mice, suggesting that when a cell becomes senescent, it may induce paracrine senescence (Nelson *et al.*, 2012). This becomes relevant when considering conditions that promote a highly inflammatory environment, such as certain viral infections. Indeed, it has been hypothesised that paracrine senescence may play a role in long-term symptoms after recovery from SARS-COV-2. Experiments have shown that the supernatant from SARS-COV-2-infected human lung diploid fibroblasts (HDFs) can induce senescence in EGFP-HDFs, which are unable to be infected with SARS-COV-2, suggesting that the secreted factors from infected cells are capable of inducing paracrine senescence (Tsuji *et al.*, 2022). This could lead to prolonged inflammatory signalling from the senescent cells after there is no detectable SARS-COV-2 infection, which could account for many of the long-term symptoms associated with infection.

1.5.3.7 Stress-induced premature senescence

Stress-induced premature senescence (SIPS) can be viewed as an umbrella term encompassing many other senescence induction methods, including DNA damage-induced senescence, oncogene-induced senescence, and mitochondrial-dysfunction-induced senescence (Dierick *et al.*, 2002; Liu *et al.*, 2015; Xie *et al.*, 2023). However, SIPS incorporates other initial effectors, such as high ROS (Xiang *et al.*, 2022), an imbalance of ribosomal factors (Turi *et al.*, 2019), disruption in proteostasis (including activation of the UPR pathway) (Hu *et al.*, 2022; Sung *et al.*, 2022), and general cellular stress

mediated by the integrated stress response (ISR) (Derisbourg, Hartman and Denzel, 2021).

High levels of ROS can induce senescence through many of the mechanisms discussed previously. ROS can cause DNA single-strand breaks, sugar moiety modifications, and deaminated and adducted bases. When these lesions occur within proximity (roughly within ten bases), forming oxidative clustered DNA lesions (OCDLs), it can lead to the formation of DSBs, subsequently with the activation of the DDR pathway, which can ultimately lead to the induction of senescence (Sharma *et al.*, 2016). High levels of ROS can also lead to the misfolding of proteins within the ER and disruption in proteostasis, which can result in the activation of the UPR (discussed previously in section 1.5.2.6), and lead to the induction of senescence.

Endogenous and exogenous stress on the cell can lead to disruption in the rate of ribosome biogenesis, which can lead to exit from the cell cycle, apoptosis, or induction of senescence. Like with many pathways associated with senescence, decoupling whether other standard induction methods, such as via p53 pathways, lead to altered ribosome biogenesis or if this is an independent step that occurs to induce senescence is challenging. Indeed, p53 activation of pRB leads to suppression of rRNA transcription (Cavanaugh *et al.*, 1995; Scott *et al.*, 2001; Turi *et al.*, 2019).

The ISR leads to phosphorylation of eIF2α which results in the suppression of protein synthesis along with preferential translation of mRNAs of the transcription factor, ATF4, which is involved in many signalling pathways, including autophagy and cell cycle regulation (Derisbourg, Hartman and Denzel, 2021). Indeed, it has been demonstrated

that AFT4 can induce senescence in renal tubular epithelial cells during ER stress (Liu *et al.*, 2015), via p16 and in mouse models, a muscle-specific knockout of AFT4 leads to protection against age-related decline in strength, muscle quality, exercise capacity, and muscle mass (Miller *et al.*, 2023).

1.5.4 Therapeutic targeting of senescent cells

There are multiple ways in which senescent cells can be targeted pharmacologically. Senolytics, such as ABT-263 (navitoclax), induce apoptosis somewhat selectively within senescent cells, and senomorphics, such as rapamycin, that prevent the cell from entering into senescence or inhibit phenotypes associated with them, such as the SASP (Zhu *et al.*, 2016; Walters and Cox, 2018). This section explores some of the various methods used to target cellular senescence.

Many senolytics drugs are being investigated, often targeting the pro-survival pathways active within senescent cells, such as the BCL-2 pathway. An example is ABT-263, which inhibits BCL-2, BCL-al, and BCL-w and enables BAX/BAK-mediated cytochrome C release from mitochondria. This induces the caspase-associated apoptosis pathway (Zhu *et al.*, 2016). Importantly, ABT-263-induced apoptosis appears to be selective for senescent cells, with experiments in HUVECS demonstrating selective decreases in senescent cell viability compared to proliferating cells (Zhu *et al.*, 2015). However, the senolytic action of ABT-263 is cell-type dependent, with studies demonstrating efficacy in HUVECS, IMR90 human lung fibroblast, and murine embryonic fibroblasts, but not in preadipocytes (Zhu *et al.*, 2016). Furthermore, ABT-263, at least in human dermal fibroblast, can selectively eliminate senescent cells from multiple inducers, for example,

RS, UV-induced senescence, and H_2O_2-induced senescence (Kim *et al.*, 2022). The same authors also demonstrated a reduction in senescence markers within the skin of aged mice, demonstrating the efficacy of ABT-263 *in vivo*. Indeed, in a mouse model investigating senolytics as a treatment to prevent periprosthetic osteolysis due to the induction of senescence by ultra-high molecular weight polyethylene, ABT-263 eliminated the senescent cells, inhibited the inflammatory response, and inhibited the formation of osteoclasts, reducing osteolysis (Su *et al.*, 2023). This provides an exciting possible avenue to prevent prosthesis failure and hints at the wide range of conditions senolytics may be able to target.

Another senolytic approach has used a combination of dasatinib and quercetin (D+Q), which likely inhibit tyrosine kinases and PI3K (Zhu *et al.*, 2015). D+Q has shown promise in trials in patients with idiopathic pulmonary fibrosis, with those receiving the treatment having significantly improved 6-minute walk distance, 4-m gate speed, and chair stand times (physical impairment associated with the disease) (Justice *et al.*, 2019). Current clinical trials with D+Q include investigating reduction in the markers of bone turnover in women over the age of 70, improvement in insulin sensitivity and glucose tolerance in obesity, and Alzheimer's disease (currently, safety/ tolerability and blood-brain barrier permeability investigations) (Espinoza *et al.*, 2023).

Another promising drug, DRI-FOXO4, acts as an antagonist for the FOXO4 binding domain on p53, inhibiting the translocation of p53 to the nucleus and activating the apoptosis pathway, selectively removing senescent cells. An example of an avenue being investigated with DRI-FOXO4 is the treatment of chondrocytes derived from

human cartilage, which are cultured *in vitro* and then implanted into sites of articular cartilage injuries to prevent post-traumatic osteoarthritis, in an attempt to improve procedure outcomes. The motivating hypothesis behind this avenue of investigation is that the *in vitro* culturing of the chondrocytes leads to the induction of senescence, potentially reducing the efficacy of treatment. The study demonstrated a reduction in senescence markers, although further work is needed to confirm if this translates into better patient outcomes (Huang *et al.*, 2021). This work demonstrates the value senolytics may provide outside the direct pharmacological treatment of conditions.

Rapamycin, a drug primarily used as an immune suppressant post-organ transplantation (Fine and Kushwaha, 2016), has also been shown to prevent the development of cellular senescence (Iglesias-Bartolome *et al.*, 2012). Its mechanism of action is through binding to FKBP12, forming a complex which can bind with mTORC1 and cause partial inhibition of the active site and inhibit its activity. Senescent cells have increased mTOR activity, increased protein synthesis, and dysfunctional autophagy. Furthermore, it is hypothesised that mTOR signalling needs to be increased for a cell to become senescent rather than quiescent (Terzi, Izmirli and Gogebakan, 2016). Indeed, rapamycin has been shown to prevent these phenotypes from occurring (Stanfel *et al.*, 2009). Associations can be made between rapamycin treatment and dietary restriction, with both impacting nutrient-sensing pathways and increasing life span in model organisms such as mice.

Interestingly, experiments have shown that treatment with rapamycin for the first 45 days of life in mice increases the life span of males by 10%, although no increase was

observed in female mice. This corresponded with lower body weight throughout their lifespan and reduced organ weight compared to control mice (Shindyapina *et al.*, 2022). In comparison, in an earlier study where rapamycin was given at 9 months of age, both male and female mice had significant increases in lifespan, although at lower doses investigated only the female mice had the increase (Miller *et al.*, 2014).

Metformin, a drug commonly used to lower blood glucose in type 2 diabetes, is a more recent pharmacological approach to target senescence, particularly the SASP. The antisenescence properties of this substance come from two different pathways. The first pathway involves stimulating adenosine monophosphate (AMP) activated protein kinase (AMPK) by increasing the AMP-ATP ratio, thus, increasing the expression of the protein deacetylase, SIRT3 (Sung *et al.*, 2022). The second pathway involves regulating insulin-like growth factor, AKT, and p38 (Park *et al.*, 2022). In a recent controlled trial involving healthy adults aged 60 and above, who underwent a simulated five-day bed rest, mimicking extended periods of immobilisation common among the elderly, muscle biopsies unveiled that metformin exhibited a notable effect in diminishing markers associated with muscle atrophy. These effects encompassed decreased type 1 myofiber atrophy, lowered muscle collagen deposition, and a diminished expression of pro-inflammatory transcriptional profiles compared to the control group. Moreover, the use of metformin was linked to a reduction in markers of cellular senescence, such as decreased levels of p21 and p53 (Petrocelli *et al.*, 2023).

While these senolytics and senomorphics display some specificity towards senescence, it is important to note that this is usually through targeting more active pathways within

these cells. Therefore, off-target effects may occur in cell types with increased activation of these pathways. Furthermore, removing senescent cells from tissues with highly proliferative cells may not be an issue; however, within tissues such as the brain, which contain cells with little proliferative capacity, removal of senescent cells may not always be beneficial. In these situations, targeting the phenotype of the senescent cells may prove more fruitful, such as inhibiting the secretion of proinflammatory mediators found in the SASP.

1.5.5 Potential role of senescence cells in atherogenesis

In the context of atherosclerosis and CVD, many of the secreted factors found in the SASP could lead to changes within the local environment of arterial lumens, increasing activation of neighbouring endothelial cells along with increasing recruitment of immune cells (e.g., monocytes), all of which are atherogenic (Bloom *et al.*, 2023a; Shang, Liu and Tu, 2023). Together with the increase in pro-inflammatory stimuli, the secretion of matrix metalloproteinases has been shown to increase SMC migration and promote degradation of the fibrous cap preventing the plaque from rupturing into the arterial lumen (Vacek *et al.*, 2015). Furthermore, with the paracrine senescence induced by the SASP, neighbouring cells within the vasculature may also begin to present with a senescent phenotype, further exacerbating the development of atherosclerosis (Nelson *et al.*, 2012; Chou, Ho and Hung, 2022).

Studies using the Ldlr$^{-/-}$ mouse model indicated the presence of senescent cells within the atherosclerotic plaques, suggesting that senescence either results from the formation of these plaques or that senescence contributes to the initiation of the disease (Childs *et al.*, 2016a). Within this same study, the removal of senescent cells either pharmacologically (using ABT-263) or genetically (p16-3MR mice; A mouse model that expresses herpes simplex virus thymidine kinase under the control of the p16^{ink4a} promoter, which induces cell death in p16^{ink4a} positive cells upon administration of ganciclovir) both reduced the senescent cell burden within the vasculature and reduced plaque burden. A later study conducted by the same author demonstrated that the removal of senescent cells using ABT-263 prevented thinning of the fibrous cap, a process that can increase the likelihood of plaque rupture, which could result in myocardial infarction (Childs *et al.*, 2021). It is possible that senescence within the vasculature is both a driver and an initiator of the disease, with both the atherogenic environment being pro-senescent (e.g., increased ROS, increased cytokine expression) and senescence being pro-atherogenic (e.g., the SASP and changes in cell morphology).

1.5.6 Targeting vascular senescence

With the detection of senescent cells within the arterial regions of atherosclerotic plaques (Minamino *et al.*, 2002a), targeting of senescent cells within the vasculature may provide an approach to prevent plaque formation or maintain plaque stability. Both senescent eCs and VSMCs have been detected within regions of plaque development, both of which may promote the development of atherosclerosis and make the plaque more likely to rupture. Senescent eCs have been shown to have

decreased nitric oxide (NO) production, which may result in a decreased response to vasodilating stimuli, resulting in local increases in blood pressure. Along with this, senescent eCs have been shown to have decreased levels of complex I, III, and IV within their mitochondria, which leads to an increase in ROS (Ungvari *et al.*, 2008). This may promote atherogenesis through increasing oxidation of lipids in the subendothelial space and increased activation of neighbouring eCs. Furthermore, the expression of monocyte chemoattractant protein 1 (MCP-1) is raised in senescent eCs (Basisty *et al.*, 2020). This may result in increased recruitment of monocytes to these areas, increasing foam cell formation and contributing to plaque development.

Senescent VSMCs have been shown to have higher calcium deposition levels than non-senescent VSMCs, which ultimately leads to increased vascular calcification (Nakano-Kurimoto *et al.*, 2009). This reduces the vesse''s ability to respond appropriately to the pulse wave, increasing local blood pressure and thus causing increased damage to the endothelial cell layer. This may enhance the early stages of atherosclerotic plaque development through EC activation, which results in the pro-atherogenic phenotype discussed earlier.

In support of the hypothesis that senescence may play a role in atherogenesis, multiple studies using mouse models have demonstrated benefits in targeting removal of senescent cells. Interestingly, the foam cells within atherosclerotic plaques also display senescence markers (Childs *et al.*, 2016b); using the INK-ATTC transgenic mouse model with a pharmacologically inducible removal of $p16^{ink4a}$ expressing cells. Removal of p16 expressing (i.e. senescent) cells resulted in a reduction in plaque burden both in the

early stages of plaque development and in already established plaques. While the focus of this study was on intimal foam cells, the transgenic model and treatment used would be expected to result in the removal of all cells positive for $p16^{ink4a}$ expression, so it would also result in the removal of senescent eCs and VSMCs. Regardless of the cell type removed, this study indicates that $p16^{ink4a}$-positive cells (likely senescent cells) play a vital role in the formation and maintenance of atherosclerosis within mice.

Furthermore, Roos *et al.* demonstrated improved vascular performance in mice treated with the senolytic combination of dasatinib and quercetin (D+Q) to a similar extent to a genetic approach (Roos *et al.*, 2016). In particular, these authors demonstrated that targeting senescent cells within older mice restored vasomotor function and reduced calcification, all of which are likely to reduce EC stress and decrease the formation of atherosclerotic plaques. While such studies show promise for the treatment and prevention of atherosclerosis, it is important to reiterate that these treatments target biochemical pathways involved in senescence that may also be active in other cells. This means that off-target effects may occur, which may either modulate the formation and maintenance of atherosclerosis through indirect means, or present complications yet to be discovered.

1.6 Aims of the thesis

With the current epidemiological and experimental evidence, this thesis aims to use both *in vitro* and *in vivo* methods to establish a link between age at the time of exposure to IR and the severity of atherosclerotic phenotype development. Firstly, with the

epidemiological evidence suggesting those exposed at a younger age have a higher CVD mortality rate, I will further investigate this using mouse models of CVD. Within this, I will also establish the use of $Ldlr^{-/-}$ mice for investigations into IR-CVD. Secondly, I will begin to investigate potential mechanisms that facilitate the development of IR-CVD and the influence of age at the time of exposure. For this, I will use Human coronary artery endothelial cells from donors of varying ages. Within this, I will investigate phenotypes that promote atherogenesis, and then interrogate molecular drivers through multi-omic approaches.

2 Materials and methods

2.1 Mouse studies

2.1.1 Mouse husbandry

For the LDL receptor knockout mouse ($Ldlr^{-/-}$) pilot study for IR-induced CVD (section 2.1.2), 12 male and 12 female mice were purchased from the Jackson Laboratory (Jax stock #002207). For both mouse models ($Ldlr^{-/-}$ and ApoE knockout mice ($ApoE^{-/-}$)) used in the main experiments, mice were purchased, and breeding colonies established. For the $Ldlr^{-/-}$ mouse study, 4 male and 4 female mice were purchased from the Jackson Laboratory. For the $ApoE^{-/-}$ breeding colony, 6 male and 6 female mice were purchased from Jackson Laboratory (Jax stock #002052). Breeding colonies were established by housing 1 male and 1 female together. Once pups were born, males were removed. After weaning, the pups were removed and housed by sex. All mice were maintained on a standard chow diet, with access to food and water *ad libitum* and housed in a temperature-controlled environment with a 12hr light/dark cycle.

2.1.2 LDL receptor knockout mouse X-ray dose pilot study

For the $Ldlr^{-/-}$ pilot study, mice were whole-body irradiated at 6-weeks old with 0, 0.5, 2, or 4 Gy X-ray (X-ray described in section 2.3). 6 months later, mice were euthanised via intraperitoneal injection of sodium pentobarbital (Schedule 1 method) with exsanguination as confirmation. Blood was collected by cardiac puncture and placed

into ETDA coated tubes. Brain, cerebellum, and liver were harvested and placed in RNA later. The whole aorta (from aortic root to iliac bifurcation) was removed using microdissection techniques and placed into formalin solution ready for processing. Quantification of plaque coverage was carried out as described in section 2.1.4.

2.1.3 Investigation into the effect of age at the time of IR exposure and the development of CVD in Ldlr$^{-/-}$ mice

To determine if age at the time of exposure affects the development of IR-induced CVD, Ldlr$^{-/-}$ mice were exposed to 2 Gy X-ray at 6 weeks, 26, and 52 weeks of age. 6 months after each irradiation time-point, mice were euthanised by overdose of anaesthesia first by use of isoflurane followed by an overdose of sodium pentobarbitone by intraperitoneal injection. I changed the euthanasia protocol compared to the pilot study as first anaesthetising with isoflurane was deemed less stressful for the mice. Death was confirmed by exsanguination. The whole aorta (from aortic root to iliac bifurcation) was removed using microdissection techniques and placed into formalin solution ready for processing. Quantification of plaque coverage was performed using Oil red O (ORO) (section 2.1.4).

2.1.4 Oil red O plaque staining and quantification

Aortas were retrieved from formalin fixative and stripped of all advential fat under a dissection microscope using superfine Vanna's scissors (8 cm, 0.015x0.015 mm, straight, Wolf Laboratories #501778) and fine point watchmaker forceps (Fisher Scientific #E010/04). Under the dissection microscope, the aortas were opened along

the outer curvature of the arch, opening the brachiocephalic/innominate, left common carotid, and right common carotid arteries. The arch was then cut down the inner curvature, following down the rest of the aorta to the iliac bifurcation. Once opened, aortas were washed in 70 % isopropanol 3 times for 5 minutes. Aortas were then incubated for 50-60 minutes in freshly prepared oil red O working solution made of 3 parts ORO and 2 parts of milliQ water. After staining, aortas were washed twice in 60 % isopropanol for 5 minutes. The aortas were then pinned open using 0.1mm insect pins. Stained aortas were then imaged using a Samsung SM-G975F, with a mount I created with polystyrene (Figure 2.1). Images were pre-processed in PowerPoint and plaque percentage coverage was calculated by thresholding for the whole aorta, then thresholding the stained plaque, using Image J.

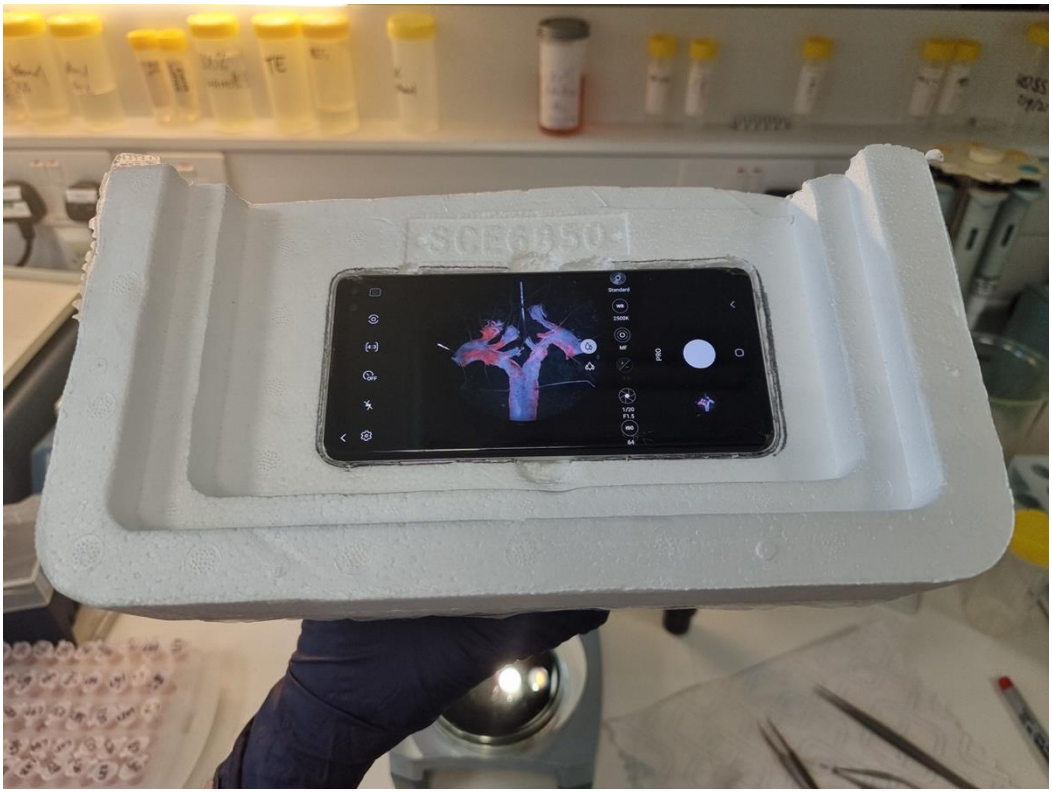


Figure 2.1 Mount for the camera to image the aortas.

To ensure consistent images of aortas, an insert was cut into polystyrene to fit a Samsung SM-G975F, with a rear hole cut to mount to the microscope eyepiece.

2.2 Cell culture

2.2.1 Cell maintenance

Human coronary artery endothelial cells (HCAECs) were obtained from Lonza, Cell Applications, and Promocell and immortalised via hTERT transfection when received. HCAECs were then either cultured or stored in a BOC Drystore refrigerator (separated

from liquid nitrogen, maintained at <-150°C) until use. For seeding of cells, 1 ml aliquots containing 5 x 10^5 cells were removed from storage, thawed rapidly in a water bath at 37°C, and then transferred to 9 ml Hanks' balanced salts without calcium, magnesium, and phenol red (HBSS, Capricorn Scientific, #HBSS-2A) in 15 ml centrifuge tubes and cells pelleted by centrifugation at 1200 RPM in a Thermo Fisher Megafuge 16 centrifuge for 5 minutes. The pellet was then resuspended by gentle trituration with 10-15 ml MesoEndo Cell Growth Medium (MEC. Cell Applications INC.) and transferred into filter-capped T75 flasks pre-coated with fibronectin. Unless otherwise stated, all cells were incubated at 37°C 5 % CO_2 in a humidified incubator. Cells were regularly checked using a Thermo Fisher Evos XL imaging system. During the week, media changes occurred every other day, with 170 μL per cm^2 MEC media applied. For weekend maintenance, 200 μL per cm^2 of MEC media was used. The age and sex of the HCAEC used for the experiments are listed in Table 2.1.

For passaging, HCAEC were detached by incubation with 2 mL Trypsin (1:100 dilution in HBSS) for 2-5 minutes, followed by gentle tapping of the flask. Following the addition of 2 mL soya bean trypsin inhibitor (1:100 dilution in HBSS), cells were removed and placed into a 15 mL centrifuge tube with 6 ml of HBSS. For cell counting using a C-Chip Haemocytometer (VWR, cat. 631-1098), a 10 μl aliquot was taken and determined using a Evos XL phase contrast imaging system (Thermo Fisher). Population doublings (PD) of cells were calculated using the formula:

$$\mathrm{PD} = \frac{\log(\text{No. cells harvested}/\text{No. cells seeded})}{\log(2)}$$

Cumulative population doublings (CPD) were calculated as a sum of all PDs. Cells were then seeded at 25,000 to 100,000 / cm^2 in the relevant vessels for the subsequent experiments (See experimental methods for details). Surplus cells were cryopreserved in freezing medium (10% DMSO in FBS) at $5x10^5$ cells per 1 mL in cryovials. After initial freezing at -80°C, vials were moved to the BOC Drystore refrigerator. Within each experiment performed using the HCAECs, the PD of each donor cell line was within 3 PDs.

The HL-60 monocyte cell line was a kind gift from Dr Kai Rothkam. Cells were cultured in suspension T75s using RPMI media with 10% FBS. Viability and cell number were assessed by mixing 20 μL aliquots with 20 μL of AccuStain solution T and another 20 μL with 20 μL of AccuStain solution N and incubating for 2 minutes. 20 μL of each was loaded into the matching sections on the AccuChip, with viability and number assessed on the ADAM-MC™ automated cell counter. The HL-60 cells were maintained between 0.1 and $1x10^6$ cells/mL.

2.2.2 Simulated flow conditions

25,000 cells/cm^2 were seeded on fibronectin coated coverslips in 4 well plates, with 500 μL MEC media. Once confluent, plates were placed on a PS-3D fixed-angle 3D rotator (Grant-Bio) and rotated at 30 RPM within the cell culture incubator, for 5 days. For control, cells from the same donor were seeded in the same conditions and were incubated in static conditions.

Table 2.1 Donor information for HCAEC cell lines used in this thesis.

Donor Code	Age	Sex
HCAEC0	19	M
HCAEC1	23	M
HCAEC2	26	M
HCAEC3	54	M
HCAEC4	17	F
HCAEC5	27	M
HCAEC6	51	F
HCAEC7	51	M
HCAEC8	48	M
HCAEC9	33	F
HCAEC10	54	M
HCAEC11	55	F

2.3 X-ray exposures

All X-ray exposures were carried out at room temperature (RT) using an A.G.O HS X-ray system (Aldermaston, Reading, UK; output 13 mA, 250 kV peak, 0.5 Gy/min). For *in vitro* experiments, the media was changed immediately after irradiation. For all sham (0 Gy) exposures, both mice and cells were exposed to the same environment, without X-ray irradiation.

2.4 In vitro assays

2.4.1 Adhesion assay

HCAEC were seeded into T-75 flasks and cultured until confluent as previously described (section 2.2). In parallel, HL-60 cells were cultured in non-adherent T-75 flasks with cell number and viability confirmed as previously mentioned (section 2.2). Within 24-well plates, 4 glass coverslips were coated with human fibronectin (1:100 in HBSS) for a minimum of 1 hour in a humidified incubator. HCAEC were then detached using trypsin and counted (as previously described), with $5x10^4$ cells then being seeded onto each coverslip and cultured under standard conditions. In experiments involving X-ray exposure, this was performed in duplicate, with one plate for irradiation, and the other for sham control. Cell confluency was monitored using an Evos XL phase contrast imaging system (Thermo Fisher). Once a confluent monolayer of HCAEC was formed (3-5 days depending on the donor), the plates were irradiated with either 0 Gy or 10 Gy. Plates were then maintained under normal cell culture conditions.

One week after irradiation, $2x10^7$ HL-60 cells were labelled with cell tracker green (CTG) by incubation in RPMI (with 10% FBS) containing 1:1000 dilution of CTG for 1 hour. Fluorescence was confirmed by microscopy using Evos XL fluorescence microscope (Fisher Scientific). HL-60 cells were then pelleted and resuspended in MEC growth media to a concentration of $2x10^6$ per 1 mL. Triplicate coverslips of HCAECs post irradiation (or control) were then incubated with $1x10^6$ CTG-labelled HL-60 cells for 4 hours at 37°C with 5% CO_2 in a humidified incubator. Coverslips were then carefully

washed 3 times by dipping into HBSS 5 times, blotting off excess HBSS. Adherent cells were then released by treatment with 250 μL trypsin and incubation at 37^{o}C for 5-10 mins, with trituration to ensure cell resuspension. The fourth coverslip, which was not incubated with HL-60 cells, was used for quantification of HCAEC cell number using a haemocytometer, as previously described (section 2.2). 200 μL of the trypsinised HCAEC/CTG-HL60 mixture was transferred to a 96-well black-walled plate. CTG-labelled HL60 cells were quantified against a standard curve, created by serial dilution of stained, HL60 cells not incubated with HCAECs (50,000, 25,000, 12,500, 6,250, 3,125, 0 cells). Fluorescence was then measured using a plate-based spectrophotometer (BioTek Synergy HT). The fluorescent signal from the CTG-HL-60 cells was then converted to cell count using the standard curve, and a ratio of HL60:HCAEC determined.

2.4.2 Permeability assay

Monolayer permeability assays were conducted using 12-well plates with 0.4 μM pore size transwell inserts (Cornig #CC403). Inserts were coated with 100-fold dilution of Matrigel in cold MEC media and then incubated at 37^{o}C for 1 hour. 5x10^{5} HCAECs from each donor were seeded in triplicate into the coated trasnwells, and 500 µL of MEC growth media placed in the well below. Once a confluent monolayer was formed, plates were irradiated 0 or 10 Gy X-ray. One week after irradiation, media was removed from both compartments and transwell inserts were placed into a fresh well with 500 µL of MEC growth media below. 500 µL of MEC growth media with 70 kDa FITC dextran (1 mg/mL) (Sigma, 4645-100MGF) was added into the insert and incubated with the HCAEC monolayer for 3 hours. Following incubation, the transwell inserts were

removed, and two aliquots of 100 μL from each bottom well was transferred into separate wells of a black-walled 96-well plate and fluorescence was measured. The amount of dextran that had permeated through the cell monolayer into the lower well was then quantified against a standard curve generated by serial dilution in Falcon tubes of the fluorescent dextran in MEC growth media.

2.4.3 Senescence-associated β-Galactosidase assay

HCAECs were grown to confluency within T-75 flasks, as previously discussed. $5x10^4$ HCAECs were then seeded in fibronectin-coated wells, in triplicate, in 24 well plates. Once a confluent cell monolayer had formed, cells were irradiated with 10 Gy or mock 0 Gy X-ray (see section 2.3). One week later, cells were detached using 200 μL undiluted Trypsin, transferred to 1.5 mL Eppendorf tubes, and 1 mL soya bean trypsin inhibitor (1:100 dilution in HBSS) was then added. Cell number in the aliquot was then counted using a haemocytometer as previously discussed (section 2.2). Cells were pelleted by centrifuging at 8,000 rpm for 5 minutes, the supernatant removed, and 200 μL of SA-β-Gal reaction buffer was used to resuspend the pellet. The reaction buffer was modified from the Senescence β-Galactosidase Staining Kit (Cell signalling Technologies, No. #9860) to include fluorescein Di-β-Galactopyranoside (FDG, Thermo Fisher #F1179), which fluoresces when hydrolysed by β-Galactosidase, enabling semi-quantitative assessment of β-Galactosidase activity (1 mL reaction buffer: 100 μL staining buffer, 10 μL solution A, 10 μL solution B, 20 μL 10% triton X-100, 2.5 μL 200 mM FDG (dissolved in 50% DMSO); 857.5 μL deionised water (dH_2O)). These were then incubated as standard for 1 hour and 150 μL of the reaction mixture was transferred to a 96 well,

black walled plate for fluorescence analysis. Fluorescence readings were normalised to cell number for each well. Fluorescence divided by the HCAEC number obtained after transferring the cells to the Falcon tube was used to determine the fluorescence per HCAEC.

2.5 Pro-inflammatory cytokine secretion analysis

Human cytokine antibody arrays on nitrocellulose were purchased from Abcam (ab133997) containing 42 target cytokines (ENA-78, GCSF, GM-CSF, GRO, GRO-α, I-309, IL-1alpha, IL-1beta, IL-2, IL-3, IL-4, IL-5, IL-6, IL-7, IL-8, IL-10, IL-12 p40/p70, IL-13, IL-15, IFN-gamma, MCP-1, MCP-2, MCP-3, MCSF, MDC, MIG, MIP-1, RANTES, SCF, SDF-1, TARC, TGF-β1, TNF-α, TNF-β, EGF, IGF-I, Angiogenin, Oncostatin M, Thrombopoietin, VEGF-A, PDGF BB, and Leptin). $5x10^5$ HCAEC were seeded in fibronectin-coated 10 cm^2 plates and incubated in 10 mL MEC growth media. Confluency was reached in roughly 5-6 days, then plates were exposed to 0 or 10 Gy X-ray.

At day 5 post irradiation, 10 mL of MEC growth media was added. Two days later, this conditioned media was collected and filtered through 0.2 μM Minisart filters (surfactant-free cellulose membrane. Fisher Scientific, #1073072) and centrifuged at 1000 rpm for 5 mins. Nitrocellulose membranes containing the immobilised anti-cytokine antibody arrays were blocked using the 1× blocking solution for 30 minutes at room temperature (RT) with gentle rocking and then 1 mL of the conditioned media was incubated on the membrane at 4^{o}C overnight with (all incubation and washed steps were performed with gentle rocking). The membrane was washed in 30 mL of wash

buffer 1 at RT with, followed by 3 × 5-minute washes with 2 mL of wash buffer 1 and 3 × 5-minute washes with 2 mL of wash buffer 2. Array membranes were then incubated with 1 mL of biotin-conjugated anti-cytokine antibodies supplied with the kit for 2 hours at RT. Following this, the wash steps were repeated (excluding the large volume wash). Arrays were then incubated with 2 mL of the supplied HRP-conjugated Streptavidin at RT for 2 hours. The wash steps were then repeated. For chemiluminescence detection, arrays were incubated with 500 μL of detection buffer mixture (1:1 detection buffer C and detection buffer D supplied with the kit) and imaged on a Bio-Rad ChemiDoc™ imaging system for luminescence. Image J analysis software was used to quantify chemiluminescence, with signal normalised to the internal standards included on the array membranes.

2.6 RNA extraction

For RNA extraction, the rNeasy Plus Mini Kit (Qiagen, #72134) was used with cells lysed directly in the vessel, following the manufacturers protocol. To homogenise, the lysate was pipetted into QIAshredder spin columns (Qiagen, #79656), and centrifuged at maximum speed for 2 mins, with the pass through collected in the collection tube. RNA yield was calculated using the Nanodrop 1000 (Thermo Fisher) and the RNA integrity number (RIN) obtained using RNA screen tape analysis kit and the TapeStation 2200 (Agilent).

2.7 Western blotting

For Western blotting, cells were seeded in 10 cm plates for the duration of the experiment. Once complete, cells were washed with 10 mL HBSS, followed by the addition of 0.75 mL HBSS and cells were removed by scraping. Cells were then transferred to 1.5 mL falcon tubes and pelleted by centrifugation at 10,000 rpm for 5 minutes. HBSS was then removed, and cell pellets were stored at -80 °C.

Cell pellets were resuspended in 30 μL cold RIPA buffer (ThermoFisher Scientific, #89901. 25 mM Tris-HCL, pH 7.6, 150 mM NaCl, 1% NP-40, 1 % sodium deoxycholate, 0.1 % SDS) with 1:100 (v/v) HALT protease/phosphatase inhibitor cocktail (ThermoFisher #1861281), vortexed, and incubated on ice for 15 minutes. Lysates were then passed through QIAshredder spin columns (Qiagen #76956) by centrifugation at 14,000 rpm for 1 minute, and the protein concentration determined using the Pierce BCA assay following the manufacturer's instructions (Thermo Scientific #23225). Lysates were then equally loaded onto Mini-Protean TGX pre-cast gels (4-20% gradient. BioRad #4561096) and separated by electrophoresis at 200 V for 35 minutes. Proteins were then transferred to 0.2 μM PVDF membranes (BioRad Trans-Blot Turbo transfer pack, #1704156) using the BioRad Trans-Blot Turbo system (7 minutes, 1.3 A, 17 V). Membranes were then blocked for 1 hour at RT in 5% non-fat dried milk in TBST (w/v). Following this, primary antibody incubation was performed overnight at RT in 5% non-fat dried milk in TBST (w/v). Membranes were then washed with TBST for 2 minutes on a rocker, 5 times, and then probed with HRP-conjugated secondary antibodies for 1

hour. Membranes were then washed as previously described and incubated with ECL Western Blotting Substrate (Thermo Scientific, #32106) for 1 minute, and chemiluminescence detected immediately using a BioRad ChemiDoc imaging system. For semi-quantitative analysis, protein band intensities were measured and normalised to loading control using Image J, with protein expression then compared between samples.

2.8 Immunofluorescence cell staining

Cells were either seeded on fibronectin-coated coverslips in 24-well plates or black-walled, glass bottomed 96 well plates. Cells were fixed in 3.7 % formaldehyde for 10 minutes at RT, permeabilised using 0.1 % Triton X-100 (in HBSS) for 10 minutes, and then washed. Cells were then blocked with 2 % Foetal Calf Serum (In HBSS) for 10 minutes, three times, and then incubated with primary antibodies for one hour at RT. After washing, cells were then incubated with Alexa secondary antibodies (in 2 % FCS/HBSS) for one hour in the dark. Cells were washed and stained for DNA with DAPI. For cells seeded on glass coverslips, forceps were used to remove the coverslip and mounted to microscope slides using Vectashield (Vector Labs).

2.9 Antibodies used for Western blotting and immunofluorescence

Antibodies used for Western blotting and immunofluorescence are listed in Table 2.2.

Table 2.2 Antibodies used in Western blotting and immunofluorescence.

	Target protein	Species raised in	Dilution	Supplier
Western blotting				
Primary antibodies	LAP2	Mouse	1:1000	BD Biosciences 611000
	Total p53	Mouse	1:20000	Santa Cruz sc-126
	P21 Warf1/Cip1	Rabbit	1:1000	Cell Signalling 2947
	S6 Ribosomal protein-Phosphorylated	Rabbit	1:1000	Cell Signalling 2211
	GAPDH	Mouse	1:100000	Proteintech 60004-1-Ig
Secondary antibodies	α-Mouse HRP-conjugated IgG	Goat	1:1000	Santa Cruz sc-2013
	α-Rabbit HRP-conjugated IgG	Donkey	1:1000	Santa Cruz sc-2313
Immunofluorescence				
Primary antibodies	γ-H2AX	Rabbit	1:500	Santa Cruz sc-101696
	VE-Cadherin	Mouse	1:200	Santa Cruz sc-9989
Secondary antibodies	α-Rabbit IgG AlexaFluor 594	Donkey	1:500	Invitrogen A21207
	α-Mouse IgG AlexaFluor 594	Goat	1:500	Invitrogen A21202

2.10 Nanopore sequencing

RNA was extracted from HCAECs as described (section 2.6), followed by the creation of barcoded cDNA libraries using the PCR-cDNA barcoding kit, following the manufacturers instructions (Oxford Nanopore Technologies, SQK-PCB111.24) in preparation for

sequencing using the GridION sequencer with MinION flow cells (Oxford Nanopore Technologies, FLO-MIN114). Briefly, for reverse transcription and strand switching, 10 μL of RNA (adjusted to 200 ng with nuclease free water (Thermo Fisher, AM9937)), 1 μL of the supplied cDNA RT adapter, and 1 μL of the supplied annealing buffer was loaded into 0.2 mL PCR tubes, incubated at 60°C for 5 minutes using a PCR thermocycler (ProFlex PCR System, Applied Biosystems, Thermo Fisher Scientific), then cooled at RT for 10 minutes. 3.6 μL of NEBNext Quick Ligation Buffer (NEB B6058), 1.4 μL T4 DNA Ligase (2M U/mL, NEB M0202), and 1 μL RNaseOUT was then added and incubated at RT for 10 minutes. 1 μL of Lambda Exonuclease (NEB M0262L) and 1 μL of uracil-specific excision reagent (USER, NEB M5505L) was added, followed by incubation at 37°C for 15 minutes in the thermocycler.

This was then transferred into fresh 1.5 mL DNA LoBind Eppendorf tubes, and 36 μL of RNAClean XP beads (Beckman Coulter, A63987) were added, mixed, and incubated at RT for 5 minutes on a Hula mixer. The samples were then spun down and pelleted on a magnet (R&D Systems MagCellect, MAG997), the supernatant removed, and the beads washed with 100 μL of the supplied short fragment buffer. This wash step was repeated once more, followed by spinning down the tube, placing back on the magnet, and removing any remaining buffer. The pellet was then allowed to air-dry for 30 seconds. The tubes were then removed from the magnet, the pellets resuspended in 12 μL of nuclease free water, and then incubated at RT for 10 minutes. The beads re-pelleted on the magnet until the elute was clear and colourless, and 12 μL of the elute was removed and added to fresh 0.2 mL thin-walled PCR tubes. To each of the tubes, 1 μL of the

supplied RT primer and 1 μL of the dNTPs (10 nM) were added, and then incubated at RT for 15 minutes. 4.5 μL Maxima H Minus 5x RT buffer (final working concentration of 1x, Thermo Fisher EP0751), 1 μL RNaseOUT (40 U/μL, Life Technologies, 10777019) and 2 μL of the supplied strand switching primer II was then added, mixed, and spun down, followed by incubation in the thermocycler for 2 minutes at 42°C. 1 μL of Maxima H Minus Reverse Transcriptase (Thermo Fisher, EP0751) was then added, incubated for 90 minutes at 42°C in the thermocycler, followed by 5 minutes at 85°C for heat inactivation, and held at 4°C.

To select for full length transcripts and barcode samples, PCR was performed. 5 μL of the preparation was added to fresh 0.2 mL PCR tubes, with 0.75 μL of the barcoded primers, 6.75 μL of nuclease free water, and 12.5 μL of 2x LongAmp Hot Start Taq Master Mix (final working concentration of 1, NEB, M0533S). PCR was then performed (initial denaturation for 30 seconds at 95°C (1 cycle), denaturation for 15 seconds at 95°C (14 cycles), annealing for 15 seconds at 62°C (14 cycles), extension for 6 minutes at 65°C (14 cycles), final extension for 6 minutes at 65°C (1 cycle), then held at 4°C). 1 μL of exonuclease I was then added to each tube and mixed by pipetting, followed by incubation at 37°C for 15 minutes, and then 80°C for 15 minutes.

The barcoded cDNA was then transferred to 1.5 mL DNA LoBind Eppendorf tubes, 20 μL of AMPure XP beads (Beckman Coulter, A63880) were added, and tubes were incubated on a Hula mixer for 5 minutes at RT. The samples were spun down and pelleted on a magnet, and the supernatant was removed. The pellet was washed twice with 70 % ethanol (in nuclease free water), spun down, and placed back on the magnet.

The ethanol was removed and pellet air dried for 30 seconds. Tubes were then removed from the magnet and the pellet resuspended in 12 μL of the supplied elution buffer and incubated at RT for 10 minutes. The beads were then pelleted on the magnet and 12 μL of the elute (cleaned, barcoded, cDNA) was removed and placed into fresh 1.5 mL DNA LoBind Eppendorf tubes. The mass of each sample was calculated using the Nanodrop 1000 and samples were pooled equally in groups of 6, with a final volume of 23 μL (with elution buffer).

For loading libraries onto the flow cell, 1.2 μL of rapid adapter T with 6.8 μL of RAP dilution buffer (manufacturer supplied) were mixed, 1 μL added to each pooled sample mix, and incubated at RT for 5 minutes. The cDNA libraries were then placed in fresh tubes with 75 μL of the supplied sequencing buffer II and 51 μL of supplied loading beads II. Flow cells were primed with 500 μL of supplied priming mix, and libraries loaded into the flow cells.

I performed all of the steps associated with the nanopore sequencing, including the bioinformatic analysis of the results.

2.11 Proteomics

Briefly, HCAEC from 3 donors in each age group (17-33 years and 48-55 years) were seeded in quadruplicate and received the following treatment at confluency: 0 Gy X-ray, 0 Gy X-ray with 10 nM rapamycin, 10 Gy X-ray, and 10 Gy X-ray with 10 nM

rapamycin. Rapamycin treatment lasted 5 days post exposure, with all cells being collected and pelleted on day 7. The cell pellets were then taken to the Advanced Proteomics Facility (University of Oxford, Department of Biochemistry), where the facility extracted the proteins and trypsin FASP digested the samples for liquid chromatography with tandem mass spectrometry (LC-MS/MS). The raw spectral results were then given to me, and I processed the files using the MaxQuant and MSStats tools on the Galaxy.eu web-based platform, outputting protein identification, quantification, and differential expression (DE) analysis.

2.12 Bioinformatics

2.12.1 Differential gene expression analysis pipeline

For differential gene expression analysis of the Nanopore transcriptome sequencing, the Epi2me labs wf-transcriptomes Nextflow workflow was used (Oxford Nanopore Technologies, https://github.com/nanoporetech/pipeline-transcriptome-de). The pipeline uses Minimap2, salmon, edgeR, DEXSeq, and stageR packages. The reference transcriptome used for transcript alignment was Homo sapiens GRCh38.

2.12.2 Differential protein analysis pipeline

For differential protein expression analysis, the raw spectra files from the Advanced Proteomics Facility (University of Oxford) were uploaded to usegalaxy.eu. Here MaxQuant was used to match the spectra to a database of matching proteins, with a false discovery rate (FDR) or 0.01. The output of this was then ran through mSstats,

which normalises between runs by intensity, and performs differential expression analysis.

2.13 Drug compounds

Rapamycin (Alfa Aesar) and ABT-263 (Apex Bio) were dissolved in DMSO and stored at -20°C, as per the manufacturer's instructions. To establish working concentrations, drugs were diluted in MEC growth media before addition to the HCAEC.

2.14 Statistical analysis

Statistical analysis and graphing (unless otherwise stated) was performed using GraphPad prism. For analysis of significance between two populations, the unpaired one-tailed Student's t-test (where the hypothesis was a change in one direction) or two-tailed Student's t-test (where direction of change was not hypothesised) were used. Where comparisons of >2 populations were needed, ANOVAs (analysis of variance) were performed with multiple comparison analysis conducted using Tukey tests. All graphs display the mean values with error bars indicating the standard error from the mean (SEM), calculated with $n \geq 3$, unless otherwise stated. Where possible, biological replicates are displayed unless stated as technical replicates.

3 Identification of an X-ray dose for investigating IR-CVD in Ldlr$^{-/-}$ mice

3.1 Introduction

While many studies have investigated CVD via plaque development within the Ldlr$^{-/-}$ mouse model, at the time of this study, literature searches suggest that this model has not yet been used to investigate ionising radiation-induced CVD (IR-CVD). Therefore, there is no information on suitable X-ray exposure doses for investigation into age-mediated effects. While studies have investigated IR-induced CVD in ApoE$^{-/-}$, age was not a factor considered (Tribble *et al.*, 1999; Stewart *et al.*, 2006; Mancuso *et al.*, 2015a). The inclusion of the Ldlr$^{-/-}$ mouse model for this study is important for several reasons: Firstly, the differences surrounding the phenotypes of these mouse models mean that contributing factors promoting atherosclerosis development differ slightly between them; for example lower circulating LDL in the Ldlr$^{-/-}$ model compared to the ApoE$^{-/-}$ model; ApoE being expressed in immune cells (Véniant, Withycombe and Young, 2001a; Emini Veseli *et al.*, 2017). Therefore, any atherogenic responses to external risk factors, such as IR, may yield different outcomes. Secondly, since the aim of this thesis is to investigate how age modulates the development of IR-CVD, the Ldlr$^{-/-}$ mouse model represents a better opportunity to investigate greater age points, compared to the ApoE$^{-/-}$ model. This is due to the severity of the ApoE$^{-/-}$ phenotype, which significantly reduces their healthy lifespan (Véniant, Withycombe and Young, 2001a; Getz and

Reardon, 2016). Therefore, using an Ldlr$^{-/-}$ mouse model would allow for investigation into age points that would not be ethically viable for study in ApoE$^{-/-}$ mice.

3.2 Chapter aims

Within this chapter, I aim to ascertain a suitable dose for investigation into IR-CVD with Ldlr$^{-/-}$ mice. My specific aims are:

1. To ascertain an X-ray dose that is tolerable to the Ldlr$^{-/-}$ mouse model.
2. To investigate any relationship between IR dose and atherosclerotic plaque development within this model.

3.3 Results

3.3.1 Identification of a suitable X-ray dose for IR-CVD investigation in Ldlr$^{-/-}$ mice

To enable the inclusion of Ldlr$^{-/-}$ mice in the main study, I conducted a pilot study with 24 mice, using 3 different exposure doses and a control group, enabling the determination of a suitable X-ray exposure dose. Within these groups, 3 males and 3 females were exposed to either a sham (0 Gy), 0.5 Gy, 2 Gy, or 4 Gy X-ray, at 6-weeks-old. 6 months after exposure, aortas were excised in a blinded fashion and analysed for plaque development with Oil-red O staining, with quantification performed in image J (as described in section 2.1.4). The data was unblinded only once all the aortas were analysed.

A small amount of plaque developed on the aortas at all doses used, across both sexes (Figure 3.1). However, some aspects of the stain were visible on the outside of the aorta, such as in the 0 Gy aorta displayed (Figure 3.1A). This is due to insufficient cleaning of fatty tissue outside the aorta. This background was easily detectable during analysis and did not affect the results.

When quantifying the plaque coverage over the whole aorta, no doses displayed a significant difference in plaque coverage compared to the control. However, the 2 Gy exposure group had a smaller distribution between the mice than the other doses investigated (Figure 3.1A). Furthermore, although not significant, a higher mean percentage coverage of 1.67 % was also observed within the 2 Gy exposure group, compared to 1.44 % in the sham control.

As the most significant plaque development is usually located in the aortic arch, a separate analysis of this region was also performed. Within the aortic arch, the results were similar, with no statistical differences between the groups (Figure 3.1). Interestingly, when isolating the analysis to the aortic arch, the 0 Gy control group had a slightly higher mean percentage plaque coverage than the X-ray exposure groups.

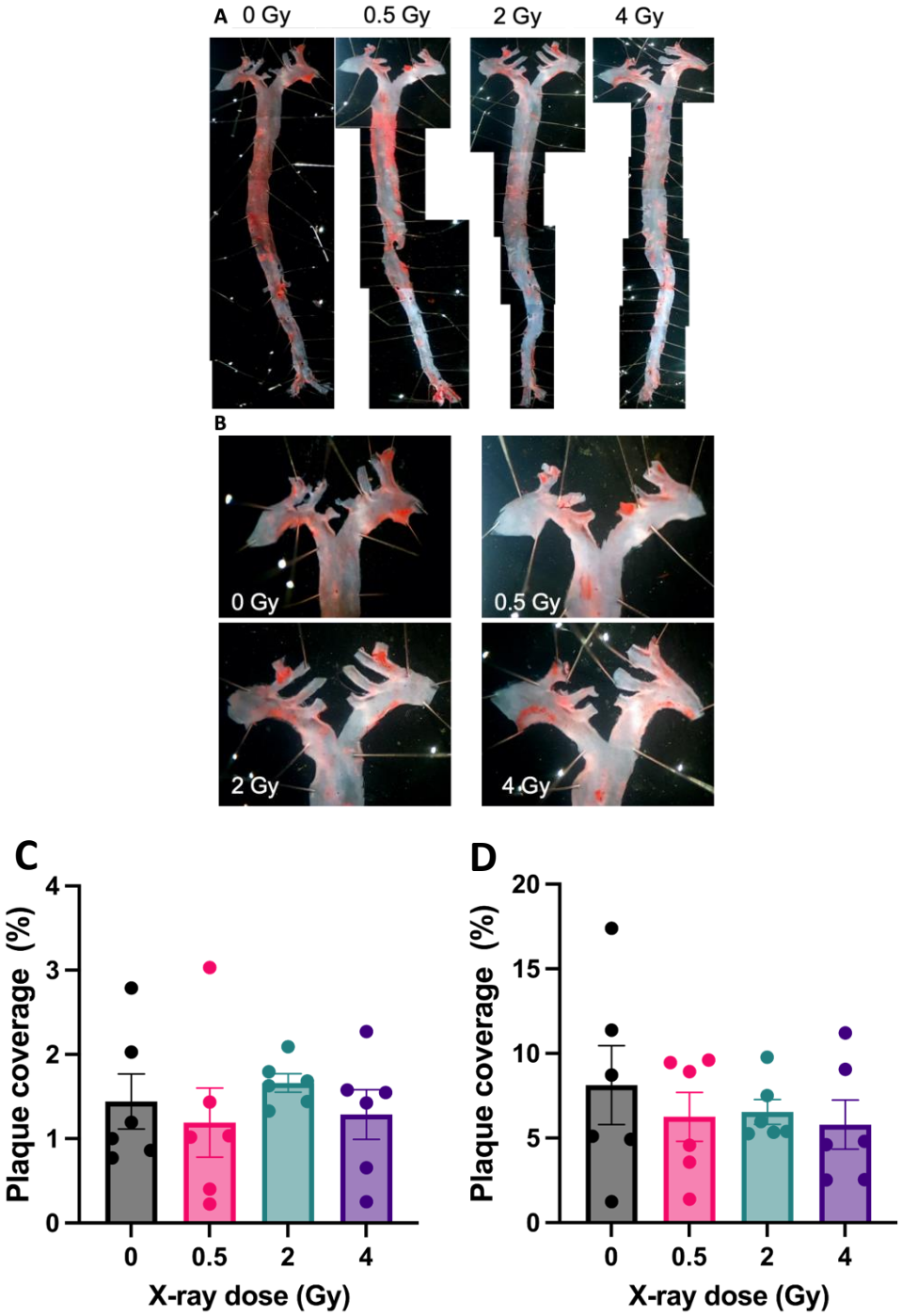


Figure 3.1. Representative images of Ldlr$^{-/-}$ Oil red O stained plaques.

Ldlr$^{-/-}$ mice were exposed to 0, 0.5, 2, and 4 Gy X-ray at 6-weeks-old and aortas were harvested 6-months post irradiation, stained with Oil red O, and area of plaque coverage was quantified with Image J. Representative images of the whole aorta (**A**) and aortic arch (**B**). Red staining indicates the presence of plaque. Percentage plaque coverage of the whole aorta (**C**) and aortic arch (**D**) following X-ray exposure. N=6, two-way ANOVA with multiple comparisons.

When comparing the plaque coverage between males and females within the whole aorta, the females had a higher mean plaque coverage in the non-irradiated group than non-irradiated male mice, although not statistically significant (

Figure 3.2A). Across all X-ray doses investigated, there was no statistical difference between male and female mice when analysing the whole aorta. However, when analysis was localised to the aortic arch, within the 0 Gy control, the female mice had a significantly higher percentage of plaque coverage across the aortic arch than the male mice (

Figure 3.2B). These findings are consistent with a study performed by Mansukhani *et al* in which they demonstrated female $Ldlr^{-/-}$ mice had greater plaque development than male mice at ages 14 weeks, 18 weeks, and 22 weeks after being on a high-fat diet (Mansukhani *et al.*, 2017a).

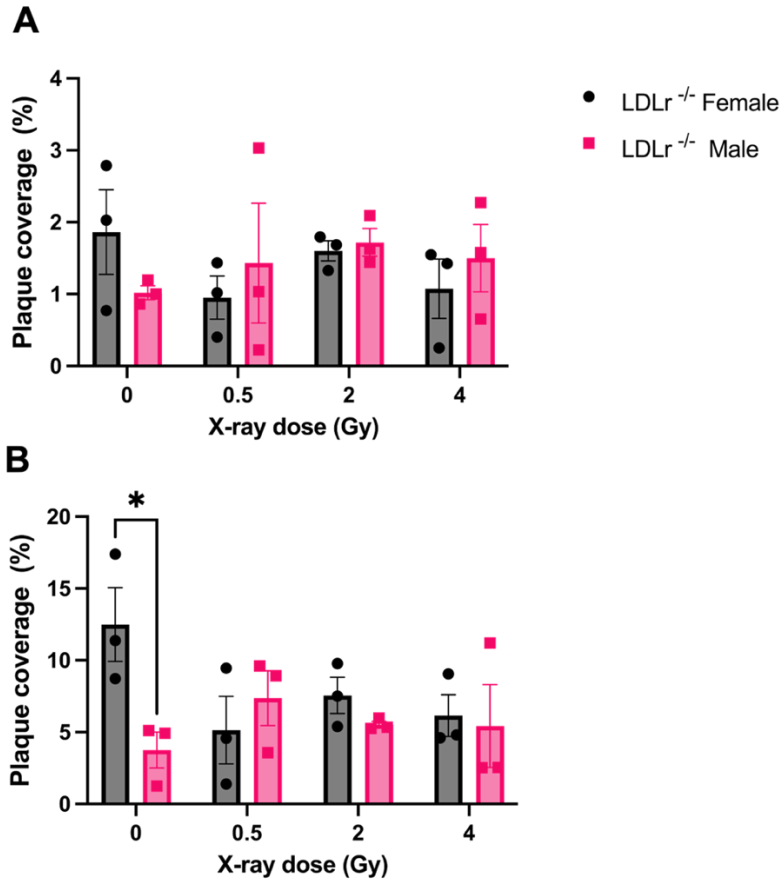


Figure 3.2. Comparison of plaque coverage after different X-ray doses in male and female Ldlr$^{-/-}$ mice.

Ldlr$^{-/-}$ mice were exposed to 0, 0.5, 2, and 4 Gy X-ray at 6-weeks-old and aortas were harvested 6-months post irradiation, stained with Oil red O, and area of plaque coverage was quantified with Image J. Percentage plaque coverage across the whole aorta (**A**) and aortic arch (**B**) after 0 Gy, 0.5 Gy, 2 Gy, and 4 Gy X-ray exposure. N=3, Two-way ANOVA with multiple comparisons, * = $p<0.05$.

The coverage within the whole aorta of the 0 Gy female mice spreads from 0.77 % to 2.79 % compared to male mice, which have a spread from 0.86 % to 1.20 %. This data may suggest that the female mice may have more variability in plaque development than the male mice, although these are low percentages, so small differences may be amplified. There is a small trend of a dose-dependent response to X-ray exposure within the male mice, with the highest mean percentage coverage occurring within the 2 Gy

exposure group (Figure 3.3A). The trends were similar when the analysis was isolated to the aortic arch, although the female mice displayed a statistically significant reduction in plaque coverage after exposure to both 0.5 Gy and 4 Gy X-ray (Figure 3.3B).

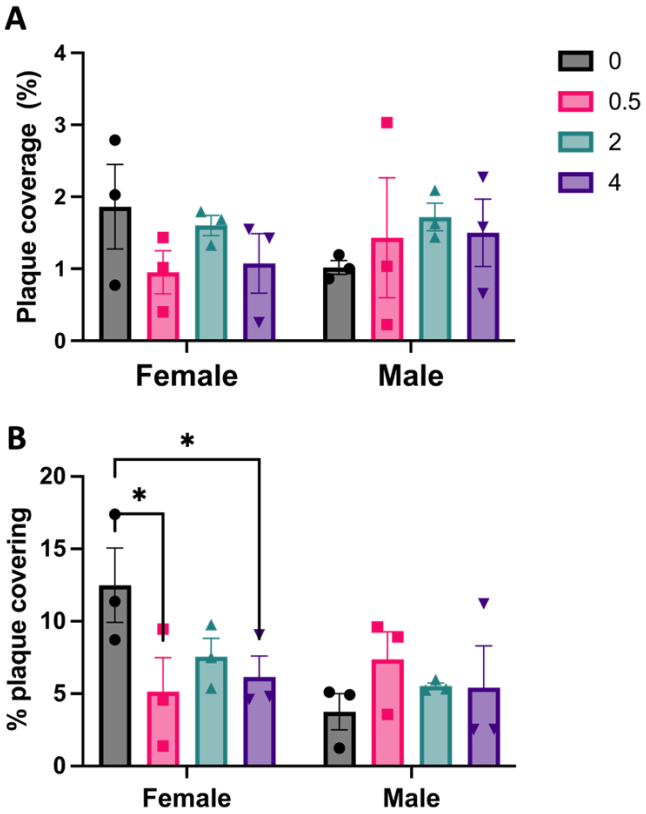


Figure 3.3. X-ray dose and plaque development in Ldlr$^{-/-}$ mice.

Ldlr$^{-/-}$ mice were exposed to 0, 0.5, 2, and 4 Gy X-ray at 6-weeks-old and aortas were harvested 6-months post irradiation, stained with Oil red O, and area of plaque coverage was quantified with Image J. The percentage plaque coverage within the whole aorta (**A**) and aortic arch (**B**) of female (left) and male (right) Ldlr$^{-/-}$ mice 6-months post X-ray exposure of either 0 Gy, 0.5 Gy, 2 Gy, or 4 Gy at 6-weeks of age. N=3, Two-way ANOVA with multiple comparisons, * = $p<0.05$.

To monitor the health of the mice and ensure any differences in plaque coverage were not due to weight loss or gain, their mass was recorded at multiple time points during the experiment. No statistical differences were observed between the groups in both

male and female mice, with no trend between X-ray dose and mass appearing (Figure 3.4). All mice sustained normal growth, which was indicated by the increase in mass over time. Furthermore, this data suggests that any difference in the aortic plaque coverage was not due to differences in weight.

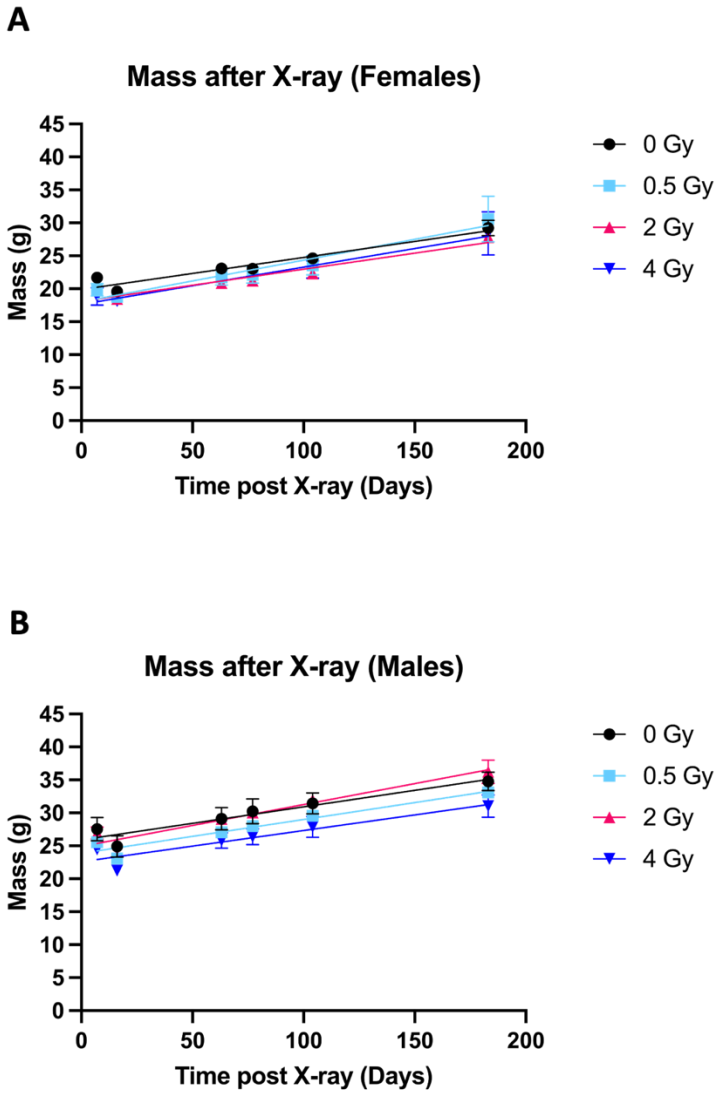


Figure 3.4. Mass of Ldlr$^{-/-}$ mice throught the experimental period after X-ray exposure.

Ldlr$^{-/-}$ mice were exposed to 0, 0.5, 2, and 4 Gy X-ray at 6-weeks-old and mice were euthanised 6-months post irradiation. At various time-points, mice were weighed. Ldlr$^{-/-}$ female (**A**) and male (**B**) mice mass recorded after exposure at 6-weeks of age to 0 Gy, 0.5 Gy, 2 Gy, or 4 Gy X-ray. N=3.

3.4 Discussion

This pilot study aimed to determine a suitable X-ray dose for investigating IR-CVD within Ldlr$^{-/-}$ mice. While there were no statistically significant increases in plaque development at any of the doses investigated in this study, trends indicated that a 2 Gy dose may be the most suitable for further investigations. This conclusion was reached for multiple reasons. Firstly, the plaque development after 2 Gy X-ray exposure had less variability between mice than the other doses investigated, suggesting that this dose may induce a more consistent response. Secondly, the 2 Gy X-ray exposure increased mean plaque coverage across the whole aorta, with the other doses trending lower. However, this increase was only 0.22 %, which is likely negligible. Thirdly, the mice seemed to tolerate all the doses used without any differences in mass between the irradiated groups and control, which is a common method of determining if the mice are suffering, along with no observable signs of ill health such as changes in coat condition, alertness, activity, and body morphology. Furthermore, at the age investigated here, along with the doses used, the plaque coverage of the aorta was low, suggesting that any subtle differences may be detectable at any of the doses investigated when moving into a larger study with a range of ages used.

Interestingly, there were differences in aortic plaque coverage between male and female mice in the control group, suggesting that female Ldlr$^{-/-}$ mice are more susceptible to plaque development at the age point used in this investigation, which fits with previously published work which demonstrated that female Ldlr$^{-/-}$ mice on a high

fat diet have greater plaque development compared to males (Mansukhani *et al.*, 2017b). Furthermore, within this pilot study, I have demonstrated a reduction in plaque burden in the female mice after exposure to 0.5 Gy and 4 Gy X-ray. A potential reason for this could be due to hormonal changes induced in the female mice by exposure to IR, although this was not investigated here, radiation exposure has been linked to changes in hormone secretion (Niazi and Niazi, 2011), and oestrogen has been suggested to be radioprotective, particularly against radiation-induced neuroinflammation (Mitra *et al.*, 2023), this combined with evidence that oestrogen levels are increased in mice exposed to IR may explain these results (Suman *et al.*, 2012). However, in contradiction to this, a previous study investigating sex mediated response to radiation injury in mice, suggests that female mice are more susceptible to radiation-induced arthrofibrosis, although this cannot be correlated with potential CVD development risk (Rodman *et al.*, 2022). This differential response depending on sex may mask any results when the sexes are combined for analysis, and importantly highlights the importance of including male and female mice in any non-sex-specific study.

From this pilot study and the points discussed above, the dose of 2 Gy was selected for the main study using $Ldlr^{-/-}$ mice. Although this pilot study raises the question of whether $Ldlr^{-/-}$ mice are susceptible to IR-CVD, if age does influence the risk associated with IR-CVD, then it is possible that older mice may be more susceptible.

4 Analysis of age-modulated X-ray-induced cardiovascular disease in Ldlr$^{-/-}$ and ApoE$^{-/-}$ mice

4.1 Introduction

The underlying cause of CVD is atherosclerosis. This is an inflammatory, age-related condition which results in the build-up of lipid-laden plaques within arteries supplying organs such as the heart (section 1.2). It is theorised that a contributing factor to the development of atherosclerosis is an increased accumulation of senescent endothelial cells lining the arteries. This could result in endothelial dysfunction and a proinflammatory environment, promoting the development of atherosclerotic plaques. Indeed, senescent cells have been detected in aortic plaques of both humans and mice (Minamino *et al.*, 2002b; Childs *et al.*, 2016a).

Furthermore, *in vitro* exposure of cells to IR is a standard method of inducing senescence (section 1.5.3.3). Therefore, it is suggested that the exposure of human vasculature to IR could prematurely induce endothelial cell senescence and promote atherogenesis.

The epidemiological evidence suggests that when exposed at a younger age, there is a greater risk of developing IR-CVD (section 1.4.1). To better assess this hypothesis, a model that accounts for the complex interactions between the different cell types and immune responses involved during the development of CVD is required. The model

needs to be complex enough to allow for the systemic effects that occur after IR exposure and also deemed the most ethically appropriate for the study. With these considerations in mind, mice were chosen for the investigation.

Many studies have used genetically modified (GM) mice to investigate the development of CVD, specifically atherosclerotic plaque development (Zhang *et al.*, 1992a; Véniant, Withycombe and Young, 2001b; Johnson *et al.*, 2005; Lo Sasso *et al.*, 2016). This is necessary as wild-type (WT) mice develop only small amounts of early-stage atherosclerosis in the form of fatty streaks, with these only occurring when mice are maintained on a high-fat diet for a prolonged period. These lesions mainly occur within the aortic root and are not comparable to the more advanced fibrous plaques observed in humans (Paigen *et al.*, 1985). The most commonly used GM models are apolipoprotein E knockout ($ApoE^{-/-}$) and low-density lipoprotein receptor knockout ($Ldlr^{-/-}$) mice, both of which have an increased abundance of circulating low-density lipoprotein (LDL), compared to WT mice, which is considered the driving force behind their development of atherosclerosis (Piedrahita *et al.*, 1992; Zhang *et al.*, 1992b). Furthermore, it has previously been reported that $ApoE^{-/-}$ mice develop IR-induced atherosclerosis, making them a clear choice for further investigation (Mancuso *et al.*, 2015b). However, at the time of this study, there was no published data involving the $Ldlr^{-/-}$ mouse model to investigate IR-induced CVD. This model was included due to the investigation into how age affects the development of IR-induced CVD (IR-CVD), which is significant when considering the life span and life quality reductions associated with the $ApoE^{-/-}$ model, meaning it is unethical to age these mice. As the $Ldlr^{-/-}$ mouse model phenotype is less severe, the experimental timeline with these mice can be longer,

allowing for a greater age range to be investigated. (Véniant, Withycombe and Young, 2001b).

4.2 Chapter aims

Within this chapter, I will investigate the effect of age at the time of exposure on the development of IR-induced atherosclerosis within the two mouse models. My specific aims are:

1. To determine if age at the time of exposure modulates IR-induced atherosclerotic plaque development within both ApoE$^{-/-}$ and Ldlr$^{-/-}$ mice.
2. To determine if these effects are sex dependent.
3. To evaluate the changes in cytokine expression after IR exposure within Ldlr$^{-/-}$ mice.

4.3 Results

4.3.1 ApoE$^{-/-}$ mouse aortic plaque quantification after X-ray exposure at varying ages

4.3.1.1 Introduction

ApoE$^{-/-}$ mice have significantly elevated cholesterol levels and develop atherosclerotic plaques within their arteries, unlike wild-type mice. It has also been shown that they are susceptible to IR-induced CVD at doses as low as 0.3 Gy (Mancuso *et al.*, 2015b). An essential consideration of this study is that aortic plaque development was assessed

300 days after irradiation, compared to my investigation, which was ~150 days after irradiation. Within this same study, mice were chronically exposed to comparable doses over 300 days; however, the sham mice in the acute study of the same period had a percentage plaque coverage of ~10 %, whereas the sham mice in the chronic study had a mean percentage plaque coverage of ~40 %, with differences being attributed to the use of different animal housing facilities, interestingly with the higher plaque coverage occurring in the mice that were housed in specific pathogen-free conditions.

4.3.1.2 ApoE$^{-/-}$ mice develop IR-CVD after exposure at 22 weeks of age

To investigate whether age modulates IR-CVD within the ApoE$^{-/-}$ model, mice were irradiated with 0 or 0.5 Gy X-ray at 6-weeks or 22-weeks old. 5 months after irradiation, mice were euthanised, aortas removed, and plaque development quantified using Oil-Red-O staining and Image J analysis (detailed in section 2.1.3 & 2.1.4). Due to the severity of the atherosclerotic phenotype developed by these mice, the highest end-point age chosen for this investigation was ten months old, with the latest irradiation occurring at 22 weeks of age.

When quantifying plaque coverage across the whole aorta using Oil-red O staining (Figure 4.1A), ApoE$^{-/-}$ mice that were exposed to 0.5 Gy X-ray at 6 weeks old had no significant difference in plaque development compared to control. However, in the mice irradiated at 22-weeks, there was a statistically significant increase in percentage plaque coverage compared to the age-matched group (Figure 4.1C). When isolating the analysis to the aortic arch, no significant difference was observed in any age group (Figure 4.1B).

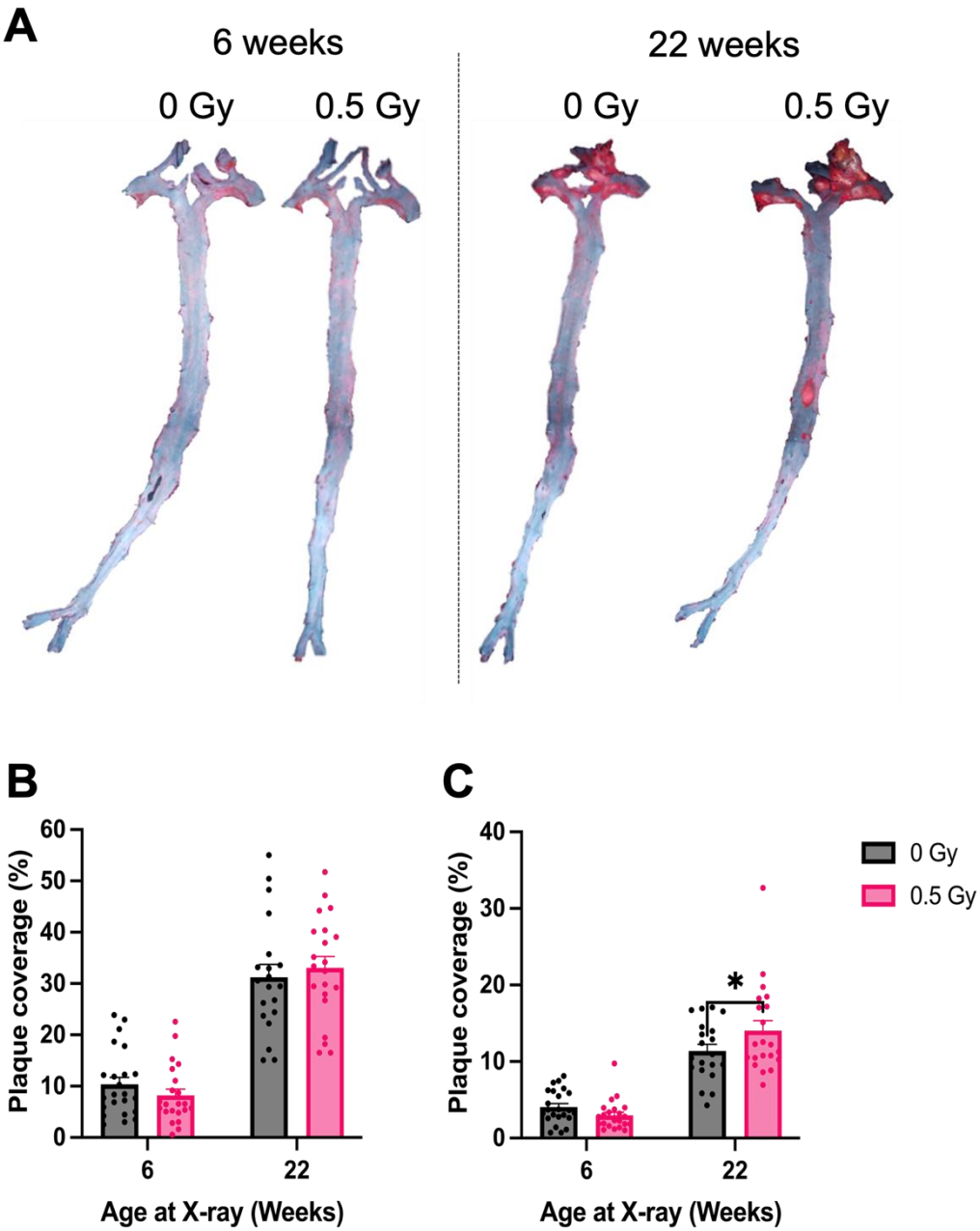


Figure 4.1. ApoE$^{-/-}$ aortic plaque coverage after X-ray exposure at 6-weeks and 22-weeks of age.

ApoE$^{-/-}$ mice were irradiated with 0 or 0.5 Gy X-ray at 6 or 22-weeks of age, with aortas harvested and stained with Oil red O 6-months post irradiation. **A)** Representative examples of Oil-red O stained plaqyes (red) 6-months after 0 Gy or 0.5 Gy X-ray exposure at ages 6-weeks (left) and 22-weeks (right) of age. Plaque coverage was quantified as a percentage of the aortic arch (**B**) and whole

aorta (**C**) using Image J. N = 20-23, Two-way ANOVA with multiple comparisons, * = $p<0.05$.

4.3.1.3 Older male ApoE$^{-/-}$ mice are more susceptible to IR-induced plaque development

Analysing the IR-induced plaque coverage from Figure 4.1 revealed a sex-mediated response to IR-CVD. The female mice had no statistically significant differences in plaque coverage between irradiated and control mice (Figure 4.2A&B). However, X-ray exposure of the male mice at 22-weeks resulted in significant increase in the percentage plaque coverage in analysis conducted of both the whole aorta (Figure 4.2B) and aortic-arch (Figure 4.2D). Importantly, there was no significant difference observed between the mice irradiated at 6-weeks old and the age-matched control mice. Interestingly, the percentage plaque coverage in male mice appears lower than female when isolating the analysis to the arch (Figure 4.2C&D), therefore a direct comparison was performed.

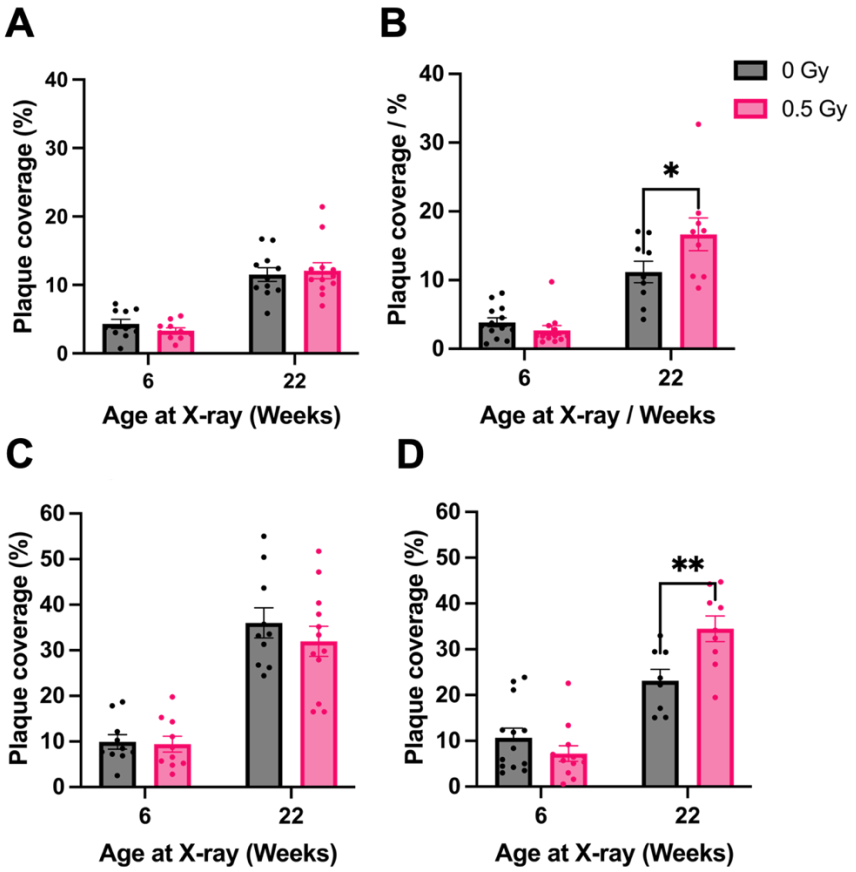


Figure 4.2. Plaque coverage in the aortas of ApoE$^{-/-}$ male and female mice after X-ray exposure.

The analysis of X-ray induced plaque development in ApoE$^{-/-}$ mice irradiated at 6-weeks or 22-weeks of age, compared to age matched controls, from Figure 4.1 was split by sex, with the perctage plaque coverage in across the aorta for female (**A**) and male mice (**B**), along with isolated analysis of the aortic arch in the female (**C**) and males (**D**) displayed. Mice were euthanised 5 months after irradiation. N=9-13, Two-way ANOVA with multiple comparisons, * = $p<0.05$, ** = $p<0.01$.

The direct comparison between male and female plaque coverage across the whole aorta, the results are comparable in all experimental conditions apart from the mice exposed to 0.5 Gy at 22 weeks of age, where the males had a statistically significant higher mean plaque coverage compared to the females (Figure 4.3A). However, this

difference is lost when the analysis is isolated to the aortic arch, with no significant difference in plaque coverage. This suggests that areas prone to plaque development may differ between sexes, with these differences being masked when analysing the whole aorta. This is likely due to increased plaque development in the thoracic and abdominal aortas in the male mice compared to females. Interestingly, the female mice in the 22-week-old control group had a significantly greater plaque coverage compared to the male (Figure 4.3B). This has been suggested within literature, however there are only a few studies that perform direct sex comparisons in mice, with even fewer comparing ApoE$^{-/-}$ mice without treatment (Caligiuri *et al.*, 1999; Kirk *et al.*, 2000; Hodgin *et al.*, 2002; Matsumoto *et al.*, 2016; Man, Beckman and Jaffe, 2020). This highlights the importance of including both sexes in scientific research.

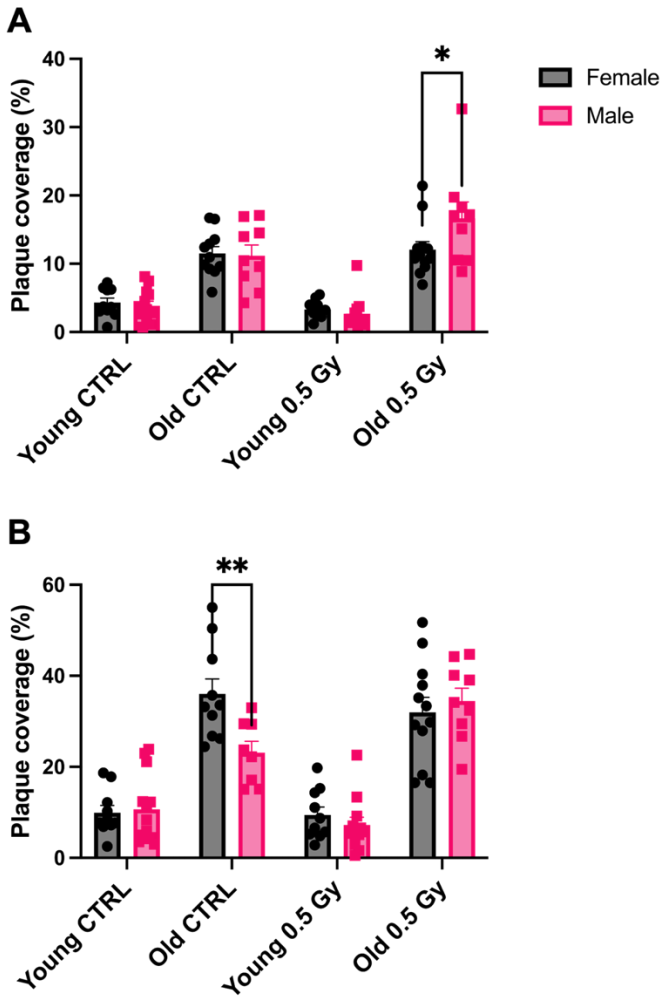


Figure 4.3. Comparison of plaque development between male and female ApoE$^{-/-}$ mice.

Comparison of plaque coverage in the whole aorta (**A**) and aortic arch (**B**) between male and female mice at 6-weeks (young) and 22-weeks (old) of age with or without 0.5 Gy X-ray exposure. N=9-13, Two-way ANOVA with multiple comparisons, * = $p<0.05$.

4.3.2 Ldlr$^{-/-}$ mouse aortic plaque analysis after X-ray exposure

Ldlr$^{-/-}$ mice have elevated cholesterol levels compared to wild-type mice, meaning that they are a commonly used model for investigation into CVD. Unlike the ApoE$^{-/-}$ mice,

Ldlr$^{-/-}$ mice have not been used to study IR-induced CVD. Having established a suitable X-ray dose in the Ldlr$^{-/-}$ pilot study, I moved forward to investigate the effect of age at the time of exposure to IR on the development of CVD. To achieve this, I irradiated Ldlr$^{-/-}$ mice with 0 or 2 Gy X-ray at either 6 weeks, 26 weeks, or 52 weeks of age and then harvested the aortas 6 months post-X-ray. To quantify atherosclerotic plaque development, I stained the aortas using the lipophilic dye, Oil Red O. This dye stains lipids and triglycerides within the plaques, enabling visualisation and quantification using Image J (detailed in section 2.1.3 & 2.1.4).

4.3.2.1 Age modulates X-ray-induced atherosclerosis within Ldlr$^{-/-}$ mice

With both sexes combined, there were no statistical differences between the control and 2 Gy exposure groups when irradiated at 6 weeks and 26 weeks of age (Figure 4.4A). However, when exposed at 52 weeks of age, there was significantly higher plaque coverage in the mice exposed to 2 Gy X-ray compared to the control. A similar trend was observed when analysing the plaque coverage within the aortic arch. However, no significant differences were observed at any of the ages investigated (Figure 4.4B). As with the ApoE$^{-/-}$ results, this suggests that IR may promote atherosclerosis to a greater extent in the abdominal aorta.

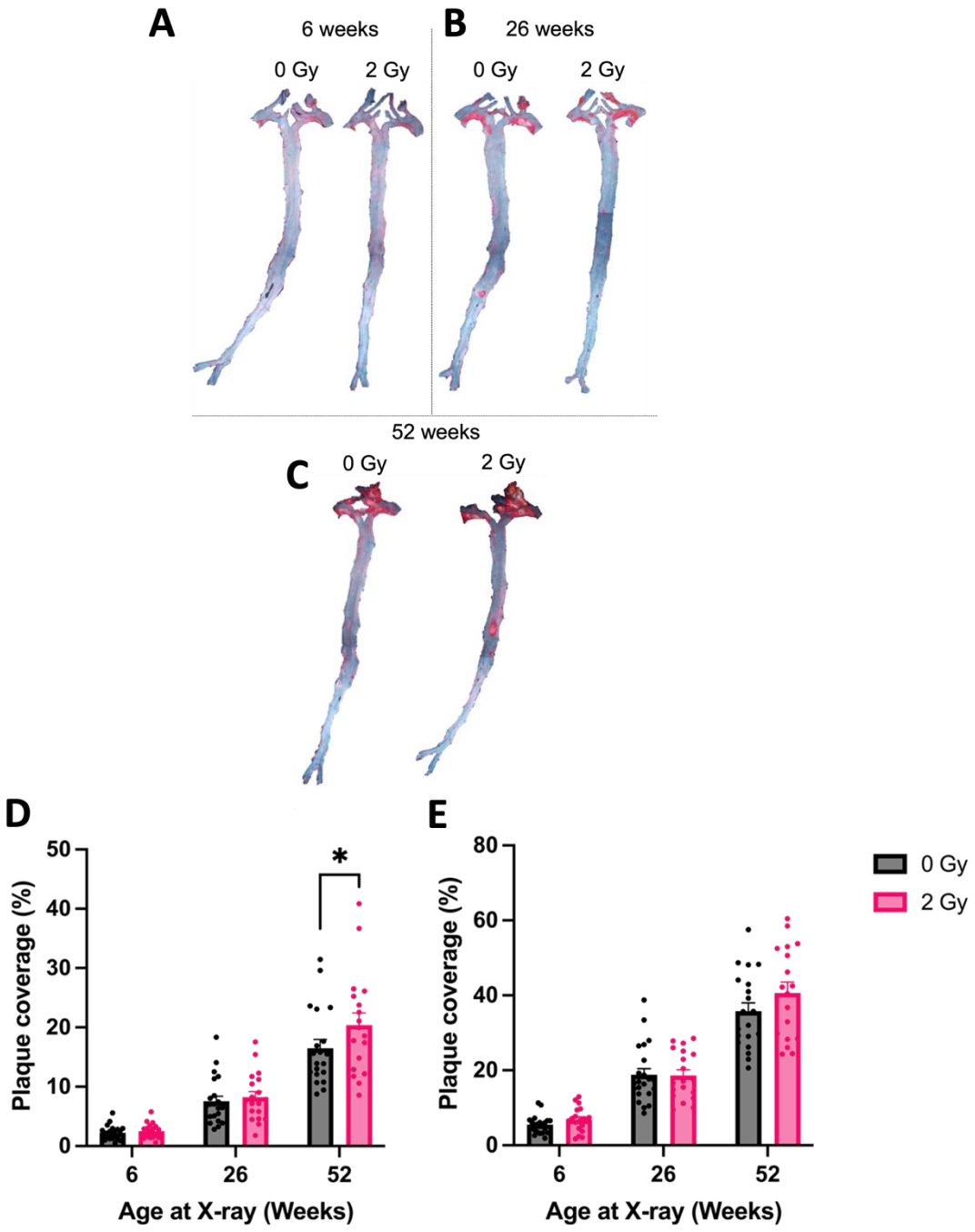


Figure 4.4. Quantification of Ldlr$^{-/-}$ mouse aortic plaque coverage after X-ray exposure.

Ldlr$^{-/-}$ mice were irradiated with 0 or 2 Gy X-ray at 6, 22, or 52-weeks, with aortas harvested and stained with Oil red O 6-months post irradiation. Representative examples of staining of aortas from mice irradiated at 6-weeks (**A**), 26-weeks (**B**), and 52-weeks (**C**). Percentage plaque coverage was determined in Image J for the

whole aorta **(D)** and aortic archI**).** N=18-22, Two-way ANOVA with multiple comparisons, * = $p<0.05$.

4.3.2.2 Female $Ldlr^{-/-}$ mice are more susceptible to IR-induced aortic plaque formation

When investigating if sex influenced the response to IR in this model, the female mice irradiated at 52-weeks had significantly greater plaque coverage in both the whole aorta (Figure 4.5A) and aortic arch (Figure 4.5C) compared to age-matched control. With no significant differences observed within the male mice at any age of irradiation, in both the whole aorta (Figure 4.5B) and aortic arch (Figure 4.5D). This contradicts my previous observations within the $ApoE^{-/-}$ mice, where only the irradiated males had a significant increase in plaque development (Section 4.3.1.3). This suggest that the genetic modifications within these mouse models may influence the sex-associated sensitivity of the mice to IR-CVD. This provides an interesting avenue for future research into potential mechanisms behind why this might be.

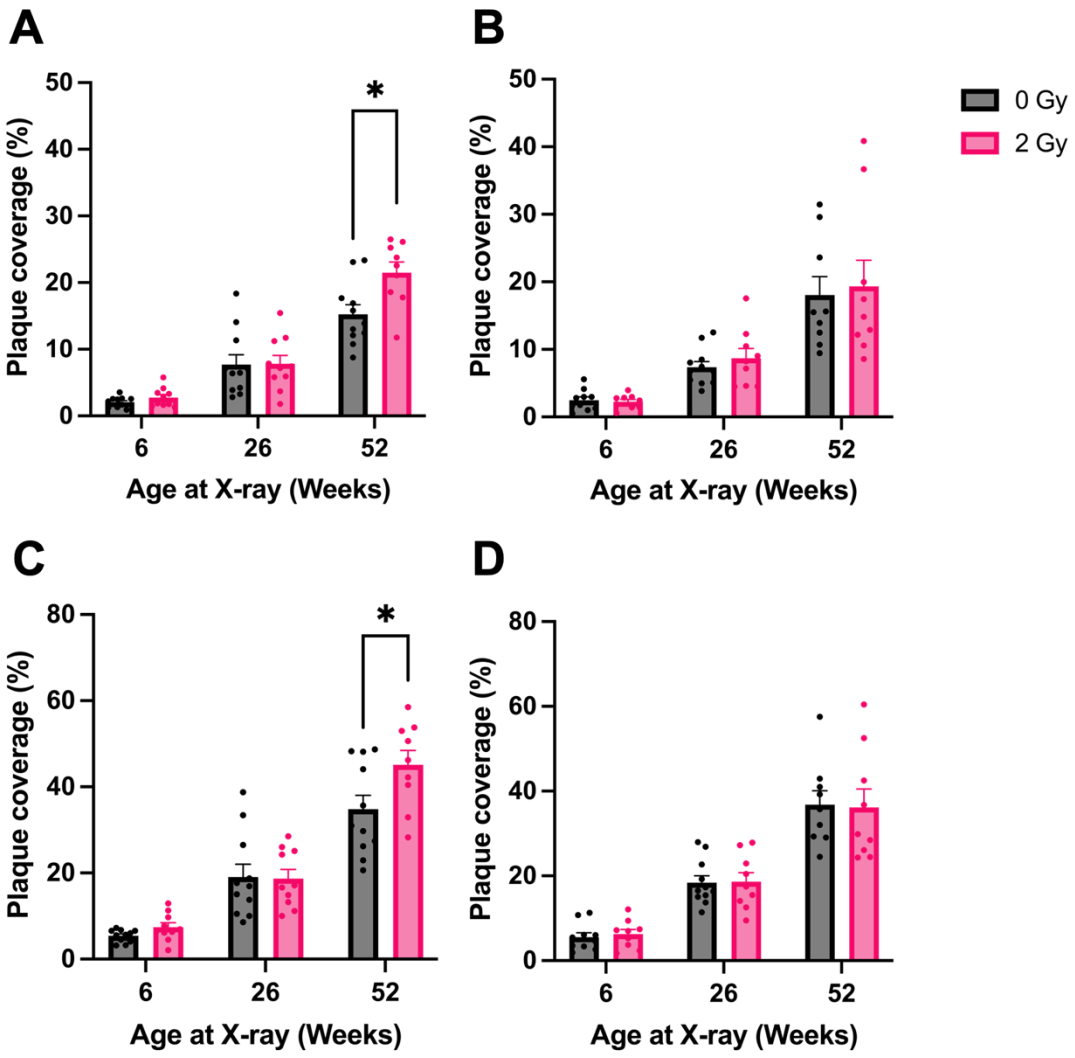


Figure 4.5 Quantification of plaque coverage after X-ray exposure at varying ages within male and female Ldlr$^{-/-}$ mice.

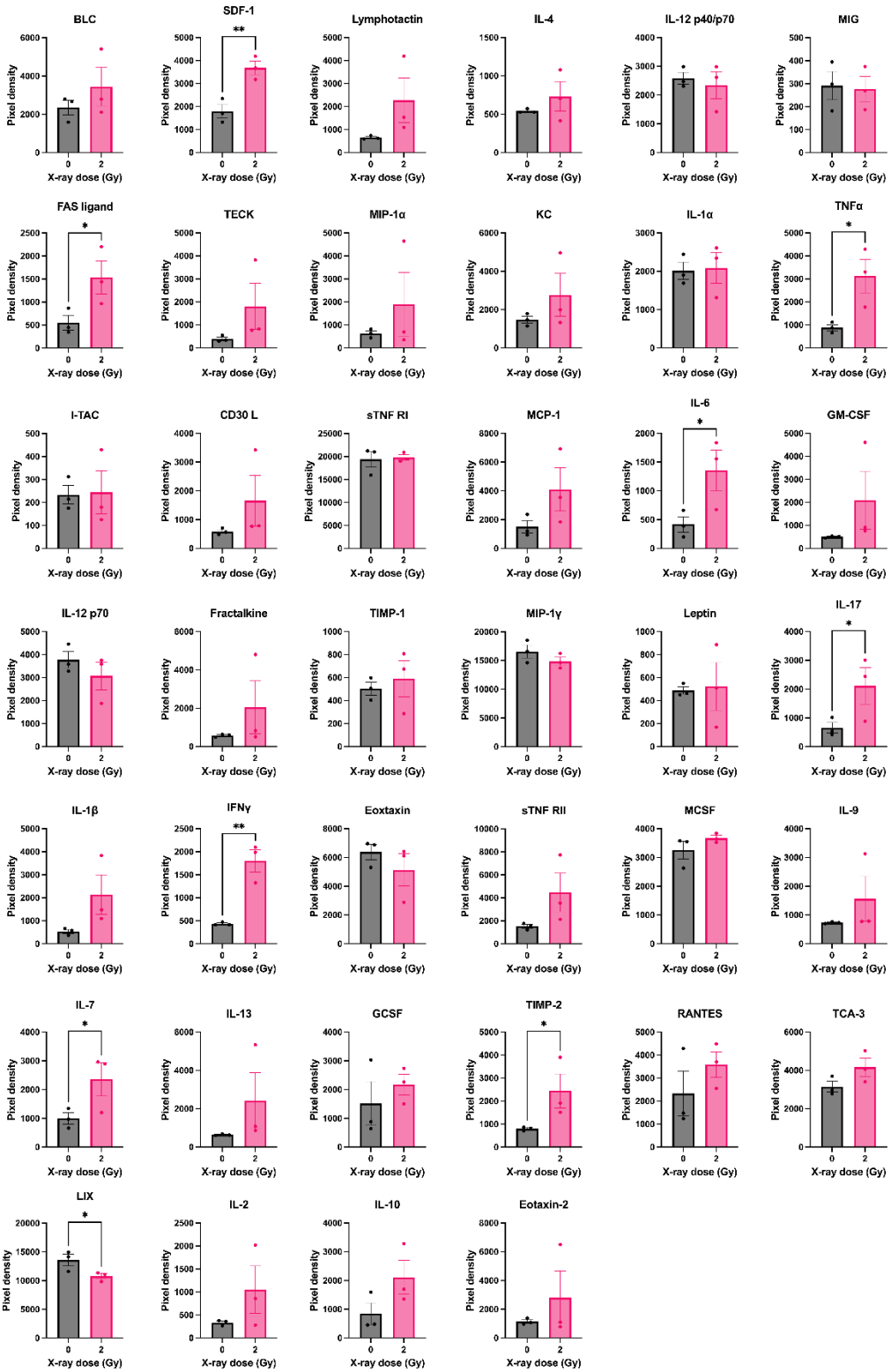
The analysis of X-ray induced plaque development in Ldlr$^{-/-}$ mice irradiated at 6-weeks, 26-weeks, or 52-weeks of age, compared to age matched controls from Figure 4.4, split by sex, with the percentage plaque coverage in across the aorta for female (**A**) and male mice (**B**), along with isolated analysis of the aortic arch in the female (**C**) and males (**D**) displayed. Mice were euthanised 5 months after irradiation. N=9-12, Two-way ANOVA with multiple comparisons, * = $p<0.05$.

4.3.2.3 Analysis of Ldlr$^{-/-}$ mouse circulating cytokines after X-ray

As atherosclerosis is an inflammatory condition, the immune response to IR may influence its development. To investigate any changes in inflammatory markers, I used mouse-specific cytokine arrays on whole blood from the mice 6 months after exposure to 2 Gy X-ray (Figure 4.6). Due to the costs associated with the arrays, I chose to only investigate the female mice in the oldest age group (52-weeks old at irradiation). These were selected as there was a significant difference in atherosclerotic plaque development between the irradiated and non-irradiated mice. Furthermore, previous studies have identified an inflammatory component of IR-CVD in ApoE$^{-/-}$ mice (Stewart *et al.*, 2006; Hoving *et al.*, 2008), therefore, assessing the cytokines within the irradiated Ldl$^{-/-}$ model will help to characterise their use for radiation research.

To assess the circulating cytokines within the Ldlr$^{-/-}$ mice, blood was collected in EDTA vacutainer tuber via cardiac punction at the time of euthanasia (6-months post irradiation). Whole blood was then diluted 1:5 to a final volume of 1 mL using the supplied blocking buffer, and incubated on the cytokine membrane for 2-hours at RT. After wash steps, antibody incubation, and application of the supplied chemiluminescence buffer, cytokine membranes were imaged using the BioRad ChemiDoc. The intensities of each cytokine were then determined using Image J, and interblot normalisation performed using the positive controls. Representative cytokine membranes for 0 and 2 Gy exposures are displayed (Figure 4.6A).

Out of the 40 cytokines that were detected, 8 were significantly upregulated 6 months after 2 Gy exposure (SDF-1, FAS Ligand, TNFα, IL-6, IL-17, IFNγ, and TIMP-2) with one, LIX, significantly downregulated


BLC
SDF-1
Lymphotactin
IL-4
IL-12 p40/p70
MIG
FAS ligand
TECK
MIP-1α
KC
IL-1α
TNFα
I-TAC
CD30 L
sTNF RI
MCP-1
IL-6
GM-CSF
IL-12 p70
Fractalkine
TIMP-1
MIP-1γ
Leptin
IL-17
IL-1β
IFNγ
Eoxtaxin
sTNF RII
MCSF
IL-9
IL-7
IL-13
GCSF
TIMP-2
RANTES
TCA-3
LIX
IL-2
IL-10
Eotaxin-2
Pixel density
X-ray dose (Gy)
0
2
*
**

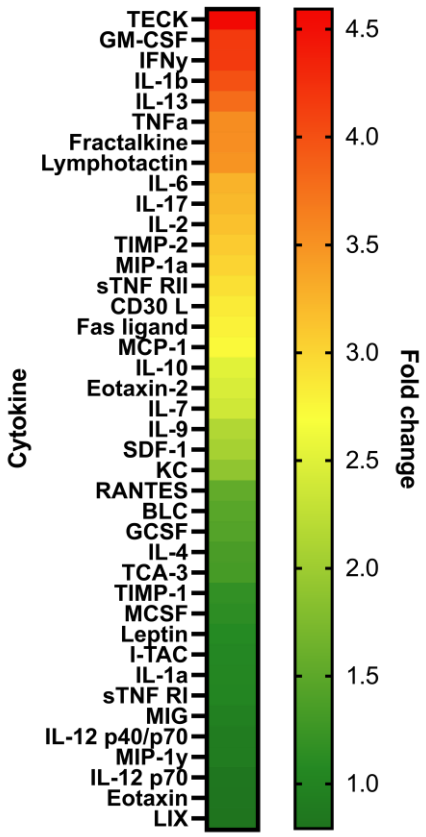
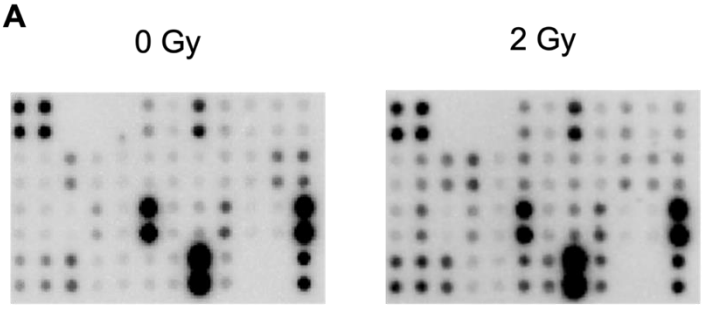


Figure 4.6). While not significant, many showed a trend of an increase after exposure (BLC, Lymphotactin, IL-4, TECK, MIP-1α, KC, CD30 L, MCP-1, GM-CSF, Fractalkine, IL-1β, sTNF RII, MCSF, IL-9, IL-13, GCSF, RANTES, TCA-3, IL-2, IL-10, and Eotaxin-2). When interpreting the results by fold change, 21 cytokines out of the 40 investigated had a fold change of >1.5 (Figure 4.6D).

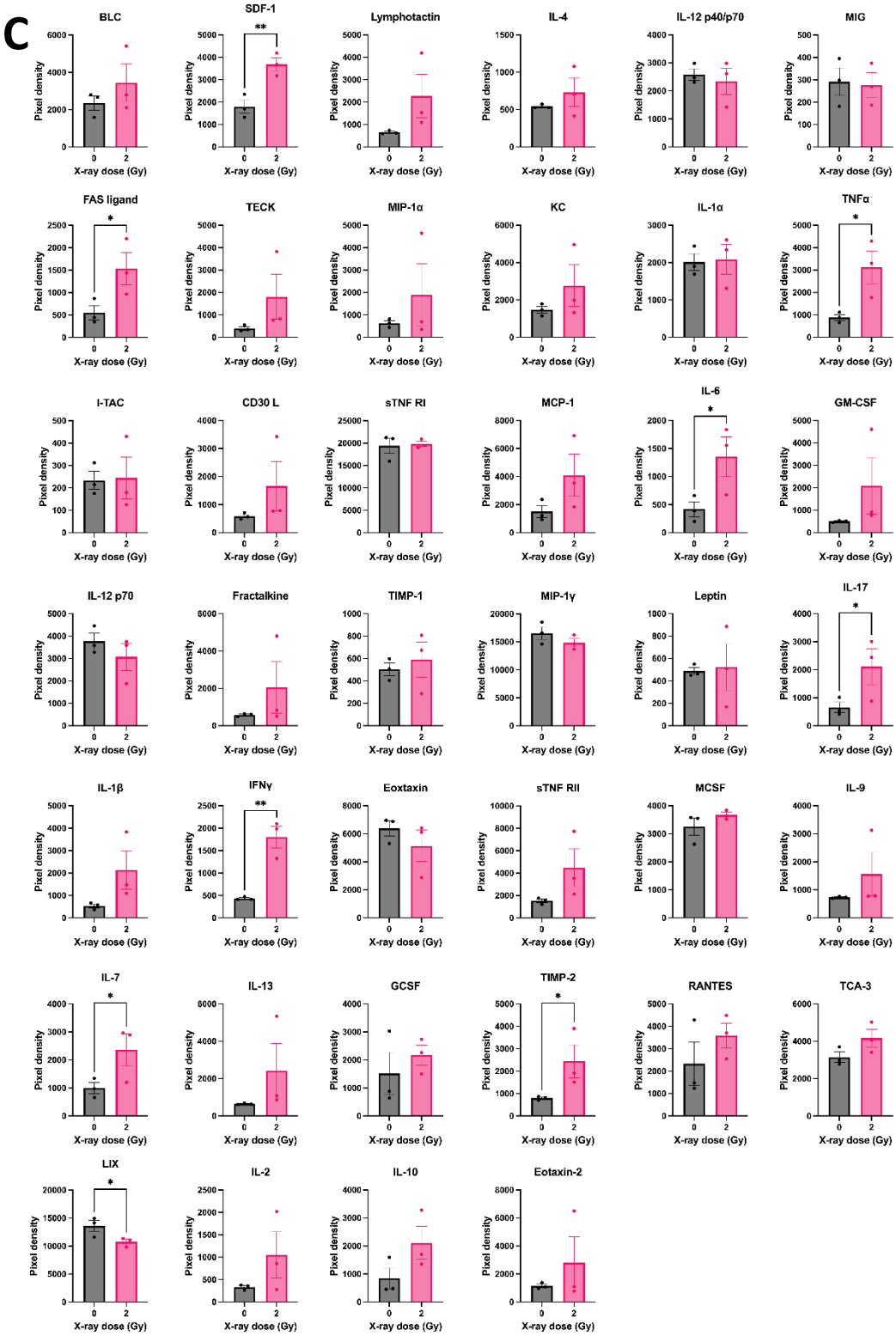
A



B

	A	B	C	D	E	F
1	POS	POS	NEG	NEG	BLANK	BLC
2	POS	POS	NEG	NEG	BLANK	BLC
3	GM-CSF	IFNγ	IL1α	IL-1β	IL-2	IL-7
4	GM-CSF	IFNγ	IL1α	IL-1β	IL-2	IL-7
5	IL-13	IL-17	I-TAC	KC	LEPTIN	LIX
6	IL-13	IL-17	I-TAC	KC	LEPTIN	LIX
7	RANTES	SDF-1	TCA-3	TECK	TIMP-1	TIMP-2
8	RANTES	SDF-1	TCA-3	TECK	TIMP-1	TIMP-2

	G	H	I	J	K	L
1	CD30 L	Eotaxin	Eotaxin-2	Fas Ligand	Fractalkine	GCSF
2	CD30 L	Eotaxin	Eotaxin-2	Fas Ligand	Fractalkine	GCSF
3	IL-4	IL-6	IL-9	IL-10	IL-12 p40/p70	IL-12 p70
4	IL-4	IL-6	IL-9	IL-10	IL-12 p40/p70	IL-12 p70
5	Lymphotactin	MCP-1	MCSF	MIG	MIP-1α	MIP-1γ
6	Lymphotactin	MCP-1	MCSF	MIG	MIP-1α	MIP-1γ
7	TNFα	sTNF RI	sTNF R II	BLANK	BLANK	POS
8	TNFα	sTNF RI	sTNF R II	BLANK	BLANK	POS


C
BLC
SDF-1
Lymphotactin
IL-4
IL-12 p40/p70
MIG
FAS ligand
TECK
MIP-1α
KC
IL-1α
TNFα
I-TAC
CD30 L
sTNF RI
MCP-1
IL-6
GM-CSF
IL-12 p70
Fractalkine
TIMP-1
MIP-1γ
Leptin
IL-17
IL-1β
IFNγ
Eoxtaxin
sTNF RII
MCSF
IL-9
IL-7
IL-13
GCSF
TIMP-2
RANTES
TCA-3
LIX
IL-2
IL-10
Eotaxin-2
Pixel density
X-ray dose (Gy)

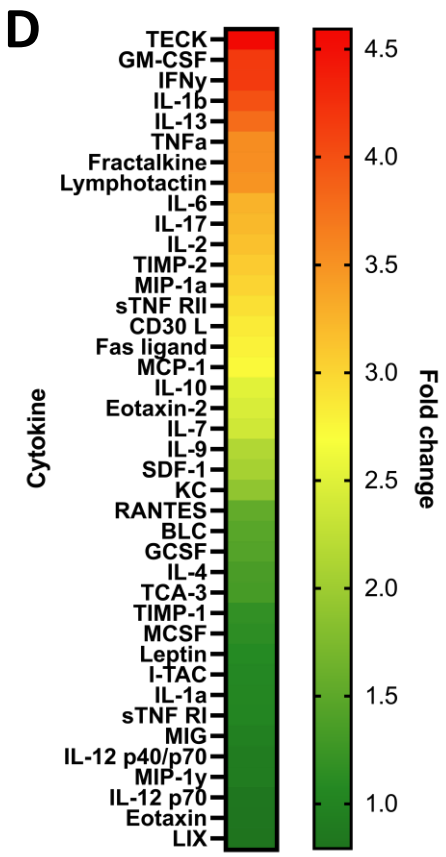


Figure 4.6. Circulating cytokines from Ldlr$^{-/-}$ mouse whole blood after X-ray exposure.

Cytokines detected in whole blood 6-months post 0 Gy or 2 Gy X-ray in female Ldlr$^{-/-}$ mice irradiated at 52-weeks of age. **A)** Representative cytokine blots for 0 (left) and 2 Gy (right) exposure groups. **B)** Map of cytokine positions on the blot. **C)** Semi-quantitative anlysis of cytokine levels in whole blood from Ldlr$^{-/-}$ female mice, 6-months after 2 Gy X-ray exsposure at 52-weeks of age. **D)** Fold change in cytokines detected after 10 Gy X-ray exposure, compared to control. N=3, unpaired T-test, * = $p<0.05$, ** = $p<0.01$. .

4.4 Discussion

In this chapter, I have demonstrated that age-modulates the development IR-CVD within both ApoE$^{-/-}$ and Ldlr$^{-/-}$ mice, with mice irradiated at an older age displaying increased atherosclerotic plaque coverage. Furthermore, I have demonstrated that this effect is sex-dependant, with IR-CVD only observed in the older male ApoE$^{-/-}$ mice and conversely in the older female Ldlr$^{-/-}$ mice. In addition, I have demonstrated IR-associated increases in circulating blood within the irradiated female Ldlr$^{-/-}$ mice.

4.4.1 Age modulated IR-CVD in ApoE$^{-/-}$ and Ldlr$^{-/-}$ mice

Atherosclerosis is the primary form of CVD (Ference *et al.*, 2017), with the plaques detected within the aortas of the ApoE$^{-/-}$ and Ldlr$^{-/-}$ mice representing the development of this condition (Véniant, Withycombe and Young, 2001a). The results in this chapter demonstrate that within the population studies here, older ApoE$^{-/-}$ and Ldlr$^{-/-}$ mice are susceptible to IR-CVD, and not younger mice. These results go against the hypothesis drawn from epidemiological evidence that suggest those exposed at a younger age are more suspectable to IR-CVD (Little *et al.*, 2012d). There are several reasons why this may be: Firstly, this may indicate that the epidemiological data does not reflect the risk associated with age and the development of IR-CVD. Indeed, a study such as this may not be able to account for all lifestyle factors surround the development of CVD. Secondly, the results may indicate that a mouse model for IR-CVD is not comparable to the development of IR-CVD within humans. While there are other animal models that have been used to study IR-CVD that have more relevant cardiac physiology, such as

rabbits and non-human primates, the ethical implication of higher order animals such as these should be carefully weighted.

Additionally, while there may be a greater increase in senescent endothelial cells lining the aorta in the younger mice, immune clearance of senescent cells may be more efficient in the younger mice compared to the older ones (Larissa G.P. Langhi Prata *et al.*, 2018; Song, An and Zou, 2020). In this regard, it is also essential to consider the implications of whole-body irradiation, which these mice were subjected to. This would mean that immune cell-producing tissues such as bone marrow will also have been irradiated, which could induce apoptosis or senescence within these cells, impacting both the development of atherosclerosis and immune clearance of senescent cells within the vasculature (Green and Rubin, 2014; Larissa G.P.Langhi Prata *et al.*, 2018).

When investigating the circulating proinflammatory cytokine profile of the $Ldlr^{-/-}$ mice 6 months after irradiation, 9 cytokines were significantly different after irradiation. Many of these have been implicated in atherosclerosis and CVD. Stromal cell-derived factor-1 (SDF-1) is associated with heart failure and all-cause mortality in humans (Subramanian *et al.*, 2014), along with evidence suggesting it is associated with platelet activation and atherogenesis (Qin, Liu and Lin, 2015; Marcos-Jubilar *et al.*, 2021). Fas ligand triggers apoptosis in cells with the Fas receptor, and literature suggests that it may prevent the progression of atherosclerotic lesions. However, there are suggestions that within mouse models of atherosclerosis, endothelial cells may become sensitive to Fas ligand, and so have increased apoptotic cell death, leading to endothelial cell dysfunction, which promotes atherogenesis (Yang *et al.*, 2004; Zadelaar *et al.*, 2005).

TNFα has been shown to stimulate atherosclerotic lesion formation, along with promoting necrosis, with inhibition demonstrated to reduce the formation of atherosclerotic plaques within mouse models of CVD (Brånén *et al.*, 2004; Boesten *et al.*, 2005). IL-6 is commonly used as a marker of SASP and has been shown to reduce the development of atherosclerotic plaques within mouse models of CVD (Huber *et al.*, 1999; Li *et al.*, 2012), and IL-7 have been shown to increase recruitment of monocytes into the endothelium (Li *et al.*, 2012), suggesting the increases in these circulating cytokines may be related to senescence, along with an inflammatory state within the mice. IFNγ has been shown to have effects on the plasma lipoproteins along with the arterial walls, promoting the progression of atherosclerosis (Gupta *et al.*, 1997). LIX (CXCL5), which was significantly downregulated in the blood of mice that had been irradiated compared to control, has been suggested as protective against atherosclerosis by regulation of foam cell formation (Rousselle *et al.*, 2013).

5 Investigation into the atherogenic effect of X-irradiation on human coronary artery endothelial cells from donors of varying age

5.1 Introduction

Endothelial cells (ECs) line the luminal side of blood vessels and play a vital role in maintaining vascular and whole-body homeostasis (Ueno *et al.*, 2017; Pi, Xie and Patterson, 2018). These cells maintain a physical barrier between the circulating blood and the tissues being supplied, locally control blood pressure, and when appropriate, drive angiogenesis. Furthermore, ECs display varying expression profiles and responses to stimuli depending on their vessel origin; therefore, it is important to use ECs that have the most closely related phenotype to the area of investigation (Lakota *et al.*, 2007a). For investigating human CVD, with a predominant focus on atherosclerosis, human coronary artery endothelial cells (HCAECs) that are found within the coronary arteries are the most relevant.

HCAECs are situated close to vascular smooth muscle cells (VSMCs), which in response to mechanical and chemical stimuli, will contract or relax, enabling control of vessel diameter. Between these two cell types is the sub-endothelial space which consists of

collagen and glycosaminoglycans (Figure 1.1). The initial stages of atherosclerosis involve the movement of lipids and immune cells into the subendothelial space, where accumulated lipids subsequently become engulfed by monocyte-derived macrophages. These lipid-laden monocytes become foam cells which form the fatty core of atherosclerotic plaques (Björkegren and Lusis, 2022). This process is often exacerbated by damage and altered junctional protein expression (e.g., occluding and claudin-5), increased chemoattractant secretion (e.g., MCP-1 and CXCL1), and increased presentation of cell surface adhesion molecules (e.g., ICAM-1 and VCAM-1) (Pober and Sessa, 2007), characteristics similar to cells that are senescent (Krouwer *et al.*, 2012a).

DNA damage, including that driven by ionising radiation (IR) is a known driver of cell senescence (discussed in section 1.5.3.3), hence it is unsurprising that exposure of ECs to IR induces senescence *in vitro*, suggesting that exposure of human coronary vasculature to IR may cause an increase in the senescent EC population, subsequently increasing the risk of developing atherosclerosis (Wang, Boerma and Zhou, 2016). Therefore, the hypothesis is that the increased accumulation of senescent ECs after radiation exposure contributes to IR-induced CVD (IR-CVD). Importantly, the HCAECs used within this thesis are immortalised with the active sub-unit of human telomerase (hTERT), limiting the induction of replicative senescence (RS). This helps to strengthen the associations made between IR-induced senescence (rather than RS) and development of the atherogenic phenotypes investigated within this chapter. Furthermore, epidemiological data suggests that younger people are more susceptible to IR-induced CVD than older adults (Little *et al.*, 2012b). It is therefore important to

understand how chronological age impacts on the cellular changes in ECs following IR exposure.

5.2 Chapter aims

In this chapter, I investigate the following questions:

1. Does the age of HCAEC donors influence intrinsic atherogenic phenotypes *in vitro*?
2. Does donor age modulate IR-induced atherogenic phenotypes in HCAECs?
3. Can the effects of IR be ameliorated pharmacologically?

5.3 Results

5.3.1 Characterisation of HCAEC

While sharing many common features of endothelial cells, human coronary artery endothelial cells (HCAECs) also show features specific to their role in the coronary artery. For example, HCAECs shower greater upregulation of IL-6 in response to IL-1 than human microvascular endothelial cells (Sodin-Semrl *et al.*, 2009). Furthermore, compared to ECs removed from the human umbilical vein (HUVECs), HCAECs display increased presentation of adhesion molecules (e.g. VCAM-1, E-selectin) in response to serum amyloid (Lakota *et al.*, 2007b). This demonstrates the importance of using an endothelial cell line with its origins from the tissue most closely related to the study

area. Hence, HCAECs are likely to represent the best cell model to study atherosclerosis in coronary artery disease.

While HCAECs are therefore a relevant cell line to study, it was necessary to establish that when grown in 2D monoculture, they represent physiological EC behaviour. HCAEC were therefore seeded at 25,000 cells/ cm^2 on fibronectin-coated plastic 24-well tissue culture plates and cultured to confluence. From Figure 5.1, it can be overserved that the cells form a monolayer and are in direct contact with neighbouring cells, creating a barrier between the media and subendothelial space.

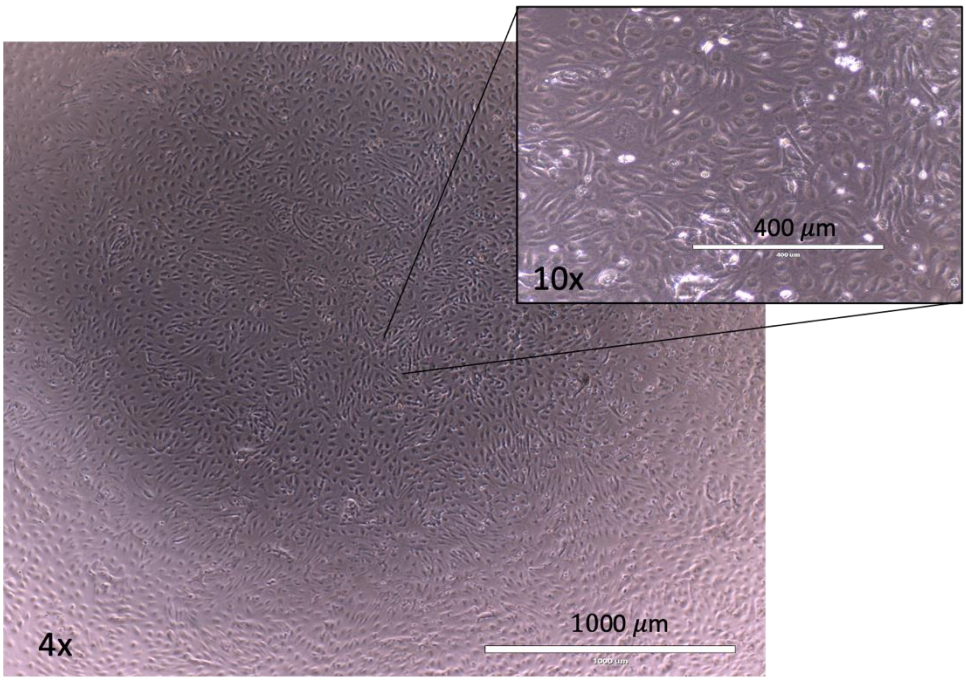


Figure 5.1 Phase contrast images of HCAEC cultured in vitro.

HCAECs were seeded at 25,000 cells/ cm^2 in 24-well plates and cultured for 2-4 days until confluent. Phase contrast images of HCAEC monolayer at 4x and 10x magnification are displayed. Scale, 4x = 1000 μm, 10x 400 μm. n=3 technical replicates.

While culturing cells *in vitro* enables investigation that may not otherwise be possible, it is important to remember the stark differences between a monolayer *in vitro* and the complex environment in which such cells exist in the body, particularly the mechanical stress caused by blood flow within the arteries. To investigate how the morphology of HCAECs may differ under flow conditions compared to the traditional static culture conditions, HCAECs were seeded onto fibronectin-coated coverslips in 4-well plates. To simulate flow conditions, the plates were incubated on an orbital rotator (rotating at 30 RPM) for 5 days, which caused the culture media to circulate within the wells, simulating flow. A control plate was maintained under static incubation conditions. Under

simulated flow conditions, the cells have an elongated morphology and appear to be less tightly packed together compared to the static culture conditions (Figure 5.2).

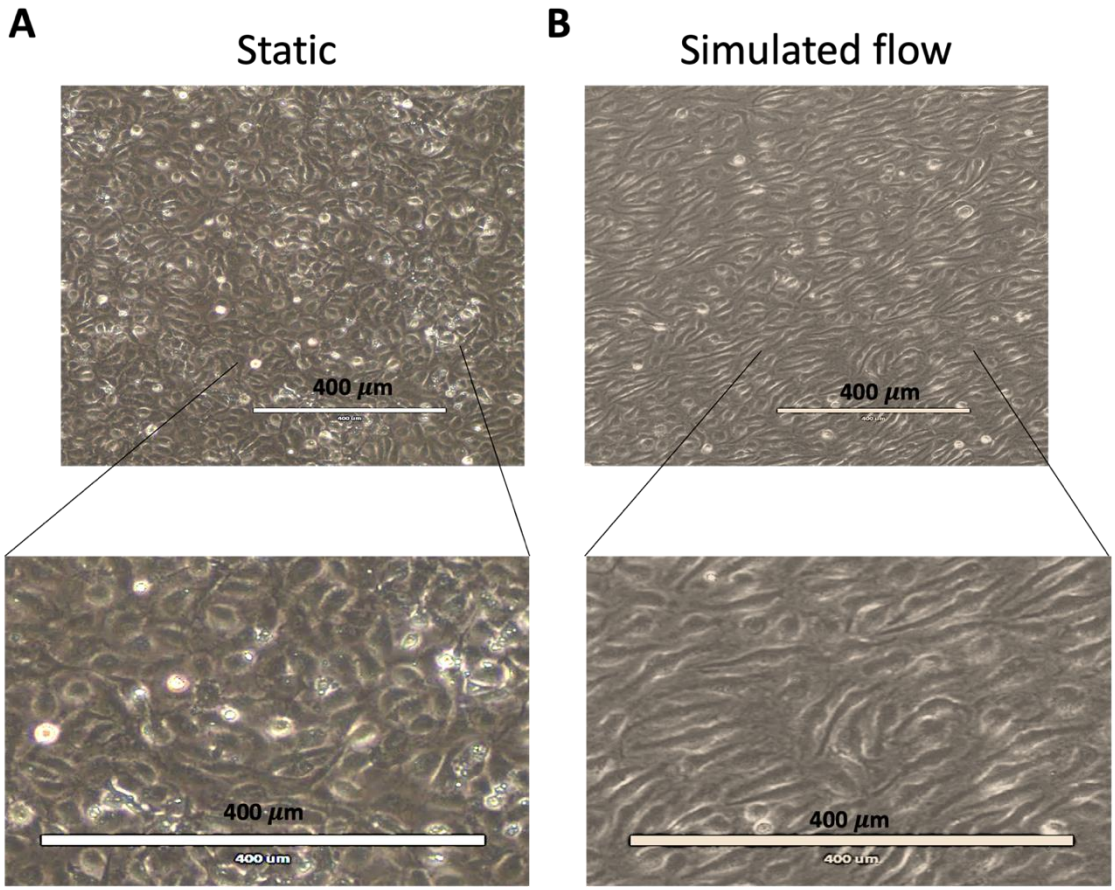


Figure 5.2 HCAEC morphology under static and flow conditions.

HCAECs were seeded at 25,000 cells/cm^2 into 4-well plates, on fibronectin-coated coverslips and incubated under static (A) or simulated flow (B) conditions (orbital rotation at 30 RPM) for 5 days, then imaged my phase contrast microscopy. Image scale bars = 400 μm, with enlargement of main image shown. N = 3 technical replicates.

This is further evidenced by immunofluorescent staining for nuclei with DAPI and the junctional protein, VE-cadherin (Figure 5.3). With a higher cell density (greater number

of nuclei within the same area) in the static culture conditions, compared to the flow conditions. Notably, cells under flow had more uniform size and shape as evidenced by VE-cadherin staining. Importantly, in both conditions, VE-cadherin staining indicates that intact monolayers have formed, enabling the barrier function to be tested *in vitro* with or without flow conditions.

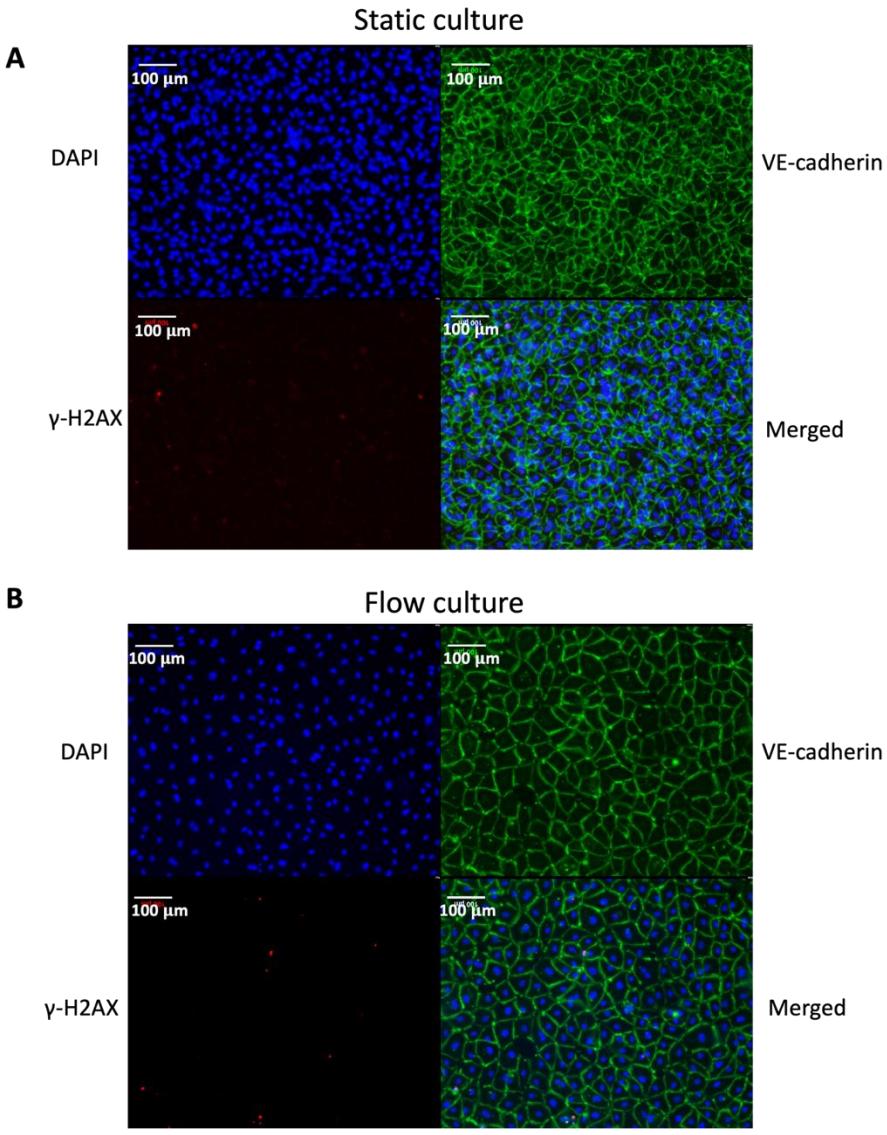


Figure 5.3 Immunofluorescence comparison of HCAEC morphology under static and flow culture conditions.

HCAECs were seeded on fibronectin-coated glass coverslips in 4-well plates at 25,000 cells/cm^2 and cultured for 2-4 days until confluent. Cells were then maintained in normal cell culture conditions (**A**) or under simulated flow conditions (using an orbital rotator at 30 RPM) for 5 days (**B**). Cells were fixed and stained with DAPI for DNA (Blue) and VE-cadherin (Green. mouse primary anti-VE-cadherin antibody, with goat anti-mouse IgG AlexFluor 595). Scale bar = 100 µm. n=3 technical replicates.

5.3.2 Effect of age on *in vitro* HCAEC atherogenic phenotypes

HCAEC monolayer barrier function (e.g., permeability), and adhesion to monocytes, are important properties that influence the development of atherosclerosis, with the attachment of circulating monocytes to the endothelial layer promoting their movement into the sub-endothelial space, and the permeability of the monolayer reflecting potential changes in the movement of both monocytes and lipids through the monolayer (Mazzone *et al.*, 1993; Cuff *et al.*, 2001; Mundi *et al.*, 2018). I therefore established baseline parameters of immortalised HCAECs, including adhesion of monocytes to, and the permeability of, the HCAEC monolayer. I then compare these phenotypes within the two HCAEC donor age groups, young (17-33 years) and middle-aged (48-55 years), with the addition of a fluorometric SA-β-Gal activity assay as an indicator of senescence. Furthermore, I investigate the effect of exposure of the HCAEC monolayers to IR, both within the young and middle-aged groups, with the assays then repeated to investigate how donor age may modulate these effects.

5.3.2.1 Establishing the HCAEC permeability assay

Since the morphological data suggested that cells formed a monolayer, it was important to test whether this provided a functional barrier. Hence, HCAECs were cultured to confluence in transwell insert chambers in 12-well plates. Fluorescent (FITC) dextran of 70 kDa was then added to the culture medium (1 mg/mL), the cells were incubated for 3 hours, and passage of the dextran through the monolayer was monitored in the culture well after removal of the insert containing the cells (see permeability assay, section 2.4.2; schematic, Figure 5.4A). The average amount of dextran that was

detected in the well below the insert was 35 μg/ mL (Figure 5.4B), with the assumption that the dextran would distribute equally throughout the 1 mL of total media in the experiment. If no barrier was in place, the expected value would be 500 μg/ mL. This suggests that the HCAECs do form a functional barrier in this setup.

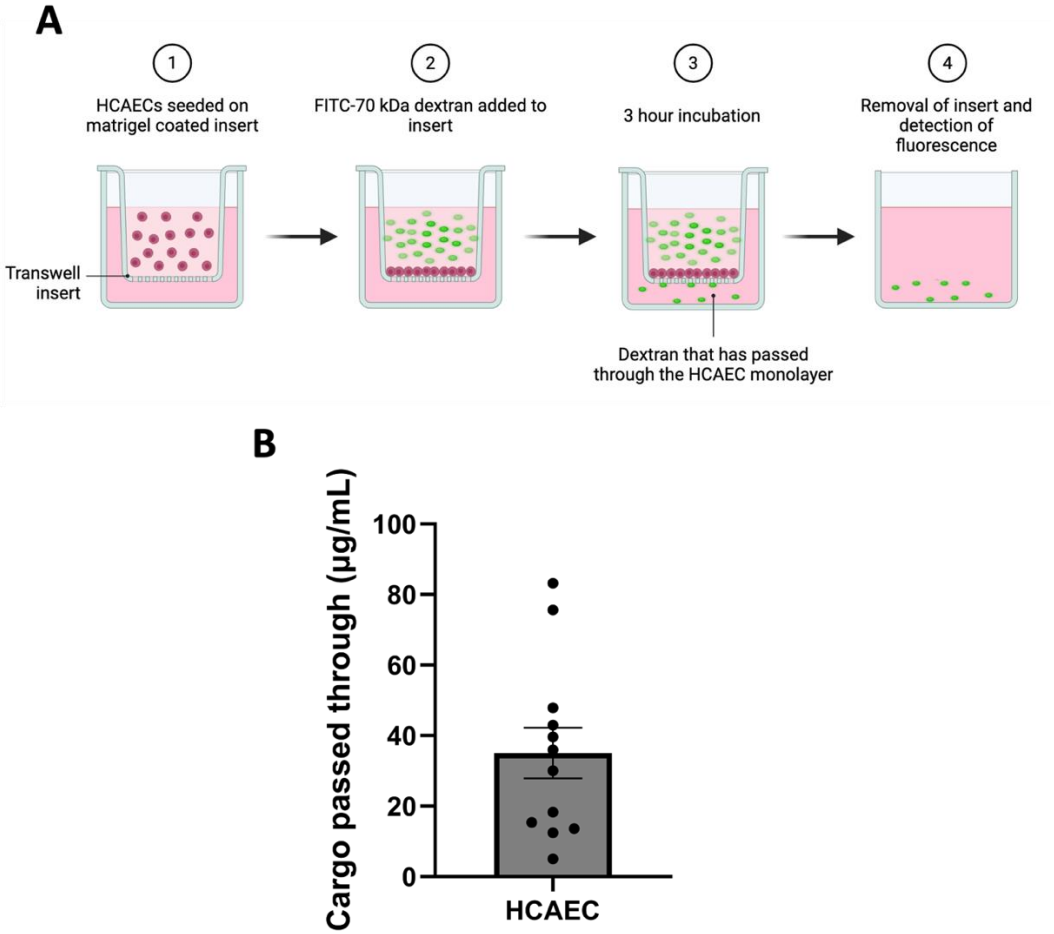


Figure 5.4 Establishing the *in vitro* permeability assay in HCAECs.

HCAECs were seeded in triplicate into diluted matrigel-coated (1:100 in MEC medium) transwell inserts (25,000 cells/ cm^2) and incubated in 12-well plates with 500 µL of MEC medium in each well and insert. Once confluent (2-4 days), 1 mg/mL 70 kDa FITC-dextran in MEC medium was added to the transwell inserts and incubated for 3 hours within the cell culture incubator. Transwell inserts were then removed, and 200 µL from each well below the inserts was pipetted into black-walled 96 well plates, in duplicate, for fluorescence reading on a plate-based spectrophotometer. A standard curve was generate using a dilution series of the stock 1 mg/mL dextran. **A**) schematic overview of the assay (created with biorender.com). **B**) The amount of fluorescent dextran detected below the transwell insert, indicating the amount that has passed through the HCAEC monolayer. N=11, 3 technical replicates.

5.3.2.2 Establishing the HCAEC adhesion assay

To assess the adhesive properties of the HCAEC monolayers, I investigated their adhesion to the monocyte-like cell line, HL60, using an adhesion assay (Lowe and Raj, 2015). Briefly, HCAECs were seeded on fibronectin-coated coverslips, in quadruplicate, within 24-well plates and cultured until confluent. Cell tracker green (CTG) stained HL60s were then added to 3 wells of each donor and incubated for 4 hours. Coverslips were then washed and placed into trypsin, with the digest being analysed for fluorescent HL60s on a spectrophotometer (the 4th coverslip was used to estimate number HCAECs per coverslip). A standard curve was created for the stained HL60s, which combined with the estimated HCAEC number allowed for quantification of the number of HL60s per HCAEC (detailed in section 2.4.1. schematic, Figure 5.5A), presenting a functional measure of HCAEC adhesion. The results indicate an average of 0.5 HL60s per HCAEC, suggesting both that not all HL60s adhere to the HCAEC monolayer and that it is possible to detect the HL60s using this method (Figure 5.5B).

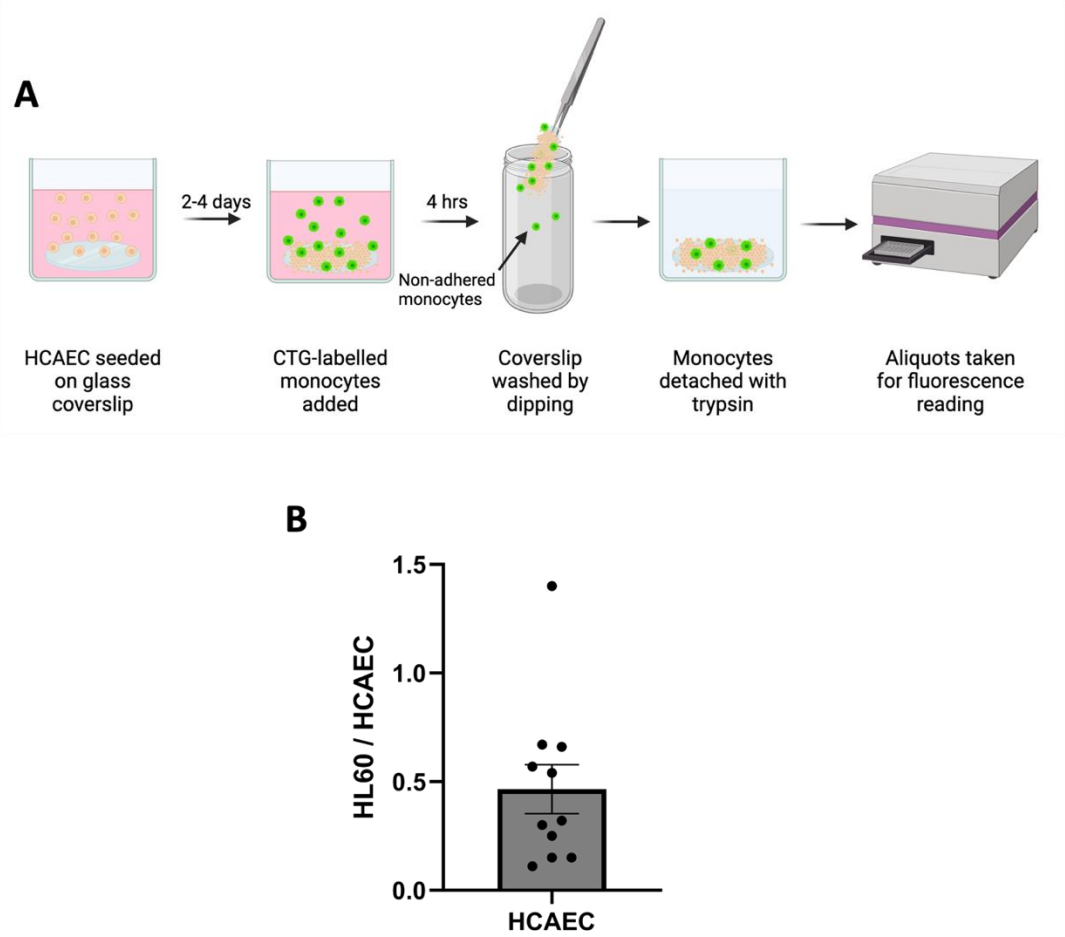


Figure 5.5 HCAEC adhesion to monocytes.

HCAECs were seeded (25,000 cells/ cm^2) onto fibronectin-coated coverslips, in quadruplicate, in 24-well plates. Once confluent (2-4 days), monocytes (HL60) stained with cell tracker green (CTG) were added to at $2x10^6$ cells/ mL and incubated for 4 hours in the cell culture incubator. The coverslips were then removed using fine forceps, washed by dipping into HBSS, and placed into fresh wells containing 250 μL of trypsin. Aliquots were taken from each digestion for detection of the fluorescent monocytes. A standard curve was created of the labelled monocytes to allow quantification. **A)** schematic overview of the assay (created with biorender.com). **B)** Number of monocytes per HCAEC. N=12, 3 technical replicates.

5.3.2.3 Effects of age on HCAEC monolayer permeability

To assess the bassline impact of HCAEC donor age on monolayer permeability, here I repeat the permeability as previously described (section 5.3.2.1), with the analysis performed by splitting the donors into two age groups, young (17-26 years) and middle-aged (48-55 years). Briefly, the HCAEC were seeded into transwell inserts, within 12 well plates and cultured until confluent. 70 kDa fluorescent dextran was then added to the transwells containing the HCAEC monolayers, and the amount of dextran that passed through the monolayer after a 3-hour incubation was determined (as detailed in section 2.4.2).

The results of this permeability assay revealed no statistically significant difference between the 2 age groups investigated (Figure 5.6A). However, the average amount of dextran that had passed into the lower well was greater in the younger age group, suggesting that the monolayer formed by the HCAEC from the younger donors may be more permeable. This trend is also overserved in the linear regression, although there is very weak correlation (R^2=0.05. Figure 5.6B).

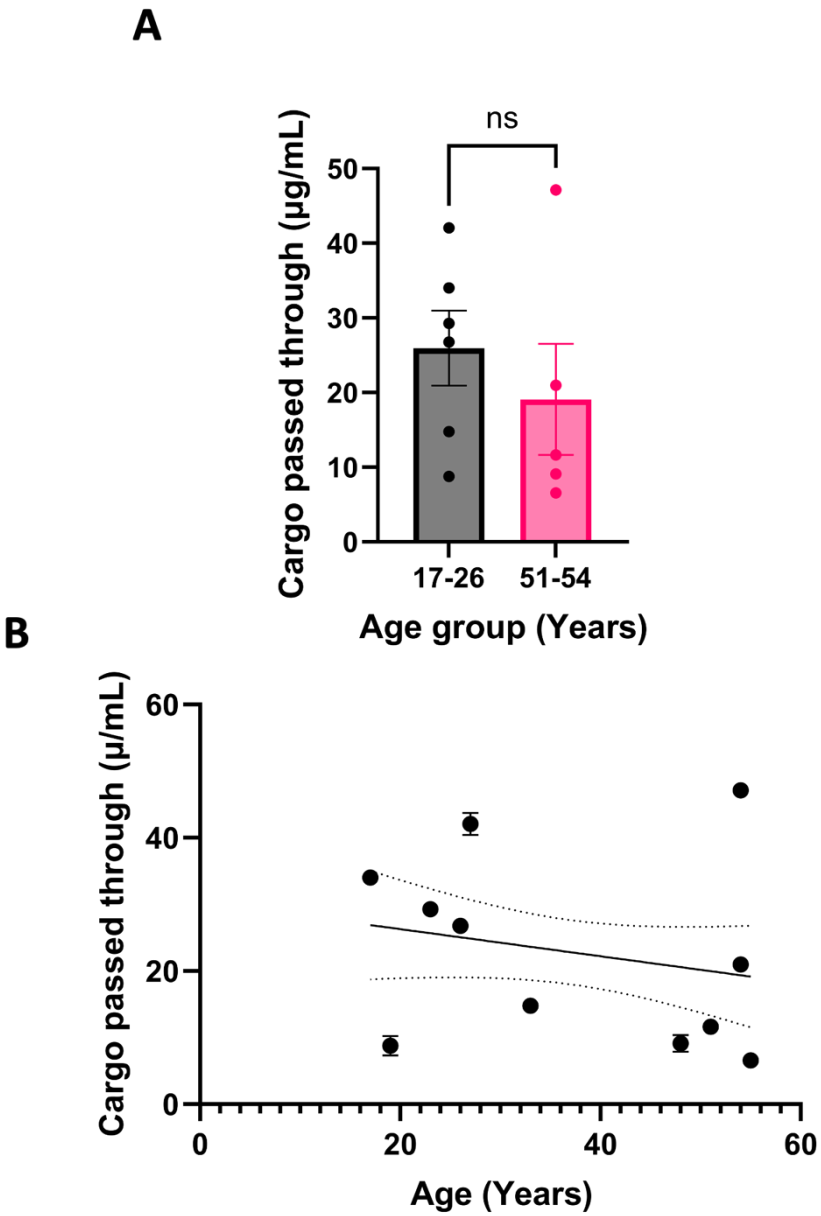


Figure 5.6 Permeability of HCAEC monolayers from donors of varying ages.

The permeability of HCAECs monolayers from donors aged 17-55 years was assessed using the FITC-labelled 70 kDa dextran (permeability assay, section 5.3.2.1). **A)** The average amount of fluorescent dextran detected in the well below the HCAEC monolayers for the two age groups, young (17-33 years old) and middle aged (51-58 years old). N=5-6, in triplicate. Student's t-test, ns = non-significant **B)** linear regression analysis of the movement of dextran across the HCAEC monolayer and donor age. N=3 technical replicates, R^2 = 0.04904

5.3.2.4 Effects of donor age on HCAEC adhesion to monocytes

I next set out to assess the baseline effect of HCAEC donor age on their adhesion. To achieve this, I repeated the adhesion assay (described in section 5.3.2.1), with the HCAECs donors split into two age groups, young (17-33 years), and middle-aged (48-55 years). Briefly, the HCAECs from each donor were seeded in quadruplicate onto fibronectin coated glass coverslips within 24-well plates, using standard cell culture conditions. Once confluent, three HCAEC coverslips were incubated with CTG-stained HL60s, with the spare for HCAEC counting. This enabled the determination of the adhesiveness of the HCAEC monolayers, measured as the number of HL60s/HCAEC.

The results indicated no statistical difference between the number of HL60 cells per HCAEC between the two age groups (Figure 5.7A). However, there was an increase in the mean number of HL60 cells per HCAEC in the middle-aged group, suggesting that HCAEC from middle-aged donors may have increased adhesion. Linear regression analysis supports this, with the trend suggesting that number of HL60 cells adhering to HCAEC increases with the age of the donor (R^2=0.349) (Figure 5.7B).

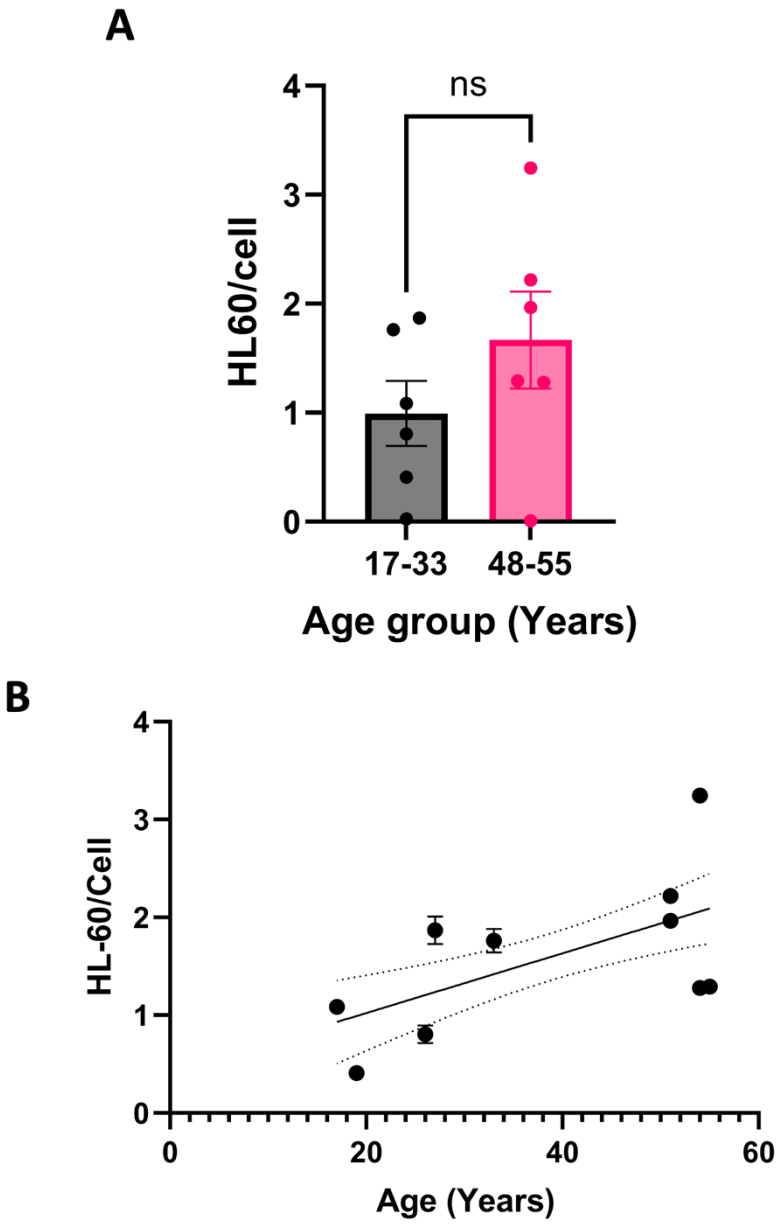


Figure 5.7 Measure of age-related HCAEC adhesion to monocytes.

HCAECs from donors aged 17-55 years were assessed for adhesion to CTG-labelled HL60s (monocyte-like). **A)** Adhesion of HL60s per HCAEC within the young (17-33) and middle-aged groups (48-55). N=6, with each point representing 3 technical replicates. Students t-test, ns = non-significant. **B) L**inear regression analysis of the HCAEC donor age compared to the number of HL60/HCAEC. N=3 technical replicates, R^2 =0.349.

5.3.2.5 Effect of HCAEC age on the SA-β-Gal activity

I next set out to establish the age-related differences in SA-β-Gal activity within the HCAECs from the donors. While not an exclusive marker of cellular senescence, it will hint towards possible changes in lysosomal mass which are observed in ageing and senescence (Kurz *et al.*, 2000). With characteristics of senescent ECs including changes to their barrier function, increases in inflammatory signalling through the SASP, and changes in cell surface adhesion molecules, senescent-like states are likely pro-atherogenic (Bloom *et al.*, 2023a).

To investigate this, HCAECs from each donor, ranging 17-55 years in age, were seeded into 24-well plates, in triplicate. Once confluent, cells were trypsinised, placed into 1.5 mL Eppendorf tubes, and analysed for SA-β-Gal activity by modifying the senescence β-galactosidase staining kit (Cell Signalling Technology #9860) to include fluorescein Di-β-D-galactopyranoside (FDG), which fluoresces when hydrolysed by SA-β-Gal , along with the addition of triton X-100 for cell permeation (complete method in section 2.4.3). To measure the level of fluorescence, 150 µL from each sample was loaded into a black walled 96-well plate and measured on a plate-based spectrophotometer. This enables a detection method that does not require imaging and subsequent processing of images, enabling higher throughput of samples.

When comparing the SA-β-Gal activity in HCAEC from young donors (17-33-years-old) to middle-aged donors (51-54-years-old), there was a statistically significant difference between them, with the middle-aged group having a high level of fluorescence, indicating greater SA-β-Gal activity (Figure 5.8B). This suggest that there is a greater

number of cells within this age group that possess, at least, the increased β-gal activity which is indicative of senescent cells. While this is not conclusive, it suggests that the HCAECs from the middle-aged donors may have a greater basal level of senescence, compared to the younger HCAECs. This is also reflected in the linear regression analysis, demonstrating that there is a trend of increasing β-gal activity with the age of the donor (Figure 5.8C).

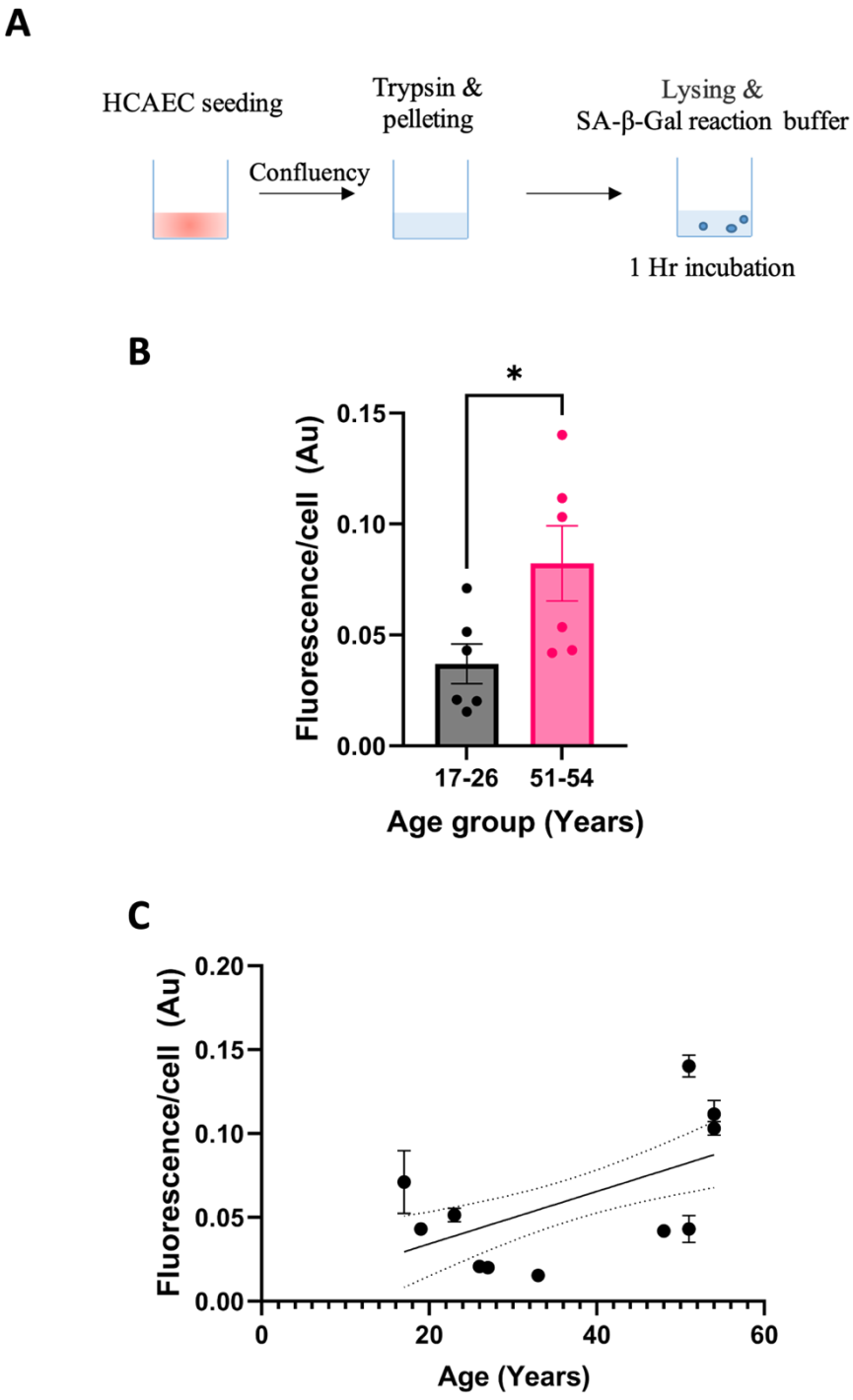


Figure 5.8 SA-β-Gal activity comparison between HCAEC from donors of varying age.

HCAECs from donors aged 17-55 were assessed for SA-β-Gal activity using a fluorescent substrate for β-Gal (detailed in section 2.4.3). The fluorescence was compared to cell count and reported as fluorescence/ HCAEC. Schematic overview given (**A**). To assess the differences in SA-β-Gal activity between HCAEC from young

and middle-aged donors, the results were grouped into age groups, 17-33- and 48-55-years. n= 6, in triplicate. Student's t-test, * = p<0.05 **(B)**. To observe any age-related trends, linear regression analysis was performed. N=3 technical replicates, R^2=0.3002 (**C**).

5.3.3 X-ray dose investigation for HCAEC

In order to investigate the effects of IR on the development of atherogenic phenotypes within HCAECs, identification of a suitable X-ray dose was needed. Previous work has investigated the response of HCAEC to varying X-ray doses (Kabacik and Raj, 2017; Philipp *et al.*, 2017b), both indicating that there is a linear dose-response relationship and that HCAEC are still viable after 10 Gy irradiation. Results published by Lowe and Raj (2014) also demonstrate that with 10 Gy X-ray exposure, these cells begin to display an increase in SA-β-Gal activity from 1 day post X-ray, with clear differences emerging from day 4 onwards.

As senescence is hypothesised to contribute to IR-CVD, I assessed SA-β-Gal activity within the HCAEC after X-ray exposure. The SA-β-Gal assay was performed as previously described (section 2.4.3), with FDG used as a substrate for β-galactosidase, enabling a plate-based fluorescent readout of SA-β-Gal activity. HCAEC from 3-6 donors were seeded into 24-well plates, and irradiated with 0, 2, or 10 Gy X-ray once confluent, with the SA-β-Gal assay performed 7-days after irradiation. The results demonstrate a significant increase in SA-β-Gal activity after 10 Gy X-ray exposure, with no significant difference between 0 or 2 Gy exposures (Figure 5.9). This suggest that at 7 days post X-ray, a 2 Gy exposure dose may not be high enough to induce senescence in all donors.

From this, combined with previous publications, the 10 Gy dose was chosen to investigate the effects of X-ray exposure on the development of atherogenic phenotypes within the HCAEC.

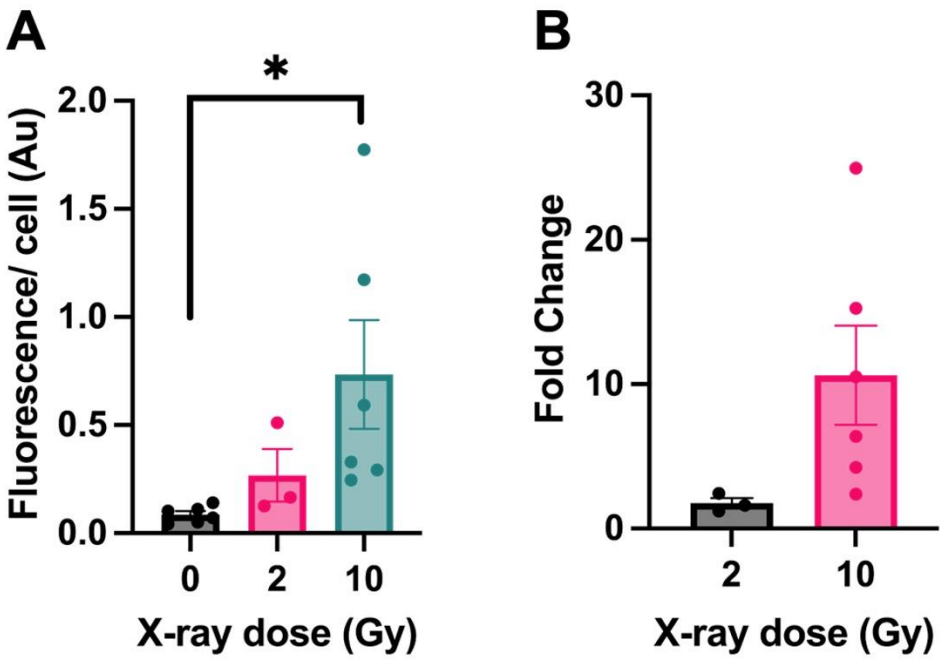


Figure 5.9 HCAEC SA-β-Gal activity after X-ray exposure.

HCAEC from 3-6 donors were seeded in 24-well plates (25,000 cells/cm^2), cultured until confluent (2-4 days), and then exposed to 0, 2, or 10 Gy X-ray. 7 days post irradiation, the SA-β-Gal assay was performed as described (section 2.4.3). **A**) SA-β-Gal activity in HCAEC 7-days post 2 Gy or 10 Gy X-ray exposure. **B**) Fold change in SA-β-Gal activity within the treatment groups. 2 Gy n=3, 0 Gy and 10 Gy n=6. Two-way ANOVA with multiple comparisons, * = $p<0.05$

5.3.4 The atherogenic response of HCAEC to IR from younger donors

After characterising the differences in adhesion, permeability, and SA-β-Gal activity within the HCAECs from young and middle-aged donors (17-33 and 48-55 years,

respectively), along with identifying a suitable X-ray dose, here I begin to investigate the effects of X-ray exposure on the development of the atherogenic phenotypes within HCAEC from young donors. As previously discussed, the adhesion assay will provide insight into the changes in HCAECs associated with their adhesion, particularly to immune cells. In addition, the permeability assay will give an indication of the HCAEC barrier function; increases in these are associated with atherogenesis. Furthermore, as the hypothesis is that the induction of senescence increases the adhesion and the permeability of the HCAEC monolayer, the SA-β-Gal assay was also performed.

5.3.4.1 X-ray induced increases in adhesion to HCAEC from young donors

Firstly, to assess the impact of 10 Gy X-ray exposure on the adhesion of HCAECs, I performed the adhesion assay on donors aged 17-33 years. Briefly, as previously discussed in Figure 5.5, HCAECs were seeded on coverslips and cultured to confluency. They were then exposed to sham or 10 Gy X-ray, and maintained in standard culture conditions for 7 days, with the adhesion assay then performed as previously described.

The results indicate that the exposure of HCAEC from donors aged 17-33 years old to 10 Gy X-ray significantly increased the adhesion of HL-60 cells to the HCAEC monolayer (Figure 5.10A). When comparing the fold change for each individual donor, there are variances between the donors, suggesting that there are individual sensitivities to X-ray induced increases in the adhesion of Hl-60 cells, although no age trend within this range was observed (Figure 5.10B).

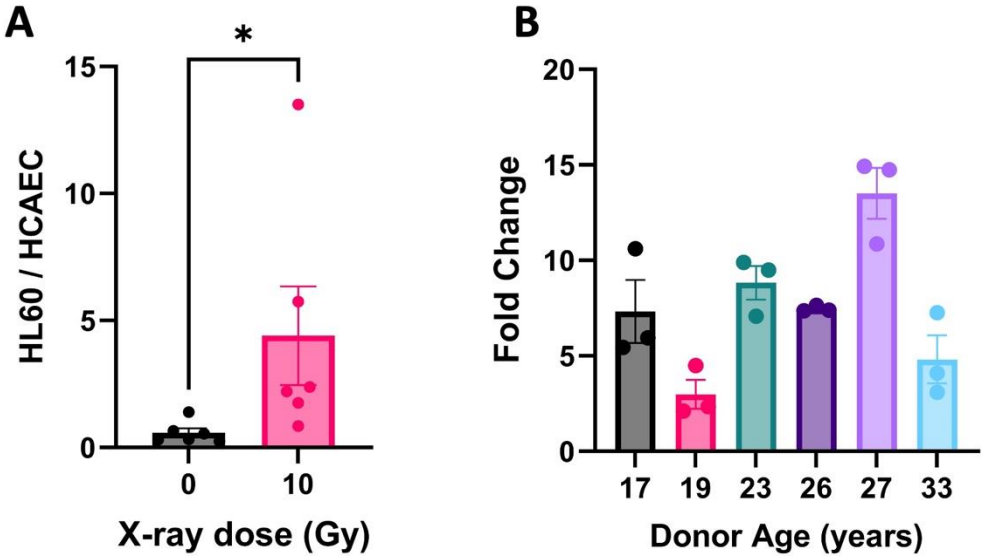


Figure 5.10 X-ray induced increases in HL-60 adhesion to HCAEC from young donors.

HCAECs from young donors were irradiated with 0 or 10 Gy X-ray once confluent. 7-days later, HCAEC adhesion to CTG-labeled HL60s was assessed. **A)** The number of HL-60 per HCAEC from young donors, with either 0 Gy or 10 Gy X-ray exposure. N=6 in triplicate, students one-tailed T-test, * = $p<0.05$. **B)** The fold change per donor after 10 Gy X-ray exposure, compared to control, n=3 technical replicates.

5.3.4.2 X-ray-induced increases in permeability of HCAEC monolayers from young donors

To assess the permeability of the HCAEC monolayers from donors aged 17-33 years, I performed the permeability assay. Briefly, as described in Figure 5.4, HCAECs from the young donors were seeded in transwell inserts and cultured to confluency. They were then exposed to sham or 10 Gy X-ray, and maintained in standard culture conditions, with the permeability assay then performed 7 days post irradiation.

The results indicate a significant increase in the permeability of HCAEC from young donors to 70 KDa dextran after 10 Gy X-ray exposure (Figure 5.11). When comparing

the fold change within each donor after 10 Gy X-ray exposure, 4 out of the 6 donors demonstrated similar changes, with 2 donors displaying greater fold changes in permeability (Figure 5.11B). This could be due to individual sensitivities to radiation exposure, or down to flaws in the transwell inserts in the experiment or damage to the monolayers from X-ray exposure.

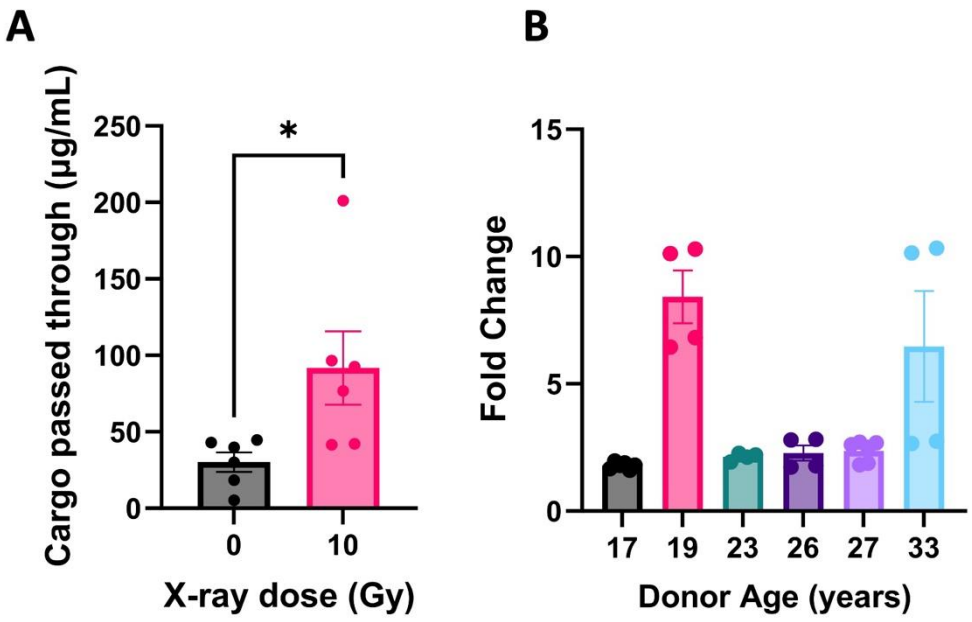


Figure 5.11 X-ray induced increases in the permeability of HCAEC monolayers from young donors.

HCAECs from young donors were irradiated with 0 or 10 Gy X-ray, with the permeability of the HCAEC monolayer assessed 7-days later using FITC-dextran (70 kDa). **A)** The amount of fluorescently labeled 70 KDa dextran that passed through the HCAEC monolayer with either 0 Gy or 10 Gy X-ray exposure. N=6 in triplicate, Students one-tailed T-test, * = $p<0.05$. **B)** The fold change in fluorescent dextran detected in the lower well, per donor after 10 Gy X-ray exposure, compared to control. 4-6 technical replicates.

5.3.4.3 Increases in SA-β-Gal activity in HCAECs from young donors after X-ray exposure

One hypothesis behind the IR-induced atherogenic phenotypes in HCAECs is that the IR is inducing senescence, which can display many of the phenotypes associated with adhesion and permeability, along with being pro-inflammatory (as discussed in section 1.5.2). Due to this, here I use the SA-β-Gal assay to provide insight into the development of senescence within the HCAECs from young donors (aged 17-33 years) 7-days post X-ray exposure.

To accomplish this, I have used the SA-β-Gal detection kit (Cell signalling technologies #9860) modified to use FDG (A substrate for β-gal which fluorescence when hydrolysed) (previously described in Figure 5.8). Briefly, HCAEC from donors aged 17-33 were plated in triplicate, in two separate 24 well plates, allowing for sham exposure and 10 Gy X-ray exposure. 7 days after the exposures, the SA-β-Gal assay was performed (detailed in section 2.4.3), providing fluorescence/HCAEC, indicating SA-β-Gal activity.

The results demonstrate a significant increase in SA-β-Gal activity in HCAEC from young donors after 10 Gy X-ray exposure (Figure 5.12A). While this is not a definitive detection method for senescence, it suggests that 10 Gy X-ray exposure of these cells leads to the induction of senescence. As with the previous assays, there appears to be individual sensitivities to X-ray induced increases in SA-β-Gal activity, ranging from ~1.5 to 5-fold increases (Figure 5.12B**).**

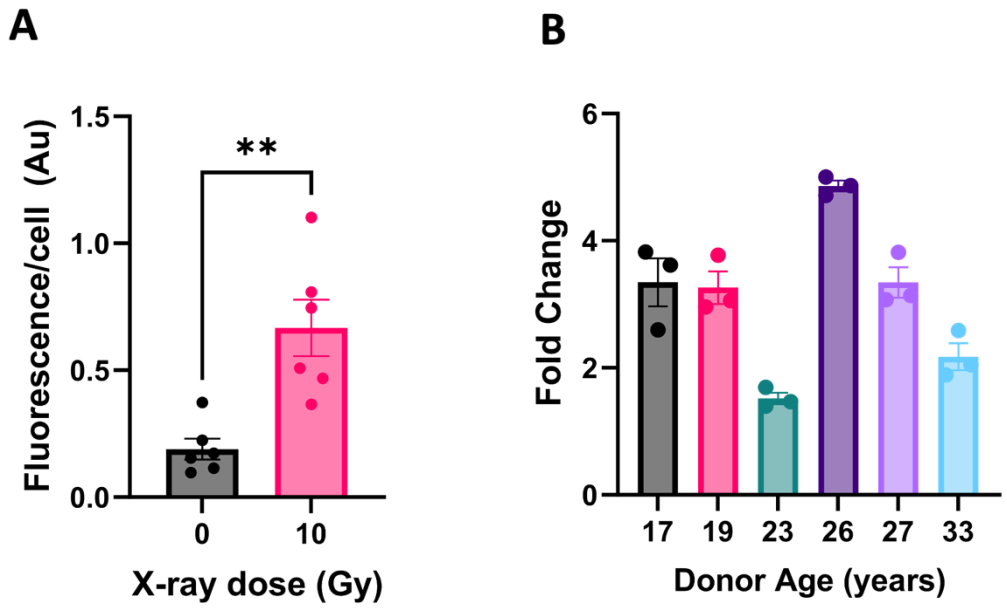


Figure 5.12 X-ray induced increases in SA-β-Gal activity of HCAEC from young donors.

HCAECs from young donors were exposed to 0 or 10 Gy X-ray once confluent. 7-days later, the fluorescent SA-β-Gal assay was performed. **A)**. The fluorescence per HCAEC with 0 or 10 Gy X-ray exposure, indicating SA-β-Gal activity. N=6 in triplicate, Students One-tailed T-test, ** = p<0.005. **B)** The fold change in fluorescence per donor after 10 Gy X-ray exposure compared to control. N=3 technical replicates per donor.

5.3.5 The atherogenic response of HCAEC from middle-aged donors to IR

Following the investigation into the effects of IR on the development of atherogenic phenotypes in HCAECs from young donors, here I again use the adhesion, permeability, and SA-β-Gal assays to investigate how the HCAECs from middle-aged donors (48-55 years) respond to IR exposure. As previously discussed, these assays investigate the adhesion of HCAEC monolayer to monocytes, mimicking the adhesion of circulating monocytes within coronary arteries; The permeability of the HCAEC monolayer using a

passive diffusion agent, mimicking the free movement of circulating lipids and immune cells into the sub-endothelial space; The SA-β-Gal assay provides insight into the potential senescence response to radiation exposure.

5.3.5.1 X-ray induced increases in adhesion of HL-60 cells to HCAEC from middle-aged donors

To investigate the changes in the adhesion of HCAECs from middle-aged donors after X-ray exposure, the adhesion assay was performed as previously described (Figure 5.5). Briefly, HCAECs from the middle-aged donors were seeded on glass coverslips and exposed to 10 Gy X-ray once confluent. 7 days after irradiation, HCAECs were incubated with monocytes (HL-60) stained with cell tracker green, and the number attached to the HCAEC monolater was quantified. The results demonstrate a significant increase in HL-60 adhesion per HCAEC after 10 Gy X-ray exposure, suggesting that X-ray exposure increases pathways associated with either recruitment of HL-60 cells, or the presentation of adhesion molecules associated with their membrane interactions with HCAECs (Figure 5.13A). When comparing the fold change in adhesion within each donor after X-ray exposure, there is variability in the response, suggesting that individual donor sensitivity to IR may affect the overall comparisons (Figure 5.13B).

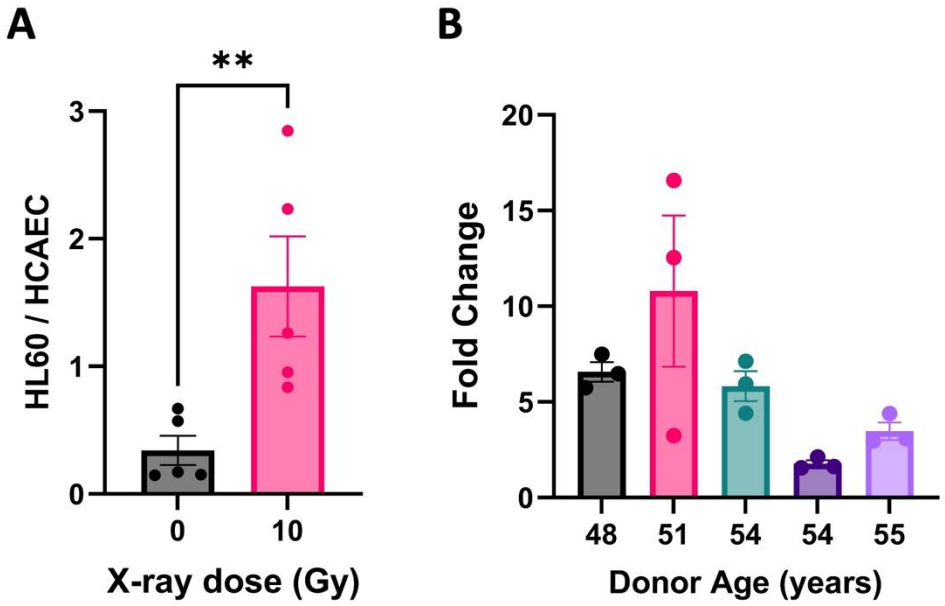


Figure 5.13 X-ray induced increases in HL-60 adhesion to HCAEC from middle-aged donors.

HCAECs from donors **A)** The number of HL-60 cells bound to HCAECs from donors ranging 48-55 years old, with either 0 Gy or 10 Gy X-ray exposure. N=5 in triplicate, Students One-sided T-test, ** = $p<0.005$. **B)** The fold change per donor after 10 Gy X-ray exposure, compared to 0 Gy control. N= 3 technical replicates per donor.

5.3.5.2 X-ray-induced increases in permeability of HCAEC monolayers from middle-aged donors

To investigate the changes in permeability of the HCAEC monolayer created by middle aged donors after IR exposure, the permeability assay was performed as previously described (Figure 5.4). Briefly, this assay involves quantifying the amount of fluorescent

dextran which has passed through confluent HCAEC monolayers 7-days post exposure to 10 Gy X-ray. The results indicate that 7-days after exposure to 10 Gy X-ray, the monolayers formed by the HCAEC from middle-aged donors become more permeable, compared to control (Figure 5.14A). When comparing the fold change between donors, four out of the six demonstrated similar changes in permeability after the X-ray exposure of around a 2-fold increase, with two donors demonstrating roughly a 3.5-fold increase (Figure 5.14B). This suggests that some donors may be more susceptible to IR induced increases in permeability than others.

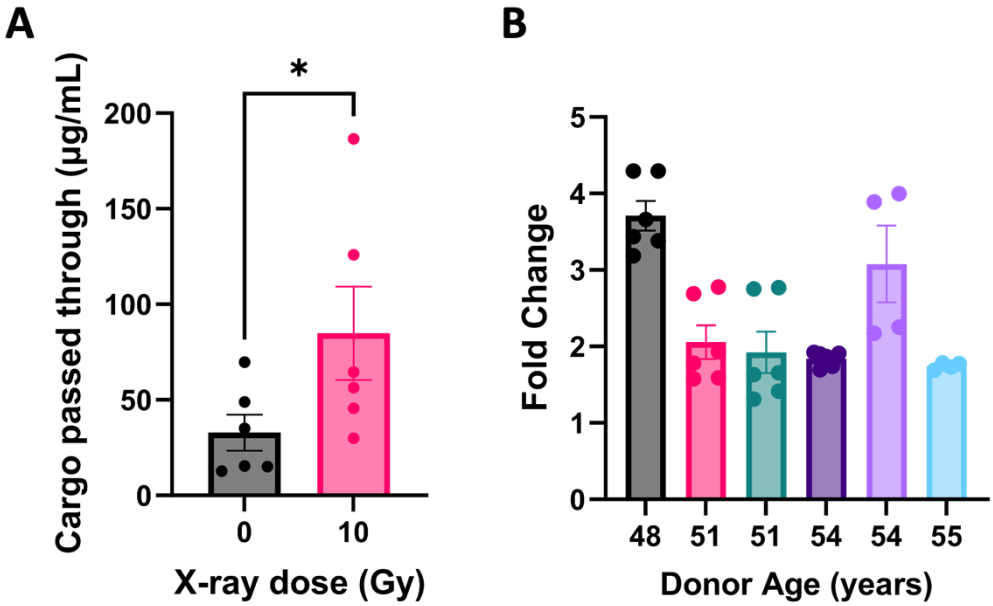


Figure 5.14 X-ray induced increases in the permeability of HCAEC monolayers from middle-aged donors.

HCAECs from middle-aged donors were irradiated with 0 or 10 Gy X-ray, with the permeability of the HCAEC monolayer assessed 7-days later using FITC-dextran (70 kDa). **A)** The amount of fluorescently labeled 70 KDa dextran that passed through the HCAEC monolayer with either 0 Gy or 10 Gy X-ray exposure. N=6 in triplicate, Students one-tailed T-test, * = $p<0.05$. **B)** The fold change in fluorescent dextran detected in the lower well, per donor after 10 Gy X-ray exposure, compared to control. 4-6 technical replicates.

5.3.5.3 Changes in SA-β-Gal activity in HCAECs from middle-aged donors after X-ray exposure

To investigate senescence within HCAECs from middle-aged donors after exposure to IR, I have used SA-β-Gal activity as an indicator, as previously described (section 5.3.2.5). While this is not a conclusive marker, it will provide insight into the potential

induction of senescence within these cells after exposure to IR. To achieve this, I performed the SA-β-Gal assay as previously described for the HCAEC from younger donors (Figure 5.12). Briefly, HCAECs from donors aged 51-55 years were cultured to confluency and exposed to IR in the form of X-ray (10 Gy dose). 7-days post irradiation, the fluorometric SA-β-Gal assay was performed. The results from this assay demonstrated an increase in the mean SA-β-Gal activity per HCAEC from the middle-aged donors. However, this increase was not significant (Figure 5.15A). When investigating the fold-change within individual donors, there is some variance between them, with the increases in SA-β-Gal activity being ~2-4 fold (Figure 5.15B).

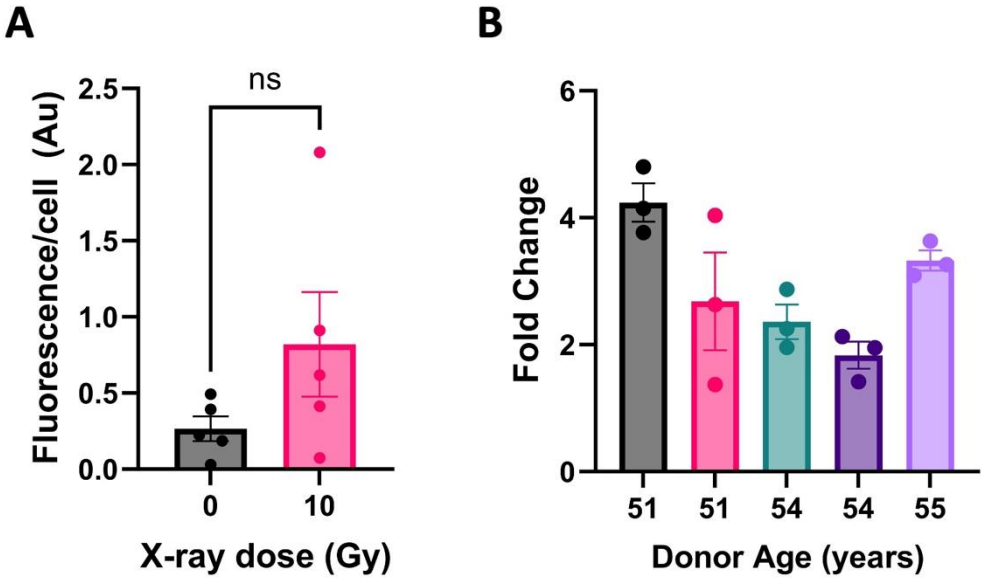


Figure 5.15 X-ray induced increases in SA-β-Gal activity of HCAEC from middle-aged donors.

HCAECs from middle-aged donors were exposed to 0 or 10 Gy X-ray once confluent. 7-days later, the fluorescent SA-β-Gal assay was performed. **A)**. The fluorescence per HCAEC with 0 or 10 Gy X-ray exposure, indicating SA-β-Gal activity. N=5 in triplicate, Students One-tailed T-test, NS = non-significant. **B)** The fold change in fluorescence per donor after 10 Gy X-ray exposure compared to control. N=3 technical replicates per donor.

5.3.6 Comparison of IR-induced atherogenic response in HCAEC from young and middle-aged donors

To assess the impact of donor age on the response of HCAEC to IR in relation to CVD, in this section I repeat the phenotypic assays which investigate the adhesion and permeability of HCAEC monolayers, along with fluorometric SA-β-Gal assay to provide insight into induction of senescence, with the focus being to compare the two HCAEC

donor age groups available, young, and middle-aged (17-33 and 48-55 years, respectively).

5.3.6.1 Age modulation of IR-induced adhesion in HCAEC

To investigate the modulation of IR-induced adhesion of HCAECs by donor age, I performed the adhesion assay, as previously described (5.3.2.2). Briefly, the HCAECs from donors aged 17-55 years were seeded on glass coverslips and exposed to 0 or 10 Gy X-ray once confluent. 7-days after irradiation, the adhesion of the HCAECs was determined by incubation and subsequent detection of adhered cell-tracker green labelled monocytes.

The results indicate that the HCAECs from young donors had, on average, a higher number of HL60s bound per HCAEC compared to the HCAEC from middle-aged donors, although this was not statistically significant (Figure 5.16A). This is reflected in the fold change compared to control within each individual donor after X-ray exposure, with the average fold change in HL60 adhesion being greater in the HCAEC from younger donors, compared to the middle-aged donors, although no significant difference was observed (Figure 5.16B). Importantly, the spread of data within both groups supports previous findings which indicate individual sensitivities to IR-induced adhesion, which suggests that the study may be underpowered.

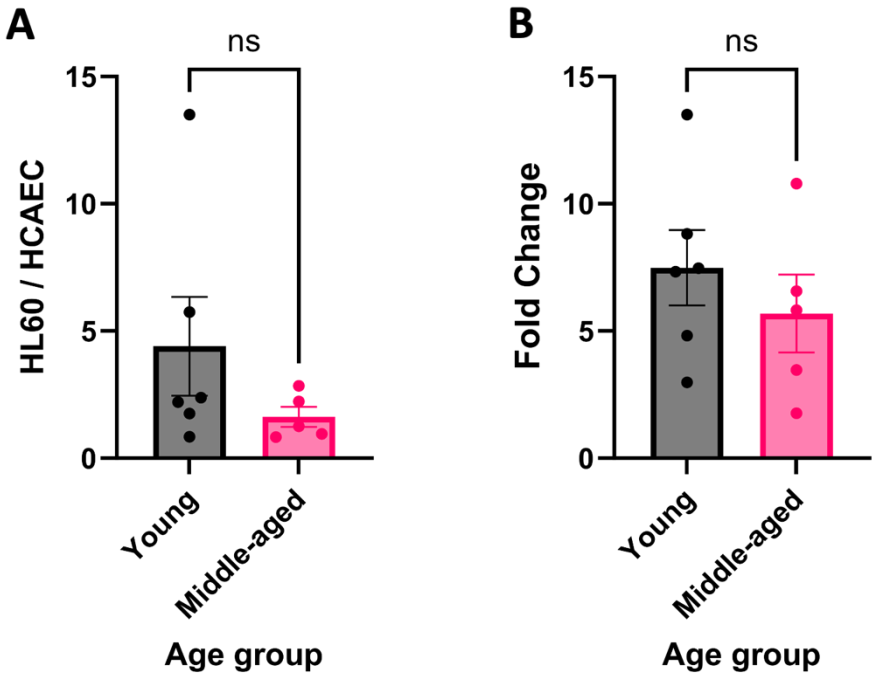


Figure 5.16 Adhesion of HL-60 to HCAECs from young and middle-aged donors after X-ray exposure.

HCAECs from donors aged 17-55 years were seeded on four fibronectin-coated glass coverslips in 2, 24-well plates and irradiated with 0 or 10 Gy X-ray once confluent. 7-days later, HCAECs were incubated with CTG-stained HL60s to assess HCAEC adhesion. **A)** The number of HL60 cells bound to HCAECs from young and middle-aged donors after 10 Gy X-ray exposure. N=5-6 in triplicate, Students two-tailed T-test, ns= not-significant. **B)** The fold change in the number of HL60 cells per HCAEC after 10 Gy X-ray exposure compared to control. N=5-6, each donor performed in triplicate. Students two-tailed t-test, ns = not-significant.

The trends in age mediated, IR-induced HL60 adhesion observed above (Figure 5.16) are reflected when plotted on a scatter graph, with a slight negative correlation between HCAEC donor age and adhesion after X-ray exposure (Figure 5.17). While not significant, they do suggest that HCAECs from younger donors may be more susceptible to IR-induced increases HCAEC adhesion. Interestingly, it appears that the HCAEC which

have a greater level of HL60 cell adhesion without X-ray exposure, particularly in the cells from younger donors, have a greater IR-induced adhesion of HL60 cells (Figure 5.17B).

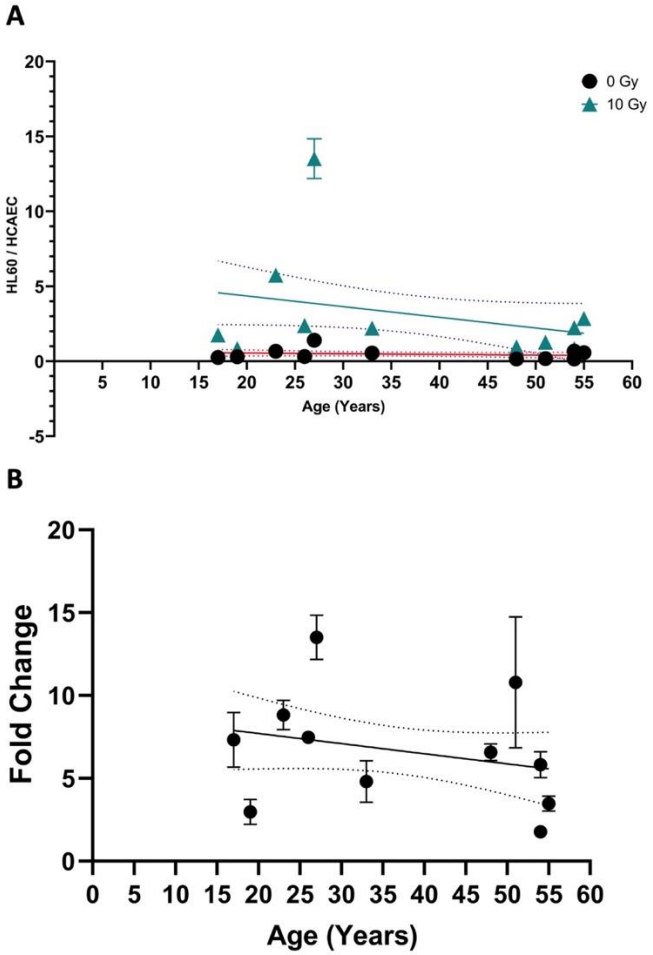


Figure 5.17 Age modulation of IR-induced HCAEC adhesion.

The results from **Figure 5.16** presented in a scatter graph with linear regression analysis. **A)** The number of HL-60 cells per HCAEC from donors ranging 17-55 years, with or without 10 Gy X-ray exposure. 0 Gy slope = -0.004646, R^2= 0.03485. 10 Gy slope = -0.07118, R^2=0.03485 **B)** Fold change in the number of HL-60 cells per HCAEC from donors ranging 17-55 years after 10 Gy X-ray exposure, compared to sham exposure. Slope = -0.06108, R^2=0.05225.

5.3.6.2 Age modulation of IR-induced permeability of HCAEC

To investigate how HCAEC donor age modulate IR-induced HCAEC monolayer permeability, the permeability assay was performed (as previously described in section 5.3.2.1) on HCAEC donor ranging 17-55 years after X-ray exposure. Briefly, this assay involves measuring the amount of dextran that passes through the HCAEC monolayer, 7 days after irradiation with 0 or 10 Gy X-ray.

The results indicate no age-modulation of IR-induced permeability of HCAEC monolayers, with the amount of dextran that passed through the monolayers of HCAEC from young or middle-aged donors 7-days after X-ray exposure being comparable (Figure 5.18). However, when the fold-change in permeability, which accounts for individual donor changes, the average increase permeability was greater in the HCAECs from the younger donors, although this was not statistically significant. However, as with the adhesion assay, there was considerable variation within the age groups, suggesting that individual responses to IR exposure may mask any impact age has on the development of IR-induced permeability, further suggesting that the study may be underpowered.

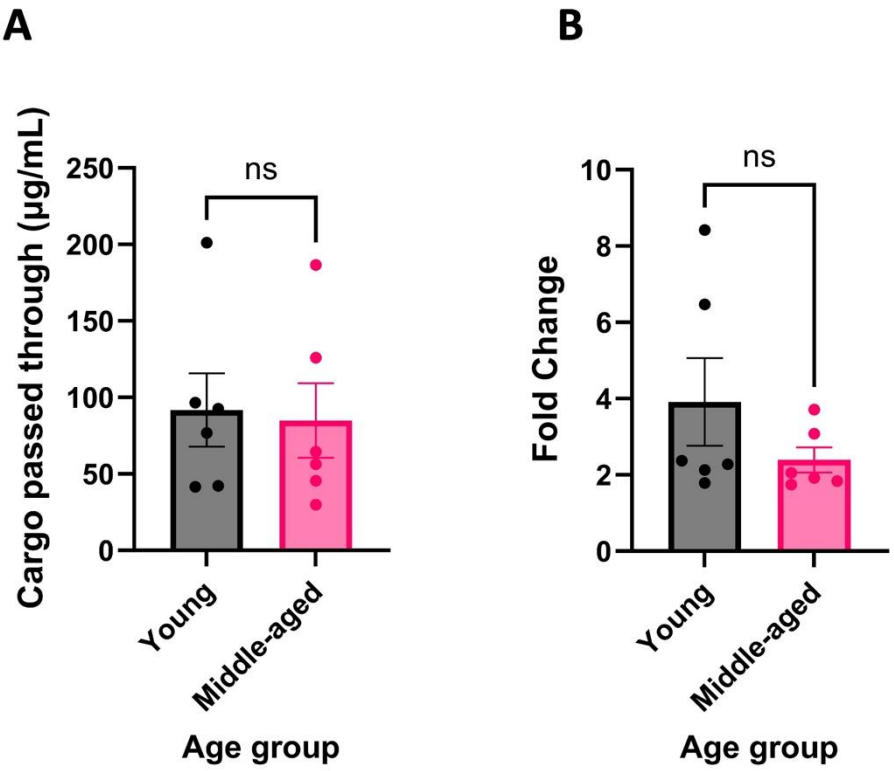


Figure 5.18 Permeability of HCAEC monolayers from young and middle-aged donors.

HCAECs from young and middle-aged donors were seeded transwell inserts coated with matrigel and irradiated with 0 or 10 Gy X-ray once confluent. 7-day later, the permeability assay was performed with FITC-labeled 70 kDa dextran (**A)** The amount of dextran that passed through the HCAEC monolayer derived from young and middle-aged donors after 10 Gy X-ray exposure. **B)** The fold change in the amount of dextran that passed through the monolayers after 10 Gy X-ray exposure, compared to sham exposure. N=6 in triplicate. Students two-tailed t-test. Ns = non-significant.

The trends above are reflected when analysing the amount of dextran which permeated the monolayers individually by age using a scatter plot (Figure 5.19). This demonstrates a slight negative correlation between age and the amount of dextran which passed through the HCAEC monolayers. When accounting for the basal level of monolayer

permeability within each donor by plotting the fold-change after 10 Gy X-ray exposure, compared to sham exposure, the correlation is moderately strengthened (Figure 5.19B).

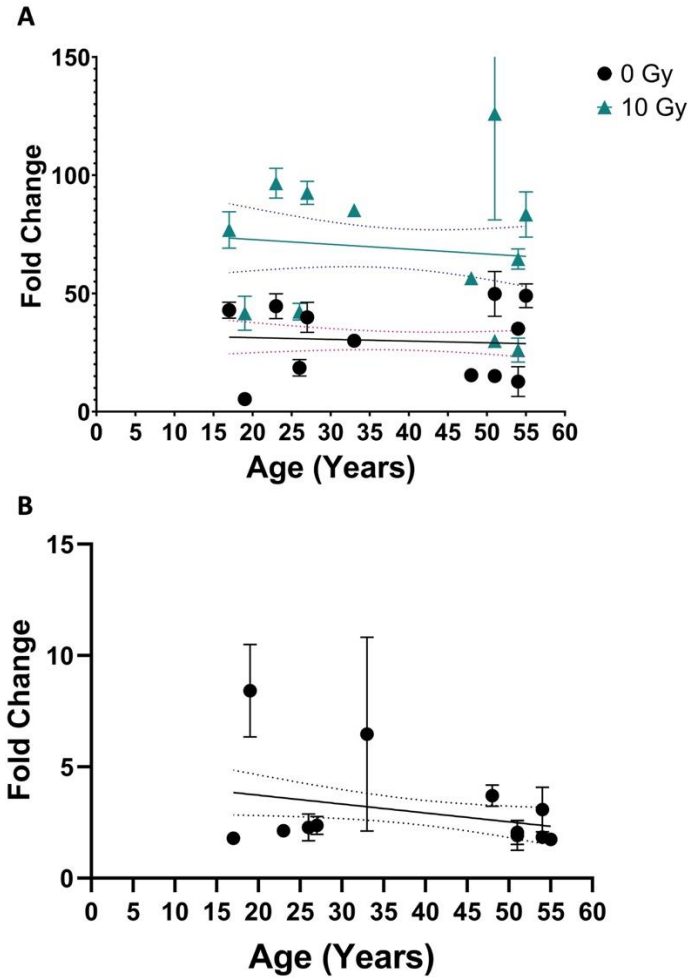


Figure 5.19 Age modulation of IR-induced HCAEC monolayer permeability.

The results from Figure 5.18 presented in a scatter graph with linear regression analysis performed. **A)** The amount of fluorescent 70 KDa dextran that passed through monolayers formed by HCAECs from donors ranging 17-55 years, with or without 10 Gy X-ray exposure. 0 Gy slope = -0.07225, R^2=0.004754. 10 Gy slope = -0.2039, R^2=0.008537 **B)** Fold change in the amount of dextran which passed through the monolayers after 10 Gy X-ray exposure, compared to sham exposure. Slope = -0.03988, R^2= 0.06933.

5.3.6.3 Age modulation of IR-induced SA-β-Gal activity in HCAEC

To investigate whether age modulates the development of IR-induced senescence in HCAECs, the fluorometric SA-β-Gal assay was used as previously described (section 5.3.2.5). Briefly, HCAECs from donors aged 17-55 years were seeded in 24-well plates and exposed to 0 or 10 Gy X-ray once confluent. 7-days after irradiation, SA-β-Gal activity was assessed using the fluorometric SA-β-Gal assay. While this alone is not sufficient, it will give an indication as to whether the cells are likely to be senescent.

The results indicate no significant difference in fluorescence per HCAEC between the two age groups, after 10 Gy X-ray exposure. However, the average fluorescence per cell was greater within the HCAEC from middle-aged donors after irradiation (Figure 5.20A). When assessing the fold-change within each donor and comparing the two age-groups, there is still no significant difference (Figure 5.20B). Within this, the average fold-change is greater in the HCAECs from younger donors.

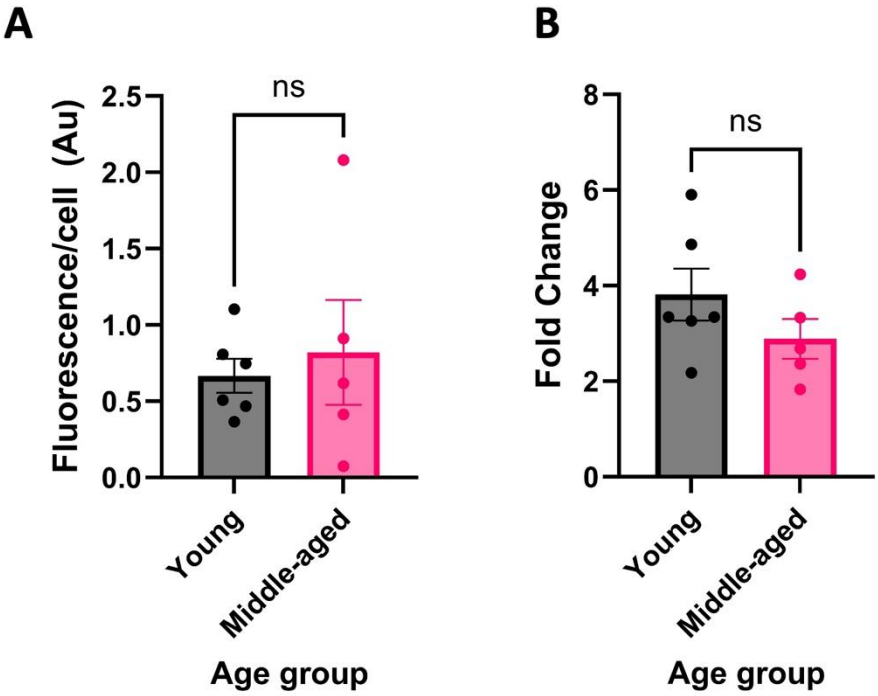


Figure 5.20 SA-β-Gal activity in HCAECs from young and middle-aged donors after X-ray exposure.

HCAECs from donors young and middle-aged donors seeded in 24-well plates and irradiated with 0 or 10 Gy X-ray once confluent. 7-days post X-ray, the fluorescence SA-β-Gal assay was performed and reported as fluorescence/ HCAEC. **A)** The amount of fluorescence detected per HCAEC from young and middle-aged donors, indicating SA-β-Gal activity. N=5-6 in triplicate, two-tailed t-test, ns= non-significant. **B)** Fold change in SA-β-Gal activity after the HCAECs from the donors were exposed to 10 Gy X-ray. N=5 in triplicate. Student's one-sided T-test. Ns = not significant.

While there is no significant difference when comparing the means of the two age groups investigated, both the 0 Gy and 10 Gy exposure linear regressions demonstrate a similar slope (0.003028 and 0.004542, respectively. Figure 5.21A). However, the linear regression analysis of the fold change of all donors investigated demonstrates a negative correlation with the age of the HCAEC and the IR-induced SA-β-Gal activity

(slope = -0.03509), suggesting that older cells may have less of an increase in SA-β-Gal activity after X-ray exposure, which may suggest less of an induction of senescence (Figure 5.21B).

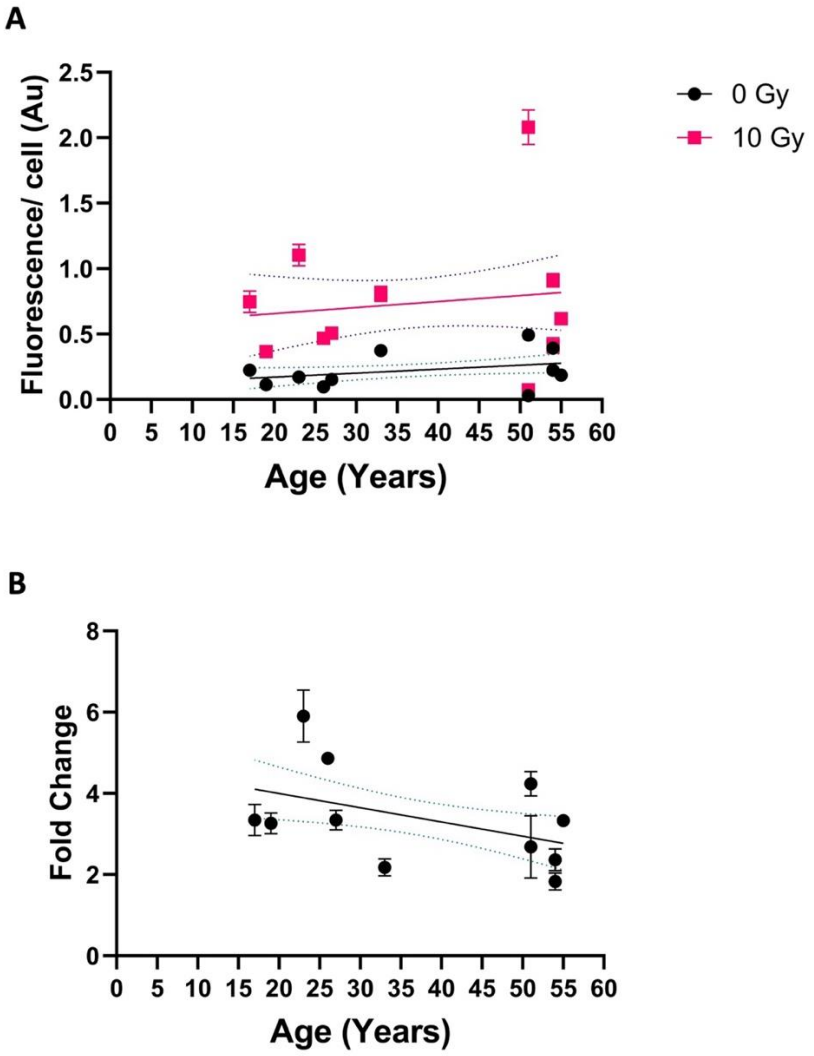


Figure 5.21 SA-β-Gal activity in HCAECs from all donors after X-ray exposure.

The results from Figure 5.20 presented in a scatter graph with linear regression analysis performed. **A**) The amount of fluorescence detected per HCAEC from donors ranging 17-55 years, with or without X-ray exposure, indicating SA-β-Gal activity. 0 Gy slope = 0.003028, R^2=0.1109. 10 Gy slope= 0.004542, R^2=0.5233 B) The fold change in SA-β-Gal activity within the donors after 10 Gy X-ray exposure, compared to sham exposure. N=3 per donor. Slope = -0.03509, R^2=0.1693.

5.3.6.4 Correlation between HCAEC senescence and atherogenic phenotypes

To investigate the association between the IR-induced changes in SA-β-Gal activity and the IR-induced changes in adhesion and permeability within the HCAECs, I compared

the fold-change after X-ray exposure results from section 5.3.6 against the fold-change in senescence. This analysis revealed there was a significant correlation between fold-increases in SA-β-Gal activity and greater fold-changes in HCAEC adhesion (Spearman r = 0.5636, p = 0.038) (Figure 5.22). For the permeability assay, there was a slight negative correlation (-0.2545), although this was not significant (p=0.2255). These results suggest that HCAECs that experience a greater fold increase in SA-β-Gal activity after irradiation, are more likely to have increased adhesion, supporting the theory that senescence increases the adhesion of HCAECs.

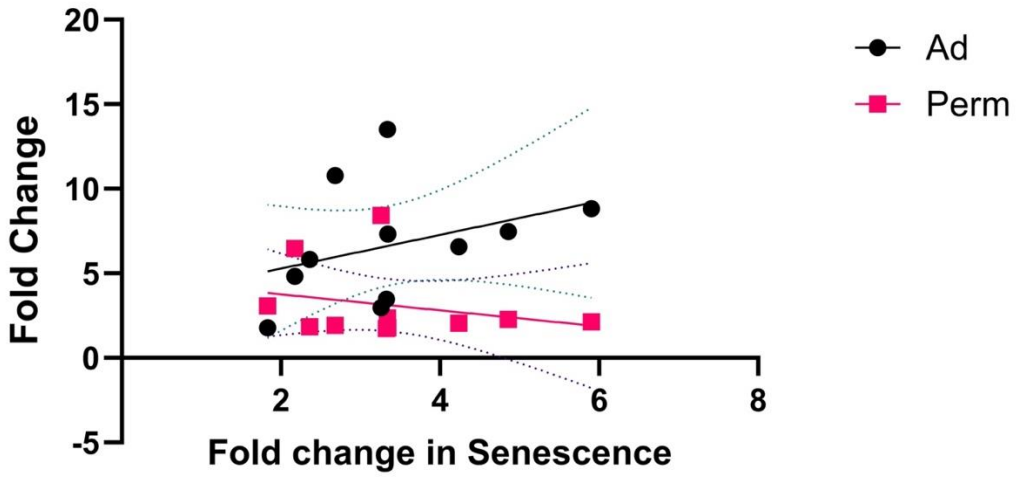


Figure 5.22 Correlation between fold-change in senescence and permeability and adhesion of HL-60s in HCAEC.

The fold-change in SA-β-Gal activity (referred to as senescence) and the matched fold-changes in adhesion of HL-60 cells to HCAEC (Black) and the fold-changes in monolayer permeability (red), from section 5.3.6. n=3 technical replicates. Correlation analysis for adhesion indicated a Spearman r= 0.5636, p=0.038. For permeability, the Spearman r = -0.2545, p=0.2255.

5.3.7 Optimising drugs for targeting senescence in HCAEC

In order to begin to address the hypothesis that radiation increases pro-atherogenic phenotypes in HCAEC, preventing or removing the senescent cells would give an indication as to whether they are affecting these phenotypes. To investigate this in a way that could be transferable to mouse and Human trials, a pharmacological approach would be best. To enable these investigations, firstly the correct dose of the drugs needs to be determined. To prevent the development of senescence after IR exposure, I have used the mTOR inhibitor, rapamycin, which predominantly targets the mTORC1 complex. To target senescent cells after their development, I have used ABT-263 which is a BCL-2 inhibitor (Discussed in more detail in 1.5.4).

5.3.7.1 ABT-263 senolytic dose investigation

For the investigation into suitable doses of ABT-263 as a senolytic for HCAEC, the doses used were 0 nM, 10 nM, 100 nM, and 1000 nM. For the senolytic treatment, ABT-263 at the doses mentioned was added on day 4, for 24 hours, with the SA-β-Gal assay performed on day 7, as previously described (section 5.3.4.3). A significant increase in SA-β-Gal activity was detected within the vehicle control HCAEC exposed to 10 Gy X-ray, compared to sham irradiation (Figure 5.23A). Interestingly, with 10 nM treatment, the SA-β-Gal activity between sham exposure and 10 Gy X-ray exposure was comparable, suggesting that ABT-263 at this dose may increase β-gal expression along with preventing X-ray induced increases in SA-β-Gal activity. At 100 nM, the sham exposed HCAEC had SA-β-Gal activity similar to that in the vehicle control, with a slight reduction in the average fluorescence per HCAEC. At 1000 nM, there was a significant

increase in the SA-β-Gal activity in the 10 Gy exposure group, suggesting that this dose was not effective at removing X-ray induced senescent cells.

When displaying the results as dose-matched, fold-change after X-ray expose, both 10 nM and 100 nM led to minimal fold-change in SA-β-Gal activity, although only the 100 nM dose was statistically significant (Figure 5.23B). This suggest that both 10 nM and 100 nM are likely to remove X-ray induced senescent cells, or at least prevent X-ray induced increases in SA-β-Gal activity.

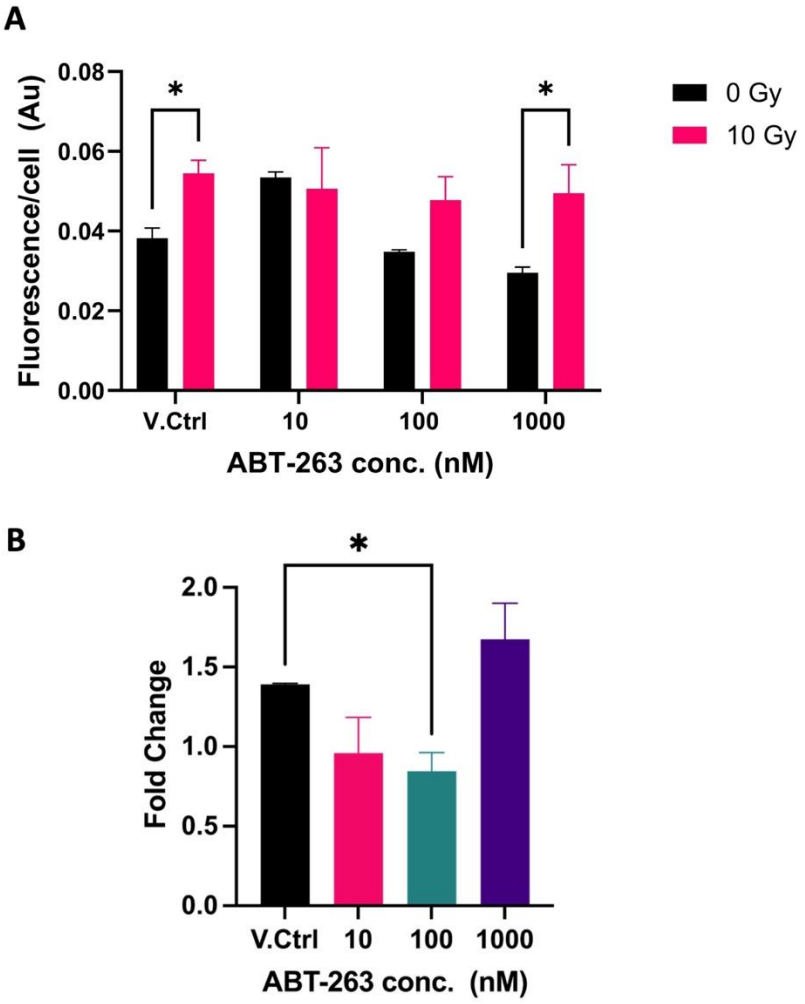


Figure 5.23 ABT-263 dose investigation in HCAEC exposed to X-rays.

HCAECs were seeded in fibronectin-coated, 24-well plates (25,000 cells/ cm^2) and once confluent (2-4 days), exposed to 0 or 10 Gy X-ray. 4 days post-irradiation, ABT-263 at concentrations of 10 nM, 100 nM, and 1000 nM was added for 24 hours. The SA-β-Gal assay was then performed on day 7 as previously described (section 5.3.2.5). **A)** Raw fluorescence per cell indicating SA-β-Gal activity with the fold change between 0 Gy and 10 Gy X-ray in each treatment group displayed **(B).** Two-way ANOVA with multiple comparisons, n=3, * = $p<0.05$.

5.3.7.2 Rapamycin senomorphic dose investigation

To investigate the ability of rapamycin to prevent the induction of X-ray induced senescence, HCAEC were irradiated with 0 or 10 Gy X-ray with the addition of 0 nM, 10 nM, 50 nM, or 100 nM rapamycin. After incubation with the rapamycin for 5 days, cells were maintained on normal MEC media, and the SA-β-gal assay was performed on day 7 as previously described (section 5.3.2.5).

As previously demonstrated, irradiation of HCAECs with 10 Gy X-ray led to a significant increase in SA-β-gal activity (Figure 5.24). Interestingly, incubation of the HCAECs with all doses of rapamycin significantly reduced the SA-β-gal activity in the non-irradiated cells, suggesting a reduction in the basal levels of the β-galactosidase activity. At all doses used, rapamycin treatment led to statistically significant reductions in SA-β-gal activity within the irradiated cells, demonstrating no significant difference in activity between the irradiated and non-irradiated HCAECs. This was reflecting when the results were presented as fold-change after irradiation, compared to non-irradiated, drug matched controls, with all doses resulting in a significant reduction in the fold change of SA-β-gal activity, compared to no-drug control (Figure 5.24B).

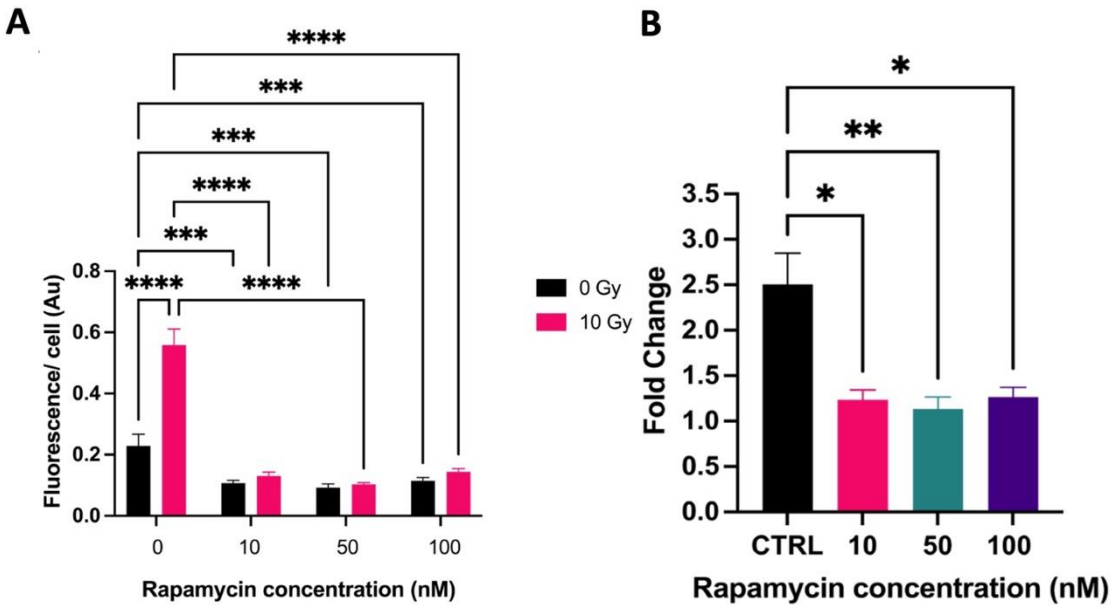


Figure 5.24 Rapamycin dose investigation in HCAEC exposed to X-rays.

HCAECs were irradiated with 0 or 10 Gy X-ray once confluent. Immediately after, rapamycin was added at concentrations of 0, 10, 50, and 100 nM, and removed after 5 days. On day 7, the SA-β-Gal assay was performed (as previously described in section 5.3.2.5). **A)** Raw fluorescence per cell indicating SA-β-Gal activity with the fold change between 0 Gy and 10 Gy X-ray in each treatment group displayed **(B).** n=3, two-way ANOVA with multiple comparisons, * = $p<0.05$, ** = $p<0.005$, *** = $p<0.001$, **** = $p<0.0001$.

To provide insight into the morphological features of the HCAECs when exposed to IR and treated with rapamycin, I performed the SA-β-Gal assay in the classical fashion with the HCAECs from a 54-year-old donor (Figure 5.25). Importantly, this is only an n=1 due to the main focus being on the fluorescent SA-β-Gal assay previously performed (Figure 5.24). To provide some level of analysis, I quantified the number of cell positive for SA-β-Gal staining as a percentage of the total number of cells in the 40x magnification images. Within these results, ~64% of the cells were positive in the control group (no IR

exposure or rapamycin treatment), with this rising to 95% when exposed to 10 Gy X-ray (Figure 5.25C). Interestingly, in all groups, rapamycin treatment reduced the percentage of positive cells present in the image, with those irradiated displaying similar SA-β-Gal staining to drug matched controls. Furthermore, the flattened and enlarged morphology observed with 10 Gy X-ray exposure appears to be reduced with rapamycin treatment, although this has not been quantified and so is subjective. In addition to this, the number of cells present in the images of the HCAECs exposed to X-rays increases with rapamycin treatment, suggesting that rapamycin may at least be delaying IR-induced apoptosis along with markers of senescence. However, minimal conclusions can be drawn from this due to no technical or biological replicates being performed.

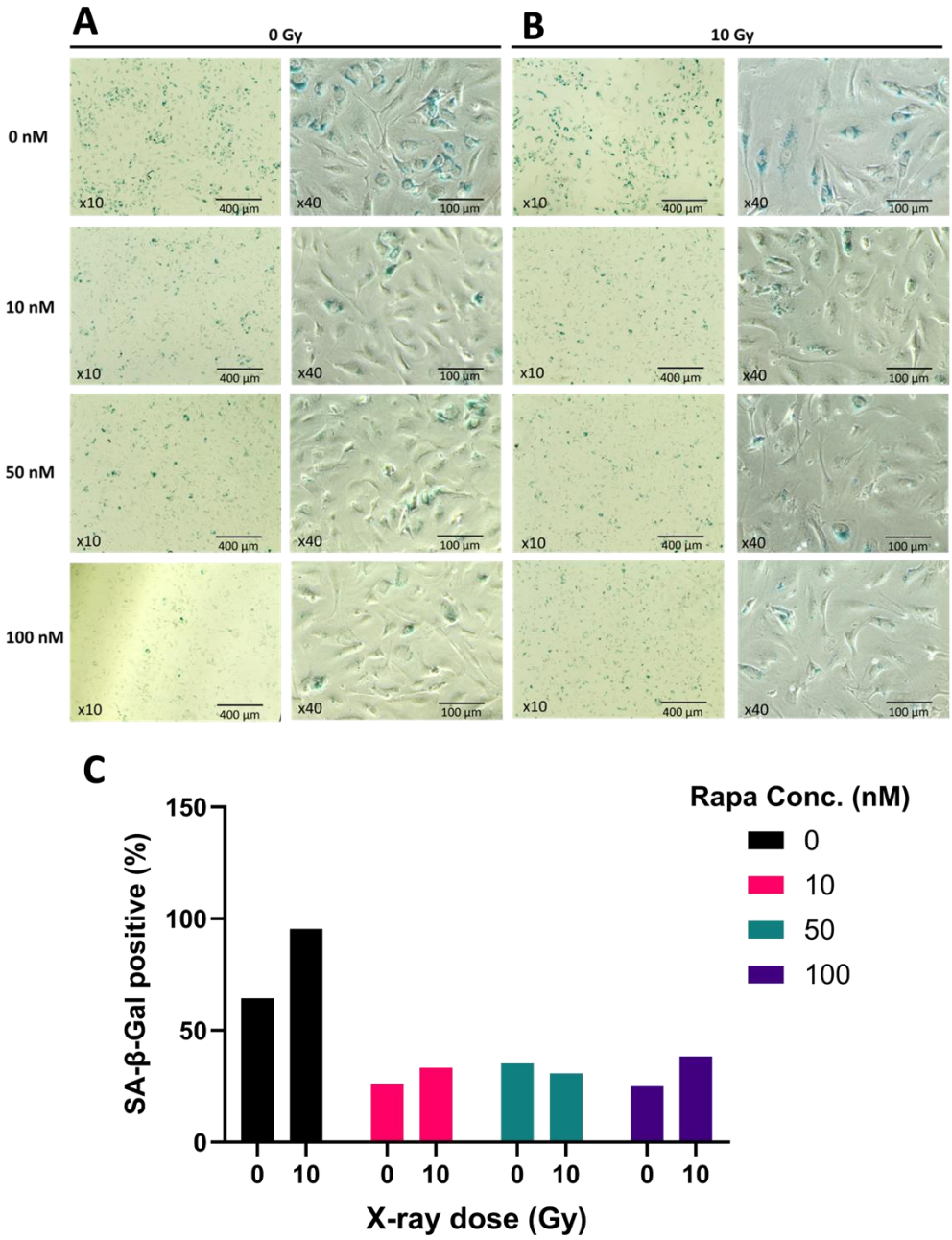


Figure 5.25 Phase contrast images of SA-β-Gal Gal stained, irradiated HCAECs with rapamycin treatment.

HCAECs from a 54-year-old donor were seeded in a 24-well plate and exposed to 0 or 10 Gy X-ray once confluent. Cells then received either 0, 10, 50, or 100 nM rapamycin for 5 days, with the assay performed 7 days post X-ray. **A-B)** Phase contrast images of SA-β-Gal stained (blue) HCAECs with 0 Gy (**A**) or 10 Gy (**B**) X-ray exposure, with 0, 10, 50, or 100 nM rapamycin treatment (top to

bottom, respectively). The percentage of SA-β-Gal positive cells was then quantified (**C**). n=1.

As rapamycin demonstrated the most promise in preventing IR-induced increases in SA-β-gal activity at low doses, I chose this as the drug to move forward with further investigations. Firstly, I investigated proteins associated with senescence and the ability of rapamycin to attenuate X-ray induced changes. When investigating the effects of rapamycin on senescence related proteins, 10 nM was sufficient enough to cause almost complete inhibition of mTOR activity as measured by phosphorylated S6 ribosomal protein (Figure 5.26D). LAP2, a protein related to nuclear membrane integrity is reduced by 10 Gy X-ray, a common occurrence when a cell enters into senescence. With no significant difference observed between rapamycin treatment after 10 Gy exposure and the control cells, this suggests that rapamycin inhibited the deterioration of the nuclear membrane integrity associated with X-ray exposure and senescence (Figure 5.26A). Furthermore, although not significant, 10 Gy X-ray induced an up-regulation of p53, which is associated with DNA damage and stress induced senescence. This increase was inhibited with 10 nM rapamycin treatment (Figure 5.26B). This was also reflected in the p21 Waf1/Cip1 protein levels, with a significant increase in the proteins abundance which was reduced to levels comparable to those observed in the control cells with rapamycin treatment (Figure 5.26C). Overall, these result support the role of X-ray exposure in inducing senescence, by providing evidence of increases in other markers associated with senescence and demonstrate the effectiveness of 10 nM rapamycin in preventing the induction of X-ray induced senescence.

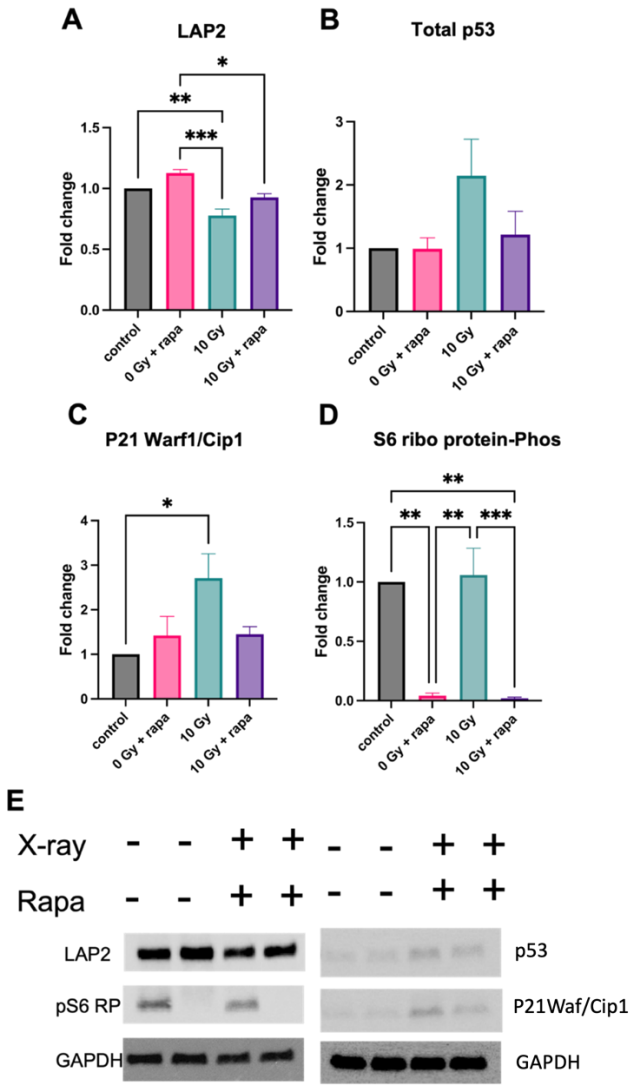


Figure 5.26 The expression of senescence-associated proteins with X-ray exposure and rapamycin treatment.

HCAECs seeded in 10cm^2 plates and irradiated with 0 or 10 Gy X-ray once confluent Within both irradiated and non-irradiated plates, 0 and 10 nM rapamycin was added immediately after irradiation. Rapamycin was removed after 5 days, and cells were pelleted on day 7. Proteins were then extracted, and Western blotting performed (as previously described in section 2.7). **A-D)** Fold change in Lap2 (**A**), total p53 (**B**), p21Waf1/Cip1 (**C**), and phosphorylated S6 ribosomal protein (D) after X-ray exposure with or without 10 nM rapamycin treatment. (**E**) Representative western blots for the associated proteins. Primary and secondary antibodies used are listed in Table 2.2. Two-way ANOVA with multiple comparisons, n=3, * = $p<0.05$, ** = $p<0.005$, *** = $p<0.001$.

An additional characteristic of cellular senescence is an increase in nuclear size (discussed in section 1.5.2.3). Therefore, I assessed the size of the nuclei within the HCAECs from young and middle-aged donors using DAPI staining, 7 days after 0 or 10 Gy X-ray exposure, with or without 10 nM rapamycin treatment (Figure 5.27). The results indicate that the nuclear area was significantly increase after 10 Gy X-ray exposure in the HCAECs from both young and middle-aged donors, with rapamycin significantly reducing this increase in the HCAECs from younger donors, and not middle-aged. This supports the SA-β-Gal assays previously performed, providing additional evidence towards the ability of rapamycin to prevent or delay the IR-induced senescence in HCAECs.

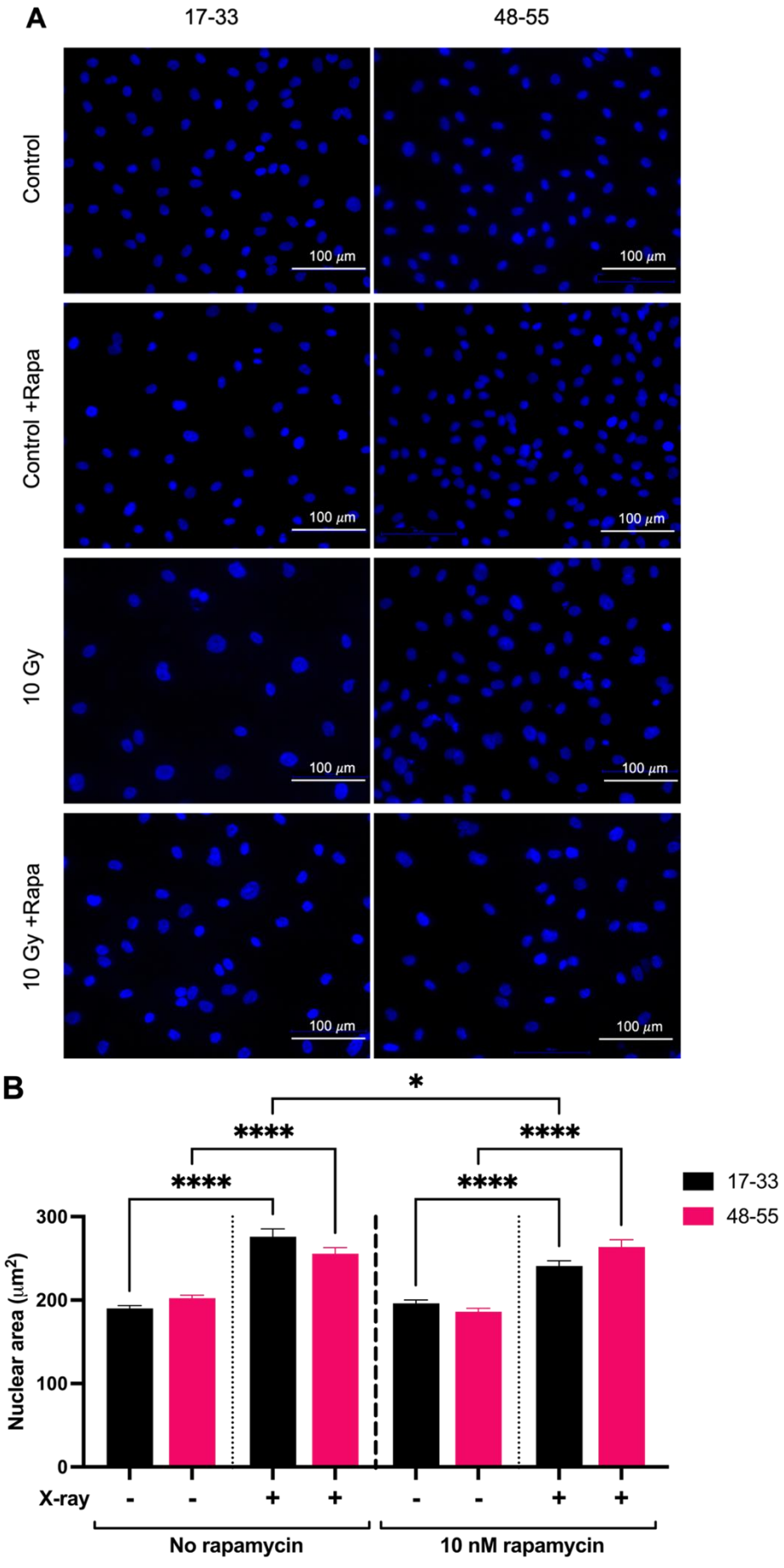

A
17-33
48-55
Control
Control +Rapa
10 Gy
10 Gy +Rapa
100 μm
B
*
****
****
****
****
17-33
48-55
Nuclear area (μm²)
300
200
100
0
X-ray
-
-
+
+
-
-
+
+
No rapamycin
10 nM rapamycin

Figure 5.27 Changes in HCAEC nuclei size with IR exposure and rapamycin treatment.

A) Representative images of HCAEC nuclei stained with DAPI (Blue), with cells from young donors (17-33 years, left) and middle-aged donors (48-55 years, right) displayed. HCAECs received no treatment, 10 nM rapamycin, 10 Gy X-ray, or 10 Gy X-ray + 10 nM rapamycin (top to bottom). Nuclear area was then calculated using Image J (**B**). n=3 per age group, with 3 technical replicates. Two-way ANOVA with multiple comparisons, * = $p<0.05$, ** = $p<0.005$, *** = $p<0.001$, **** = $p<0.0001$.

5.3.8 Targeting senescence to prevent IR-induced atherogenic phenotypes in HCAECs

Having demonstrated that IR in the form of X-rays can increases both the adhesion and permeability of HCAEC monolayers from both young and middle-aged donors, within this section I use the senomorphic, rapamycin, and the senolytic, ABT-263 in an attempt to inhibit these responses. From the experiments investigating suitable doses of senolytics and senomorphics, 10 nM rapamycin was chosen as the drug to move forward into the phenotypic investigations. This was due to it being the lowest dose that provided a significant reduction in SA-β-Gal activity (section 5.3.7.2). Furthermore, I have previously demonstrated rapamycin halts epigenetic ageing in HUVECs (Kabacik *et al.*, 2022b), along with having vast amounts of safety data with its use in people since 1999, allowing for easier repurposing in the future than other mTOR inhibitor alternatives (Kraig *et al.*, 2018). The dose chosen for ABT-263 was 10 nM ABT-263 due to its reduction in fold change in SA-β-Gal activity (section 5.3.7.1). For all the assays

performed in this section, 10 nM rapamycin was added immediately after X-ray exposure, for 5 days, with a 2-day recovery period. 10 nM ABT-263 treatment was applied at day-4 post X-ray exposure, for 1 day, followed by a 2-day recovery period and the assays performed on day-7.

5.3.9 Targeting senescence to prevent IR-induced HL-60 adhesion in HCAEC from young and middle-aged donors

Building upon previous comparisons between the HCAECs from young and middle-aged donors, here I repeat the adhesion assay and include senomorphic treatment with rapamycin and senolytic treatment with ABT-263. The adhesion assay was performed as previously described (section 0), using fluorescently labelled HL-60 cells, and quantifying the number bound to the HCAEC monolayers 7-days post 0 Gy or 10 Gy X-ray exposure, with or without rapamycin or ABT-263 treatment.

Firstly, these results reinforce my previous findings that exposure of HCAECs to 10 Gy X-ray increases the adherence of HL-60 cells to the monolayer, with a significant increase in HL60/HCAEC after 10 Gy X-ray exposure (Figure 5.28A). ABT-263 treatment had no significant affect. However, the HCAECs treated with rapamycin had no significant difference in the number of HL-60s/HCAEC between the irradiated and non-irradiated, drug matched HCAECs (Figure 5.28A). This was reflected when analysing the fold-change in HCAEC adhesion after irradiation, with a significant reduction in the fold change observed with 10 nM rapamycin treatment (Figure 5.28B), these results suggest that rapamycin can inhibit X-ray induced HL60 adhesion to HCAECs.

When looking at the results split into the young (17-33 years) and middle-aged (48-55 years) experimental groups, the HCAEC from younger donors had a significant increase in the number of HL-60 cells per HCAEC after 10 Gy X-ray exposure, within both the non-drug control cells and the ABT-263 treated cells (Figure 5.28C-D). However, 10 nM rapamycin inhibited this increase, with the number of HL-60 per HCAEC being comparable to drug matched, non-irradiated control (Figure 5.28C).

The adhesion assays performed on the HCAEC from middle-aged donors demonstrated no significant increases in any of the treatment groups, including control, after irradiation (Figure 5.28D). However, I have previously demonstrated increases in the adhesion of HCAEC from middle-aged donors (5.3.2.2), however, fewer HCAECs could be used in these experiments due to one of the cell lines presenting with unusual morphology and therefore, were excluded from the experiment.

These results were reflected when considering the basal level of HL-60 adhesion without X-ray exposure. There was a significantly higher fold-change in adhesion seen in the HCAECs from younger donors compared to those from middle-aged donors when no drug treatment was applied (Figure 5.28E). Treatment of the HCAEC with rapamycin led to comparable fold-changes in HL-60 adhesion between both age groups, with a significant reduction in fold-change observed in the HCAEC from younger donors. Furthermore, senolytic treatment with ABT-263 showed no significant reduction in HL60 per HCAEC, although there was a reduction in the average number of HL-60 per HCAEC within the cells from the younger donors. Overall, these results demonstrate

that HCAEC from younger donors have greater IR-induced increases in HL60 adhesion, compared to HCAEC from older donors.

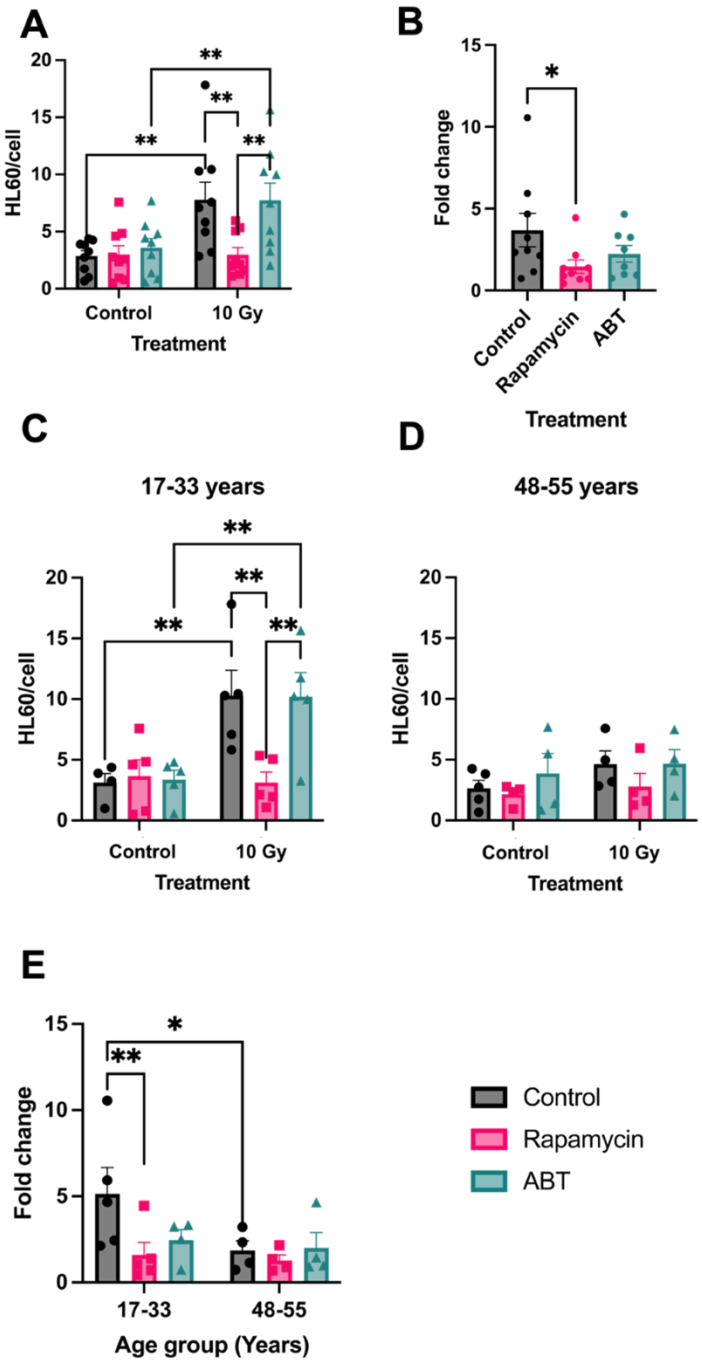


Figure 5.28 Adhesion of HL-60 cells to HCAEC from donors of different ages after X-ray exposure and treatment with rapamycin or ABT-263.

HCAECs from donors aged 17-55 years were irradiated with 0 and 10 Gy X-ray once confluent. For rapamycin treatment, 10 nM was added immediately for 5 days after exposure. For ABT-263 treatment, 10 nM ABT-263 was added on day 4 for 24 hours. 7-days post irradiation, CTG-stained HL60s were incubated with the HCAECs for four

hours, and the number of HL60/HCAEC determined. **A-B)** Hl-60 per HCAEC with all ages combined with or without 10 nM rapamycin treatment or 10 nM ABT-263 (**A**), with the associated fold change **(B**). N=8 per group. **C-E)** HL-60 per HCAEC with or without drug treatment in cells from donors ranging from 17-33 (**C**) and 48-55 (**D**), with a comparison between the associated fold changes within the age groups (**E**). N=3-5 per group. Two-way ANOVA with multiple comparisons, * = $p<0.05$, ** = $p<0.005$.

5.3.10 Targeting senescence to prevent X-ray-induced permeability of HCAEC monolayers

After the success of reducing X-ray induced adhesion with rapamycin treatment, I focused on investigating whether it was possible to mitigate the changes in permeability associated with X-ray exposure, again using senomorphic, rapamycin and senolytic, ABT-263. To achieve this, I performed the permeability assay, as previously described (section 5.3.2.1).

Briefly, HCAECs from the young (17-33 year) and middle-aged (48-55 years) donors were seeded in transwell inserts coated with diluted matrigel, allowing for the movement of fluorescent 70 KDa dextran into the wells below the insert. Once a confluent monolayer was formed, the transwells were exposed to 0 Gy or 10 Gy X-ray. For rapamycin treatment, the HCAEC were then incubated with rapamycin for 5 days immediately after exposure. For ABT-263 treatment, the drug was applied for 1 day, 4 days post X-ray. 7 days after irradiation, the permeability assay was performed.

Using a standard curve to quantify the amount of cargo that passed through the monolayers, in the experimental groups without drug treatment, there was a significant

increase in the amount of fluorescent dextran detected, supporting my previous work demonstrating X-ray exposure increases HCAEC monolayer permeability (Figure 5.29A). However, there was also a significant increase observed between the ABT-263 treated cells after 10 Gy X-ray exposure, suggesting that ABT-263 did not reduce X-ray induced permeability. On the other hand, the rapamycin treated monolayers did not display a significant increase in permeability after 10 Gy X-ray exposure, although the average amount of dextran detected was still higher after X-ray exposure. This suggest that rapamycin treatment may have reduced the severity of X-ray-induced permeability.

When calculating the fold change in permeability after irradiation for the individual donors, there was no significant difference observed, although rapamycin resulted in a reduced mean fold-increase in permeability (Figure 5.29B). When analysing the changes in permeability within the HCAEC from younger donors, within the HCAEC without drug treatment, there was no significant increase in the average amount of dextran detected after X-ray exposure (Figure 5.29C). However, rapamycin treatment results in a lower average permeability within the non-irradiated cells, and only a marginal reduction in the 10 X-ray exposed cells. This has led to a significant increase in permeability between the sham and 10 Gy exposure cells within this experimental group.

Within the HCAECs from middle-aged donors, there was no significant differences between any of the drug treatment, sham or irradiated groups (Figure 5.29D). However, there was a considerable increase in the average amount of dextran detected after X-ray exposure with no drug treatment and ABT-263 treatment. Within the rapamycin

treatment group, there was less of an increase in dextran detection after irradiation, suggesting a lower increase in permeability with this treatment after X-ray exposure.

When interpreting the data using fold-change to account for non-irradiated levels of permeability within the groups, there was no significant differences between any of the treatment groups, or the matched drug treatment groups between the HCAECs from young and middle-aged donors (Figure 5.29E). However, the middle-aged donors had a greater average fold-increase after irradiation in both the non-drug treatment cells and the ABT-263 treated cells. Rapamycin treatment was comparable between the age groups.

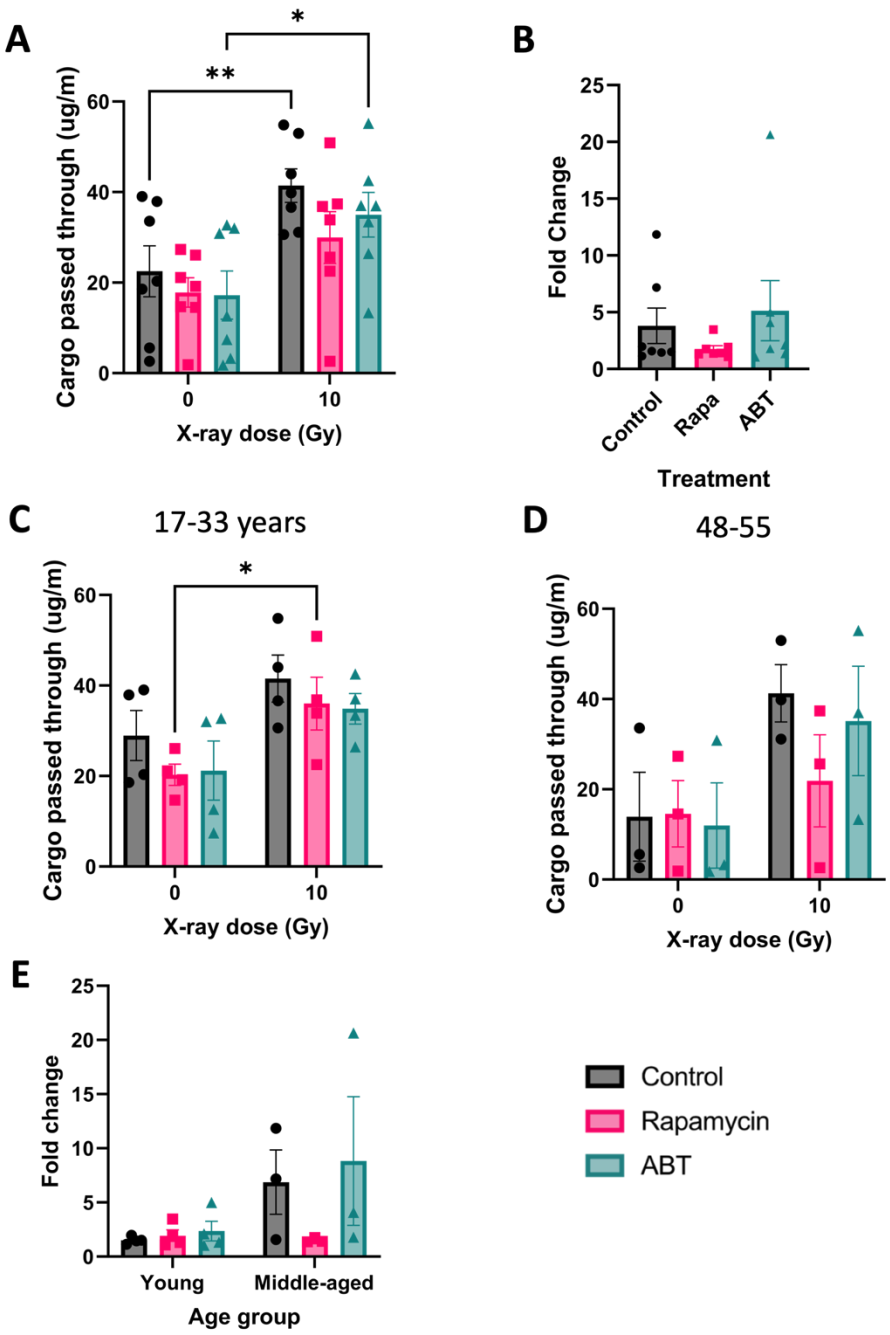


Figure 5.29 Permeability of HCAEC monolayers after X-ray exposure and treatment with rapamycin or ABT-263.

HCAECs from young and middle-aged donors were irradiated with 0 or 10 Gy X-ray when confluent. For rapamycin treatment, 10 nM was added immediately after irradiation, for 5 days. For ABT-263 treatment, 10 nM was added 4 days post irradiation for 24 hours. **A)** The amount of cargo that passed through the HCAEC monolayer with all ages combined, with 0 or 10 Gy X-ray exposure, with or without

10 nM rapamycin treatment or 10 nM ABT-263, with the associated fold change after irradiation, compared to drug matched control **(B**). N=7 per group. **C-E)** The amount of cargo that passed through the HCAEC monolayer with or without drug treatment in cells from young donors (**C**) and middle-aged donors (**D**), with a comparison between the associated fold-changes within the age groups (**E**). N=3-4 per group. Two-way ANOVA with multiple comparisons, * = p<0.05, ** = p<0.005.

5.3.10.1 Efficacy of targeting HCAEC senescence with rapamycin and ABT-263

To investigate the efficacy of rapamycin and ABT-263 treatment in preventing senescence phenotypes within HCAECs, I first performed the SA-β-Gal assay as previously described (section 5.3.2.5). Briefly, HCAECs were culture until confluent and exposed to 0 or 10 Gy X-ray, with 5-day incubation with 10 nM rapamycin immediately after 10 Gy X-ray, 1 day incubation with ABT-263 at day 4 post X-ray, or standard cell culture conditions, with the SA-β-Gal assay performed 7-days post X-ray.

Firstly, the results are consistent with that seen previously, with 10 Gy X-ray irradiation resulting in an increase in the average fluorescence per HCAEC, indicating increased SA-β-Gal activity, suggesting that the number of senescence HCAEC has increased (Figure 5.30A). The incubation of the cells exposed to 10 Gy X-ray with 10 nM rapamycin resulted in a reduction of SA-β-Gal activity back to levels similar to that seen in the non-irradiated control group. ABT-263 only resulted in a slight reduction in the average fluorescence per HCAEC, suggesting that it may not be as effective in all the donor HCAEC. Furthermore, rapamycin slight lowered the average fluorescence per HCAEC in the non-irradiated cells, suggesting that either rapamycin is preventing other stress inducers of senescence or is modulating the production of the β-Galactosidase enzyme.

These results were reflected in the matched fold-change in SA-β-Gal activity, with rapamycin resulting in a significantly lower fold change after X-ray exposure, compared to the non-rapamycin treated cells, suggesting that rapamycin may be protecting the cells from IR induced senescence (Figure 5.30B). ABT-263 had less of an impact and only slightly reduced the fold-increase SA-β-Gal activity.

When investigating the effect age has on the response to 10 Gy X-ray, a statistically significant increase in SA-β-Gal activity was observed in the 17-33 age group, but not in the 48-55-years old age group, suggesting the HCAECs from the younger donors are more susceptible to X-ray induced increases in SA-β-Gal activity (Figure 5.30C-D). In the HCAECs from older donors, as before, the baseline SA-β-Gal activity was higher compared to those from younger donors, suggesting that there may be a higher proportion of cells in a senescent like state. Incubation of the HCAEC with rapamycin significantly reduced the SA-β-Gal activity after 10 Gy X-ray exposure compared to the age matched, non-drug treated, irradiated cell groups within both age ranges investigated. Rapamycin only resulted in a significant reduction in the fold-change of SA-β-Gal activity within the HCAEC from younger donors, which is likely due to only a small increase in SA-β-Gal activity being detected after irradiation in the HCAEC from middle-aged donors (Figure 5.30E). ABT-263 displayed a similar trend to that observed with the age groups combined, with only a slight trend in reduction of SA-β-Gal activity being observed in the 17-33 age group after 10 Gy X-ray exposure, with no difference observed in the 48-55-year-old cell group (Figure 5.30C-E).

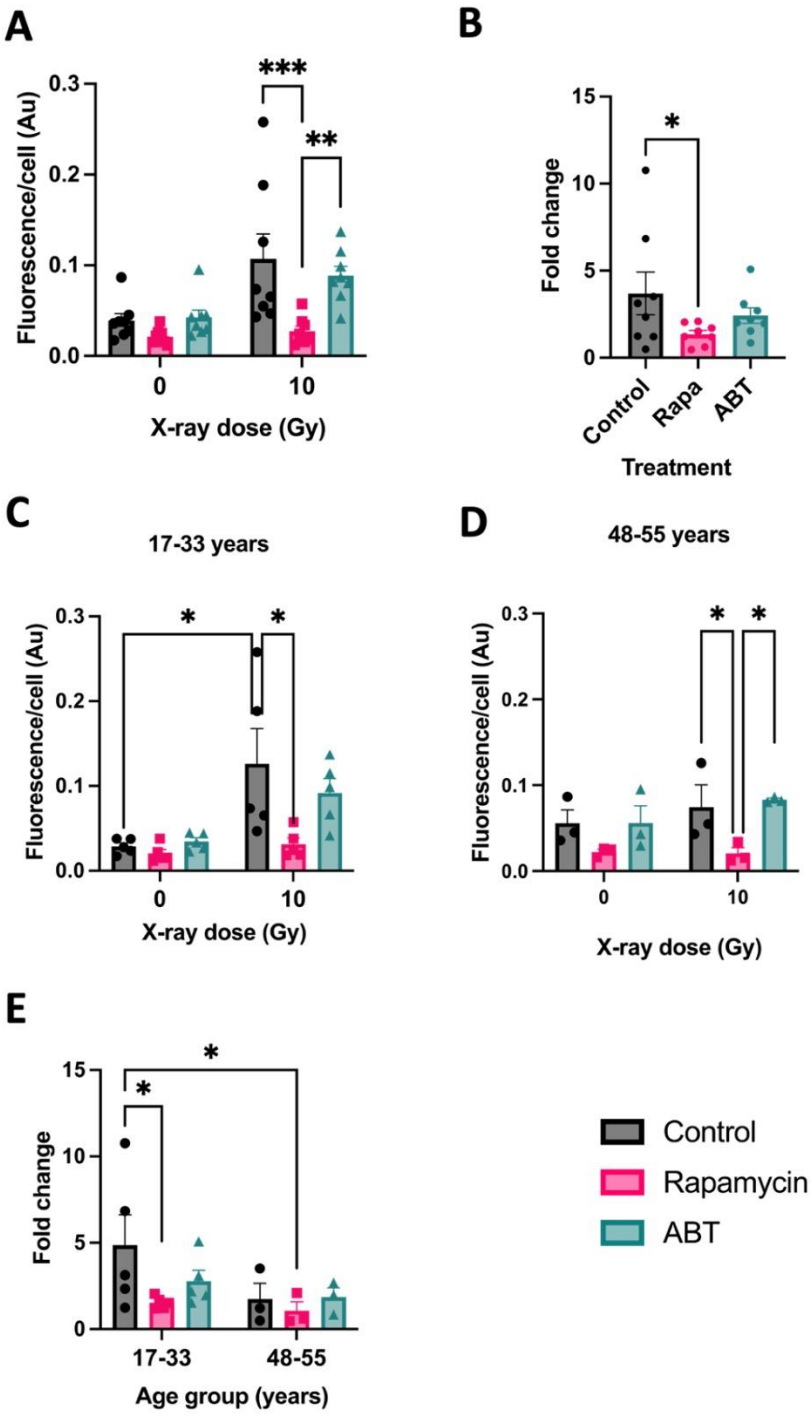


Figure 5.30 SA-β-Gal activity in HCAEC from donors of different ages after X-ray exposure and treatment with rapamycin or ABT-263.

HCAECs from young and middle-aged donors were irradiated with 0 or 10 Gy X-ray when confluent. For rapamycin treatment, 10 nM was added immediately after irradiation, for 5 days. For ABT-263 treatment, 10 nM was added 4 days post

irradiation for 24 hours. The fluorescent SA-β-Gal assay was performed 7 days after irradiation. **A)** Raw SA-β-Gal fluorescence per HCAEC for all donors irradiated with 0 or 10 Gy X-ray, with or without 10 nM rapamycin treatment or 10 nM ABT-263, with the associated fold change after irradiation, compared to drug matched control (**B**). N=8 per group. **C-E)** Raw fluorescence per HCAEC with or without drug treatment in HCAECs from donors from young (**C**) and middle-aged (**D**) donors, with a comparison between the associated fold changes within the age groups (**E**). N=3-5 per group. Two-way ANOVA with multiple comparisons, * = p<0.05, ** = p<0.005, *** = p<0.001.

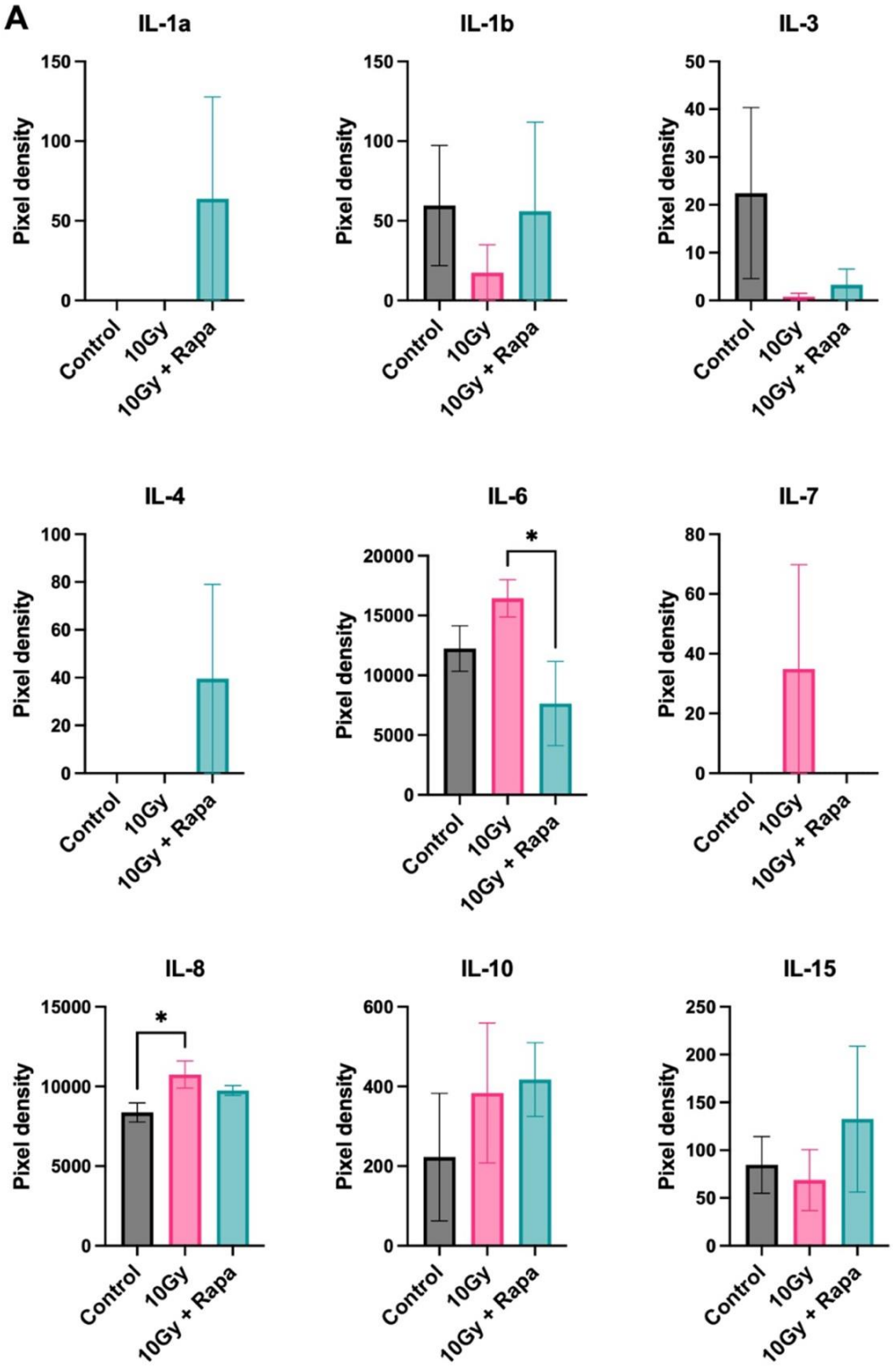
5.3.11 The effect of rapamycin treatment on X-ray-induced SASP

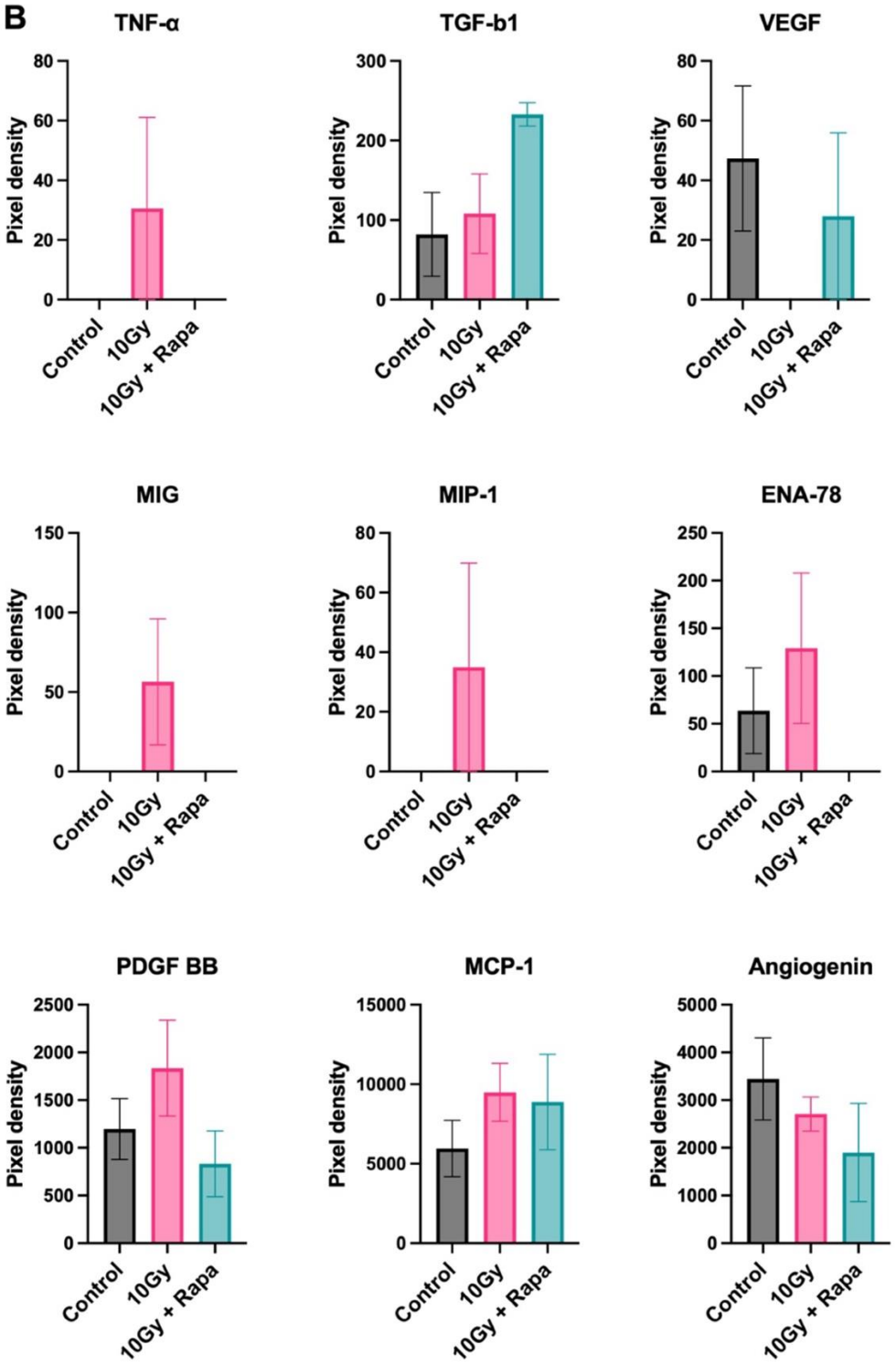
With the inflammatory component of atherosclerosis being considerable, the ability to prevent any upregulation in SASP factors induced by IR exposure will be beneficial (Shang, Liu and Tu, 2023). Therefore, here I investigate the SASP of HCAEC from the donors exposed to X-ray, including rapamycin treatment. Rapamycin was chosen as the drug of choice due to the promising reductions observed in the atherosclerosis associated assays and its reduction in senescence markers. For the rapamycin treatment, the same protocol was followed as in the previous assays, with immediate addition after X-ray exposure for 5 days, with a 2-day recovery period. In all experimental groups, fresh MEC media was applied 2-days before collecting for assessment at day 7 post irradiation.

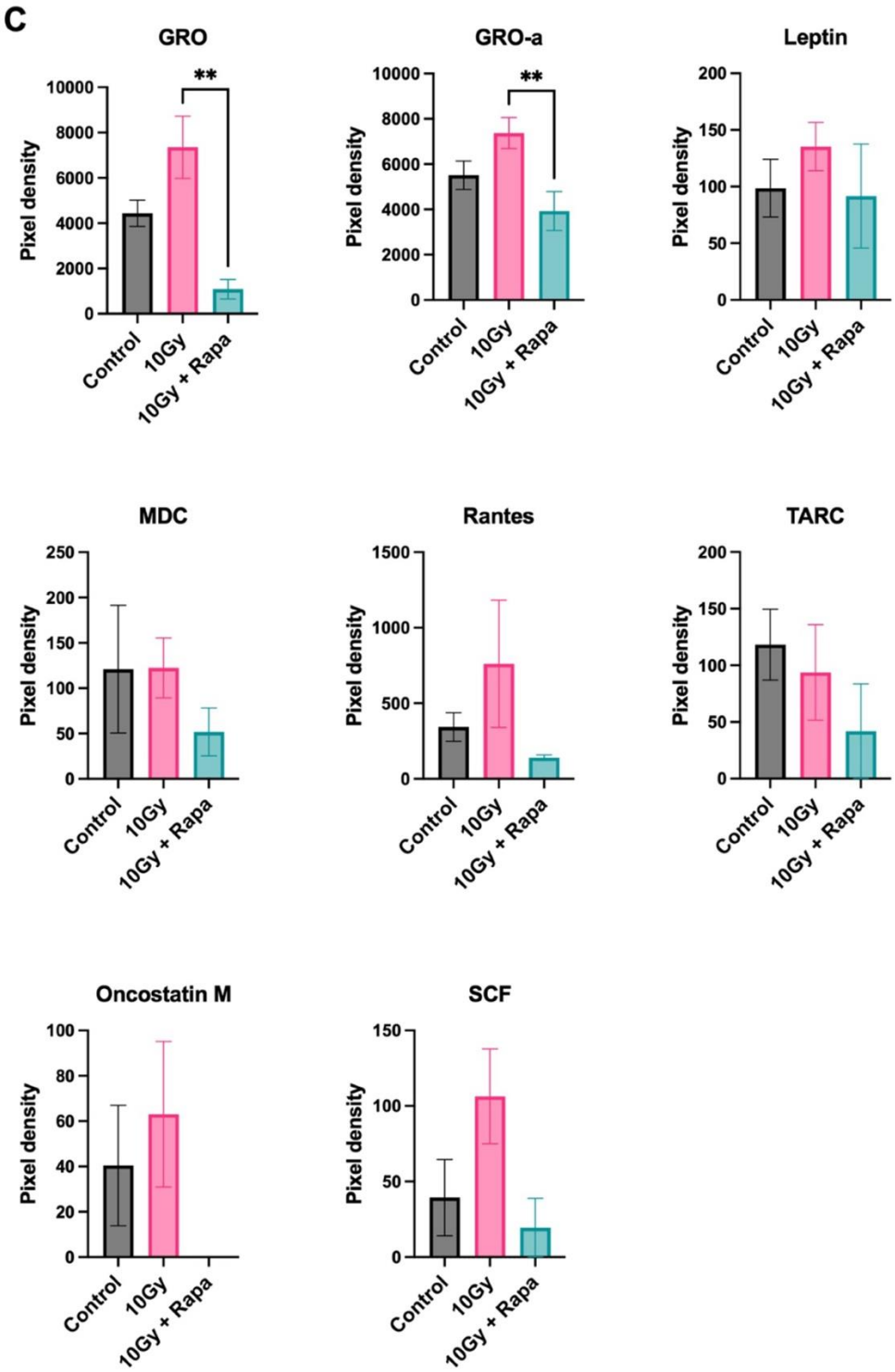
Out of the 42 cytokines investigated, 26 were secreted by the HCAEC (Figure 5.31). Out of these, 17 were upregulated after 10 Gy X-ray exposure (IL-6, IL-7, IL-8, IL-10, TNF-α, TGF-β1, MIG, MIP-1, ENA-78, PDGF BB, MCP-1, GRO, GRO-a, Rantes, Oncostatin M, SCF, Leptin), with IL-8 being significantly upregulated. IL-6 is of particular interest as it is a

commonly used marker of SASP. Out of these, rapamycin prevented the upregulation of 15 (IL-6, IL-7, IL-8, TNF-α, MIG, MIP-1, ENA-78, PDGF BB, MCP-1, GRO, GRO-α, Rantes, Oncostatin M, SCF, Leptin), significantly reducing the levels of IL-6, GRO, and GRO-α.

The fold-change in cytokine expression with rapamycin treatment compared to without, after 10 Gy X-ray exposure, in 23 cytokines that were present in both experimental groups demonstrate a prevention in change of cytokine levels for the majority investigated (Figure 5.31D). However, there was a greater increase in MCP-1 and a greater decrease in IGF-1 with rapamycin treatment. These results suggest that 10 nM rapamycin attenuates the majority of IR-induces inflammatory mediators investigated within these cells, suggesting that it may reduce IR-induced SASP.


A
IL-1a
IL-1b
IL-3
IL-4
IL-6
IL-7
IL-8
IL-10
IL-15
Pixel density
Control
10Gy
10Gy + Rapa
*


B
TNF-α
TGF-b1
VEGF
MIG
MIP-1
ENA-78
PDGF BB
MCP-1
Angiogenin
Pixel density
Control
10Gy
10Gy + Rapa


C
GRO
GRO-a
Leptin
MDC
Rantes
TARC
Oncostatin M
SCF
Pixel density
Control
10Gy
10Gy + Rapa
**

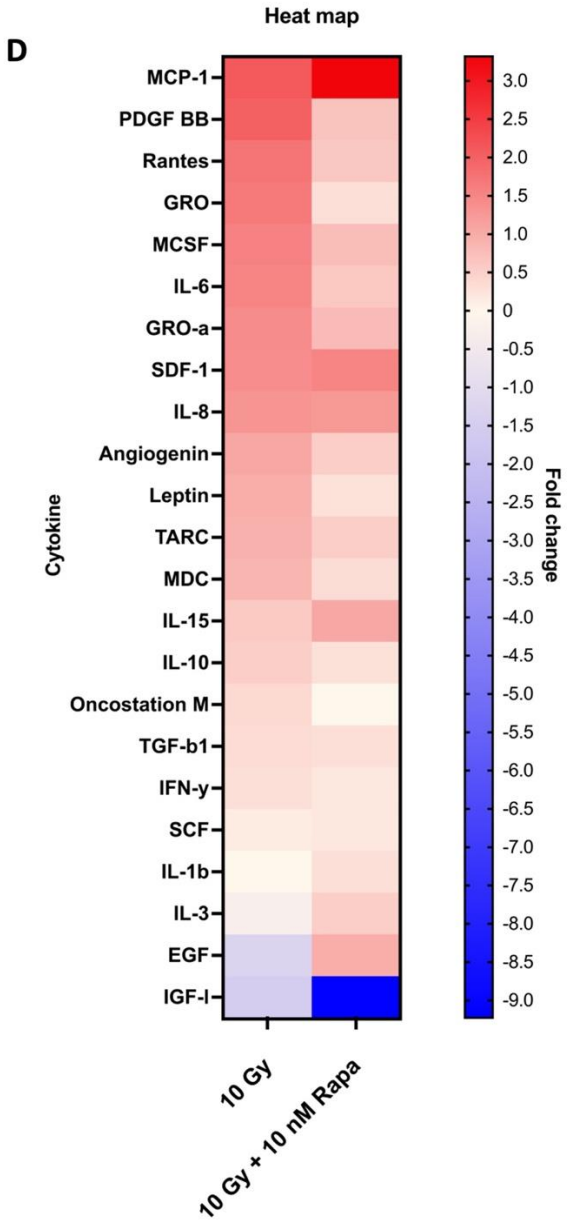


Figure 5.31 Secreted cytokines from HCAEC exposed to X-ray with or without rapamycin.

HCAECs were seeded on fibronectin-coated 10 cm^2 plates (10,000 cells/cm^2) and cultured until confluent (4-6 days). Cells were then exposed to 0 or 10 Gy X-ray and were treated with 10 nM rapamycin or cultured under normal conditions. On day 5, rapamycin was removed, and fresh media was applied to all plates. Media was collected and filtered on day 7. 1 mL of the conditioned media was then incubated on Abcam 42-cytokine arrays (#ab133997) overnight at 4°C. **A-C)** Cytokines detected in the media of HCAEC after 0 Gy or 10 Gy X-ray exposure, with or without 10 nM

rapamycin. **D**) The associated fold change in cytokine expression. N=6 per group. Two-way ANOVA with multiple comparisons, * = p<0.05, ** = p<0.005.

5.4 Discussion

In this chapter, I have demonstrated that HCAECs form intact monolayers that are suitable for the study of permeability and adhesion, phenotypes that are related to atherogenesis. Furthermore, I have demonstrated no significant difference in the adhesion or permeability of the HCAEC monolayers from young or middle-aged donors. However, the HCAECs from middle-aged donors had significantly higher SA-β-Gal activity, suggesting an increased likelihood of displaying aged or senescence characteristics.

In addition, I have demonstrated that irradiation of HCAEC monolayers increases their adhesion and permeability, along with SA-β-Gal activity. Following this, I repeated the experiments with the aim of investigating whether age of the HCAEC donor influences IR-induced adhesion and permeability of the monolayer. I report that there were trends of greater IR-induced increases in adhesion and permeability in the HCAECs from young donors, than middle-aged, although these differences were not statistically significant.

I further investigated the role of senescence in X-ray-induced increases in adhesion and permeability by targeting senescent cells with rapamycin and ABT-263. Firstly, I demonstrated the efficacy of rapamycin and ABT-263 in alleviating X-ray-induced

increases in SA-β-Gal activity within HCAECs. Furthermore, I report that rapamycin treatment reduces IR-induced adhesion, with the trend observed suggesting that it may also reduce IR-induced permeability. Finally, within this chapter, I have also demonstrated differences IR-induced increases in HCAEC cytokine secretion, with rapamycin alleviating many of the changes observed.

5.4.1 Characterising HCAEC for CVD investigations

With the basic characterisation of HCAEC monolayer formation, investigations into the effects of flow culture conditions on HCAEC morphology suggested simulated flow results in less densely populated HCAEC monolayers, which may impact on monolayer barrier functions. While these conditions may be more physiologically relevant, due to the time constraints, required assay optimisations, and technical issues associated with the placing an orbital rotator within a cell culture incubator, further investigations into HCAEC under flow conditions were not carried out.

While there was no significant difference in the permeability and adhesion between HCAECs from young and middle-aged donors, the trend observed suggests that HCAECs from middle-aged donors are more likely to have increased adhesion to monocytes than those from younger donors. To the best of my knowledge, at the time of writing, the use of HCAEC from donors of different ages to investigate age-mediated changes in HCAEC adhesion has not been carried out. However, these results correlate with a previous study that suggested increased HL-60 adhesion to HCAECs which have been aged *in vitro* by serial passaging and begun to enter into RS, compared to early passage cells (Lowe and Raj, 2014b).

In contrast, the permeability of the HCAEC monolayers displayed a slight negative correlation with age, suggesting that the monolayers formed by HCAEC from younger donors are more permeable. However, again these results were also not significant. This is inconsistent with published data which has demonstrated that mimicking age-related changes in the extracellular matrix (ECM) increased the permeability of endothelial monolayers (Huynh *et al.*, 2011), along with HUVECs that have entered into RS having increased permeability (Krouwer *et al.*, 2012b). Importantly, these publications used HUVECs and bovine arterial endothelial cells which will differ to HCAEC, along with artificially generating an aged ECM, which may not be fully representative. However, this does highlight a potential flaw in the permeability assay I have used for this study, as the HCAECs from young and middle-aged donors were seeded on a matrigel matrix of the same consistency. Therefore, if it is an aged ECM that promotes EC permeability, it is likely that this would not be observed. Furthermore, if it is the development of RS that increases EC permeability, this will be minimally observed in the h-tert immortalised cells I have used within these studies. However, the SA-β-Gal assay performed on the HCAECs within this chapter demonstrated a significant increase in SA-β-Gal activity in the cells from middle-aged donors. While this is not a definitive marker of senescence, this result suggests that these cells may be displaying some senescence characteristics.

5.4.2 IR and CVD phenotypes in HCAECs

When investigating the atherogenic response of HCAEC from young and middle-aged donors to IR, I have demonstrated that both age groups have increased HL-60 adhesion

after IR exposure. Furthermore, the trend suggests that IR-induced adhesion is more prominent in HCAEC from younger donors, although initially not significant. However, during later repeats, a significant difference in fold-change in HCAEC adhesion was observed within the HCAECs from young donors compared to middle-aged. However, while the trends support this in both experimental runs, it suggests caution should be taken with forming conclusions on these results. Importantly, many studies have reported varied degrees of radiation sensitivity between people (Rajaraman *et al.*, 2018a; Palumbo *et al.*, 2019), suggesting this study may be underpowered.

Similarly, I have demonstrated that IR exposure significantly increases the permeability of the HCAEC monolayer, in HCAEC from both young and middle-aged donors. However, no significant age-modulation of IR-induced permeability of HCAEC monolayers was observed.

While these monolayers were inspected under a phase contrast microscope before conducting the assay, it is possible that the radiation exposure leads to cell death and gaps within the monolayer, rather than a senescence associated increase in permeability. However, the increase in permeability after X-ray exposure aligns with studies that demonstrate increased permeability with the development of senescence (Huynh *et al.*, 2011; Krouwer *et al.*, 2012b; Uzarski, Scott and McFetridge, 2013). Indeed, this is supported with the SA-β-Gal assays within this chapter, which demonstrated an increase in SA-β-Gal activity.

Interestingly, this was only significantly increase in the HCAEC exposed to IR from the younger donors, although the average measure of activity was still considerably raised in the HCAEC from older donors.

When investigating the correlation between SA-β-Gal activity and the atherogenic phenotypes, there was a clear, significant increase in adhesion with increased SA-β-Gal activity, supporting the hypothesis that senescence may be driving IR-induced increases in adhesion. However, there was a slight negative correlation in relation to the permeability of the HCAEC monolayer. Although this was not significant, it suggests that if indeed senescence increases monolayer permeability, then the permeability assay set-up may not be the right approach to detect any related changes.

Within this chapter, I also investigated using a pharmacological approach to target X-ray induced senescent cells in an attempt to ameliorate the X-ray induced atherogenic phenotypes described. Within this, the mTOR inhibitor rapamycin and BCL-2 inhibitor, ABT-263, were chosen. However, the senolytic ABT-263 was not successful in any of the age groups investigated. This may be due to a number of reasons; Firstly, 4 days may not have been long enough to allow for sufficient development of senescence within the cell populations. Secondly, the amount of time the cells were incubated with the drug may not have been long enough. The time frames used were needed in order to be able to compare all of the assays. In contrast, rapamycin was successful in reducing the X-ray associated increases in adhesion, particularly in the HCAEC from younger donors, which had a more significant increase in SA-β-Gal activity. The effect of rapamycin on IR-induced permeability was similar, although not significant, it resulted

in a reduction in the average IR-induced permeability of the HCAEC from older donors. Again, the effect of rapamycin is more pronounced in the conditions where there is a greater increase in the associated atherogenic phenotype. I also provided strong evidence that the beneficial effects of rapamycin were a result of reducing the senescent cell burden, with both the SA-β-Gal assay and assessment of nuclear morphology, combined with the observed reductions in secreted SASP factors, such as IL-6.

Furthermore, I have demonstrated that cytokines related to the progression of atherosclerosis, such as GROα which has been implicated in increasing unstable coronary artery disease and IL-8 which increases the risk of CVD (Geiser *et al.*, 1993; Zernecke, Shagdarsuren and Weber, 2008b), which are upregulated with X-ray exposure in HCAECs can be reduced with rapamycin treatment. Similarly, the chemokine RANTES, which is a monocyte chemoattractant and has been implicated in the early pathogenesis of atherosclerosis (Podolec *et al.*, 2016; Jongstra-Bilen *et al.*, 2021), was upregulated with X-ray exposure, with rapamycin demonstrating an ability to prevent this from occurring. These results suggest that targeting HCAEC with rapamycin may be a viable option for preventing the IR-induced SASP, which if similar observations are made *in vivo*, may reduce the severity of IR-induced atherosclerosis.

Some considerations and limitations of the work carrier out in this chapter revolve around the use of immortalised HCAECs. This is particularly relevant when considering non-IR exposure evidence, as there will be limited development of RS, which may result in a less pronounced age phenotype in the HCAEC from older donors. This also has

relevance when considering the hypothesis involving age mediating the effects of IR exposure, with one hypothesis being that the increased senescent cell burden within age *in vivo* would result in fewer non-senescent cells for the IR to interact with, and thus would lead to less of an increase in senescent cell burden when compared to someone of a younger age who is exposed. Furthermore, the nature of *in vitro* cell culture results in the selection of cells within a population which proliferate more rapidly, which may not reflect a cell population *in vivo*. Furthermore, as demonstrated within this chapter, the effects of culturing cells in flow conditions alters their morphology, meaning the static cell culture conditions used for the assays performed here may not reflect the response of the cells *in vivo*. Indeed, previous experiments have demonstrated changes in the adhesion of HL-60 cells to ECs, depending on the type of flow applied to them (Uzarski, Scott and McFetridge, 2013).

6 Comparative transcriptomics of HCAECs

6.1 Introduction

As clear associations between irradiation of HCAECs and the development of pro-atherogenic phenotypes have been made (Chapter 5), identification of any IR-induced changes in gene expression will help aid future investigations into potential mechanisms. Rather than selecting genes of interest and taking a targeted approach, comparative transcriptomics allows for an unbiased approach, which may result in the identification of genes or pathways that might otherwise have been overlooked. Furthermore, it is then possible to mine the resultant datasets for genes of interest, providing a comprehensive method for early-stage mechanistic investigations. While there are different methods of transcriptome sequencing, within this chapter I utilise Nanopore sequencing technology (Oxford Nanopore Technologies)

6.1.1 Oxford Nanopore sequencing

Oxford Nanopore sequencing uses flow cells which contain nanopores that allow the movement of DNA or RNA sequences through a synthetic membrane. As the nucleic acid sequence passes through the pore, it disrupts an ionic current, which is then translated into a nucleotide sequence by the MinKNOW software (Oxford Nanopore Technologies). Unlike other sequencing technology, the nanopore system allows for full-length transcript analysis, rather than breaking the sequences into smaller sections.

For the sequencing conducted in this chapter, I created barcoded, cDNA libraries from HCAEC RNA, which enabled pooling of different samples for multiplexing. While this approach reduces the amount of genes sequenced per sample, it reduces the cost per sample and enables for the inclusion of more experimental groups. The initial steps involved reverse transcription and strand-switching of the sample RNA, selecting for full-length transcripts by PCR, followed by the addition of barcoded primers and adapters to facilitate movement through the nanopores. The cDNA library was then loaded onto the flow cells for sequencing over 72 hours. The base-called sequences were then aligned to the genome, normalised between samples using the number transcripts per million reads, and analysed for differential gene expression (detailed in section 2.10).

6.2 Chapter aims

In this chapter, I set out to investigate the following questions:

1. Are there differences in the transcriptome of HCAECs from young and middle-aged donors?
2. Does age of the HCAEC donor affect X-ray-induced gene expression changes?
3. Does rapamycin alleviate IR-induced changes in atherosclerosis related gene expression?

6.3 Results

6.3.1 Age difference in the transcriptome of HCAECs

Searches through sequencing databases such as GEO Datasets and EMBL Expression Atlas, along with publication searches, failed to identify any studies that investigated age-related changes in the HCAEC transcriptome. Therefore, to provide a novel overview of transcriptome changes with age in HCAECs, I performed comparative transcriptomics using Nanopore sequencing to identify differences in gene expression between HCAECs from young (17-26 years old) and middle-aged (54-55 years old) donors.

To achieve this, HCAECs were seeded in 10 cm^2 tissue culture plates and maintained in standard cell culture conditions (detailed in section 2.2.1) until confluent. The RNA was then isolated, and a cDNA library was prepared for nanopore sequencing (described in section 2.10). The sequencing was performed over 72 hours, with the WF-transcriptomes pipeline (Oxford Nanopore Technologies, described in section 2.10) used for the differential gene expression analysis.

The differential gene expression analysis indicated 750 statistically significant, differently expressed genes within the HCAECs from the middle-aged donors, compared to the young (Figure 6.1A), 67 of these genes had a false discovery rate (FDR) of <0.05 (supplementary S6.1), with the top 10 most significantly differentially expressed listed (Figure 6.1B). Due to the number of significantly differentially expressed genes, here I

focus on the top 10 most significant. Within these genes, two were found to have reduced expression in the HCAECs from middle-aged donors, compared to young, Uclh*1* (ubiquitin carboxy-terminal hydrolase 1) and *Cd24* (cluster of differentiation 24). *Uclh1* has been implicated in the progression of age-related diseases, such as Alzheimer's and Parkinson's disease (Coulombe *et al.*, 2014). Furthermore, pharmacological inhibition with LDN-5744 and siRNA knockdown within pulmonary endothelial cells has been shown to lead to an increase in the permeability of the endothelial barrier (Mitra *et al.*, 2021), suggesting that the lower expression observed in HCAECs from middle-aged donors may be associated with increased monolayer permeability. However, this was not observed in the permeability assays performed in Chapter 5.

Upregulation of *Cd24* has been associated with increased tumour progression and vascularisation, along with silencing resulting in decreased HUVEC migration and reduced wound healing (Wang *et al.*, 2016; Altevogt *et al.*, 2021). Therefore, the lower expression levels observed in HCAECs from middle-aged donors suggests that these cells may be less likely to migrate in response to vascular injury, which may have implications for the initiation of atherosclerosis, of which damage to the HCAEC monolayer can drive (Section 1.2.3).

Within this analysis, I also overserved increased expression of 8 genes in the HCAECs from middle-aged donors, compared to young. *Plat* is a secreted serine protease that is essential for fibrinolysis and the breakdown of blood clots (Suzuki *et al.*, 2011). Furthermore, PLAT degrades ECM components, which will affect the binding of HCAECs to the ECM, along with the retention of lipids in the sub-endothelial space. Indeed, early

studies demonstrated a correlation between increased blood plasma levels of PLAT and advanced atherosclerosis (Lupu *et al.*, 1995; Steins *et al.*, 1999). Furthermore, upregulation of *Plat* has been associated with aged and senescent brain endothelial cells in mice (Kiss *et al.*, 2020). Therefore, the upregulation of *Plat* within HCAECs from middle-aged donors suggests that they may have altered ECM interactions, which may affect monolayer permeability, potentially resulting in a pro-atherogenic phenotype.

Crip1 (cysteine rich intestinal protein 1) was significantly upregulated in the middle-aged HCAEC. This is a member of the LIM/double zinc finger protein family and has been shown to down-regulate the expression of Fas proteins, with overexpression reducing 5-fluorouracil-induced apoptosis in SW620 and RKO cells (colorectal cancer cell lines) (Zhang *et al.*, 2019). Furthermore, a mouse model overexpressing CRIP was shown to have an altered cytokine expression pattern compared to control, with greater upregulation of cytokines such as IL-10 and IL-6 in response to pathogenic infection (Lanningham-Foster *et al.*, 2002). More recently, it was shown that CRIP1 silencing upregulates the axin protein in acute myeloid leukaemia cells *in vitro*, resulting in inactivation of the Wnt/β-catenin signalling pathway, leading to induction of apoptosis and G1/S cell cycle transition arrest (Deng *et al.*, 2023). While no studies have investigated these effects in HCAECs, they hint towards upregulation of *Crip1* promoting the survival of aged or damaged cells. Furthermore, if *Crip1* expression increases with age, as these results suggest, then it may result in increased inflammatory cytokine secretion with age in response to infection, as observed with the increased prevalence of COVID-19-induced cytokine storms with age (Nidadavolu and Walston, 2021). This

suggests possible avenues of investigation into any relationship between *Crip1* expression, senescence, and the SASP.

Cox7A1, which was significantly upregulated in the HCAEC from middle-aged donors, encodes the subunit 7A1 for cytochrome c oxidase. Studies have demonstrated that overexpression of COX7A1 blocks autophagic flux within human non-small cell lung cancer cell lines by downregulating PGC-1α along with upregulating NOX2 (Zhao *et al.*, 2019). Ultimately, it was demonstrated that overexpression of COX7A1 promoted apoptosis within these cells along with inhibiting autophagy. Therefore, the increased expression observed in HCAECs from middle-aged donors suggests that autophagy may be differentially modulated, compared to HCAECs from young donors.

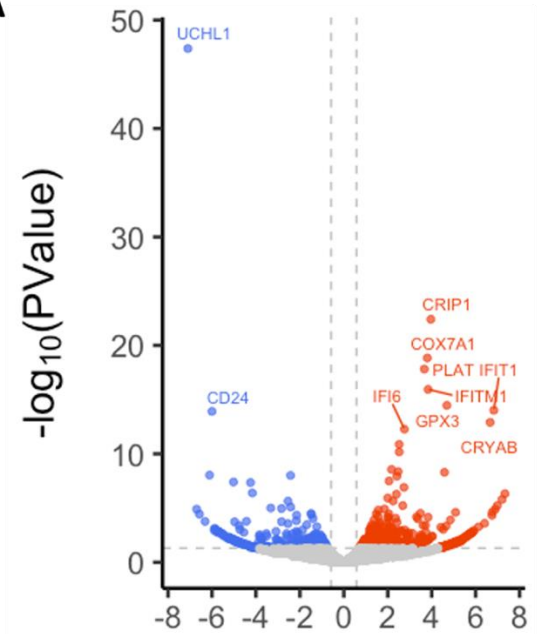
The increased expression of *CRYAB* in the HCAEC from middle-aged donors is also interesting. This has been suggested as a gene that is upregulated in many different cell types (e.g., hCMECs, hLSCs, IMR90) during senescence, along with different senescence inducers (doxorubicin and IR), with targeting this gene being proposed as a potential senolytic (Limbad *et al.*, 2022). This upregulation within the older HCAECs may suggest that they are more likely to be in senescence or developing a senescent phenotype, which supports the findings in Chapter 5 where I observed increased SA-β-Gal activity in the HCAECs from middle-aged donors, compared to young.

Lastly, *Ifi6* (interferon α inducible protein 6) is induced by interferon, with overexpression in human vascular endothelial cells inhibiting apoptosis in conjunction with increased BCL-2 expression (Qi *et al.*, 2015), suggesting activation of pro-survival

pathways in the HCAECs from middle-aged donors similar to those observed in senescence (Zhu *et al.*, 2015).

Overall, the gene expression observed in the HCAECs from middle-aged donors compared to young is suggestive of an aged phenotype, supporting the SA-β-Gal assay performed in Chapter 5 which suggested an increased likelihood of the HCAECs from middle-aged donors being senescent. Furthermore, the expression of genes discussed here suggests that the HCAECs may have a pro-atherogenic phenotype. However, this was not reflected in the permeability and adhesion assays previously performed (Chapter 5). Importantly, due to the vast number of genes found to be significantly differentially expressed with age in the HCAECs, individually investigating each gene is not feasible, along with potentially missing the complex molecular interactions associated with the interplay in their expression. Furthermore, it is not possible to state that a certain genes expression will result in a particular characteristic. However, from the few genes discussed here, future research can be targeted to identify whether they influence cellular functions with HCAECs.

A



B

gene	logFC	pvalue	FDR	diffexpressed
UCHL1	-7.098146445	4.25E-48	6.17E-44	Down
CRIP1	3.963254264	3.91E-23	2.84E-19	Up
COX7A1	3.799163613	1.45E-19	6.99E-16	Up
PLAT	3.664848307	1.54E-18	5.58E-15	Up
IFITM1	3.836473938	1.14E-16	3.3E-13	Up
GPX3	4.692367954	3.39E-15	8.2E-12	Up
IFIT1	6.827866953	9.53E-15	1.97E-11	Up
CD24	-5.998216758	1.21E-14	2.18E-11	Down
CRYAB	6.66150479	1.25E-13	2.01E-10	Up
IFI6	2.759059614	5.3E-13	7.68E-10	Up

Figure 6.1 Differential gene expression analysis of young and middle-aged HCAEC.

WF-transcriptome (Oxford Nanopore Technologies) pipeline processing of nanopore sequencing performed on cDNA from HCAECs from young (17-26 years) and middle-aged (54-55 years) donors. The resultant differential gene expression in the middle-aged HCAEC cells compared to young as $\log_2$ fold change and statistical significance as $\log_{10}$(PValue) is displayed (A), with the top 10 most significantly differentially expressed listed. N=3, T-test.

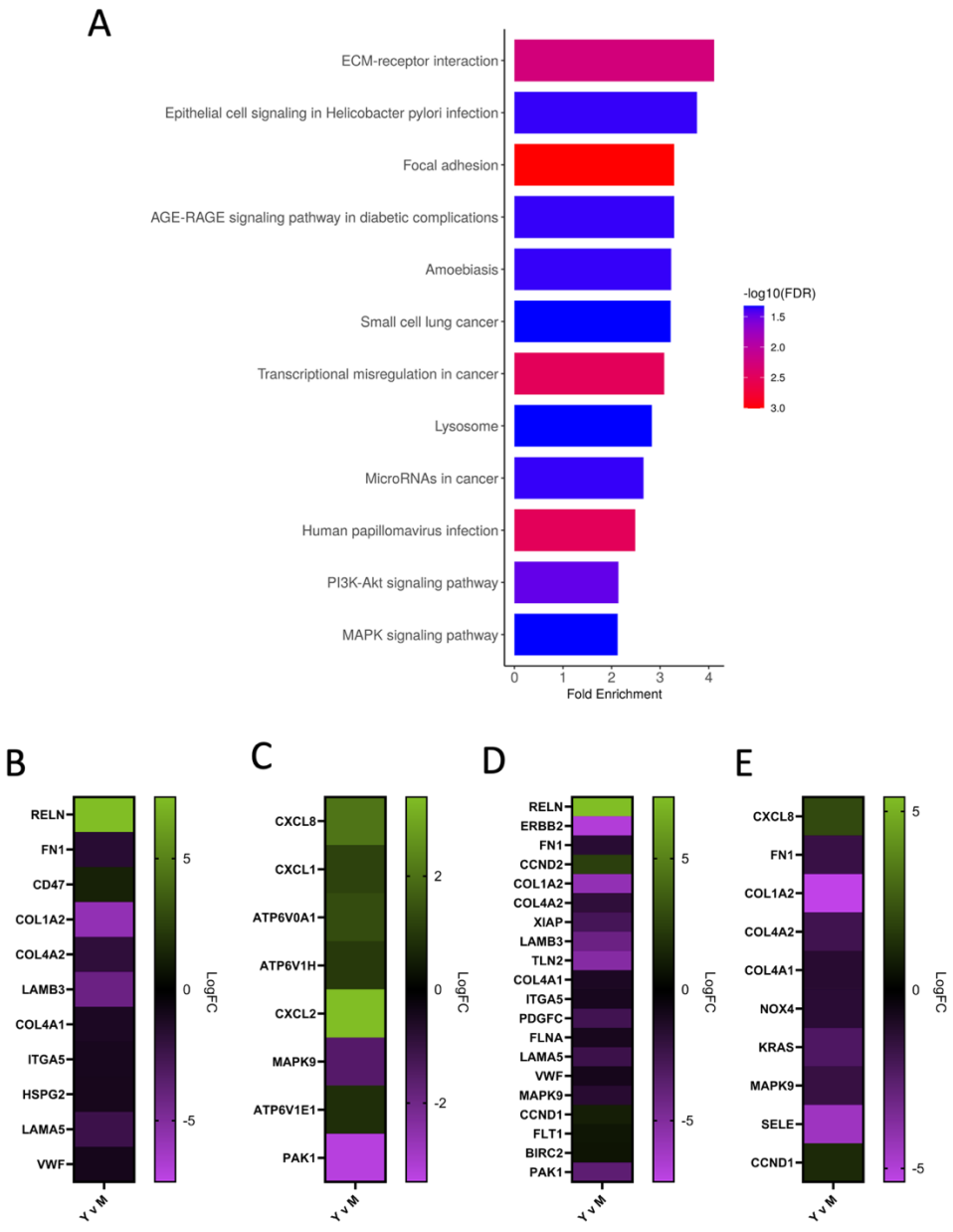
To provide insight into the wider biological context of the genes differentially expressed between HCAECs from young and middle-aged donors, I used ShinyGO to perform gene ontology (GO) analysis on those that were found to be significantly differentially expressed (Ge *et al.*, 2020). GO analysis uses databases of genes related to biological processes and compares experimental datasets to predict the processes likely to be associated with the gene expression profile. In the context of changes in HCAEC gene expression with age, this enables prediction of the biological processes that may be associated with age.

The GO analysis of the significantly differentially expressed genes in the HCAECs from middle-aged donors compared to young identified 12 likely biological process (Figure 6.2A). From these pathways, I identified the associated genes and their differential expression (Figure 6.2B-M). Many of the predicted processes are related to cellular ageing, senescence, and HCAEC monolayer maintenance, such as ECM-receptor interaction, AGE-RAGE signalling, lysosome processes. Differential modulation of the ECM-receptor interaction pathway may have both direct and indirect effects on cellular adhesion, proliferation, and apoptosis (Bloom *et al.*, 2023b). Many of the genes associated with this pathway were significantly downregulated in HCAEC from older donors, including *Col1A2* (encoding pro-α chain type 1 collagen) and *Lamb3* (encoding the β-subunit of laminin), suggesting that these cells have changes in both their ECM and their interaction with it (Figure 6.2A), with similar changes observed in ageing and senescence (Woldhuis *et al.*, 2020).

Another pathway of interest is the AGE-RAGE (advanced glycation end products - receptor for advanced glycation end products) signalling pathway in diabetic complications (Figure 6.2). This pathway elicits many intracellular signalling cascades, such as the MAPKs, and results in NF-κ B activity and has been associated with age related diseases along with effecting vascular homeostasis (Senatus and Schmidt, 2017). Furthermore, downstream pathways may promote the expression of inflammatory cytokines, such as IL-1 and IL-6 (Liu *et al.*, 2017), along with RAGE induction of JAK-STAT-mediated and PI3K-Akt-dependent pathways, with are involved in cell proliferation, apoptosis, and inflammatory signalling (Ariyoshi *et al.*, 2001; Rai *et al.*, 2012; Dong *et al.*, 2022).

In addition to this, upregulation of the cytokine and chemokine genes *Cxcl8*, *Cxcl1*, *Cxcl2* (encoding IL-8, GROα, and GROβ, respectively) was noted in many of the pathways mentioned (Figure 6.2B-M). These chemokines and cytokines are involved in inflammatory signalling and immune cell recruitment (Breland *et al.*, 2008; Qin *et al.*, 2013). Indeed, IL-8 has been shown to increase the adhesion of the monocyte like THP-1 cells to HUVEC monolayers, suggesting that the increased *Cxcl8* expression may result in increased monocyte adhesion to the HCAEC from middle-aged donors (Xu *et al.*, 2022). The upregulation of secreted factors such as these is also observed in the SASP of senescent cells. Furthermore, an upregulation of a number of the genes associated with the lysosome was observed (Figure 6.2I), suggesting that there may be increased lysosome biogenesis, which is another hallmark of senescence (Discussed in section 1.5.2).

Overall, the pathways and direction of the associated differential gene expression in the HCAEC from middle-aged donors suggest that they would be more likely to display atherogenic phenotypes, along with pro-senescent characteristics, which provides some insight into the findings in chapter 5, along with future avenues of investigation to identify potential mechanisms. Furthermore, this section has provided evidence of the changes in HCAECs gene expression with age, with literature searches only revealing age related changes in coronary artery ECs in animal models.


A
ECM-receptor interaction
Epithelial cell signaling in Helicobacter pylori infection
Focal adhesion
AGE-RAGE signaling pathway in diabetic complications
Amoebiasis
Small cell lung cancer
Transcriptional misregulation in cancer
Lysosome
MicroRNAs in cancer
Human papillomavirus infection
PI3K-Akt signaling pathway
MAPK signaling pathway
0 1 2 3 4
Fold Enrichment
-log10(FDR)
1.5
2.0
2.5
3.0
B
RELN
FN1
CD47
COL1A2
COL4A2
LAMB3
COL4A1
ITGA5
HSPG2
LAMA5
VWF
Y v M
LogFC
5
0
-5
C
CXCL8
CXCL1
ATP6V0A1
ATP6V1H
CXCL2
MAPK9
ATP6V1E1
PAK1
Y v M
LogFC
2
0
-2
D
RELN
ERBB2
FN1
CCND2
COL1A2
COL4A2
XIAP
LAMB3
TLN2
COL4A1
ITGA5
PDGFC
FLNA
LAMA5
VWF
MAPK9
CCND1
FLT1
BIRC2
PAK1
Y v M
LogFC
5
0
-5
E
CXCL8
FN1
COL1A2
COL4A2
COL4A1
NOX4
KRAS
MAPK9
SELE
CCND1
Y v M
LogFC
5
0
-5

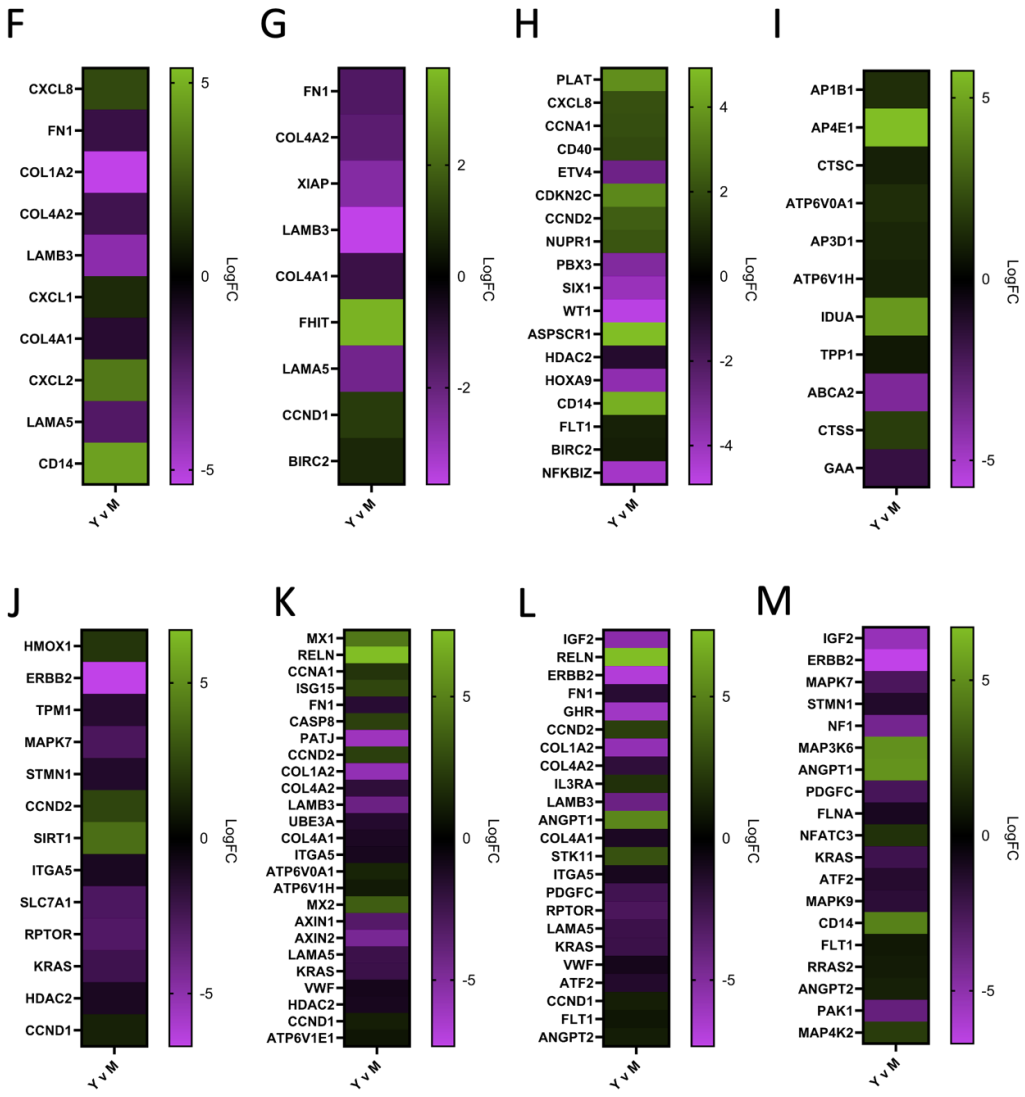


Figure 6.2 GO pathways of differentially expressed genes in HCAEC from middle-aged donors.

Genes significantly differentially expressed between HCAEC from young and middle-aged donors were submitted for GO analysis using ShinyGO. Significantly predicted GO pathways associated with the differentially expressed genes is shown (**A**). N=3, hypergeometric tests. B-M) The genes found to be significantly differentially expressed in HCAEC from middle-aged donors, compared to young, that are associated with the significantly predicted KEGG pathways. B) ECM-receptor interaction. C) Epithelial cell signaling in Helicobacter pylori infection. D) Focal adhesion. E) AGE-RAGE signaling pathway in diabetic complications. F) Amoebiasis. G) Small cell lung cancer. H) Transcription misregulation in cancer. I) Lysosome. J) MicroRNAs in cancer. K) Human papillomavirus infection. L) PI3K-Akt signaling

pathway. M) MAPK signaling pathway. Log fold change is displayed. N=3, student's T-test.

6.3.2 Age differences in IR-induced differential gene expression in HCAEC

To investigate if age of the HCAEC donor affects IR-induced changes in gene expression, HCAECs from young and middle-aged donors were seeded on 10 cm^2 plates and exposed to 0 or 10 Gy X-ray once confluent. 7-days post irradiation, RNA was extracted from the cells and a cDNA library was prepared for nanopore sequencing (as described in section 2.10). Raw sequences were then matched to the corresponding genes, differential gene expression analysis performed including students t-tests for statistical analysis. This revealed 2057 genes that were significantly differentially expressed in irradiated HCAECs from young donors (Figure 6.3A), with 28 having an FDR <0.05 (Supplementary Table S6.2). Within the irradiated HCAECs from middle-aged donors, 534 genes were significantly differentially expressed (Figure 6.3B), with *Troap* reaching an FDR<0.05. Comparing the differentially expressed genes in irradiated HCAECs from middle-aged donors compared to young identified 1466 that were significantly differentially expressed (Figure 6.3C), with none having an FDR<0.05.

Firstly, I visualised the IR-induced changes in gene expression using volcano plots (Figure 6.3A-B). I then filtered the results for statistical significance (student's t-test, $p<0.05$), ranked them using log_2 fold-change, and performed gene ontology enrichment analysis using the GOrilla web-based platform (Eden *et al.*, 2009). This revealed 11 GO process predicted to be active in HCAECs from young donors after irradiation and 5 in the

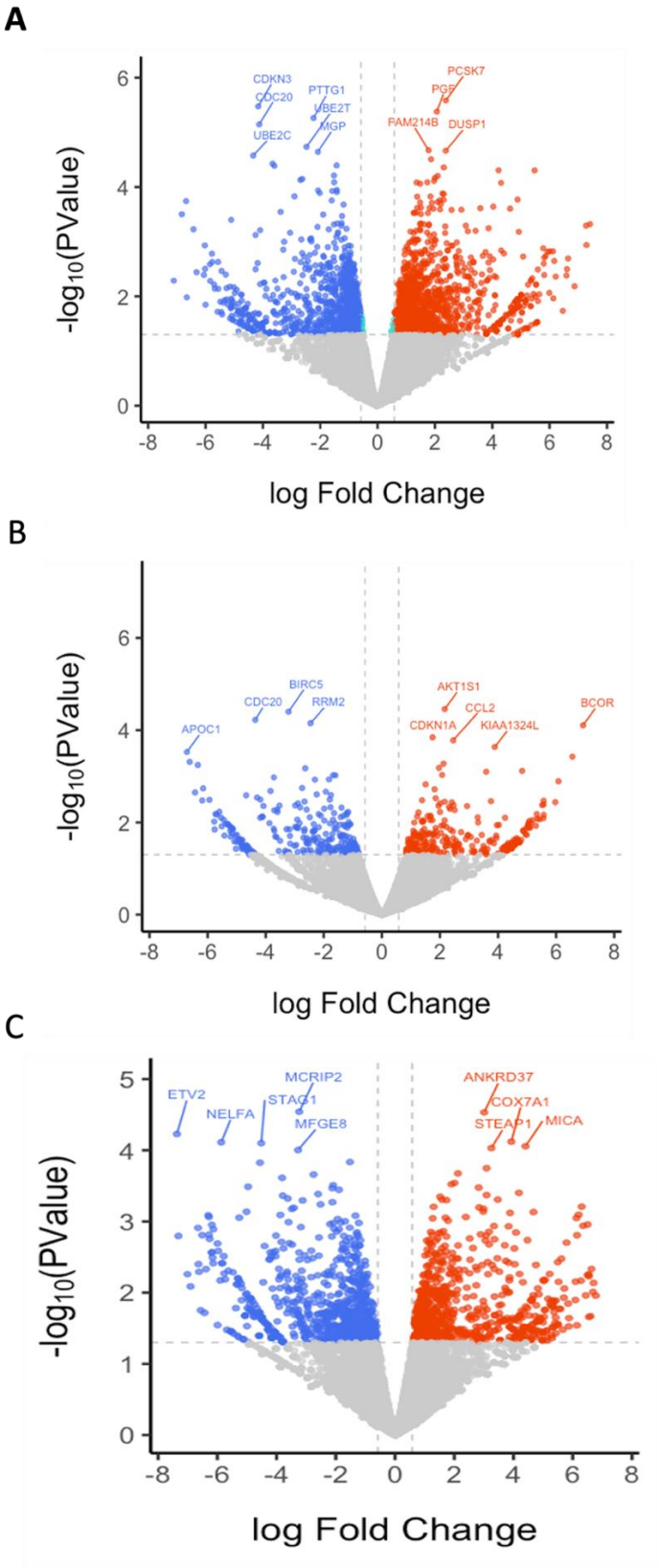
HCAECs from middle-aged donors (Figure 6.3D-E). In addition to this, GO analysis of the differential gene expression in HCAECs from middle-aged donors compared to young after irradiation revealed 14 GO process that are likely to be active (Figure 6.3E).

Within the irradiated HCAECs from young donors, X-ray exposure appears to have affected molecular processes associated with the regulation of transcription, with identification of GO processes such as: regulation of transcription by RNA polymerase II, regulation of transcription (DNA templated), regulation of nucleic acid-templated transcription, and regulation of RNA biosynthetic processes (Figure 6.3D). Furthermore, processes such as the regulation of cellular component movement and processes related to modification of peptidyl-lysine and peptidyl-tyrosine, we predicted to be active. These suggest that IR exposure of HCAECs from young donors causes a shift in gene expression and modification of proteins, which is unsurprising given the number of genes significantly differentially expressed. Indeed, IR-induced changes in transcription in ECs has been documented previously, with identification of potential markers of exposure at 72-hours post irradiation (Chopra *et al.*, 2022). Furthermore, changes in the transcriptome are well documented in senescence, along with its induction by IR (Section 1.5.3.3) (Casella *et al.*, 2019; Kandhaya-Pillai *et al.*, 2023). In addition, regulation of secretion within these cells was also affected by irradiation, suggesting that the increases in inflammatory cytokines observed in section 5.3.11 may have been due to IR-induced changes in gene expression.

However, the GO processes related to the differential gene expression in the irradiated HCAECs from middle-aged donors indicates changes in processes such as lipid catabolic

processes, detection of chemical stimuli, and regulation of G protein-coupled receptor signalling pathways (Figure 6.3E). Firstly, the prediction of different GO processes between the two age groups suggests that age modulates the biological response of HCAECs to IR. Furthermore, these processes suggest that IR exposure changes the interaction of the HCAECs with their environment, along with how they respond to intercellular signalling.

When assessing the GO pathways associated with the differential gene expression between the irradiate HCAECs from young and middle-aged donors (Figure 6.3F), the results suggest that regulation of inclusion body assembly is greatly changed in the irradiated HCAECs from middle-aged donors, which may suggest a greater accumulation of un-folded proteins and potentially increases disruption in proteostasis, which are characteristics of ageing and senescent cells (Sabath *et al.*, 2020). Furthermore, a number of the detected processes are involved in atherogenesis, such as cell-cell adhesion via plasma-membrane adhesion molecules and cell chemotaxis (Gimbrone and García-Cardeña, 2016a; Gencer *et al.*, 2021).


A
CDKN3
CDC20
UBE2C
PTTG1
UBE2T
MGP
PCSK7
PGF
FAM214B
DUSP1
-log10(PValue)
log Fold Change
B
APOC1
BIRC5
CDC20
RRM2
AKT1S1
CCL2
CDKN1A
KIAA1324L
BCOR
-log10(PValue)
log Fold Change
C
ETV2
NELFA
MCRIP2
STAG1
MFGE8
ANKRD37
COX7A1
STEAP1
MICA
-log10(PValue)
log Fold Change

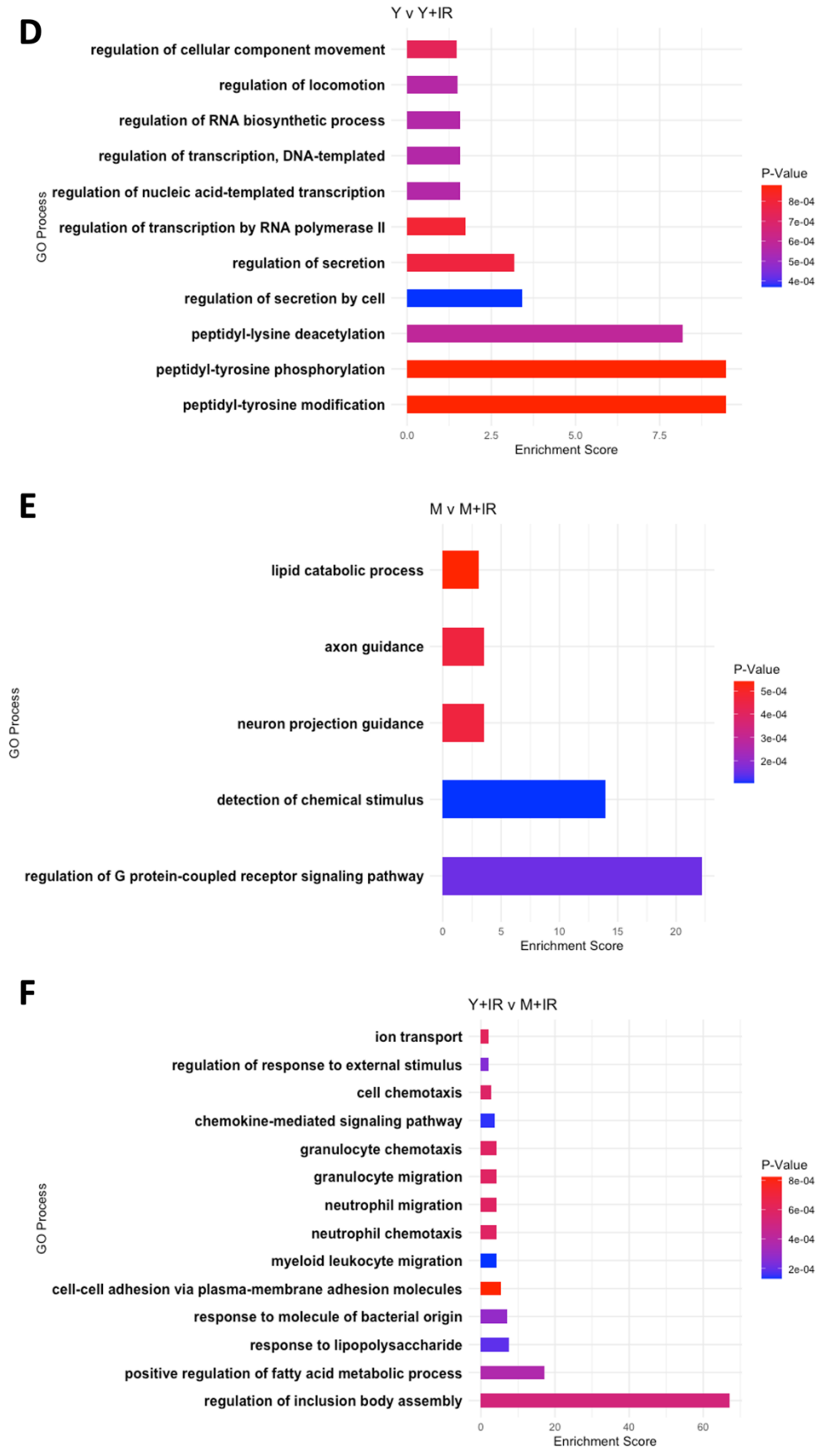

D
Y v Y+IR
regulation of cellular component movement
regulation of locomotion
regulation of RNA biosynthetic process
regulation of transcription, DNA-templated
regulation of nucleic acid-templated transcription
regulation of transcription by RNA polymerase II
regulation of secretion
regulation of secretion by cell
peptidyl-lysine deacetylation
peptidyl-tyrosine phosphorylation
peptidyl-tyrosine modification
GO Process
0.0
2.5
5.0
7.5
Enrichment Score
P-Value
8e-04
7e-04
6e-04
5e-04
4e-04
E
M v M+IR
lipid catabolic process
axon guidance
neuron projection guidance
detection of chemical stimulus
regulation of G protein-coupled receptor signaling pathway
GO Process
0
5
10
15
20
Enrichment Score
P-Value
5e-04
4e-04
3e-04
2e-04
F
Y+IR v M+IR
ion transport
regulation of response to external stimulus
cell chemotaxis
chemokine-mediated signaling pathway
granulocyte chemotaxis
granulocyte migration
neutrophil migration
neutrophil chemotaxis
myeloid leukocyte migration
cell-cell adhesion via plasma-membrane adhesion molecules
response to molecule of bacterial origin
response to lipopolysaccharide
positive regulation of fatty acid metabolic process
regulation of inclusion body assembly
GO Process
0
20
40
60
Enrichment Score
P-Value
8e-04
6e-04
4e-04
2e-04

Figure 6.3 GO analysis of age-mediated, X-ray-induced differential gene expression in HCAECs.

HCAECs from young (17-26 years) and middle-aged (54-55 years) donors were seeded (10,000 cells/cm^2) on fibronectin-coated, 10 cm^2 plates and when confluent (4-6 days), exposed to 0 Gy or 10 Gy X-ray. Cells were maintained under standard cell culture conditions and RNA extracted 7-days post irradiation, and nanopore sequencing was performed. **A-C**) Differential gene expression after X-ray exposure in HCAECs from young donors (**A**), middle-aged donors (**B**), and the differences in gene expression in HCAECs from middle-aged donors irradiated with 10 Gy compared to HCAECs from young donors after irradiation (**C**). N=3, student's t-test, log_2 fold-change and log_{10} p-values. Above the horizontal dotted line indicates a significance threshold of $p<0.05$, vertical dotted lines indicate a fold-change of >1.5 or <-1.5. **D-F)** Significantly differentially expressed genes were ranked by descending fold-change, and likely associated GO processes were predicated using GOrilla.

To assess the extent the genes associated with the GO pathways were differentially expressed, the datasets of the irradiated HCAECs from young and middle-aged donors were mined for the corresponding genes. For this, I focused on 8 key GO process due to their connection to cell homeostasis and potential involvement in the development of pro-atherogenic phenotypes. These were: regulation of secretion, cell chemotaxis, cell-cell adhesion via plasma membrane adhesion molecules, peptide-lysine deacetylation, peptide-tyrosine deacetylation, regulation of response to external stimuli, regulation of transcription by RNA polymerase II, and chemokine mediated signalling (Figure 6.4).

In processes related to the regulation of secretion, I noted 14 genes that were upregulated in the irradiated HCAECs from young donors, including sirtuin 4 (*Sirt4*), scribble cell polarity complex component (*Llgl2*), and paired box 8 (*Pax8*). When comparing the expression of the genes in the irradiated HCAECs from middle-aged donors, the upregulation was less remarkable (Figure 6.4A), with minimal change or

slight upregulation observed. Comparing the expression of these genes between the irradiated HCAECs from young and middle-aged confirms that the abundance of the majority genes involved in the regulation of secretion is lower in the cells from middle-aged donors. These results suggest that X-ray exposure has a greater impact on the expression of genes related to secretion in HCAECs from younger donors.

In contrast, the genes related to cell chemotaxis displayed greater IR-induced upregulation in the HCAECs from middle-aged donors, with notable differences in chemokine (c-c motif) ligand 2 (*Ccl2*, aka, monocyte chemoattractant protein-1) and *Ccl14*, which are involved in the attraction of immune cells such as monocytes. Indeed, higher expression of MCP-1 has been associated with decreased atherosclerotic plaque stability and increased likelihood of symptoms associated with the disease (Georgakis *et al.*, 2021). The comparison between the irradiated HCAECs form young and middle-aged donors suggests that these genes, along with the others associated with cell chemotaxis, have increased abundance in the irradiated HCAECs from middle-aged donors. This suggest that *in vivo*, IR exposure of older people or animal models may result in increased attraction of immune cells to positions where endothelial cells are irradiated.

The genes associated with the cell-cell adhesion via plasma membrane adhesion molecules were downregulated in the irradiated HCAECs from young donors, with comparatively small changes observed in the HCAECs from middle-aged donors (Figure 6.4C). Notable differences were observed in *Cldn7* (claudin 7) expression which is a

component of tight junctions between cells, with changes in expression likely to affect EC monolayer barrier function (Alexandre *et al.*, 2007).

Furthermore, I observed a greater upregulation of genes within the irradiated HCAECs from young donors which are related to the deacetylation of peptidyl-lysine and peptidyl-tyrosine (Figure 6.4D-E). Within this, *Sirt1*, *Sirt4*, *Hdac4*, and *Hdac9* were upregulated within irradiated HCAEC from young donors, with downregulation of these (excluding *Hdac9*) observed in the irradiated HCAECs from middle-aged donors. The *Hdac* genes encode histone deacetylases, which are involved with epigenetic regulation, with studies demonstrating a reduction in *Hdac4* during UV and oxidative stress induced senescence (Di Giorgio *et al.*, 2021; Lee *et al.*, 2022). These results suggests that epigenetic regulation of IR-induced senescence associated genes may differ with age in HCAECs, a potential novel route of investigation. Furthermore, sirtuins directly link cellular metabolic signalling to the state of protein PTMs. SIRT1 deacetylates histones H1k26 and H4K16 along with non-histone targets such as WRN, p53, and mTORC1, which have been associated with longevity (Dang, 2014). Among their cellular functions are transcription silencing, mitochondria regulation, stress response, cell proliferation and survival, and apoptosis (Maxwell *et al.*, 2011; Dang, 2014). Taken together, the upregulation of sirtuin genes in irradiated HCAECs from young donors, and not from middle-aged, suggests that IR-induced senescence may have different mechanisms in HCAECs, depending on the age of the donor.

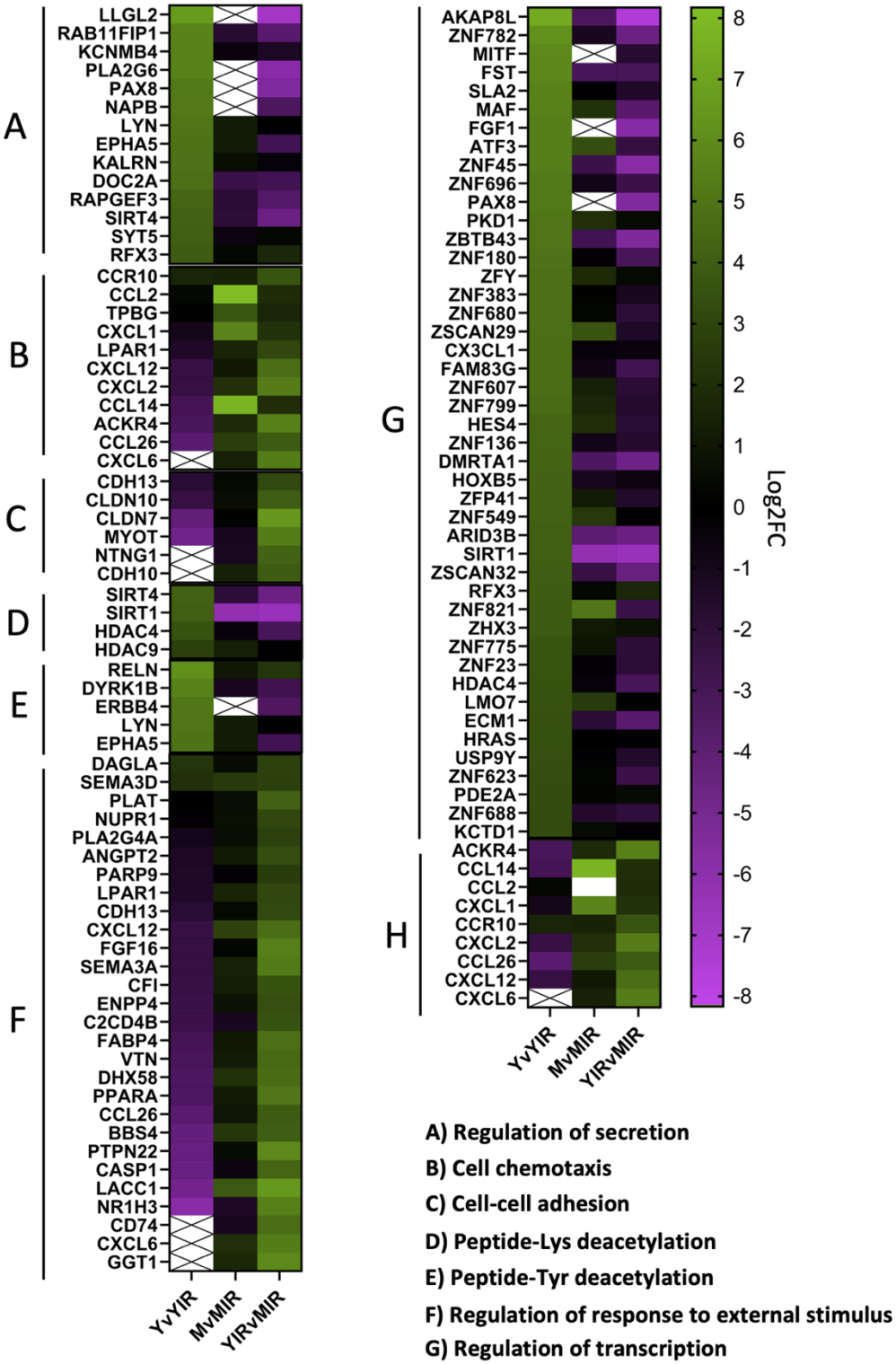
In addition, the genes related to response to external stimulus were downregulated in the irradiated HCAECs from young donors, with minimal change observed in the HCAECs

from middle-aged donors (Figure 6.4F). Within these, *Lacc1* (laccase domain-containing 1) was downregulated in the irradiated HCAECs from young donors, with upregulation in those from middle-aged donors. In *Lacc1* knockout mouse models, it has been observed that reduction in *Lacc1* expression result in increased in TNF-α transcription along with exacerbated arthritis, suggesting that reduced *Lacc1* expression may cause an inflammatory phenotype (Skon-Hegg *et al.*, 2019). In addition, *Sema3d* was upregulated in both age groups, which is interesting as this has been suggested as a potential tumour suppressor due to its potential role as a prognostic marker for colorectal cancer, along with cell migration assays that have demonstrated increases in the colorectal cancer cell line RKO migration with knockdown of *Sema3d* (Wang *et al.*, 2017). The expression differences of genes in this GO process suggests that irradiated HCAECs from young donors may respond differently to external stimulus, potentially affecting their ability to maintain vascular homeostasis (Halcox *et al.*, 2002; Chuaiphichai *et al.*, 2023).

Furthermore, I observed a greater increase in genes associated with the regulation of transcription in irradiated HCAECs from young donors with those from middle-aged donors mainly being downregulated (Figure 6.4G). *Akap8l* encodes protein kinase A anchoring protein 8L, which binds to mTORC1, was upregulated in irradiated HCAECs from young donors and downregulated in those from middle-aged. Loss of AKAP8L has been shown to cause decreased mTORC1 related processes, such as translation, cell growth, and cell proliferation (Melick, Meng and Jewell, 2020), suggesting that these processes are increased in HCAECs from young donors and downregulated in those from middle-aged. In contrast, overexpression of *Arid3b* (AT-rich interaction domain 3B)

has tumour suppressor qualities in gastric cancer cell lines, leading to reduced cell migration and wound healing (X. Zhang *et al.*, 2023).

I observed a greater upregulation of genes related to chemokine-mediated signalling within the irradiated HCAECs from middle-aged donors (Figure 6.4H), such as *Ccl14*, *Ccl2*, and *Cacl2*, suggesting that the irradiated HCAECs from middle-aged donors may recruit immune cells to a greater extent, which is an important step in atherogenesis (Gencer *et al.*, 2021).



A) Regulation of secretion

B) Cell chemotaxis

C) Cell-cell adhesion

D) Peptide-Lys deacetylation

E) Peptide-Tyr deacetylation

F) Regulation of response to external stimulus

G) Regulation of transcription

H) Chemokine mediated signaling

Figure 6.4 Differential expression of genes related to GO pathways within irradiated HCAEC.

From the GO processes predicted to be affected by IR exposure in HCAECs from young and middle-aged donors (Figure 6.3), the genes which relate to those process were identified, and the fold-change after X-ray exposure was determined. Data represents the log_2 fold-change after 10 Gy X-ray exposure in HCAECs from young (YvYIR), middle-aged (MvMIR), and the differential expression between the young and middle-aged donors after irradiation (YIRvMIR). N=3.

In summary, the prediction of different biological process associated with IR-induced changes in gene expression within the two age groups investigated, demonstrates potential age-modulation of the biological response to IR within these cells. The data presented here suggests that the expression of genes related to different aspects of atherogenesis are modulated differently depending on age, such as those related to secretion and cell chemotaxis. These results reveal added complexity in identifying potential age-associated mechanisms behind IR-CVD as it is not possible to state one process will be more atherogenic than another. Furthermore, they highlight the difficulty in assessing IR-induced atherogenic phenotypes *in vitro*, with many processes being associated with the interaction of cells with their environment. Creating a physiologically relevant environment for cells *in vitro* is challenging, with the added complexity of ageing environments, IR-induced characteristics that differ between age related to these interactions may be missed.

6.3.3 Modulation of IR-induced CVD related gene expression with rapamycin

With the observed reductions in IR-induced atherogenic phenotypes in Chapter 5, here I investigate the effects of rapamycin on IR-induced CVD related gene expression in HCAECs. While focusing the investigation on genes related to atherosclerosis will lead to omission of potentially interesting effects of rapamycin treatment, I chose this targeted approach to potentially enable correlations to be drawn between the atherogenic phenotypes observed in Chapter 5 and transcript level differences which may be relate to them. To achieve this, HCAECs from young (17-33 years) and middle-aged (48-55 years) donors were seeded in 10 cm^2 plates and irradiated with 0 or 10 Gy X-ray when confluent. Plates then received 0 or 10 nM rapamycin treatment for 5 days, with RNA harvested on day 7 and cDNA libraries prepared for nanopore sequencing as previously described (section 2.10). From the results differential gene expression analysis, I visualised the statistically significant (student's t-test, $p<0.05$) results in volcano plots (Figure 6.5). the comparisons made identified differentially expressed genes between: rapamycin treated HCAECs to control from young (Figure 6.5A) and middle-aged donors (Figure 6.5B), irradiated HCAECs treated with rapamycin compared to control from young (Figure 6.5C) and middle-aged (Figure 6.5D) donors, and irradiated HCAECs with rapamycin treatment compared to irradiated cells from young (Figure 6.5E) and middle-aged (Figure 6.5F) donors.

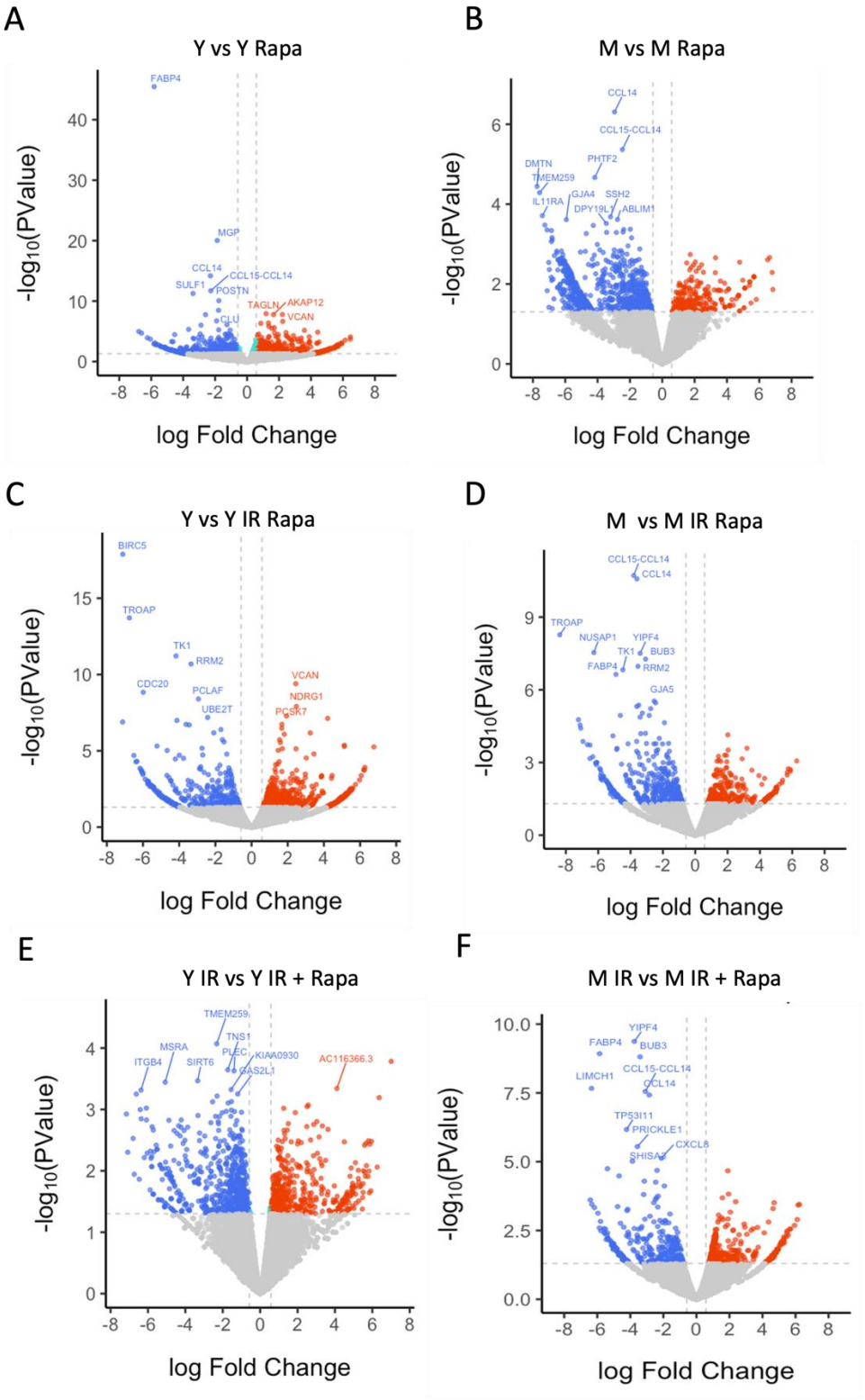


Figure 6.5 Modulation of IR-induced differential gene expression in HCAECs.

To assess the changes in the transcriptome of HCAECs from young and middle-aged donors following rapamycin treatment and whether this treatment modulated IR-induced changes, HCAECs were seeded in 10 cm^2 plates (10,000 cells/cm^2) and exposed to 0 or 10 Gy X-ray once confluent (4-6 days). Within both the 0 Gy and 10 Gy exposure groups, 0 or 10 nM rapamycin treatment was received. RNA was then extracted, a cDNA library created, and nanopore sequencing performed. A-B) The differential gene expression following rapamycin treatment compared to control, without IR exposure in HCAECs from young (a) and middle-aged (B) donors. C-D) The differential gene expression in HCAECs exposed to 10 Gy X-ray and treated with rapamycin compared to control from young (C) and middle-aged (D) donors. E-F) comparison of the gene expression in HCAECs exposed to 10 Gy X-ray and treated with rapamycin compared to irradiated cells without drug treatment, from young (E) and middle-aged (F) donors. N=3 student's t-test. log_2 fold-change and log_{10} p-values. Above the horizontal dotted line indicates a significance threshold of $p<0.05$, vertical dotted lines indicate a fold-change of >1.5 or <-1.5.

Following the differential gene expression analysis, I mined the datasets for the expression of genes related to senescence, cellular adhesion, and cellular junctions. These are related to the adherence of immune cells (e.g. monocytes) to the endothelium, adhesion of the endothelial cells to the ECM, and the permeability of the vascular endothelial cell barrier, all of which contribute to the early stages of atherogenesis. Furthermore, I investigated these genes within the HCAECs from young and middle-aged donors, to assess whether the efficacy of rapamycin differed depending on age. To achieve this, for genes related to senescence, I used a gene set that was created and validated for genes associated with senescence (SenMayo gene set) (Saul *et al.*, 2022). For genes related to cellular adhesion and cellular junctions, I used Ingenuity Pathway Analysis (IPA™, Qiagen) to create gene sets by searching for cellular adhesion and junctional pathways, and identifying the genes associated with them (gene sets used in Supplementary Table S6.3, S6.4, & S6.5). To mine the

differential gene expression dataset, I used R Studio to identify the genes that match those within the gene sets. To allow for total comparison, in both age groups, I analysed the changes in the expression of these genes in HCAECs which were exposed to 10 Gy X-ray compared to non-irradiated control, the expression of these genes with both X-ray exposure and treatment with 10 nM rapamycin compared to no-treatment control, and the expression of the genes in with X-ray exposure and rapamycin treatment compared to X-ray exposure alone (Figure 6.6). While comparing the effects of irradiated HCAECs with rapamycin treatment to a rapamycin non-irradiated control would be informative, as I was interested in the potential of rapamycin to modulate IR-induced changes, I focused on comparing the gene expression to non-rapamycin control cells.

Firstly, the differential expression of junction related genes after X-ray exposure differed between the age groups investigated, with *Tubb3*, *Parvb*, *Tubb6* being upregulated in HCAECs from young donors and little changes observed in the irradiated HCAECs from middle-aged donors (Figure 6.6A). Similarly, *Tugb1*, Rab5a*,* and *Dnm1l* which were downregulated with X-ray exposure of the HCAECs from young donors displayed little change in the irradiated HCAECs from middle-aged donors. Furthermore, the IR-induced changes in *Mapre2*, *Arpc1b*, *Mapre1*, Actn*4*, *Cadm3*, *Rab5b*, *Exoc2*, *F11r*, and *Cdh13* were opposite in direction of change within the two age groups.

When comparing the effect of rapamycin on the expression of junction related genes, attenuation of many IR-induced changes in gene expression was observed (Figure 6.6A). For example, the upregulation of *Plec*, *Clip1*, *Ctnnb1*, and *Mapre2* with irradiation of

HCAECs from young donors was reduced to levels similar to non-irradiated control. This was also observed for genes that were downregulated with IR exposure, such as *Fermt2*, *Cdh5*, *Jup*, *Rab5a*, *Tubb*, *F11r*, *Cdh13*. Within the HCAECs from middle-aged donors, rapamycin attenuated IR-induced differential expression of *Nectin*, *Fermt2*, *Jup, Dnm2*, *Arpc1b*, *Afdn*, *Arf6*, *Arpc3*, *Tuba12*, *Arpc4*, *Arpc1a*, *tubb*, and *F11r*.

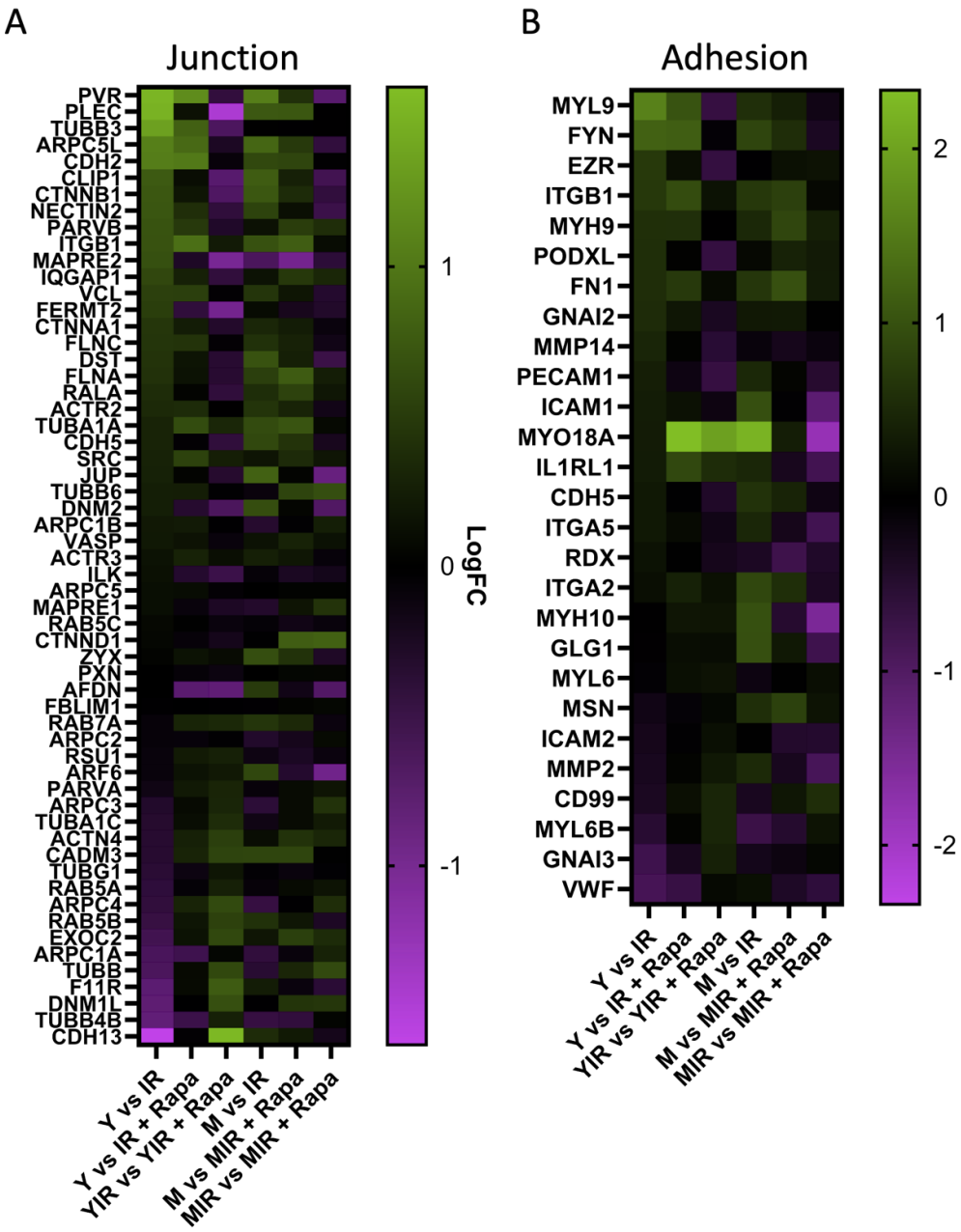
The investigation into the differentially expressed genes within the HCAECs which were related to cellular adhesion revealed some differences in IR-induced changes between the HCAECs from young and middle-aged donors (Figure 6.6B). Within these genes, *Ezr*, and *Mmp14* were upregulated in response to IR in the HCAECs from young donors, with little change observed in those from middle-aged donors. On the other hand, *Myh10*, *Glg1*, and *Myl6* displayed little change in the irradiated HCAECs from young donors, with upregulation of *Myh10* and *Glg1*, and downregulation of *Myl6* in irradiated HCAECs from middle-aged. Furthermore, *Rdx*, *Msn*, *Mmp2*, and *Vwf* displayed opposing directions of change following IR exposure of the HCAECs within the two age groups.

Within the irradiated HCAECs from the young donors, the IR-induced changes in *Ezr*, *Podxl, Mmp14*, *Cdh5*, *Rdx*, *Msn*, *Icam2*, *Mmp2*, and *Myl6b* genes were reduced to levels similar to control when rapamycin treatment was received (Figure 6.6B). Interestingly, rapamycin treatment increased the expression of *Myo18a* in the irradiated HCAECs from young donors. In contrast, the expression of *Myo18a* was reduced in the irradiated HCAECs from middle-aged donors. This encodes a member of the myosin family and has been implicated in regulation of actin, vesicle budding, and focal adhesions (Buschman and Field, 2018). Furthermore, within the irradiated HCAECs from the middle-aged

donors, rapamycin treatment reduced the IR-induced expression of *Peacam1*, *Icam1*, *Il1rl1*, and *Itga5*.

When assessing the differential expression of genes associated with senescence, 10 genes were found to be upregulated in irradiated HCAECs from young donors, with differential expression of other genes observed in the irradiated HCAECs from middle-aged donors (Figure 6.6C). Furthermore, 10 genes were found to show little change in expression in the irradiated HCAECs from young donors, with these genes being either upregulated or downregulated with IR exposure in the HCAECs from middle-aged donors. In addition to this, 11 genes were found to be downregulated with IR exposure of the HCAECs from young donors with these genes being either upregulated or having no change in the irradiated HCAECs from middle-aged donors. This suggests that IR-induced senescence-associated gene expression may differ with age in HCAECs. Furthermore, within the HCAECs from young donors, rapamycin treatment reduced 17 IR-induced increases in senescence associated gene expression, with 7 of these being reduced to expression levels similar to non-irradiated control (Figure 6.6C). Additionally, rapamycin prevented the IR-induced decrease of 11 genes, with 6 of these being comparable to non-irradiated control. Within the HCAECs from middle-aged donors, rapamycin treatment reduced IR-induced increases in expression of 20 genes, with 4 of these being expressed at levels similar to non-irradiated control. Similar was observed in the genes that had decreased expression in response to IR with rapamycin reducing the decreases in 7 genes, with 3 displaying expression levels similar to control.

In summary, IR radiation exposure of HCAECs results in changes in gene expression that are likely to promote atherogenic and senescence characteristics. Furthermore, these results demonstrate the ability of rapamycin to modulate some of these changes, suggesting that the reduction in IR-induced atherogenic phenotypes observed in Chapter 5 may be partly related to regulation of gene expression. While not investigating the individual possible effects of the genes reported here may miss potentially relevant biological effects, this analysis provides an overview of the changes in genes associated with senescent and atherosclerotic characteristics, along with providing evidence that rapamycin alleviates some of the IR-induced changes in gene expression. This also provides genes that may be of interest in future investigations.


A
Junction
PVR
PLEC
TUBB3
ARPC5L
CDH2
CLIP1
CTNNB1
NECTIN2
PARVB
ITGB1
MAPRE2
IQGAP1
VCL
FERMT2
CTNNA1
FLNC
DST
FLNA
RALA
ACTR2
TUBA1A
CDH5
SRC
JUP
TUBB6
DNM2
ARPC1B
VASP
ACTR3
ILK
ARPC5
MAPRE1
RAB5C
CTNND1
ZYX
PXN
AFDN
FBLIM1
RAB7A
ARPC2
RSU1
ARF6
PARVA
ARPC3
TUBA1C
ACTN4
CADM3
TUBG1
RAB5A
ARPC4
RAB5B
EXOC2
ARPC1A
TUBB
F11R
DNM1L
TUBB4B
CDH13
1
0
-1
LogFC
Y vs IR
Y vs IR + Rapa
YIR vs YIR + Rapa
M vs IR
M vs MIR + Rapa
MIR vs MIR + Rapa
B
Adhesion
MYL9
FYN
EZR
ITGB1
MYH9
PODXL
FN1
GNAI2
MMP14
PECAM1
ICAM1
MYO18A
IL1RL1
CDH5
ITGA5
RDX
ITGA2
MYH10
GLG1
MYL6
MSN
ICAM2
MMP2
CD99
MYL6B
GNAI3
VWF
2
1
0
-1
-2
Y vs IR
Y vs IR + Rapa
YIR vs YIR + Rapa
M vs IR
M vs MIR + Rapa
MIR vs MIR + Rapa

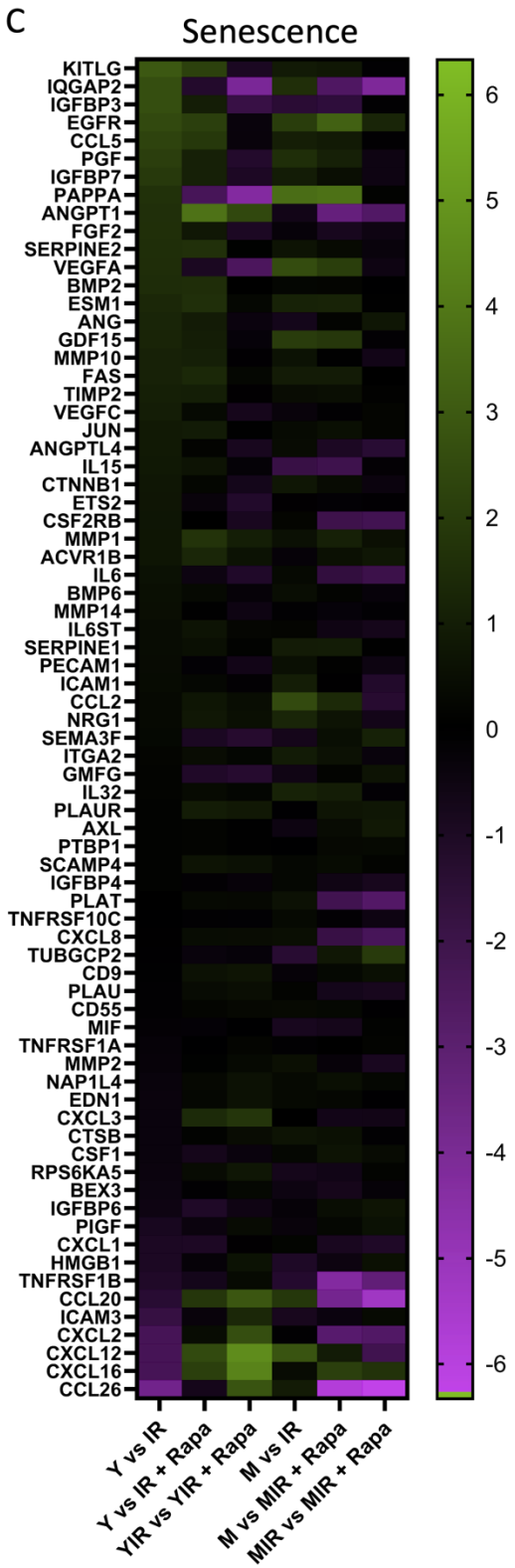

C
Senescence
KITLG
IQGAP2
IGFBP3
EGFR
CCL5
PGF
IGFBP7
PAPPA
ANGPT1
FGF2
SERPINE2
VEGFA
BMP2
ESM1
ANG
GDF15
MMP10
FAS
TIMP2
VEGFC
JUN
ANGPTL4
IL15
CTNNB1
ETS2
CSF2RB
MMP1
ACVR1B
IL6
BMP6
MMP14
IL6ST
SERPINE1
PECAM1
ICAM1
CCL2
NRG1
SEMA3F
ITGA2
GMFG
IL32
PLAUR
AXL
PTBP1
SCAMP4
IGFBP4
PLAT
TNFRSF10C
CXCL8
TUBGCP2
CD9
PLAU
CD55
MIF
TNFRSF1A
MMP2
NAP1L4
EDN1
CXCL3
CTSB
CSF1
RPS6KA5
BEX3
IGFBP6
PIGF
CXCL1
HMGB1
TNFRSF1B
CCL20
ICAM3
CXCL2
CXCL12
CXCL16
CCL26
6
5
4
3
2
1
0
-1
-2
-3
-4
-5
-6
Y vs IR
Y vs IR + Rapa
YIR vs YIR + Rapa
M vs IR
M vs MIR + Rapa
MIR vs MIR + Rapa

Figure 6.6 modulation of IR-induced expression of genes associated with adhesion, cellular junctions, and senescence in HCAECs with rapamycin.

The differential gene expression datasets from HCAECs from young and middle-aged donors exposed to 10 Gy X-ray, with or without rapamycin treatment from Figure 6.5 were mined for genes related to cellular junctions (A), cellular adhesion (B), and senescence (c). n=3, log_2 fold change. Y vs IR, irradiated HCAECs from young donors compared to young control. Y vs IR + Rapa, irradiated HCAECs from young donors with rapamycin treatment compared to young control. YIR vs YIR + Rapa, irradiated HCAECs from young donors with rapamycin treatment compared to irradiated HCAECs from young without rapamycin treatment. M vs IR, irradiated HCAECs from middle-aged donors compared to middle-aged control. M vs IR + Rapa, irradiated HCAECs from middle-aged donors with rapamycin treatment compared to middle-aged control. MIR vs MIR + Rapa, irradiated HCAECs from middle-aged donors with rapamycin treatment compared to irradiated HCAECs from Middle-aged without rapamycin treatment.

6.4 Discussion

Within this chapter I have used nanopore sequencing to assess the differences in the transcriptome of HCAECs from young and middle-aged donors, with the results presented here demonstrating clear differences in transcription with age. Within this, the differences in the expression of genes observed with age in the HCAECs suggest that those from middle-aged donors may have greater EC monolayer permeability compared to those from young donors (an atherogenic phenotype). Furthermore, the differences in gene expression between the two age groups suggests that the HCAECs from middle-aged donors may display aged and senescence characteristics. This analysis has also potentially generated a novel dataset indicating likely changes in HCAEC gene expression with age, which will facilitate future targeted investigations.

In addition, I have explored the effect of HCAEC donor age on IR-induced changes in gene transcription, demonstrating that age does modulate these changes, with the GO analysis revealing increased expression of genes related to regulation of secretion, peptide-lysine/tyrosine deacetylation, and regulation of transcription within the HCAECs from young donors, compared to those from middle-aged. In contrast, the genes associated with regulation of response to external stimulus, cell chemotaxis, and cell-cell adhesion were downregulated in response to IR in the HCAECSs from young donors. These provide avenues for future investigations into why age may modulate IR-induced atherosclerotic phenotypes in HCAECs. Finally, I have demonstrated the efficacy of rapamycin in alleviating many of the observed IR-induced changes in gene expression, suggesting an mTOR centred mechanism behind many of the IR-induced changes.

6.4.1 Differences in HCAECs gene expression between young and middle-aged donors

When interrogating the top 10 most significantly differentially expressed genes between HCAECs from young and middle-aged donors, I observed upregulation in genes such as *Plat,* which have been associated with EC senescence in mice (Kiss *et al.*, 2020), and *Cryab*, which has been associated with senescence (Limbad *et al.*, 2022), suggesting HCAECs form middle-aged donors may present with senescence characteristics. Furthermore, I noted upregulation of pro-survival genes such as *Ifi6* and *Crip*, which may promote apoptosis resistance through BCL-2, similar to that observed in senescence

(Lanningham-Foster *et al.*, 2002; Childs *et al.*, 2014). Indeed, the expression of these genes aligns with the increased SA-β-Gal activity observed in the HCAECs from middle-aged donors compared to young (section 5.3.2.5).

In addition to an aged phenotype, the gene expression profile is suggestive of a pro-atherogenic phenotype, with reduced transcription of *Uclh1* in the HCAECs from middle-aged donors compared to young, suggesting reduced monolayer barrier functionality. However, there was no significant differences in monolayer permeability between the young and middle-aged donors when investigated in Chapter 5.

Due to the complex nature of cellular signalling and regulation, stating that a change in one gene will affect a particular cellular phenotype may not be accurate. Therefore, to gain a greater understanding of the potential processes implicated in the differences in gene expression overserved between the HCAECs from young and middle-aged donors, GO analysis was performed. This revealed processes such as ECM-receptor interaction, AGE-RAGE signalling, PI3K-AKT signalling, and MAPK signalling, with the combination of genes within these pathways supporting an aged phenotype within the HCAECs from middle-aged donors (Denoyelle *et al.*, 2006; Yentrapalli *et al.*, 2013; Senatus and Schmidt, 2017; Levi *et al.*, 2020).

6.4.2 Age-modulation of IR-induced gene expression in HCAECs

The differential gene expression analysis performed on the irradiated HCAECs from young and middle-aged donors revealed differences in IR-induced gene expression

between the two age groups. In this sample population, this suggests that age does modulate HCAEC response to IR at a transcriptional level.

To assess the potential processes associated with the changes in transcription, GO analysis was performed. This revealed changes in different molecular process, depending on the age group investigated. Of note, in the irradiated HCAECs from young donors, many processes involved in the regulation of transcription were identified, suggesting that IR exposure impacts gene transcription to a greater extent in HCAECs from younger donors. Indeed, this was supported when investigating the transcription-associated individual gene expression changes, with the majority of genes upregulated in irradiated HCAECs from young donors and not in those from middle-aged donors. Furthermore, regulation of secretion along with process related to protein PTMs were predicted to be affected to a greater extent by IR exposure in HCAECs from young donors compared to middle-aged, confirmed by the observed upregulation of the associated genes in the irradiated HCAECs from young donors. These observations fit with studies that have assessed changes in the HUVEC transcriptome with TNF-α induced senescence, where expression of gene related to transcriptional control were observed and cytokine secretion were observed (Kandhaya-Pillai *et al.*, 2017, 2023) .

6.4.3 Limitations

While transcriptomic analysis provides a detailed overview of the changes in gene expression within a population of cells, these changes may not be reflected in protein translation, therefore drawing conclusions on phenotypic effects due to the changes in gene expression may not be accurate. Rather, this analysis enables the identification of

changes in the modulation of gene transcription between the experimental groups. Furthermore, a small change in a gene that is highly translated may result in a greater increase in the associated protein expression, meaning that arbitrary targets (e.g. 1.5-fold-change) may miss relevant changes in gene expression. Additionally, investigating fold-changes in gene expression requires the gene to be detected in both experimental groups. This would result in the omission of genes that are only expressed in response to the experimental question. Importantly, individuals have varying sensitivity to IR(Rajaraman *et al.*, 2018b), therefore, the sample size used here may not be large enough to gain a true picture of age-modulated gene expression in response to IR. Lastly, the wealth of data collected here and the feasibility to analyse all observations is limited by the scope of this thesis. However, it does provide the opportunity for future analysis.

7 Comparative proteomics of HCAECs

7.1 Introduction

While Chapter 6 identified differences in gene transcription with age and IR exposure in the HCAECs, these changes may not be reflected in the proteome. Therefore, within this chapter, I build upon this previous work using liquid chromatography-tandem mass spectrometry (LC-MS/MS) to assess the differences in protein expression between HCAECs from young and middle-aged donors, along with the changes induced by IR exposure. Furthermore, I assess the use of rapamycin to ameliorate IR-induced changes in protein expression.

This dual omics approach was used due to the complex nature of protein expression and regulation. While the mRNA levels in a cell can provide insights into gene expression, they do not always correlate with protein expression (Guo *et al.*, 2008; O'Sullivan *et al.*, 2017). Indeed, research suggests that the correlation between global mRNA and protein levels can be as low as 40 % (de Sousa Abreu *et al.*, 2009; Maier, Güell and Serrano, 2009). This can be due to various reasons. Firstly, post-transcriptional modifications like splicing, editing, and mRNA degradation can reduce the translation of mRNA to protein (Gagliardi and Dziembowski, 2018; H. Shi *et al.*, 2020; Pederiva *et al.*, 2023). Secondly, variations in translation efficiency can lead to different protein expression levels, meaning that while mRNA levels may remain constant, the amount of protein translated can fluctuate (Tuller, Kupiec and Ruppin, 2007; Siwiak and

Zielenkiewicz, 2010; Nieuwkoop *et al.*, 2023). Evidence of this can be drawn from the average production of mRNA and protein; for example, in mammalian cells, an average of 2 copies of a given mRNA are produced per hour; in comparison, 20 or more copies of the corresponding proteins may be translated (Schwanhüusser *et al.*, 2011). Thirdly, differences in protein degradation rates can affect protein abundance, meaning that fluctuations in degradation can lead to increased or decreased protein abundance independently of mRNA levels (Eden *et al.*, 2011; Zhao *et al.*, 2022). This can also be influenced by post-translational modifications to the proteins, affecting their abundance independently of mRNA levels (Zecha *et al.*, 2022). Therefore, use of both transcriptomic and proteomic techniques will provide a comprehensive overview of the molecular changes within the HCAECs.

7.1.1 LC-MS/MS overview

The proteomic workflow used within this chapter involves the lysis of the cells to liberate proteins, which are then subjected to enzymatic digestion using trypsin. The resulting peptides are separated via liquid chromatography, an essential step in reducing sample complexity and enhancing detection specificity. Within the LC step, the liquid sample is separated by passing through a column with a stationary phase. Different compounds interact differently with the stationary phase based on their polarity and molecular size. A mobile phase carries the peptides through the column, where they are then eluted at different times (depending on their interactions with the stationary phase). These compounds are then detected by a UV-vis detector and introduced into the mass spectrometer (Pitt, 2009).

Within the mass spectrometer, the compounds are ionised to form charged particles and become separated based on their mass-to-charge ratio (m/z). Ions of a particular size are selected and fragmented by collision with an inert gas, producing a unique pattern of fragments that can be used to deduce the molecule's structure. The separation of fragments based on their m/z is then detected in a second mass analyser, and the resulting spectra are detected. The fragmentation spectrum is characteristic of the original molecule and is then used for its identification (Pitt, 2009). This is achieved by comparing the fragments' retention times, mass spectra, and the intensity of the ions to theoretical spectra in databases using algorithms such as MaxQuant.

For the proteomic analysis within this chapter, cell pellets were collected and taken to the Advanced Proteomics Facility (Department of Biochemistry, University of Oxford). Here, the proteins from each pellet were extracted, trypsin FASP digested, and then detected using Orbitrap LC-MS/MS with a 2-hour gradient, including protmix and wash control steps. After receiving the raw data, I processed it using the Galaxy platform (www.usegalaxy.eu) (section 2.12.2).

7.2 Aims

Within this chapter, I set out to address the following questions:

1. Are there differences in protein expression within the HCAECs depending on the donors age?
2. Does age of the HCAEC donor effect IR-induced changes in protein expression?

3. Can IR-induced atherogenic related changes in the proteome be ameliorated with rapamycin treatment?

7.3 Results

7.3.1 Differences in protein expression in HCAECs with age

To assess the differences in the proteome between HCAECs from 3 young donors (17, 23, and 26 years old) and middle-aged (54,55, and 55 years old) donors, HCAECs were seeded in 10 cm^2 plates and cultured to confluency using standard techniques (outlined in section 2.2.1). 7-days after confluency was reached, cell pellets were collected, and LC-MS/MS performed. After analysing the changes in expression for significance (student's t-test, $p<0.05$), those that reached significance were visualised using a volcano plot (Figure 7.1A).

Within these results, 233 proteins were found to be significantly differentially expressed in the HCAEC from middle-aged donors compared to the young. Due to the number of proteins significantly differentially expressed, I focused on the top 10 most significantly differentially expressed (listed Figure 7.1B). Within this, I observed increased expression of proteins associated with intracellular protein trafficking within the HCAECs from middle-aged donors (KIF13B (kinesin family member 13B), AP1B1 (adapter related protein complex 1 subunit β 1), and PRAF2 (prenylated rab acceptor 1 domain family member 2)). Of note is KIF13B, which when adjusting for multiple comparisons using the adjusted p-value, was the only protein to meet the enhanced statistical significance

level of <0.05. This has been shown to be associated with the transport of VEGFR2 cargo from the Golgi apparatus to the endothelial cell surface, with a knockdown of KIF13B resulting in a reduction in angiogenesis within HUVECs (Yamada *et al.*, 2014). The upregulation in HCAECs from middle-aged donors suggests that there may be increased transport of VEGFR2 to the cell membrane, which if combined with increased activation of VEGFR2, may result in increased activation of the associated signalling cascades (PI3K-Akt, which promotes vascular permeability; Raf-MEK-MAPK, which is involved in control of cell proliferation; Src-FAK, which is involved with cell motility) (Zhuang *et al.*, 2013). Further adding to changes in protein transport with age in HCAECs is the upregulation of AP1B1, which forms a heterotetrametric complex known as clathrin adaptor proteins (or adapter proteins) (Shin, Nile and Oh, 2021). PRAF2, along with being involved with protein and vesicle transport, is classed as an oncogene which has been associated with promoting the proliferation and invasion of the MCF-7 cancer cell line (Qian *et al.*, 2019; Wang *et al.*, 2022).

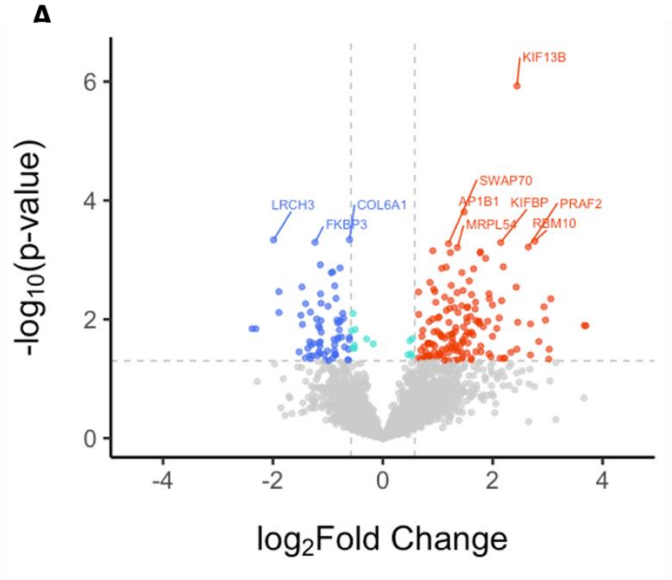
In addition to protein trafficking, of proteins significantly differentially expressed between the HCAEC age groups are involved in cellular structure and attachment to the ECM (CO6A1 (collagen type VI alpha 1 chain protein), KIFBP (kinesin family member binding protein), SWAP70 (switch-associated protein 70), and LRCH3 (leucine rich repeats and calponin homology domain containing 3)). CO6A1 forms a heterotrimeric complex with collagen VI alpha2 and alpha 3 chains. This is a major structural component for microfibrils which link the cellular cytoskeleton to the ECM, meaning downregulation of this protein in the HCAEC from middle-aged donors may make them less tightly associated with the ECM, potentially effecting monolayer permeability

(Zanotti *et al.*, 2023). Furthermore, KIFBP, which was upregulated in the HCAEC from middle-aged donors, binds to and inhibits the catalytic motor heads of kinesin superfamily member proteins, again involved in the regulation of microtubule formation (Solon *et al.*, 2021). SWAP70 was also upregulated and is involved with the regulation of the actin cytoskeleton (Baranov *et al.*, 2016). Furthermore, SWAP70 is a guanine exchange factor involved in the activation of endothelial cells in response to viral G protein-coupled receptor activation (Dwyer *et al.*, 2015). Additionally, the reduced expression of LRCH3 supports changes in the regulation of HCAEC cell structure, as it is a negative regulator of GTPase CDC42, which is involved in regulating actin dynamics and acts as a cytoskeleton (Rivière *et al.*, 2020).

The protein, RBM10 (RNA binding motif protein 10) promotes apoptosis through the regulation of MDM2-p53 negative feedback loop, BCL-2, and Bax. It also inhibits proliferation through Notch signalling and rap1a/Akt/CREB pathways (Cao *et al.*, 2021). This was upregulated in the HCAEC from middle-aged donors, suggesting that they may have greater activity in their apoptosis pathways. Furthermore, the FKBP3 (FK506-binding protein 3) protein, a prolyl isomerase, which was downregulated in HCAEC from middle-aged donors, is needed for cell cycle progression, suggesting that these HCAEC may be less proliferative than those from younger donors. In addition to this, FKBP3 has been associated with regulation of microtubules and assisted protein folding, potentially contributing to proteostasis which is dysregulated with ageing (Dilworth *et al.*, 2018). Furthermore, the upregulation of MRPL54 (mitochondrial ribosomal protein 54) observed in the HCAECs from middle-aged donors suggest that there may be increased mitochondrial translation, which may suggest increased mitochondrial

biogenesis. While this is speculation without further investigation, this may be indicative of dysfunctional mitochondria, a hallmark of ageing and senescence (section 1.5.2) (López-Otín *et al.*, 2013; Hernandez-Segura, Nehme and Demaria, 2018). Indeed, studies have demonstrated that knockdown of the *Mrpl54* gene in *C. elegans* increases the mitochondrial UPR and increases lifespan (Houtkooper *et al.*, 2013). However, a more recent study conducted in a *Mrlp54* knockdown mouse model failed to demonstrate any increase in lifespan, suggesting that this may not be translatable to other models (Reid *et al.*, 2023).

A



B

Protein	log2FC	pvalue	adj.pvalue	diffexpressed
KIF13B	2.44	1.18E-06	3.41E-03	Up
AP1B1	1.48	1.56E-04	1.57E-01	Up
COL6A1	-0.61	4.55E-04	1.57E-01	Down
LRCH3	-1.99	4.60E-04	1.57E-01	Down
RBM10	2.77	4.84E-04	1.57E-01	Up
FKBP3	-1.24	5.06E-04	1.57E-01	Down
KIFBP	2.15	5.09E-04	1.57E-01	Up
SWAP70	1.20	5.33E-04	1.57E-01	Up
PRAF2	2.65	6.06E-04	1.57E-01	Up
MRPL54	1.36	6.18E-04	1.57E-01	Up

Figure 7.1 Differentially expressed proteins in HCAEC from middle-aged donors compared to young.

Comparative proteomic analysis of HCAECs from young and middle-aged donors maintained in standard culture conditions for 7-days post confluency. The proteins found to be differentially expressed in HCAECs from middle-aged donors compared to young are displayed as Log_2 fold change with the associated significance as $-log_{10}$(p value) (**A**). The top ten most significantly differentially expressed proteins are displayed (**B**). N=3, students t-test. Horizontal dotted line

indicates a significance threshold of $p<0.05$, vertical dotted lines indicate a fold-change of >1.5 or <-1.5.

The differences in protein expression presented here provide a narrow view of the potential changes with age in HCAEC. Analysing each protein individually, while informative, will potentially miss complex interactions and is outside the scope of this thesis. Therefore, in the next section, I assess the potential cellular processes effected by the combined differences in protein expression.

7.3.1.1 GO pathways associated with HCAEC proteome changes with age

To gain a greater understanding of the potential biological context behind the changes in protein expression observed in Figure 7.1, I performed GO analysis of the differentially expressed proteins between the HCAECs from young and middle-aged donors to assess the potential difference in biological processes. To achieve this, the differentially expressed proteins that were found to be significant (students t-test) were analysed using ShinyGO, producing predicted GO process (Top 20 displayed, Figure 7.2). Within this, many of the processes have associations with cellular ageing and senescence, including processes associated with mTOR signalling, protein processing in the ER, and changes in proteins associated with the spliceosome. These suggest that there are differences in the regulation of the proteome, along with regulation of cell growth, the actin cytoskeleton, gene transcription, and cell survival. This further support the analysis of the top 10 differentially expressed proteins, suggesting that the HCAECs from middle-aged donors, unsurprisingly, display more characteristic of cellular ageing than those from young donors (Tang and Xiao, 2023; Thompson and De-Souza, 2023).

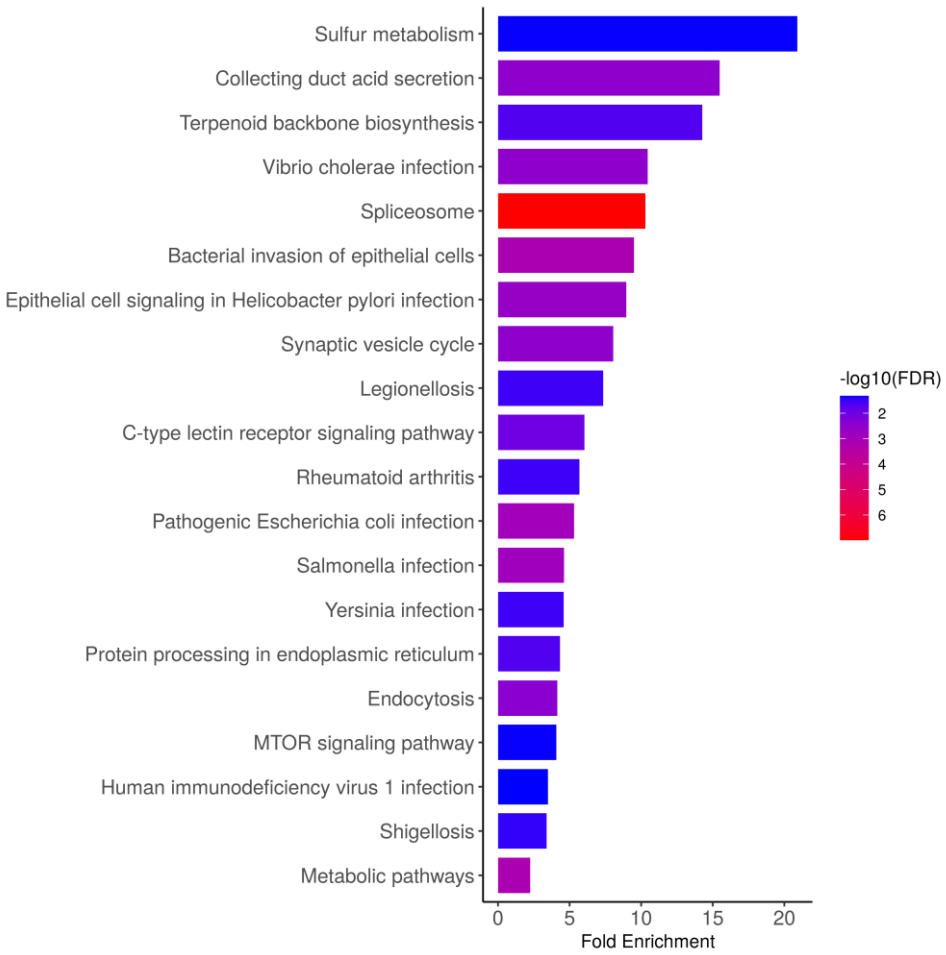


Figure 7.2 GO pathways associated with the differently expressed proteins in the HCAEC from middle-aged donors.

Significantly differentially expressed proteins in HCAECs from middle-aged donors (54-55 years) compared to young (17-26 years) were uploaded to ShinyGO for GO analysis. The top 20 most significantly predicted KEGG pathways associated with the differentially expressed genes is shown. N=3, hypergeometric tests for pathway significance, t-tests for differential gene expression significance.

7.3.2 Age modulation of IR-induced protein changes in HCAECs

To assess whether age modulates IR-induced changes in protein expression, HCAECs from young and middle-aged donors were seeded and grown to confluency, followed by exposure to 0 or 10 Gy X-ray. 7-days after irradiation, the cell pellets were collected, and LC-MS/MS performed. After determining the abundance of the detected proteins, differential expression analysis was performed and the differences in protein expression after irradiation within the HCAECs from young (Figure 7.3A) and middle-aged (Figure 7.3B) donors compared to age-matched control was visualised in volcano plots. This analysis revealed 423 proteins significantly differentially expressed (student's t-test, $p<0.05$) in irradiated HCAECs from young donors, with 14 having an adjusted p-value <0.05; with 308 within the irradiated HCAECs from middle-aged donors, none with an adjusted p-value <0.05.

To assess any common protein level response to IR between the two age groups, I filtered the datasets for the proteins that were significantly differentially expressed in both age groups, detecting 49 proteins upregulated in irradiated HCAECs from both young and middle-aged donors, and 44 downregulated (Supplementary Table S7.). Additionally, 4 proteins were found to be upregulated in irradiated HCAECs from young donors, and down regulated in those from middle-aged donors (PRAF2 (prenylated rab acceptor 1 domain family member 2), VATF (ATPase H+ transporting V1 subunit F), S10AG (S100 calcium binding protein A16), and KI13B (KIF13B; kinesin family member 13B)) (Figure 7.3D). As this section is focusing on the differences between IR-induced

changes in HCAEC protein expression between the two age groups, I chose to focus on the proteins that displayed opposite modulation.

PRAF2, as discussed previously (section 7.3.1), is involved in ER-Golgi transport and vesicular traffic, along with being proposed to act as an oncogene (Qian *et al.*, 2019; Wang *et al.*, 2022). This was observed to be upregulated in the HCAECs from middle-aged donors, compared to young when investigating the differences in protein expression with age (with no irradiation) in the HCAECs (section 7.3.1). However, irradiation of the HCAECs led to an increase in PRAF2 expression in the HCAECs from young donors, and a decrease in those from middle-aged (Figure 7.3D).

VATF forms vacuolar-type H^+ ATPases (V-ATPase) situated on vacuoles, which acidify intracellular organelles, such as lysosomes (Wang *et al.*, 2020). Importantly, mTORC1 has been suggested to regulate that movement of V-ATPases from the cytosol to the lysosomal membrane, with increased mTORC1 activity preventing its trafficking to the lysosome via TRiC (T-complex protein ring complex, a chaperonin), reducing its acidification, and thus reducing its catabolic activity (Ratto *et al.*, 2022). VATF was found to be upregulated in the irradiated HCAECs from young donors and downregulated in those from middle-aged. However, as the abundance of VATF does not necessarily correspond to it localisation to vacuoles such as lysosomes, it is not possible to state the differences observed here result in differences in vacuolar acidification between the two age groups. It does, however, provide an interesting line of investigation for future studies.

S10AG, which was upregulated in irradiated HCAECs from young donors, and downregulated in those from middle-aged, is involved in ER-Golgi transport and along with playing a role in cell decision pathways such as proliferation, migration, and apoptosis (Sturchler *et al.*, 2006), with more recent studies investigating S10AG expression in cervical cancer revealing strong association with S10AG mRNA levels and pathways such as the p53 regulatory pathway, and proteosome and ribosome signalling pathways (H. Zhang *et al.*, 2023). However, as with most other proteins discussed, understanding how the differences in S10AG expression between the age groups effects cellular characteristics requires an approach which accounts for combined changes in protein expression.

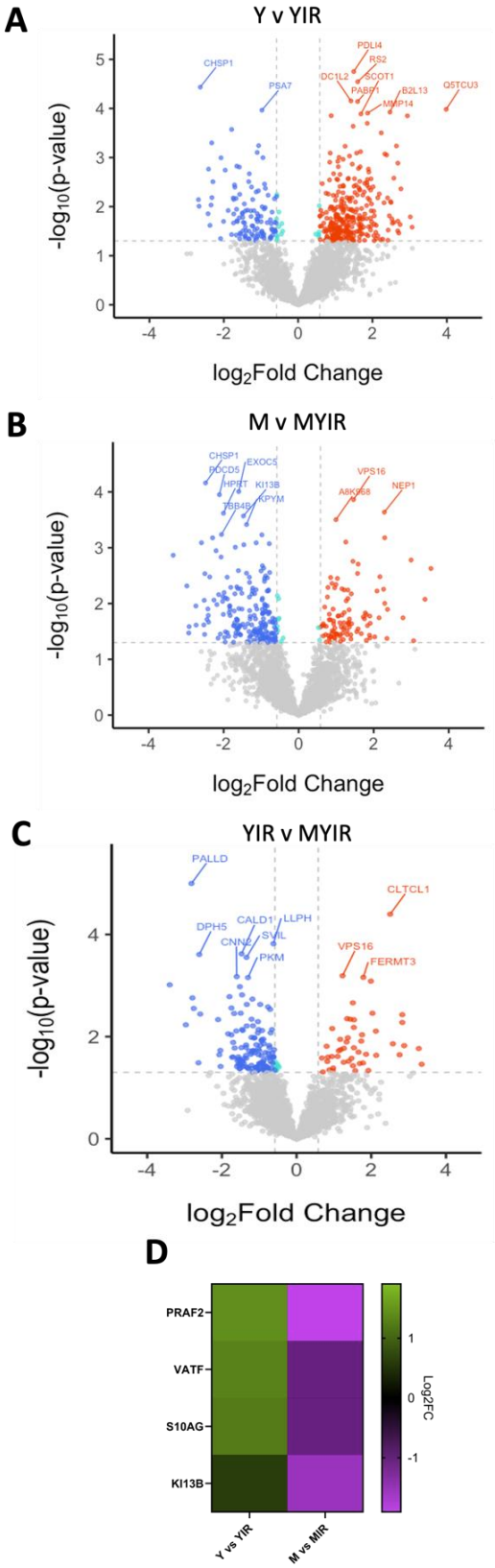
KI13B is involved in cytoskeletal organisation and vesicle trafficking (Serra-Marques *et al.*, 2020). Interestingly, I previously noted this to be more highly expressed in non-irradiated HCAECs from middle-aged donors compared to young (7.3.1). Furthermore, research suggests that KIF13B-mediated VEGFR2 trafficking is increased in wet age-related macular degeneration (a disease of the eye associated with ageing), with KIF13B inhibition proposed as a therapeutic avenue to prevent progression of the disease through preventing EC-related angiogenesis (Yamada *et al.*, 2014; Waters *et al.*, 2021; Cho *et al.*, 2023). While tenuous, the targeting of KIF13B for an age-related disease involving ECs, and the increased expression I observed in HCAECs from younger donors, suggests that its expression may increase with age. Therefore, it is possible that IR exposure of HCAECs from young donors is inducing age-associated changes in protein expression.

In summary, the expression profile of the proteins found to be differentially modulated with age in the HCAEC suggests that there are increases ER-Golgi trafficking in response to IR in HCAECs from young donors, and a reduction in those from middle-aged. This may have implications in proteostasis within the cells and suggests further research into age-modulation of IR response should investigate changes in intracellular cellular trafficking.

Next, I analysed the expression profile of the irradiated HCAECs from middle-aged donors, compared to young donors. This comparison revealed 192 significantly differentially expressed proteins, with only PALLD (paladin) having an adjusted p-value <0.05 (Figure 7.3C). PALLD is a cytoskeletal protein that is required for organising the actin cytoskeleton, therefore, is involved in control of cell shape, adhesion, and cell-cell junctions (Mykkänen *et al.*, 2001; Rönty *et al.*, 2007; Jin *et al.*, 2010). With this being significantly downregulated in irradiated HCAECs from both young and middle-aged donors, it suggests that this may play an important role in the HCAEC response to IR, and may be implicated in the development of pro-atherogenic phenotypes.

To gain a greater understanding of the molecular pathways associated with the IR-induced changes in protein expression, I uploaded the raw datasets to Ingenuity Pathway Analysis (IPA^{TM}) software, which analyses the protein expression profiles, provides molecular pathways which are likely to be active or reduced, and calculates their significance. From this analysis, I identified the common pathways between each age-group that were statistically significant (Figure 7.3E). Of note, this analysis suggested that pathways related to proteostasis were increased in the irradiated

HCAECs from young donors, such as the protein sorting signalling and protein folding pathways. However, within the HCAECs form middle-aged donors, the analysis suggested the protein sorting signalling pathway was minimally activated and the protein folding pathway was downregulated. This suggests that IR induces different modulation of proteostasis in HCAECs depending on the age of the donor. In addition to this, pathways associated with senescence, such as regulation of eIF4 and p70S6K and mTOR signalling were predicated to be activated within the irradiated HCAECs from young donors, and to a lesser extent, in the irradiated HCAECs from middle-aged donors.


A
Y v YIR
CHSP1
PSA7
PDLI4
RS2
DC1L2
SCOT1
PABP1
B2L13
Q5TCU3
MMP14
-log10(p-value)
log2Fold Change
B
M v MYIR
CHSP1
EXOC5
DCD5
HPRT
KI13B
KPYM
TBB4B
VPS16
A8K968
NEP1
-log10(p-value)
log2Fold Change
C
YIR v MYIR
PALLD
CLTCL1
DPH5
CALD1
LLPH
CNN2
SVIL
PKM
VPS16
FERMT3
-log10(p-value)
log2Fold Change
D
PRAF2
VATF
S10AG
KI13B
Y vs YIR
M vs MIR
Log2FC

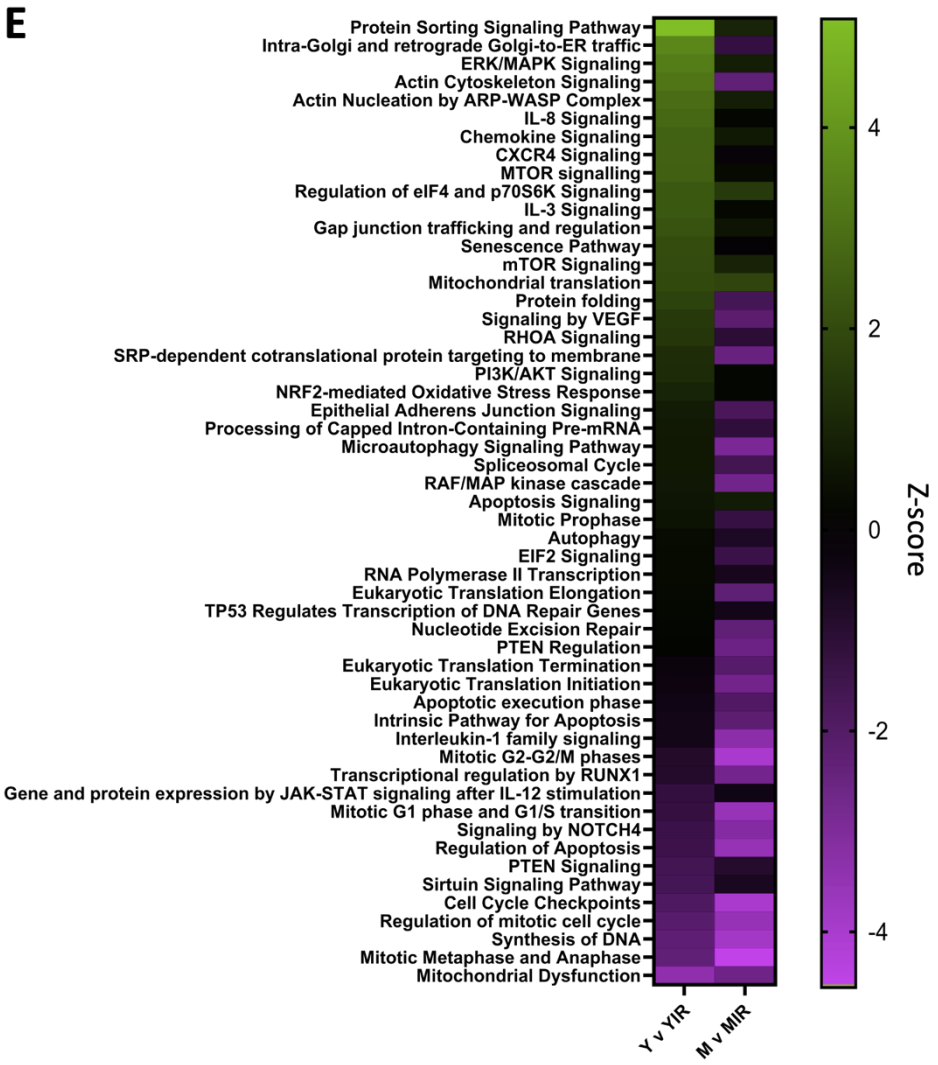


Figure 7.3 Differential IR-induced protein expression in HCAECs from young and middle-aged donors.

HCAECs from young and middle-aged donors were irradiated with 0 or 10 Gy X-ray. 7 days after irradiation, cell pellets were collected, and proteomic analysis performed. **A-C**) Significantly differentially expressed proteins after irradiation of HCAECs from young donors (**A**) and middle-aged donors (**B**) compared to age matched control, with the differences in protein expression after IR exposure compared between the age groups (**C**). Blue = significantly downregulated, red = significantly upregulated, calculated using student t-tests (n=3), with the $\log_2$ fold-change and $\log_{10}$ p-values displayed. Horizontal dotted line indicates a significance threshold of $p<0.05$, vertical dotted lines indicate a fold-change of >1.5 or <-1.5. **D**) The significantly differentially expressed proteins with opposite change in direction in the irradiated HCAECs from young and middle-aged donors. **E**)

Datasets were uploaded to IPA™ for pathway comparison analysis, identifying pathways predicted to be differentially modulated with IR exposure within the HCAEC from young and middle-aged donors, with the heatmap representing z-score for activation of each pathway. N=3, student's t-test. log_2 fold-change and log_{10} p-values. Horizontal dotted line indicates a significance threshold of $p<0.05$, vertical dotted lines indicate a fold-change of >1.5 or <-1.5.

7.3.3 Rapamycin alleviates IR-induced CVD-related protein expression in HCAEC

With processes related to mTOR signalling suggested to be affected by IR exposure (section 7.3.2), the well documented increases in mTOR signalling in senescence (Walters, Deneka-Hannemann and Cox, 2016; Walters and Cox, 2018; Weichhart, 2018), the reduction in IR-induced CVD phenotypes and related gene expression with the mTOR inhibitor, rapamycin (e.g., HCAEC monolayer adhesion and permeability) observed in Chapters 5&6, in this section, I investigate the modulation of IR-induced changes in protein expression using rapamycin. To accomplish this, HCAECs from young and middle-aged donors were exposed to 0 or 10 Gy X-ray, with immediate addition of 10 nM rapamycin to the irradiated cells for 5 days. 7-days post irradiation, cell pellets were collected, and proteomic analysis performed as previously described (7.1.1). This resulted in the generation of datasets outlining the differentially expressed proteins between the groups investigated. As the interest of this section is in the ability of rapamycin to alleviate IR-induced changes in protein expression, here I will only discuss

the differences in protein expression between the non-treated control and the irradiated with rapamycin treated HCAECs.

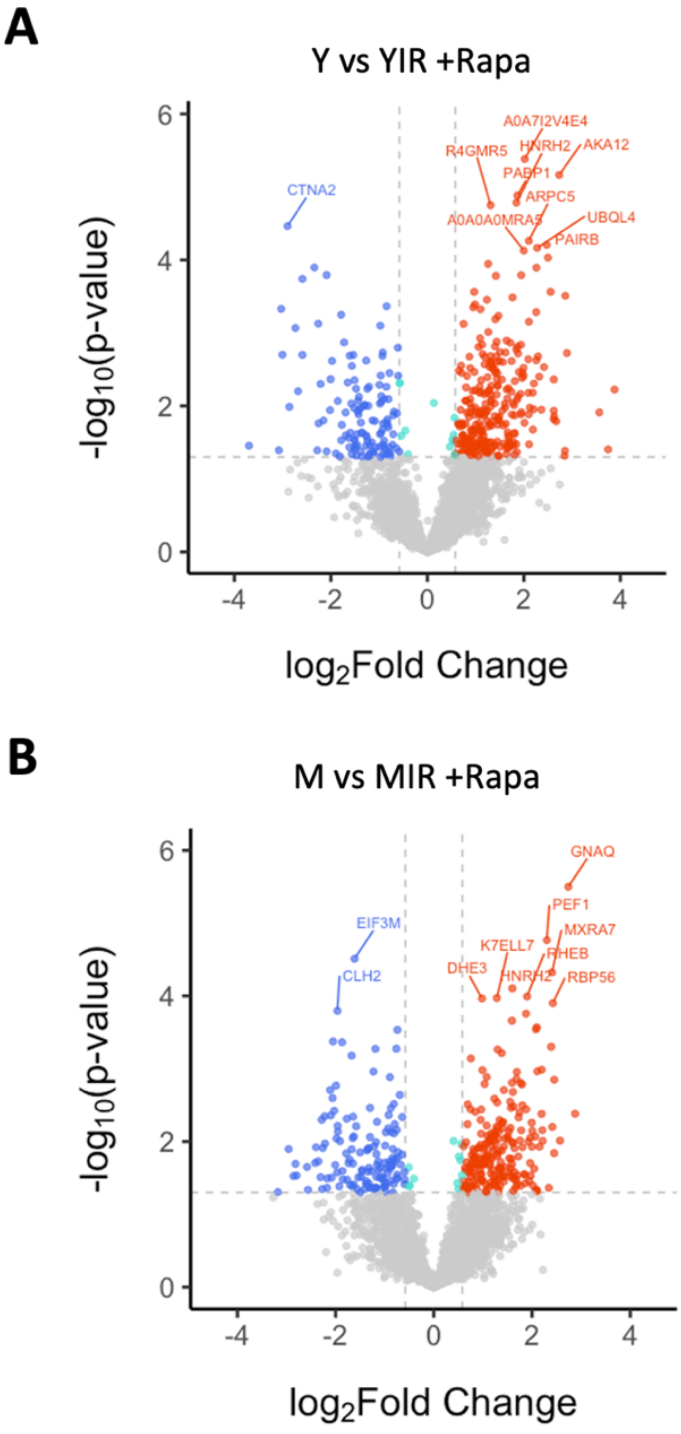
From the differential protein expression analysis, within the HCAECs from young donors, 415 proteins were found to be significantly differentially expressed after irradiation and rapamycin treatment, compared to control (student's t-test, $p<0.05$), with 28 having an adjusted p-value <0.05 (Figure 7.4A). Within the HCAECs from middle-aged donors, 759 proteins were found to be significantly differentially expressed (student's t-test, $p<0.05$), with 11 have an adjusted p-value <0.05 (Figure 7.4B). Using these datasets, along with those from Figure 7.3, I mined the differential protein expression results for the proteins related to cellular senescence, adhesion, and junctions (gene sets used in Supplementary Table S6.3, S6.4, & S6.5). With this, I compare the protein expression changes, within both age groups, between irradiated HCAECs and control, along with irradiated HCAECs + rapamycin, compared to control (Figure 7.4C-E).

When comparing the IR-induced changes in protein expression associated with senescence, proteins such as MMP14, IGFBP7, and SERPINE1 have greater upregulation in the irradiated HCAECs from young donors compared to middle-aged (Figure 7.4C). Interestingly, expression of IGFBP7 has been associated with chronic heart failure in people and mouse models, with *Igfbp7* knockout mice displaying reduced severity along with a reduction in cardiac cell senescence (Zhang *et al.*, 2022). This suggests that further *in vitro* investigation into the effect of IGFBP7 on senescence in HCAECs may provide insight into the differing protein expression profile observed between the ages

here. Conversely, there was a greater upregulation observed in MMP2, and ICAM1 within the HCAECs from middle-aged donors. Importantly, rapamycin treatment alleviated the majority of IR-induced protein expression changes associated with senescence. Many of the proteins are associated with the SASP, complementing the SA-β-Gal assay performed in Chapter 5, which suggested X-ray exposure was likely inducing senescence in these HCAECs (Saul *et al.*, 2022).

Furthermore, the IR-induced differential expression of proteins associated with adhesion suggests that the HCAECs from young donors will have a varied adhesion phenotype compared to those from middle-aged. Examples include the upregulation of MYH14 and MYL9 in the irradiated HCAECs from young donors and not in those from middle-aged. While this does not enable direct correlation between differences in IR-induced adhesion, future functional investigations into the effects of overexpression or knockdown of these proteins may shed light on those that may result in age-mediated differences in IR-induced adhesion. Importantly, within the irradiated HCAECs from young donors, rapamycin alleviated the increase in a high number of proteins, such as ESM1, MMP14, MYL9, and IL1RL1, suggesting that the significant reduction in HCAEC monolayer adhesion observed with rapamycin treatment in Chapter 5 may be due to preventing upregulation of these proteins. Indeed, *Esm1* (endothelial cell-specific molecule-1) knockout mouse models have been shown to have reduced immune cell migration across the EC monolayer, suggesting this may play an important role in HCAEC monolayer permeability and immune cell recruitment (Rocha *et al.*, 2014).

Similar trends were observed in the IR-induced changes in expression of proteins related to cellular junctions, with greater increases in proteins such as CADM3, ARF6, and TUBA1A, with the majority of down-regulated proteins displaying similar decreases between the two age groups. Furthermore, rapamycin inhibited the upregulation of the vast majority of proteins in irradiated HCAECs from young donors. Within the irradiated HCAECs from middle-aged donors, the main effects of rapamycin were preventing IR-induced decreases in proteins such as FERMT2, CTNND1, and TUBB8. As with those related to adhesion and senescence, these results provide potential targets for investigation into their effects on functional adhesion *in vitro*.


A
Y vs YIR +Rapa
A0A7I2V4E4
HNRH2
AKA12
R4GMR5
PABP1
CTNA2
ARPC5
A0A0A0MRA5
UBQL4
PAIRB
-log10(p-value)
log2Fold Change
B
M vs MIR +Rapa
GNAQ
PEF1
EIF3M
MXRA7
K7ELL7
RHEB
DHE3
HNRH2
RBP56
CLH2
-log10(p-value)
log2Fold Change

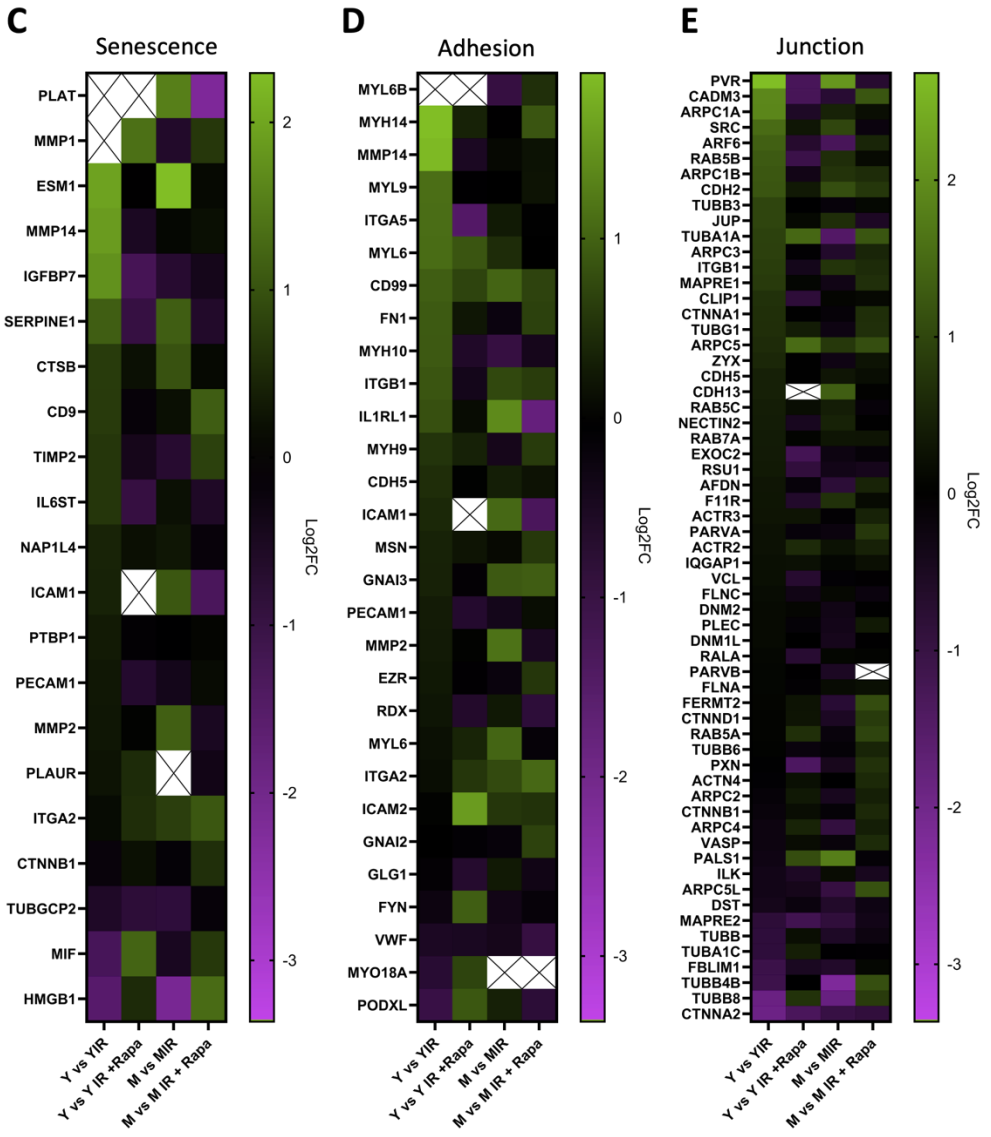


Figure 7.4 The effect of rapamycin on IR-induced protein expression in HCAECs

HCAECs from young and middle-aged donors were irradiated with 0 or 10 Gy X-ray, with exposure groups receiving 0 or 10 nM rapamycin treatment for 5 days immediately after irradiation. 7-days after irradiation, cells were pelleted, and comparative proteomic analysis performed. **A-B)** Significantly differentially expressed proteins ($p<0.05$) visualised using volcano plots, indicating those differentially expressed with irradiation and rapamycin treatment, compared to control, in HCAECs from young (**A**) and middle-aged (**B**) donors. N=3, student's t-test. $\log_2$ fold-change and $\log_{10}$ p-values displayed. Horizontal dotted line = $p<0.05$, vertical dotted lines = fold-change of >1.5 or <-1.5. Blue = downregulated, red = upregulated. The resultant datasets and those from

Figure 7.3 were then mined for proteins associated with cellular senescence (**C**), adhesion (**D**), and junctions (E).

7.3.4 Comparison between HCAEC differential gene and protein expression

To further solidify potential molecular targets for future investigations into the mechanisms behind IR-CVD, here I compare the expression of genes and proteins which are related to cellular senescence and CVD phenotypes (cellular adhesion and cellular junctions) using the gene sets used previously (SenMayo, adhesion, and junction. As discussed in section 6.3.3). This analysis will also help to identify whether the differences observed in protein expression is a result of changes in gene expression, mRNA translation, or protein degradation. Within this analysis, I focus on comparing the proteome and transcriptome in HCAECs from young and middle-aged donors and investigate the expression changes within each age group 7 days after exposure to 10 Gy X-ray.

When comparing the differences in gene and protein expression in the HCAECs from middle-aged donors compared to young, a number of the proteins related to senescence are differentially modulated with little change observed in the genes coding those proteins (Figure 7.5A). For example, the proteins HMGB1, ICAM1, and IL6ST show differential expression in the HCAECs, with the expression of the genes coding for these displaying little to no change. This suggests that there is either different post-transcriptional regulation of these genes which results in altered translation from the mRNA, or that the clearance of these proteins is differentially modulated with age, both

of which would be interesting avenues for future investigation. Indeed, it has been well noted in literature that protein translation differs with age in many different organisms and tissues, which results in altered protein expression (Demontis and Perrimon, 2010; Depuydt *et al.*, 2016; Ravi *et al.*, 2018; Stein *et al.*, 2022). In contrast, the increased abundance of the PECAM1 protein is reflected in the associated genes expression, suggesting that PECAM1 protein expression is increased with age in HCAECs, at least in part, by increased gene expression. Interestingly, PECAM1 is also associated with cellular adhesion (Figure 7.5B) and has been associated with endothelial cell disfunction and atherosclerosis making this a strong candidate for future investigations into age alone as a risk factor for CVD (Harry *et al.*, 2008; Xie *et al.*, 2020).

Similarly to the senescence associated analysis, the age-related changes in the expression of many proteins related to cellular adhesion did not correlate with changes in gene expression (Figure 7.5B). This was also the case for many of the genes and proteins associated with cellular junctions (Figure 7.5C), which suggests that there may be a decline in the degradation of junctional proteins with age in HCAEC, or increased translation from the associated mRNA. Ultimately, these results suggest that the association between gene expression and the expression of the related proteins may have reduced correlation with age. This should be confirmed with more robust measures of gene and protein expression (e.g., PCR and Western blot), along with comparison of the whole proteome and transcriptome within each age to group to identify any changes in correlation between transcription and translation with age.

When reviewing the effect of IR on gene and protein expression, a number of interesting candidates for further study arise. Within the senescence associated analysis, *Esm1* and *Hmgb1* show IR-induced changes in gene expression that are reflected in protein expression in both age groups (Figure 7.5A). This not only increases the confidence in these as potential targets for future investigations, it also suggests that the IR-induced changes in the expression of these proteins is related to changes transcription of these genes. Again, initial first steps would be to confirm these findings using PCR and Western blot analysis.

When investigating the IR-induced changes in gene and protein expression that were related to cellular adhesion, within both age groups, many of the IR-induced increases in proteins were reflected by increases in gene expression, suggesting that the expression changes in these proteins is, at least in part, due to IR-induced changes in gene expression (Figure 7.5B). Furthermore, this comparison strengthens targets such as ICAM1, IL1RL1, and ITGB1 for future investigations into the molecular effects of IR exposure of HCAECs. Interestingly, IR-induced increases in expression of the *Fn1* gene was similar between the two age groups, however, this was only reflected in increased protein expression in the HCAECs from younger donors, suggesting there may be age-modulated, IR-induced changes in translation of some proteins. Indeed, the IR-induced changes in junctional proteins only displayed a similar concordance in the HCAECs from young donors, with fewer of the changes in proteins reflected in changes in gene expression in the HCAECs from middle-aged donors (Figure 7.5C).

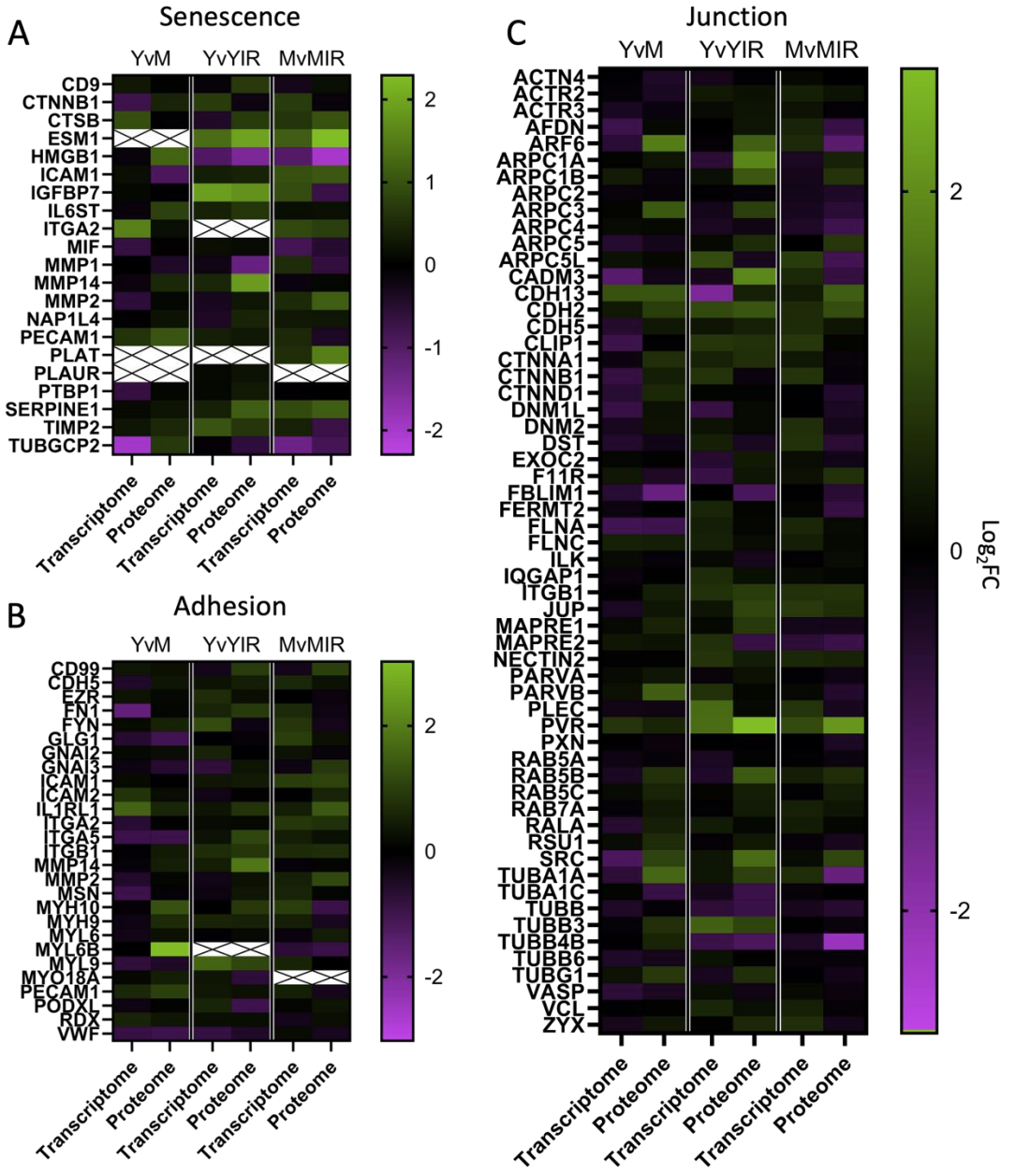


Figure 7.5 Comparison between the IR-induced differential gene and protein expression within HCAECs from young and middle-aged donors.

Comparison between the differential gene and protein expression within HCAECs associated with cellular senescence (**A**), cellular adhesion (**B**), and cellular junctions (**C**). The differential expression profiles displayed are the $\log_2$ fold change in HCAECs from middle-aged donors compared to young (YvM), young with 10 Gy X-ray exposure compared to age matched control (YvYIR), and

middle-aged with 10 Gy X-ray exposure compared to age matched control. Cell pellet and RNA harvesting was performed 7 days after X-ray exposure. N=3.

Overall, the comparison between the transcriptome and proteome changes with age suggests that many of the proteins associated with cellular senescence, adhesion, and junctions may primarily be associated with differences in control of post-transcriptional regulation of translation and degradation of these proteins. Furthermore, many of the changes in these proteins after exposure to IR appear to be related to changes in gene expression, suggesting that IR is inducing changes at a protein level through inducing changes in gene expression. However, this does not hold true for all proteins presented here, indicating the complex nature of the cellular response at a molecular level to IR. Furthermore, differences were observed in the translation of proteins between the age groups investigated, in some cases where changes in gene expression were similar. This suggests that age may affect the translation of the observed IR-induced gene expression changes, further suggesting that age related changes in translation may be associated with the age-related phenotypic responses in HCAECs and mouse models presented in previous chapters (Chapters 4&5, respectively).

A limitation of comparing the transcriptomic and proteomic analysis carried out in this thesis is the differences in read depth between the two techniques, with greater depth achieved in the transcriptomics compared to the proteomics. The result of this is that a gene may have been detected, which was not found at the protein level simply because the technique did not capture it.

7.4 Discussion

Within this chapter, I have demonstrated differences in protein expression between HCAECs from young and middle-aged donors, providing an indication of the potential changes in their proteome with age. Furthermore, I report that the protein expression profile in the HCAECs from middle-aged donors is indicative of an aged cellular phenotype, supporting the previous data presented in Chapters 5&6. GO analysis of the differences in protein expression between the two age groups identified likely differences in intracellular trafficking of molecules along with processes associated with the regulation of cell structure and interaction with the ECM, processes that are related to atherogenesis and senescence, suggesting avenues of investigation for age-related CVD. In addition, I have demonstrated that age-modulates IR-induced protein expression within HCAECs to an extent, with expression of proteins associated with ER-Golgi and vesicle trafficking, along with organelle acidification demonstrating the greatest differences between the two age groups. Finally, I demonstrated varying changes in the expression of proteins related to cellular senescence, adhesion, and junctions within age in the irradiated HCAECs. Finally, I demonstrated that mTOR inhibition with rapamycin alleviates many of the IR-associated changes in protein expression.

7.4.1 Differences in HCAEC protein expression with age

The differential protein expression analysis performed, which demonstrated the proteins that were differentially expressed in HCAECs from middle-aged donors

compared to young, provides an insight into the molecular changes that may occur in HCAECs with age. Importantly, as these cells were maintained in cell culture conditions along with being immortalised, this expression profile may not be truly representative of HCAEC ageing *in vivo*. However, from the most significantly differentially expressed proteins, such as KIF13B, AP1B1, and PRAF2 were upregulated in the HCAECs from middle-aged donors. KIF13B was particularly interesting as studies have linked increased expression and age in synapses (Aenlle and Foster, 2010), along with its role in mediated the trafficking of VEGFR2 to EC membranes. Indeed, *Kif13B* knockdown mouse models demonstrated reduced vascular leakage (Waters *et al.*, 2022), suggesting it may be important for HCAEC permeability. If the upregulation observed within the middle-aged HCAECs observed here is reflected *in vivo*, the this may provide a novel mechanism that contributes to age related atherosclerosis.

7.4.2 Age-modulation of IR-induced changes in protein expression within HCAECs

The analysis of the differentially expressed proteins in irradiated HCAECs from young and middle-aged donors revealed different protein level responses to IR between the age groups. Within this, I identified 4 proteins that were significantly upregulated in the irradiated HCAECs from young donors, with these being significantly downregulated in the irradiated HCAECs from middle-aged donors. Of note was KIF13B, which was previously found to be upregulated when comparing the HCAEC expression changes with age (discussed above 7.4.1). This upregulation within irradiated HCAECs from

young and the opposite in those from middle-aged further suggests that this may prove to be an interesting avenue for further investigation.

In addition, IPA^{TM} analysis of biological pathways likely to be active with the observed protein expression suggested that senescence related pathways such as mTOR signalling, multiple cytokine signalling pathways, and the senesce pathway were likely to have increased activity in the irradiated HCAECs from young donors, and not in those from middle-age. This suggest that age of the HCAEC donor may modulate IR-induced senescence. To the best of my knowledge, there is little evidence surrounding age-modulation of IR-induced senescence. However, the senescence related hits in the IPA^{TM} analysis, the 192 detected proteins with significantly different expression, and IR-induced SA-β-Gal activity in Chapter 5, suggests that HCAECs from younger donors respond differently to IR than those from middle-aged.

7.4.3 Rapamycin modulation of IR-induced changes in the proteome

The induction and maintenance of senescence via the mTOR pathway has been established for some time (Iglesias-Bartolome *et al.*, 2012; Walters, Deneka-Hannemann and Cox, 2016), with many studies demonstrating its ability to inhibit senescence or phenotypes associated with it such as the SASP (Schreml *et al.*, 2007; Demidenko *et al.*, 2009; Nacarelli and Sell, 2017), along with demonstrating effective prevention of epigenic ageing (Horvath *et al.*, no date; Kabacik *et al.*, 2022a). Therefore, with the hypothesis being IR-induced senescence contributes to IR-CVD, targeting this pathway further elucidates the role of senescence in IR-CVD. Indeed, rapamycin prevented or reduced IR-induced changes associated with CVD, such as cellular

adhesion and junctions. As previously discussed (section 1.2.3), atherogenesis involves the attraction and adherence of immune cells to the EC layer within coronary arteries, followed by their migration into the subendothelial space, where combined with lipids, they form atherosclerotic plaques (Skålén *et al.*, 2002b; Georgakis *et al.*, 2021). Therefore, the prevention of IR-induced increases in adhesion and permeability with rapamycin in Chapter 5, combined with the observations here that rapamycin inhibits IR-induced change in proteins associated with these characteristics, suggests that IR induces these in an mTOR-dependant manner. This lends support to the role of IR-induced senescence increasing CVD risk.

8 Discussion

8.1 Summary

In this thesis, I have demonstrated the suitability of the $Ldlr^{-/-}$ mouse model for investigation into IR-CVD, along with identifying suitable X-ray exposure doses (Chapter 3&4), providing an alternative model for investigations into IR-CVD. Using this model and the $ApoE^{-/-}$ mouse model, I have demonstrated that age does mediate IR-induced CVD within these mice, with older mice displaying significant increases in atherosclerotic plaque development, with no increases observed in younger mice (Chapter 4).

In addition to the animal studies, I have also demonstrated that IR induces pro-atherogenic phenotypes in HCAECs from different biological donors (Chapter 5). Within this, I demonstrated increases in HCAEC monolayer permeability and adhesion (pro-atherogenic characteristics) after irradiation of the cells with X-rays. Furthermore, I demonstrated a corelation between increasing SA-β-Gal activity and increasing HCAEC adhesion, suggesting that X-ray induced adhesion may be associated with increased senescence. Importantly, in initial experiments I observed trends suggesting that HCAECs from younger donors are more likely to have a greater fold-increase in adhesion, permeability, and SA-β-Gal activity post irradiation, although these differences were not statistically significant. However, when repeated in additional experiments, a significant increase in IR-induced adhesion of HCAECs from young

donors, compared to middle-aged, was observed. While just a singular aspect of the mechanisms behind atherogenesis, along with being a small sample size, this supports the epidemiological evidence which suggests IR exposure at a younger age carries a greater risk of IR-CVD (Little *et al.*, 2012c). Additionally, within Chapter 5 I have also demonstrated the ability of rapamycin to prevent IR-induced increases in HCAEC monolayer adhesion, permeability, and SA-β-Gal activity. This provides functional evidence of the suitability of rapamycin to reduce or inhibit pro-atherogenic phenotypes caused by IR exposure in HCAECs, and further adds to the hypothesis of senescence contributing to the development of IR-CVD.

Using comparative transcriptomics and proteomics, I generated transcriptome and proteome profiles of ageing in HCAECs (Chapter 6&7). Within these, a number of genes and proteins have been suggested for more targeted approaches to identify their role in age-related CVD development. With the aim of identifying avenues for future work into the mechanisms behind IR-CVD and how age may modulate these, I further utilised omics techniques, demonstrating that age of the HCAEC affects IR-induced expression changes in genes and proteins related to CVD phenotypes, highlighting potential targets for future investigation (Chapter 6&7). Lastly, I demonstrated the ability of rapamycin to alleviate some of the IR-induced changes in genes associated with CVD phenotypes, further supporting the hypothesis that IR-induced senescence contributes to IR-CVD.

8.1.1 Disparity between age affects in mice and cells

Epidemiological evidence suggests that people exposed to IR at a younger age are more likely to develop IR-CVD (Little *et al.*, 2012d, 2023), therefore, my hypothesis was mice

exposed to IR at a younger age would have a greater degree of plaque development compared to those exposed at an older age. However, the opposite was observed. Furthermore, I had a similar hypothesis with regards to the *in vitro* studies with HCAECs from young to middle-aged donors, hypothesising that the irradiated HCAECs from young donors would display greater increases in phenotypes associated with CVD development, than those from middle-aged. Here, the evidence suggests that HCAECs from younger donors may be more susceptible to IR-induced increases in adhesion, a characteristic that promotes CVD (Galkina and Ley, 2007; Gimbrone and García-Cardeña, 2016b). This raises multiple questions, firstly, as discussed in Chapter 4, does the epidemiological evidence sufficiently factor in lifestyle differences, particularly surrounding changes in culture that would have occurred over lifespan studies? Secondly, is a mouse model of CVD suitably translatable for investigating IR-CVD?

Additionally, while there may be a greater increase in senescent endothelial cells lining the aorta in the younger mice, immune clearance of senescent cells may be more efficient in the younger mice compared to the older ones (Larissa G.P. Langhi Prata *et al.*, 2018; Song, An and Zou, 2020). In this regard, it is also essential to consider the implications of whole-body irradiation, which these mice were subjected to. This would mean that immune cell-producing tissues such as bone marrow will also have been irradiated, which could induce apoptosis or senescence within these cells, impacting both the development of atherosclerosis and immune clearance of senescent cells within the vasculature (Green and Rubin, 2014; Larissa G.P.Langhi Prata *et al.*, 2018). Finally, the *in vitro* assays may not have included HCAECs from donors of a high enough

age. With 55 years being the oldest donor, this is likely not a comparable age with the oldest mice used in the animal studies (Dutta and Sengupta, 2016).

8.2 Future work

With the combination of IR-induced increases in plaque development within the mouse models of atherosclerosis (Chapter 4) and the observed reductions in IR-induced atherogenic phenotypes in HCAECs with rapamycin treatment (Chapter 5), a logical next step would be to investigate whether rapamycin can prevent IR-induced atherosclerosis within the mouse models. Within this, it would also be beneficial to assess the senescent cell content of the aortic plaques and healthy aorta, allowing for any correlation between IR-induced vascular senescence and plaque development to be drawn. In addition to this, development of an irradiation technique that would allow for targeted exposure of mouse aortas, rather than whole body exposure, would help to reduce confounding factors, such as exposure of immune cell producing tissues. An important measure missing from my analysis of the mouse aortic plaques is the depth of the plaque. Using imaging techniques such as microCT would allow for both quantification of plaque coverage and depth (Douglas *et al.*, 2019).

Within this thesis, my *in vitro* studies have only focused on one cell type (HCAECs) from the coronary arteries. While there are a number of reasons why *in vitro* studies are not truly representative, investigation into the effects of IR on co-cultures of HCAECs and VSMCs would be a step closer to *in vivo* conditions, with EC interaction with VSMCs being an important component of atherogenesis (Noonan *et al.*, 2019). Furthermore, I

have demonstrated that culturing HCAECs under flow conditions, which are more physiologically relevant, results in differences in cellular morphology, suggesting that these cells have differences in their transcriptomic and proteomic profiles compared to those cultured in static conditions. Indeed, this is supported by literature demonstrating flow responsive changes in gene and protein expression (Dardik *et al.*, 2005; Afshar *et al.*, 2023), meaning that the molecular response to IR may differ under flow conditions.

With the multi-omic investigations carried out in this thesis, comes a wealth of data and extensive possibilities for exploring it. To be concise, I have selected the most relevant points of investigation. However, this provides an opportunity for further exploration into the proteome and transcriptome of HCAECs, with datasets available for 8 different experimental populations (young, middle-aged, young + rapamycin, middle-aged + rapamycin, irradiated young, irradiated middle-aged, irradiated young + rapamycin, and irradiated middle-aged + rapamycin). Furthermore, only a targeted comparison between the transcriptome and proteome has been made within this thesis, however, the data provides the opportunity for further analysis into the relationship between the two.

9 References

Acosta, J.C. *et al.* (2013) 'A complex secretory program orchestrated by the inflammasome controls paracrine senescence', *Nature Cell Biology*, 15(8), pp. 978–990. Available at: https://doi.org/10.1038/ncb2784.

Adams, K.E. *et al.* (2006) 'Recruitment of ATR to sites of ionising radiation-induced DNA damage requires ATM and components of the MRN protein complex', *Oncogene*, 25(28), pp. 3894–3904. Available at: https://doi.org/10.1038/sj.onc.1209426.

Adams, P.D. *et al.* (2013) 'Lysosome-mediated processing of chromatin in senescence', *Journal of Cell Biology*, 202(1), pp. 129–143. Available at: https://doi.org/10.1083/jcb.201212110.

Aenlle, K.K. and Foster, T.C. (2010) 'Aging alters the expression of genes for neuroprotection and synaptic function following acute estradiol treatment', *Hippocampus*, 20(9), pp. 1047–1060. Available at: https://doi.org/10.1002/hipo.20703.

Afshar, Y. *et al.* (2023) 'Transcriptional drifts associated with environmental changes in endothelial cells', *eLife*, 12, pp. 1–29. Available at: https://doi.org/10.7554/elife.81370.

Alcorta, D.A. *et al.* (1996) 'Involvement of the cyclin-dependent kinase inhibitor p16 (INK4a) in replicative senescence of normal human fibroblasts', *Proceedings of the National Academy of Sciences of the United States of America*, 93(24), pp. 13742–13747. Available at: https://doi.org/10.1073/pnas.93.24.13742.

Alexandre, M.D. *et al.* (2007) 'The first extracellular domain of claudin-7 affects paracellular Cl- permeability', *Biochemical and Biophysical Research Communications*, 357(1), pp. 87–91. Available at: https://doi.org/10.1016/j.bbrc.2007.03.078.

Altevogt, P. *et al.* (2021) 'Novel insights into the function of CD24: A driving force in cancer', *International Journal of Cancer*, 148(3), pp. 546–559. Available at: https://doi.org/10.1002/ijc.33249.

Anand, R. *et al.* (2016) 'Phosphorylated CtIP Functions as a Co-factor of the MRE11-RAD50-NBS1 Endonuclease in DNA End Resection', *Molecular Cell*, 64(5), pp. 940–950. Available at: https://doi.org/10.1016/j.molcel.2016.10.017.

Appella, E. and Anderson, C.W. (2001) 'Post-translational modifications and activation of p53 by genotoxic stresses', *European Journal of Biochemistry*, 268(10), pp. 2764–2772. Available at: https://doi.org/10.1046/j.1432-1327.2001.02225.x.

Appelqvist, H. *et al.* (2013) 'The lysosome: From waste bag to potential therapeutic target', *Journal of Molecular Cell Biology*, 5(4), pp. 214–226. Available at: https://doi.org/10.1093/jmcb/mjt022.

Ariyoshi, H. *et al.* (2001) 'Role of receptor for advanced glycation end-product (RAGE) and the JAK/STAT-signaling pathway in AGE-induced collagen production in NRK-49F cells', *Journal of Cellular Biochemistry*, 81(1), pp. 102–113. Available at: https://doi.org/10.1002/1097-4644(20010401)81:1<102::AID-JCB1027>3.0.CO;2-Y.

Armitage, J. *et al.* (2019) 'Efficacy and safety of statin therapy in older people: a meta-analysis of individual participant data from 28 randomised controlled trials', *The Lancet*,

393(10170), pp. 407–415. Available at: https://doi.org/10.1016/S0140-6736(18)31942-1.

Atun, R. *et al.* (2015) 'Expanding global access to radiotherapy', *The Lancet Oncology*, 16(10), pp. 1153–1186. Available at: https://doi.org/10.1016/S1470-2045(15)00222-3.

Azimzadeh, O. *et al.* (2015) 'Integrative proteomics and targeted transcriptomics analyses in cardiac endothelial cells unravel mechanisms of long-term radiation-induced vascular dysfunction', *Journal of Proteome Research*, 14(2), pp. 1203–1219. Available at: https://doi.org/10.1021/pr501141b.

Bailey, S.M. and Murnane, J.P. (2006) 'Telomeres, chromosome instability and cancer', *Nucleic Acids Research*, 34(8), pp. 2408–2417. Available at: https://doi.org/10.1093/nar/gkl303.

Bainton, D.F. (1981) 'The discovery of lysosomes.', *The Journal of cell biology*, 91(3), pp. 66s–76s. Available at: https://doi.org/10.1083/jcb.91.3.66s.

Baker, J.E., Moulder, J.E. and Hopewell, J.W. (2011) 'Radiation as a risk factor for cardiovascular disease', *Antioxidants and Redox Signaling*, 15(7), pp. 1945–1956. Available at: https://doi.org/10.1089/ars.2010.3742.

Ball, A.J. and Levine, F. (2005) 'Telomere-independent cellular senescence in human fetal cardiomyocytes', (October 2004), pp. 21–30. Available at: https://doi.org/10.1111/j.1474-9728.2004.00137.x.

Baran, R. *et al.* (2022) 'The Cardiovascular System in Space: Focus on In Vivo and In Vitro Studies', *Biomedicines*, 10(1), pp. 1–29. Available at: https://doi.org/10.3390/biomedicines10010059.

Baranov, M. V. *et al.* (2016) 'SWAP70 Organizes the Actin Cytoskeleton and Is Essential for Phagocytosis', *Cell Reports*, 17(6), pp. 1518–1531. Available at: https://doi.org/10.1016/j.celrep.2016.10.021.

Barnes, P.J., Baker, J. and Donnelly, L.E. (2019) 'Cellular senescence as a mechanism and target in chronic lung diseases', *American Journal of Respiratory and Critical Care Medicine*, 200(5), pp. 556–564. Available at: https://doi.org/10.1164/rccm.201810-1975TR.

Barnes, R.P. *et al.* (2022) 'Telomeric 8-oxo-guanine drives rapid premature senescence in the absence of telomere shortening', *Nature Structural and Molecular Biology*, 29(7), pp. 639–652. Available at: https://doi.org/10.1038/s41594-022-00790-y.

Bartolomé, A. *et al.* (2017) 'MTORC1 Regulates both General Autophagy and Mitophagy Induction after Oxidative Phosphorylation Uncoupling', *Molecular and Cellular Biology*, 37(23). Available at: https://doi.org/10.1128/mcb.00441-17.

Basisty, N. *et al.* (2020) 'A proteomic atlas of senescence-associated secretomes for aging biomarker development', *PLoS biology*, 18(1), p. e3000599. Available at: https://doi.org/10.1371/journal.pbio.3000599.

Bentzon, J.F. *et al.* (2014) 'Mechanisms of plaque formation and rupture', *Circulation Research*, 114(12), pp. 1852–1866. Available at: https://doi.org/10.1161/CIRCRESAHA.114.302721.

Biran, A. *et al.* (2017) 'Quantitative identification of senescent cells in aging and disease', *Aging Cell*, 16(4), pp. 661–671. Available at: https://doi.org/10.1111/acel.12592.

Birch, J. and Gil, J. (2020) 'Senescence and the SASP: Many therapeutic avenues', *Genes and Development*, 34(23–24), pp. 1565–1576. Available at: https://doi.org/10.1101/gad.343129.120.

Björkegren, J.L.M. and Lusis, A.J. (2022) 'Atherosclerosis: Recent developments.', *Cell*, pp. 1–16. Available at: https://doi.org/10.1016/j.cell.2022.04.004.

Blagosklonny, M. V. (2012) 'Cell cycle arrest is not yet senescence, which is not just cell cycle arrest: Terminology for TOR-driven aging', *Aging*, 4(3), pp. 159–165. Available at: https://doi.org/10.18632/aging.100443.

Blokland, K.E.C. *et al.* (2020) 'Regulation of cellular senescence by extracellular matrix during chronic fibrotic diseases', *Clinical Science*, 134(20), pp. 2681–2706. Available at: https://doi.org/10.1042/CS20190893.

Bloom, S.I. *et al.* (2023a) 'Mechanisms and consequences of endothelial cell senescence', *Nature Reviews Cardiology*, 20(1), pp. 38–51. Available at: https://doi.org/10.1038/s41569-022-00739-0.

Bloom, S.I. *et al.* (2023b) 'Mechanisms and consequences of endothelial cell senescence', *Nature Reviews Cardiology*, 20(1), pp. 38–51. Available at: https://doi.org/10.1038/s41569-022-00739-0.

Bochkov, V.N. *et al.* (2002) 'Oxidized phospholipids stimulate tissue factor expression in human endothelial cells via activation of ERK/EGR-1 and Ca++/NFAT', *Blood*, 99(1), pp. 199–206. Available at: https://doi.org/10.1182/blood.V99.1.199.

Bodnar, A.G. *et al.* (1998) 'Extension of life-span by introduction of telomerase into normal human cells', *Science*, 279(5349), pp. 349–352. Available at: https://doi.org/10.1126/science.279.5349.349.

Boerma, M. (2015) 'Space radiation and cardiovascular disease risk', *World Journal of Cardiology*, 7(12), p. 882. Available at: https://doi.org/10.4330/wjc.v7.i12.882.

Boesten, L.S.M. *et al.* (2005) 'Tumor necrosis factor-α promotes atherosclerotic lesion progression in APOE*3-leiden transgenic mice', *Cardiovascular Research*, 66(1), pp. 179–185. Available at: https://doi.org/10.1016/j.cardiores.2005.01.001.

Borrego-Soto, G., Ortiz-López, R. and Rojas-Martínez, A. (2015) 'Ionizing radiation-induced DNA injury and damage detection in patients with breast cancer', *Genetics and Molecular Biology*, 38(4), pp. 420–432. Available at: https://doi.org/10.1590/S1415-475738420150019.

Braakman, I. and Bulleid, N.J. (2011) 'Protein folding and modification in the mammalian endoplasmic reticulum', *Annual Review of Biochemistry*, 80, pp. 71–99. Available at: https://doi.org/10.1146/annurev-biochem-062209-093836.

Bradshaw, P.T. *et al.* (2016) 'Cardiovascular Disease Mortality among Breast Cancer Survivors', *Epidemiology*, 27(1), pp. 6–13. Available at: https://doi.org/10.1097/EDE.0000000000000394.

Braig, M. and Schmitt, C.A. (2006) 'Oncogene-induced senescence: Putting the brakes on tumor development', *Cancer Research*, 66(6), pp. 2881–2884. Available at: https://doi.org/10.1158/0008-5472.CAN-05-4006.

Brånén, L. *et al.* (2004) 'Inhibition of tumor necrosis factor-α reduces atherosclerosis in apolipoprotein E knockout mice', *Arteriosclerosis, Thrombosis, and Vascular Biology*, 24(11), pp. 2137–2142. Available at: https://doi.org/10.1161/01.ATV.0000143933.20616.1b.

Bravo-Sagua, R. *et al.* (2017) 'Calcium transport and signaling in mitochondria', *Comprehensive Physiology*, 7(2), pp. 623–634. Available at: https://doi.org/10.1002/cphy.c160013.

Breland, U.M. *et al.* (2008) 'A potential role of the CXC chemokine GROα in atherosclerosis and plaque destabilization: Downregulatory effects of statins', *Arteriosclerosis, Thrombosis, and Vascular Biology*, 28(5), pp. 1005–1011. Available at: https://doi.org/10.1161/ATVBAHA.108.162305.

Brenner, D.J. and Hall, E.J. (2007) 'Computed Tomography — An Increasing Source of Radiation Exposure', *New England Journal of Medicine*, 357(22), pp. 2277–2284. Available at: https://doi.org/10.1056/NEJMra072149.

Brown, M.S. and Goldstein, J.L. (1986) 'A receptor-mediated pathway for cholesterol homeostasis', *Science*, 232(4746), pp. 34–47. Available at: https://doi.org/10.1126/science.3513311.

Buschman, M.D. and Field, S.J. (2018) 'MYO18A: An unusual myosin', *Advances in Biological Regulation*, 67, pp. 84–92. Available at: https://doi.org/10.1016/j.jbior.2017.09.005.

Cairns, J.A. *et al.* (1985) 'Aspirin, Sulfinpyrazone, or Both in Unstable Angina', *New England Journal of Medicine*, 313(22), pp. 1369–1375. Available at: https://doi.org/10.1056/NEJM198511283132201.

Caligiuri, G. *et al.* (1999) 'Effects of sex and age on atherosclerosis and autoimmunity in apoE-deficient mice', *Atherosclerosis*, 145(2), pp. 301–308. Available at: https://doi.org/10.1016/S0021-9150(99)00081-7.

Camacho-Pereira, J. *et al.* (2016) 'CD38 Dictates Age-Related NAD Decline and Mitochondrial Dysfunction through an SIRT3-Dependent Mechanism', *Cell Metabolism*, 23(6), pp. 1127–1139. Available at: https://doi.org/10.1016/j.cmet.2016.05.006.

Cao, Y. *et al.* (2021) 'RBM10 Regulates Tumor Apoptosis, Proliferation, and Metastasis', *Frontiers in Oncology*, 11(February), pp. 1–12. Available at: https://doi.org/10.3389/fonc.2021.603932.

Carney, J.P. *et al.* (1998a) 'The hMre11/hRad50 protein complex and Nijmegen breakage syndrome: Linkage of double-strand break repair to the cellular DNA damage

response', *Cell*, 93(3), pp. 477–486. Available at: https://doi.org/10.1016/S0092-8674(00)81175-7.

Carney, J.P. *et al.* (1998b) 'The hMre11/hRad50 protein complex and Nijmegen breakage syndrome: Linkage of double-strand break repair to the cellular DNA damage response', *Cell*, 93(3), pp. 477–486. Available at: https://doi.org/10.1016/S0092-8674(00)81175-7.

Carroll, B. *et al.* (2017) 'Persistent mTORC1 signaling in cell senescence results from defects in amino acid and growth factor sensing', *Journal of Cell Biology*, 216(7), pp. 1949–1957. Available at: https://doi.org/10.1083/jcb.201610113.

Casella, G. *et al.* (2019) 'Transcriptome signature of cellular senescence', *Nucleic Acids Research*, 47(14), pp. 7294–7305. Available at: https://doi.org/10.1093/nar/gkz555.

Cavanaugh, A.H. *et al.* (1995) 'Activity of RNA polymerase I transcription factor UBF blocked by Rb gene product', *Nature*, 374(6518), pp. 177–180. Available at: https://doi.org/10.1038/374177a0.

Ceccaldi, R., Rondinelli, B. and D'Andrea, A.D. (2016) 'Repair Pathway Choices and Consequences at the Double-Strand Break', *Trends in Cell Biology*, 26(1), pp. 52–64. Available at: https://doi.org/10.1016/j.tcb.2015.07.009.

Chan, S.W.L. and Blackburn, E.H. (2002) 'New ways not to make ends meet: Telomerase, DNA damage proteins and heterochromatin', *Oncogene*, 21(4 REV. ISS. 1), pp. 553–563. Available at: https://doi.org/10.1038/sj/onc/1205082.

Chen, Q.M. *et al.* (2000) 'Involvement of Rb family proteins, focal adhesion proteins and protein synthesis in senescent morphogenesis induced by hydrogen peroxide', *Journal of Cell Science*, 113(22), pp. 4087–4097. Available at: https://doi.org/10.1242/jcs.113.22.4087.

Cheng, Y.J. *et al.* (2017) 'Long-term cardiovascular risk after radiotherapy in women with breast cancer', *Journal of the American Heart Association*, 6(5). Available at: https://doi.org/10.1161/JAHA.117.005633.

Chiarito, M. *et al.* (2020) 'Monotherapy with a P2Y12 inhibitor or aspirin for secondary prevention in patients with established atherosclerosis: a systematic review and meta-analysis', *Lancet (London, England)*, 395(10235), pp. 1487–1495. Available at: https://doi.org/10.1016/S0140-6736(20)30315-9.

Childs, B.G. *et al.* (2014) 'Senescence and apoptosis: dueling or complementary cell fates?', *EMBO reports*, 15(11), pp. 1139–1153. Available at: https://doi.org/10.15252/embr.201439245.

Childs, B.G. *et al.* (2016a) 'Senescent intimal foam cells are deleterious at all stages of atherosclerosis', *Science*, 354(6311), pp. 472–477. Available at: https://doi.org/10.1126/science.aaf6659.

Childs, B.G. *et al.* (2016b) 'Senescent intimal foam cells are deleterious at all stages of atherosclerosis', *Science*, 354(6311), pp. 472–477. Available at: https://doi.org/10.1126/science.aaf6659.

Childs, B.G. *et al.* (2021) 'Senescent cells suppress innate smooth muscle cell repair functions in atherosclerosis', *Nature Aging*, 1(8), pp. 698–714. Available at: https://doi.org/10.1038/s43587-021-00089-5.

Cho, H.D. *et al.* (2023) 'KIF13B mediates VEGFR2 recycling to modulate vascular permeability', *Cellular and Molecular Life Sciences*, 80(4), pp. 1–21. Available at: https://doi.org/10.1007/s00018-023-04752-5.

Chopra, S. *et al.* (2022) 'Profiling mRNA, miRNA and lncRNA expression changes in endothelial cells in response to increasing doses of ionizing radiation', *Scientific Reports*, 12(1), pp. 1–17. Available at: https://doi.org/10.1038/s41598-022-24051-6.

Chou, L., Ho, C. and Hung, S. (2022) 'Paracrine Senescence of Mesenchymal Stromal Cells Involves', pp. 1–17.

Chua, R.L. *et al.* (2020) 'COVID-19 severity correlates with airway epithelium–immune cell interactions identified by single-cell analysis', *Nature Biotechnology*, 38(8), pp. 970–979. Available at: https://doi.org/10.1038/s41587-020-0602-4.

Chuaiphichai, S. *et al.* (2023) 'Endothelial cell vasodilator dysfunction mediates progressive pregnancy-induced hypertension in endothelial cell tetrahydrobiopterin deficient mice', *Vascular Pharmacology*, 150(March), p. 107168. Available at: https://doi.org/10.1016/j.vph.2023.107168.

Coleman, O.I. and Haller, D. (2019) 'ER Stress and the UPR in Shaping Intestinal Tissue Homeostasis and Immunity', *Frontiers in Immunology*, 10(December), pp. 1–13. Available at: https://doi.org/10.3389/fimmu.2019.02825.

Collins, C.J. and Sedivy, J.M. (2003) 'Involvement of the INK4a/Arf gene locus in senescence.', *Aging cell*, 2(3), pp. 145–150. Available at: https://doi.org/10.1046/j.1474-9728.2003.00048.x.

Collins, K. and Mitchell, J.R. (2002) 'Telomerase in the human organism', *Oncogene*, 21(4 REV. ISS. 1), pp. 564–579. Available at: https://doi.org/10.1038/sj/onc/1205083.

Collins, P.L. *et al.* (2020) 'DNA double-strand breaks induce H2Ax phosphorylation domains in a contact-dependent manner', *Nature Communications*, 11(1). Available at: https://doi.org/10.1038/s41467-020-16926-x.

Condon, J. *et al.* (2002) 'Telomerase immortalization of human myometrial cells', *Biology of Reproduction*, 67(2), pp. 506–514. Available at: https://doi.org/10.1095/biolreprod67.2.506.

Coppé, J. *et al.* (2014) 'The Senescence-Associated Secretory Phenotype: The Dark Side of Tumor Suppression', *Annual Review of Pathology: Mechanisms of Disease*, pp. 99–118. Available at: https://doi.org/10.1146/annurev-pathol-121808-102144.The.

Coppé, J.P. *et al.* (2008) 'Senescence-associated secretory phenotypes reveal cell-nonautonomous functions of oncogenic RAS and the p53 tumor suppressor.', *PLoS biology*, 6(12). Available at: https://doi.org/10.1371/journal.pbio.0060301.

Correia-Melo, C. *et al.* (2016) 'Mitochondria are required for pro-ageing features of the senescent phenotype', *The EMBO Journal*, 35(7), pp. 724–742. Available at: https://doi.org/10.15252/embj.201592862.

Cory, S. and Adams, J.M. (1998) 'Matters of life and death: Programmed cell death at cold spring harbor', *Biochimica et Biophysica Acta - Reviews on Cancer*, 1377(2), pp. 25–44. Available at: https://doi.org/10.1016/S0304-419X(98)00003-1.

Coulombe, J. *et al.* (2014) 'Loss of UCHL1 promotes age-related degenerative changes in the enteric nervous system', *Frontiers in Aging Neuroscience*, 6(JUN), pp. 1–10. Available at: https://doi.org/10.3389/fnagi.2014.00129.

Cox, L.S. and Redman, C. (2017) 'The role of cellular senescence in ageing of the placenta', *Placenta*, 52, pp. 139–145. Available at: https://doi.org/10.1016/j.placenta.2017.01.116.

Cuff, C.A. *et al.* (2001) 'The adhesion receptor CD44 promotes atherosclerosis by mediating inflammatory cell recruitment and vascular cell activation', *Journal of Clinical Investigation*, 108(7), pp. 1031–1040. Available at: https://doi.org/10.1172/jci12455.

Curnock, R. *et al.* (2023) ' TFEB -dependent lysosome biogenesis is required for senescence ', *The EMBO Journal*, 42(9). Available at: https://doi.org/10.15252/embj.2022111241.

Dalle Pezze, P. *et al.* (2014) 'Dynamic Modelling of Pathways to Cellular Senescence Reveals Strategies for Targeted Interventions', *PLoS Computational Biology*, 10(8). Available at: https://doi.org/10.1371/journal.pcbi.1003728.

Dang, W. (2014) 'The controversial world of sirtuins', *Drug Discovery Today: Technologies*, 12, p. e9. Available at: https://doi.org/10.1016/j.ddtec.2012.08.003.

Dardik, A. *et al.* (2005) 'Differential effects of orbital and laminar shear stress on endothelial cells', *Journal of Vascular Surgery*, 41(5), pp. 869–880. Available at: https://doi.org/10.1016/j.jvs.2005.01.020.

Debacq-Chainiaux, F. *et al.* (2009) 'Protocols to detect senescence-associated beta-galactosidase (SA-βgal) activity, a biomarker of senescent cells in culture and in vivo', *Nature Protocols*, 4(12), pp. 1798–1806. Available at: https://doi.org/10.1038/nprot.2009.191.

Delacroix, S. *et al.* (2007) 'The Rad9-Hus1-Rad1 (9-1-1) clamp activates checkpoint signaling via TopBP1', *Genes and Development*, 21(12), pp. 1472–1477. Available at: https://doi.org/10.1101/gad.1547007.

Della-Maria, J. *et al.* (2011) 'Human Mre11/human Rad50/Nbs1 and DNA ligase IIIα/XRCC1 protein complexes act together in an alternative nonhomologous end joining pathway', *Journal of Biological Chemistry*, 286(39), pp. 33845–33853. Available at: https://doi.org/10.1074/jbc.M111.274159.

Demidenko, Z.N. *et al.* (2009) 'Rapamycin decelerates cellular senescence', *Cell Cycle*, 8(12), pp. 1888–1895. Available at: https://doi.org/10.4161/cc.8.12.8606.

Demontis, F. and Perrimon, N. (2010) 'FOXO/4E-BP signaling in Drosophila muscles regulates organism-wide proteostasis during aging', *Cell*, 143(5), pp. 813–825. Available at: https://doi.org/10.1016/j.cell.2010.10.007.

Deng, X. *et al.* (2023) 'CRIP1 supports the growth and migration of AML-M5 subtype cells by activating Wnt/β-catenin pathway', *Leukemia Research*, 130, p. 107312. Available at: https://doi.org/10.1016/j.leukres.2023.107312.

Denoyelle, C. *et al.* (2006) 'Anti-oncogenic role of the endoplasmic reticulum differentially activated by mutations in the MAPK pathway', *Nature Cell Biology*, 8(10), pp. 1053–1063. Available at: https://doi.org/10.1038/ncb1471.

Depuydt, G. *et al.* (2016) 'Increased protein stability and decreased protein turnover in the caenorhabditis elegans ins/igf-1 daf-2 mutant', *Journals of Gerontology - Series A Biological Sciences and Medical Sciences*, 71(12), pp. 1553–1559. Available at: https://doi.org/10.1093/gerona/glv221.

Derisbourg, M.J., Hartman, M.D. and Denzel, M.S. (2021) 'Modulating the integrated stress response to slow aging and ameliorate age-related pathology', *Nature Aging*, 1(9), pp. 760–768. Available at: https://doi.org/10.1038/s43587-021-00112-9.

Dierick, J.F. *et al.* (2002) 'Stress-induced premature senescence and replicative senescence are different phenotypes, proteomic evidence', *Biochemical Pharmacology*, 64(5–6), pp. 1011–1017. Available at: https://doi.org/10.1016/S0006-2952(02)01171-1.

Dilworth, D. *et al.* (2018) 'The prolyl isomerase FKBP25 regulates microtubule polymerization impacting cell cycle progression and genomic stability', *Nucleic Acids Research*, 46(5), pp. 2459–2478. Available at: https://doi.org/10.1093/nar/gky008.

Dimri, G.P. *et al.* (1995) 'A biomarker that identifies senescent human cells in culture and in aging skin in vivo', *Proceedings of the National Academy of Sciences of the United States of America*, 92(20), pp. 9363–9367. Available at: https://doi.org/10.1073/pnas.92.20.9363.

Dong, H. *et al.* (2022) 'Pathophysiology of RAGE in inflammatory diseases', *Frontiers in Immunology*, 13(July), pp. 1–16. Available at: https://doi.org/10.3389/fimmu.2022.931473.

Dou, Z. *et al.* (2015) 'Autophagy mediates degradation of nuclear lamina', *Nature*, 527(7576), pp. 105–109. Available at: https://doi.org/10.1038/nature15548.

Dou, Z. *et al.* (2017) 'Cytoplasmic chromatin triggers inflammation in senescence and cancer', *Nature*, 550(7676), pp. 402–406. Available at: https://doi.org/10.1038/nature24050.

Douglas, G. *et al.* (2019) 'A key role for the novel coronary artery disease gene JCAD in atherosclerosis via shear stress mechanotransduction', *Cardiovascular Research* [Preprint]. Available at: https://doi.org/10.1093/cvr/cvz263.

Druelle, C. *et al.* (2016) 'ATF6a regulates morphological changes associated with senescence in human fibroblasts', *Oncotarget*, 7(42), pp. 67699–67715. Available at: https://doi.org/10.18632/oncotarget.11505.

Duca, L. *et al.* (2016) 'Matrix ageing and vascular impacts: Focus on elastin fragmentation', *Cardiovascular Research*, 110(3), pp. 298–308. Available at: https://doi.org/10.1093/cvr/cvw061.

Dutta, S. and Sengupta, P. (2016) 'Men and mice: Relating their ages', *Life Sciences*, 152, pp. 244–248. Available at: https://doi.org/10.1016/j.lfs.2015.10.025.

Dwyer, J. *et al.* (2015) 'The guanine exchange factor SWAP70 mediates vGPCR-induced endothelial plasticity', *Cell Communication and Signaling*, 13(1), pp. 1–7. Available at: https://doi.org/10.1186/s12964-015-0090-1.

Eden, E. *et al.* (2009) 'GOrilla: A tool for discovery and visualization of enriched GO terms in ranked gene lists', *BMC Bioinformatics*, 10, pp. 1–7. Available at: https://doi.org/10.1186/1471-2105-10-48.

Eden, E. *et al.* (2011) 'Proteome Half-Life Dynamics in Living Human Cells', *Science*, 331(6018), pp. 764–768. Available at: https://doi.org/10.1126/science.1199784.

Emini Veseli, B. *et al.* (2017) 'Animal models of atherosclerosis', *European Journal of Pharmacology*, 816(April), pp. 3–13. Available at: https://doi.org/10.1016/j.ejphar.2017.05.010.

Esashi, F. *et al.* (2005) 'CDK-dependent phosphorylation of BRCA2 as a regulatory mechanism for recombinational repair', *Nature*, 434(7033), pp. 598–604. Available at: https://doi.org/10.1038/nature03404.

Espinoza, S.E. *et al.* (2023) 'Drugs Targeting Mechanisms of Aging to Delay Age-Related Disease and Promote Healthspan: Proceedings of a National Institute on Aging Workshop', *The Journals of Gerontology: Series A*. Edited by D. Le Couteur, 78(Supplement_1), pp. 53–60. Available at: https://doi.org/10.1093/gerona/glad034.

Fatima, S. *et al.* (2022) 'ER-Stress and Senescence Coordinately Promote Endothelial Barrier Dysfunction in Diabetes-Induced Atherosclerosis', *Nutrients*, 14(14). Available at: https://doi.org/10.3390/nu14142786.

Feng, S. *et al.* (2016) 'Ewing tumor-associated antigen 1 interacts with replication protein A to promote restart of stalled replication forks', *Journal of Biological Chemistry*, 291(42), pp. 21956–21962. Available at: https://doi.org/10.1074/jbc.C116.747758.

Ference, B.A. *et al.* (2017) 'Low-density lipoproteins cause atherosclerotic cardiovascular disease. 1. Evidence from genetic, epidemiologic, and clinical studies. A consensus statement fromthe European Atherosclerosis Society Consensus Panel', *European Heart Journal*, 38(32), pp. 2459–2472. Available at: https://doi.org/10.1093/eurheartj/ehx144.

Ferrucci, L. and Fabbri, E. (2018) 'Inflammageing: chronic inflammation in ageing, cardiovascular disease, and frailty', *Nature Reviews Cardiology*, 15(9), pp. 505–522. Available at: https://doi.org/10.1038/s41569-018-0064-2.

Finch, W., Shamsa, K. and Lee, M.S. (2014) 'Cardiovascular complications of radiation exposure', *Reviews in Cardiovascular Medicine*, 15(3), pp. 232–244. Available at: https://doi.org/10.3909/ricm0689.

Fine, N.M. and Kushwaha, S.S. (2016) 'Recent Advances in Mammalian Target of Rapamycin Inhibitor Use in Heart and Lung Transplantation', *Transplantation*, 100(12), pp. 2558–2568. Available at: https://doi.org/10.1097/TP.0000000000001432.

Freund, A. *et al.* (2012) 'Lamin B1 loss is a senescence-associated biomarker', *Molecular Biology of the Cell*, 23(11), pp. 2066–2075. Available at: https://doi.org/10.1091/mbc.E11-10-0884.

Fujii, S. *et al.* (2012) 'Insufficient autophagy promotes bronchial epithelial cell senescence in chronic obstructive pulmonary disease', *OncoImmunology*, 1(5), pp. 630–641. Available at: https://doi.org/10.4161/onci.20297.

Fumagalli, M. *et al.* (2012) 'Telomeric DNA damage is irreparable and causes persistent DNA-damage-response activation', *Nature Cell Biology*, 14(4), pp. 355–365. Available at: https://doi.org/10.1038/ncb2466.

Gagliardi, D. and Dziembowski, A. (2018) '5' and 3' modifications controlling RNA degradation: from safeguards to executioners', *Philosophical Transactions of the Royal Society B: Biological Sciences*, 373(1762), p. 20180160. Available at: https://doi.org/10.1098/rstb.2018.0160.

Galbiati, A., Beauséjour, C. and d'Adda di Fagagna, F. (2017) 'A novel single-cell method provides direct evidence of persistent DNA damage in senescent cells and aged mammalian tissues', *Aging Cell*, 16(2), pp. 422–427. Available at: https://doi.org/10.1111/acel.12573.

Galkina, E. and Ley, K. (2007) 'Vascular adhesion molecules in atherosclerosis', *Arteriosclerosis, Thrombosis, and Vascular Biology*, 27(11), pp. 2292–2301. Available at: https://doi.org/10.1161/ATVBAHA.107.149179.

Galley, H.F. and Webster, N.R. (2004) 'Physiology of the endothelium', *British Journal of Anaesthesia*, 93(1), pp. 105–113. Available at: https://doi.org/10.1093/bja/aeh163.

Gary, R.K. and Kindell, S.M. (2005) 'Quantitative assay of senescence-associated β-galactosidase activity in mammalian cell extracts', *Analytical Biochemistry*, 343(2), pp. 329–334. Available at: https://doi.org/10.1016/j.ab.2005.06.003.

Ge, S.X. *et al.* (2020) 'ShinyGO: A graphical gene-set enrichment tool for animals and plants', *Bioinformatics*, 36(8), pp. 2628–2629. Available at: https://doi.org/10.1093/bioinformatics/btz931.

Geisel, D. *et al.* (2012) 'DNA double-strand breaks as potential indicators for the biological effects of ionising radiation exposure from cardiac CT and conventional coronary angiography: A randomised, controlled study', *European Radiology*, 22(8), pp. 1641–1650. Available at: https://doi.org/10.1007/s00330-012-2426-1.

Geiser, T. *et al.* (1993) 'The interleukin-8-related chemotactic cytokines GRO alpha, GRO beta, and GRO gamma activate human neutrophil and basophil leukocytes', *Journal of Biological Chemistry*, 268(21), pp. 15419–15424. Available at: https://doi.org/10.1016/s0021-9258(18)82274-8.

Gencer, S. *et al.* (2021) 'Inflammatory Chemokines in Atherosclerosis', *Cells*, 10(2), p. 226. Available at: https://doi.org/10.3390/cells10020226.

Georgakis, M.K. *et al.* (2021) 'Monocyte-Chemoattractant Protein-1 Levels in Human Atherosclerotic Lesions Associate with Plaque Vulnerability', *Arteriosclerosis,*

Thrombosis, and Vascular Biology, 41(6), pp. 2038–2048. Available at: https://doi.org/10.1161/ATVBAHA.121.316091.

Geserick, C*. et al.* (2006) 'Expression of mTert in primary murine cells links the growth-promoting effects of telomerase to transforming growth factor-β signaling', *Oncogene*, 25(31), pp. 4310–4319. Available at: https://doi.org/10.1038/sj.onc.1209465.

Getz, G.S. and Reardon, C.A. (2016) 'Do the Apoe −/− and Ldlr −/− Mice Yield the Same Insight on Atherogenesis?', *Arteriosclerosis, Thrombosis, and Vascular Biology*, 36(9), pp. 1734–1741. Available at: https://doi.org/10.1161/ATVBAHA.116.306874.

Gharavi, N.M. *et al.* (2007) 'Role of the JAK/STAT pathway in the regulation of interleukin-8 transcription by oxidized phospholipids in vitro and in atherosclerosis in vivo', *Journal of Biological Chemistry*, 282(43), pp. 31460–31468. Available at: https://doi.org/10.1074/jbc.M704267200.

Gimbrone, M.A. and García-Cardeña, G. (2016a) 'Endothelial Cell Dysfunction and the Pathobiology of Atherosclerosis', *Circulation Research*, 118(4), pp. 620–636. Available at: https://doi.org/10.1161/CIRCRESAHA.115.306301.

Gimbrone, M.A. and García-Cardeña, G. (2016b) 'Endothelial Cell Dysfunction and the Pathobiology of Atherosclerosis', *Circulation Research*, 118(4), pp. 620–636. Available at: https://doi.org/10.1161/CIRCRESAHA.115.306301.

Di Giorgio, E. *et al.* (2021) 'HDAC4 degradation during senescence unleashes an epigenetic program driven by AP-1/p300 at selected enhancers and super-enhancers',

Genome Biology, 22(1), pp. 1–25. Available at: https://doi.org/10.1186/s13059-021-02340-z.

Glück, S. *et al.* (2017) 'Innate immune sensing of cytosolic chromatin fragments through cGAS promotes senescence', 19(9). Available at: https://doi.org/10.1038/ncb3586.

Goldstein, J.L. and Brown, M.S. (1984) 'Progress in understanding the LDL receptor and HMG-CoA reductase, two membrane proteins that regulate the plasma cholesterol', *Journal of Lipid Research*, 25(13), pp. 1450–1461.

Gonçalves, R.C. *et al.* (2021) 'Strategies for re-vascularization and promotion of angiogenesis in trauma and disease', *Biomaterials*, 269(August 2020). Available at: https://doi.org/10.1016/j.biomaterials.2020.120628.

Goodarzi, A.A. *et al.* (2006) 'DNA-PK autophosphorylation facilitates Artemis endonuclease activity', *EMBO Journal*, 25(16), pp. 3880–3889. Available at: https://doi.org/10.1038/sj.emboj.7601255.

Gorgoulis, V. *et al.* (2019) 'Cellular Senescence: Defining a Path Forward', *Cell*, 179(4), pp. 813–827. Available at: https://doi.org/10.1016/j.cell.2019.10.005.

Graner, M.W., Lillehei, K.O. and Katsanis, E. (2015) 'Endoplasmic reticulum chaperones and their roles in the immunogenicity of cancer vaccines', *Frontiers in Oncology*, 4(January), pp. 1–12. Available at: https://doi.org/10.3389/fonc.2014.00379.

Gray, A., Petersen, S. and Rayner, M. (2006) 'Economic burden of cardiovascular diseases in the enlarged European Union', pp. 1610–1619. Available at: https://doi.org/10.1093/eurheartj/ehi733.

Green, D.E. and Rubin, C.T. (2014) 'Consequences of irradiation on bone and marrow phenotypes, and its relation to disruption of hematopoietic precursors', *Bone*, 63(631), pp. 87–94. Available at: https://doi.org/10.1016/j.bone.2014.02.018.

Griffith, J.D. *et al.* (1999) 'Mammalian telomeres end in a large duplex loop', *Cell*, 97(4), pp. 503–514. Available at: https://doi.org/10.1016/S0092-8674(00)80760-6.

Grishko, V.I. *et al.* (1999) 'Nitric oxide-induced damage to mtDNA and its subsequent repair', *Nucleic Acids Research*, 27(22), pp. 4510–4516. Available at: https://doi.org/10.1093/nar/27.22.4510.

Guo, Y. *et al.* (2008) 'How is mRNA expression predictive for protein expression? A correlation study on human circulating monocytes', *Acta Biochimica et Biophysica Sinica*, 40(5), pp. 426–436. Available at: https://doi.org/10.1111/j.1745-7270.2008.00418.x.

Gupta, S. *et al.* (1997) 'IFN-γ, potentiates atherosclerosis in ApoE knock-out mice', *Journal of Clinical Investigation*, 99(11), pp. 2752–2761. Available at: https://doi.org/10.1172/JCI119465.

Halcox, J.P.J. *et al.* (2002) 'Prognostic value of coronary vascular endothelial dysfunction', *Circulation*, 106(6), pp. 653–658. Available at: https://doi.org/10.1161/01.CIR.0000025404.78001.D8.

Hall, E. and Giacia, A. (2006) *Radiobiology for the Radiologist*. 6th edn. Philadelphia: Lippincott Williams & Wilkins.

Harris, S.L. and Levine, A.J. (2005) 'The p53 pathway: Positive and negative feedback loops', *Oncogene*, 24(17), pp. 2899–2908. Available at: https://doi.org/10.1038/sj.onc.1208615.

Harry, B.L. *et al.* (2008) 'Endothelial cell PECAM-1 promotes atherosclerotic lesions in areas of disturbed flow in ApoE-deficient mice', *Arteriosclerosis, Thrombosis, and Vascular Biology*, 28(11), pp. 2003–2008. Available at: https://doi.org/10.1161/ATVBAHA.108.164707.

Hayflick, L. (1965) 'The limited in vitro lifetime of human diploid cell strains', *Experimental Cell Research*, 37(3), pp. 614–636. Available at: https://doi.org/10.1016/0014-4827(65)90211-9.

Hayflick, L. and Moorhead, P.S. (1961) 'The serial cultivation of human diploid cell strains', *Experimental Cell Research*, 25(3), pp. 585–621. Available at: https://doi.org/10.1016/0014-4827(61)90192-6.

Heagerty, A.M. *et al.* (1993) 'Small artery structure in hypertension: Dual processes of remodeling and growth', *Hypertension*, 21(4), pp. 391–397. Available at: https://doi.org/10.1161/01.HYP.21.4.391.

Herbst, A. *et al.* (2007) 'Accumulation of Mitochondrial DNA Deletion Mutations in Aged Muscle Fibers: Evidence for a Causal Role in Muscle Fiber Loss', *The Journals of*

Gerontology Series A: Biological Sciences and Medical Sciences, 62(3), pp. 235–245. Available at: https://doi.org/10.1093/gerona/62.3.235.

Hernandez-Segura, A., Nehme, J. and Demaria, M. (2018) 'Hallmarks of Cellular Senescence', *Trends in Cell Biology*, 28(6), pp. 436–453. Available at: https://doi.org/10.1016/j.tcb.2018.02.001.

Herrmann, J. (2020) 'Adverse cardiac effects of cancer therapies: cardiotoxicity and arrhythmia', *Nature Reviews Cardiology*, 17(8), pp. 474–502. Available at: https://doi.org/10.1038/s41569-020-0348-1.

Hiebert, P. *et al.* (2018) 'Nrf2-Mediated Fibroblast Reprogramming Drives Cellular Senescence by Targeting the Matrisome', *Developmental Cell*, 46(2), pp. 145-161.e10. Available at: https://doi.org/10.1016/j.devcel.2018.06.012.

Hodgin, J.B. *et al.* (2002) 'Interactions between endothelial nitric oxide synthase and sex hormones in vascular protection in mice', *Journal of Clinical Investigation*, 109(4), pp. 541–548. Available at: https://doi.org/10.1172/JCI0214066.

Hofmann, J. and Sernetz, M. (1983) 'A kinetic study on the enzymatic hydrolysis of fluoresceindiacetate and fluorescein-di-β-d-galactopyranoside', *Analytical Biochemistry*, 131(1), pp. 180–186. Available at: https://doi.org/10.1016/0003-2697(83)90151-3.

Hollander, M.C. *et al.* (1993) 'Analysis of the mammalian gadd45 gene and its response to DNA damage', *Journal of Biological Chemistry*, 268(32), pp. 24385–24393. Available at: https://doi.org/10.1016/s0021-9258(20)80537-7.

Holmes, D.R. *et al.* (2002) 'Results of prevention of REStenosis with tranilast and its outcomes (PRESTO) trial', *Circulation*, 106(10), pp. 1243–1250. Available at: https://doi.org/10.1161/01.CIR.0000028335.31300.DA.

Horvath, S. *et al.* (2018) 'Epigenetic clock for skin and blood cells applied to Hutchinson Gilford Progeria Syndrome and ex vivo studies', *Aging*, 10(7), pp. 1758–1775. Available at: https://doi.org/10.18632/aging.101508.

Horvath, S. *et al.* (no date) 'Rapamycin retards epigenetic ageing of keratinocytes independently of its effects on replicative senescence, proliferation and differentiation'.

Houtkooper, R.H. *et al.* (2013) 'Mitonuclear protein imbalance as a conserved longevity mechanism', *Nature*, 497(7450), pp. 451–457. Available at: https://doi.org/10.1038/nature12188.

Hoving, S. *et al.* (2008) 'Single-Dose and Fractionated Irradiation Promote Initiation and Progression of Atherosclerosis and Induce an Inflammatory Plaque Phenotype in ApoE-/- Mice', *International Journal of Radiation Oncology Biology Physics*, 71(3), pp. 848–857. Available at: https://doi.org/10.1016/j.ijrobp.2008.02.031.

Hsu, C.H., Altschuler, S.J. and Wu, L.F. (2019) 'Patterns of Early p21 Dynamics Determine Proliferation-Senescence Cell Fate after Chemotherapy', *Cell*, 178(2), pp. 361-373.e12. Available at: https://doi.org/10.1016/j.cell.2019.05.041.

Hu, R. *et al.* (2022) 'Role of Proteostasis Regulation in the Turnover of Stress Granules', *International Journal of Molecular Sciences*, 23(23), pp. 1–12. Available at: https://doi.org/10.3390/ijms232314565.

Huang, R.X. and Zhou, P.K. (2020) 'DNA damage response signaling pathways and targets for radiotherapy sensitization in cancer', *Signal Transduction and Targeted Therapy*, 5(1). Available at: https://doi.org/10.1038/s41392-020-0150-x.

Huang, Y. *et al.* (2021) 'Senolytic Peptide FOXO4-DRI Selectively Removes Senescent Cells From in vitro Expanded Human Chondrocytes', *Frontiers in Bioengineering and Biotechnology*, 9(April), pp. 1–9. Available at: https://doi.org/10.3389/fbioe.2021.677576.

Huang, Y. *et al.* (2022) 'Biliverdin Reductase A Protects Lens Epithelial Cells against Oxidative Damage and Cellular Senescence in Age-Related Cataract', *Oxidative Medicine and Cellular Longevity*, 2022. Available at: https://doi.org/10.1155/2022/5628946.

Huber, S.A. *et al.* (1999) 'Interleukin-6 exacerbates early atherosclerosis in mice', *Arteriosclerosis, Thrombosis, and Vascular Biology*, 19(10), pp. 2364–2367. Available at: https://doi.org/10.1161/01.ATV.19.10.2364.

Huynh, J. *et al.* (2011) 'Age-Related Intimal Stiffening Enhances Endothelial Permeability and Leukocyte Transmigration', *Science Translational Medicine*, 3(112), pp. 1–7. Available at: https://doi.org/10.1126/scitranslmed.3002761.

Hwang, J. and Qi, L. (2018) 'Quality Control in the Endoplasmic Reticulum: Crosstalk between ERAD and UPR pathways', *Trends in Biochemical Sciences*, 43(8), pp. 593–605. Available at: https://doi.org/10.1016/j.tibs.2018.06.005.

IAEA (2010) *Radiation biology: A Handbook for Teachers and Students*. Vienna.

Iglesias-Bartolome, R. *et al.* (2012) 'MTOR inhibition prevents epithelial stem cell senescence and protects from radiation-induced mucositis', *Cell Stem Cell*, 11(3), pp. 401–414. Available at: https://doi.org/10.1016/j.stem.2012.06.007.

International Commission on Radiological Protection (ICRP) (2007) *The 2007 recommendations of the international commission on radiological protection*, *ICRP Publication 103, annals of ICRP 37*.

Ivanov, V.K. *et al.* (2000) 'Radiation-epidemiological analysis of incidence of non-cancer diseases among the chernobyl liquidators', *Health Physics*, 78(5), pp. 495–501. Available at: https://doi.org/10.1097/00004032-200005000-00005.

Izzo, C. *et al.* (2018) 'The impact of aging on cardio and cerebrovascular diseases', *International Journal of Molecular Sciences*. MDPI AG. Available at: https://doi.org/10.3390/ijms19020481.

Jacobs, J.J.L. and de Lange, T. (2004) 'Significant Role for p16INK4a in p53-Independent Telomere-Directed Senescence', *Current Biology*, 14(24), pp. 2302–2308. Available at: https://doi.org/10.1016/j.cub.2004.12.025.

Jiang, X. and Wang, J. (2019) 'Down-regulation of TFAM increases the sensitivity of tumour cells to radiation via p53/TIGAR signalling pathway', *Journal of Cellular and Molecular Medicine*, 23(7), pp. 4545–4558. Available at: https://doi.org/10.1111/jcmm.14350.

Jimi, S. *et al.* (1994) 'Low density lipoproteins bind more to type I and III collagens by negative charge-dependent mechanisms than to type IV and V collagens',

Atherosclerosis, 107(1), pp. 109–116. Available at: https://doi.org/10.1016/0021-9150(94)90146-5.

Jin, L. *et al.* (2010) 'The actin associated protein palladin is important for the early smooth muscle cell differentiation', *PLoS ONE*, 5(9), pp. 1–13. Available at: https://doi.org/10.1371/journal.pone.0012823.

Johnson, J. *et al.* (2005) 'Plaque rupture after short periods of fat feeding in the apolipoprotein E-knockout mouse: Model characterization and effects of pravastatin treatment', *Circulation*, 111(11), pp. 1422–1430. Available at: https://doi.org/10.1161/01.CIR.0000158435.98035.8D.

Jongstra-Bilen, J. *et al.* (2021) 'Role of myeloid-derived chemokine CCL5/RANTES at an early stage of atherosclerosis', *Journal of Molecular and Cellular Cardiology*, 156(March), pp. 69–78. Available at: https://doi.org/10.1016/j.yjmcc.2021.03.010.

Justice, J.N. *et al.* (2019) 'Senolytics in idiopathic pulmonary fibrosis: Results from a first-in-human, open-label, pilot study', *EBioMedicine*, 40, pp. 554–563. Available at: https://doi.org/10.1016/j.ebiom.2018.12.052.

Kabacik, S. *et al.* (2022a) 'The relationship between epigenetic age and the hallmarks of ageing in human cells', *Nature Aging*, 2(6), pp. 484–493. Available at: https://doi.org/10.1038/s43587-022-00220-0.

Kabacik, S. *et al.* (2022b) 'The relationship between epigenetic age and the hallmarks of ageing in human cells', *Nature Aging*, 2(6), pp. 484–493. Available at: https://doi.org/10.1038/s43587-022-00220-0.

Kabacik, S. and Raj, K. (2017) *Ionising radiation increases permeability of endothelium through ADAM10-mediated cleavage of VE-cadherin*, *Oncotarget*. Available at: https://doi.org/10.18632/oncotarget.18282.

Kandhaya-Pillai, R. *et al.* (2017) 'TNFα-senescence initiates a STAT-dependent positive feedback loop, leading to a sustained interferon signature, DNA damage, and cytokine secretion', *Aging*, 9(11), pp. 2411–2435. Available at: https://doi.org/10.18632/aging.101328.

Kandhaya-Pillai, R. *et al.* (2023) 'Key elements of cellular senescence involve transcriptional repression of mitotic and DNA repair genes through the p53-p16/RB-E2F-DREAM complex', *Aging*, 15(10), pp. 4012–4034. Available at: https://doi.org/10.18632/aging.204743.

Kastan, M. and Bakkenist, C. (2003) 'DNA damage activates ATM through intermolecular autophosphorylation and dimmer association', *Nature*, 421, pp. 499–506.

Kiang, J.G. and Olabisi, A.O. (2019) 'Radiation: A poly-traumatic hit leading to multi-organ injury', *Cell and Bioscience*, 9(1), pp. 1–15. Available at: https://doi.org/10.1186/s13578-019-0286-y.

Kim, H. *et al.* (2022) 'Attenuation of intrinsic ageing of the skin via elimination of senescent dermal fibroblasts with senolytic drugs', *Journal of the European Academy of Dermatology and Venereology*, 36(7), pp. 1125–1135. Available at: https://doi.org/10.1111/jdv.18051.

Kim, J. *et al.* (2011) 'AMPK and mTOR regulate autophagy through direct phosphorylation of Ulk1', *Nature Cell Biology*, 13(2), pp. 132–141. Available at: https://doi.org/10.1038/ncb2152.

Kirk, E.A. *et al.* (2000) 'Impaired superoxide production due to a deficiency in phagocyte NADPH oxidase fails to inhibit atherosclerosis in mice', *Arteriosclerosis, Thrombosis, and Vascular Biology*, 20(6), pp. 1529–1535. Available at: https://doi.org/10.1161/01.ATV.20.6.1529.

Kirkland, J.L. and Tchkonia, T. (2017) 'Cellular Senescence: A Translational Perspective', *EBioMedicine*, 21, pp. 21–28. Available at: https://doi.org/10.1016/j.ebiom.2017.04.013.

Kiss, T. *et al.* (2020) 'Single-cell RNA sequencing identifies senescent cerebromicrovascular endothelial cells in the aged mouse brain', *GeroScience*, 42(2), pp. 429–444. Available at: https://doi.org/10.1007/s11357-020-00177-1.

Kojima, H. *et al.* (2012) 'The STAT3-IGFBP5 axis is critical for IL-6/gp130-induced premature senescence in human fibroblasts', *Cell Cycle*, 11(4), pp. 730–739. Available at: https://doi.org/10.4161/cc.11.4.19172.

Kojima, H. *et al.* (2013) 'IL-6-STAT3 signaling and premature senescence', *Jak-Stat*, 2(4), p. e25763. Available at: https://doi.org/10.4161/jkst.25763.

Kolodgie, F.D. *et al.* (2003) 'Intraplaque Hemorrhage and Progression of Coronary Atheroma', *New England Journal of Medicine*, 349(24), pp. 2316–2325. Available at: https://doi.org/10.1056/NEJMoa035655.

von Koschembahr, A. *et al.* (2020) 'Metabolism and genotoxicity of polycyclic aromatic hydrocarbons in human skin explants: mixture effects and modulation by sunlight', *Archives of Toxicology*, 94(2), pp. 495–507. Available at: https://doi.org/10.1007/s00204-019-02650-z.

Kou, Y. *et al.* (2023) 'Eldecalcitol prevented OVX-induced osteoporosis through inhibiting BMSCs senescence by regulating the SIRT1-Nrf2 signal', *Frontiers in Pharmacology*, 14(March), pp. 1–12. Available at: https://doi.org/10.3389/fphar.2023.1067085.

Kourtis, N. and Tavernarakis, N. (2009) 'Autophagy and cell death in model organisms', *Cell Death and Differentiation*, 16(1), pp. 21–30. Available at: https://doi.org/10.1038/cdd.2008.120.

Kowalski, J. *et al.* (2013) 'Senescent cells harbour features of the cancer epigenome', *Nature cell biology*, 50(4), pp. 381–389. Available at: https://doi.org/10.1038/ncb2879.Senescent.

Kraig, E. *et al.* (2018) 'A randomized control trial to establish the feasibility and safety of rapamycin treatment in an older human cohort: Immunological, physical performance, and cognitive effects', *Experimental Gerontology*, 105(3), pp. 53–69. Available at: https://doi.org/10.1016/j.exger.2017.12.026.

Krauth, M.T. *et al.* (2006) 'Effects of various statins on cytokine-dependent growth and IgE-dependent release of histamine in human mast cells', *Allergy: European Journal of*

Allergy and Clinical Immunology, 61(3), pp. 281–288. Available at: https://doi.org/10.1111/j.1398-9995.2006.00997.x.

Krouwer, V.J.D. *et al.* (2012a) 'Endothelial cell senescence is associated with disrupted cell-cell junctions and increased monolayer permeability', *Vascular Cell*, 4, pp. 1–10. Available at: https://doi.org/10.1186/2045-824X-4-12.

Krouwer, V.J.D. *et al.* (2012b) 'Endothelial cell senescence is associated with disrupted cell-cell junctions and increased monolayer permeability', *Vascular Cell*, 4, pp. 1–10. Available at: https://doi.org/10.1186/2045-824X-4-12.

Kuhfittig-Kulle, S. *et al.* (2007) 'The mutagenic potential of non-homologous end joining in the absence of the NHEJ core factors Ku70/80, DNA-PKcs and XRCC4-LigIV', *Mutagenesis*, 22(3), pp. 217–233. Available at: https://doi.org/10.1093/mutage/gem007.

Kujoth, G.C. *et al.* (2005) 'Mitochondrial DNA Mutations, Oxidative Stress, and Apoptosis in Mammalian Aging', *Science*, 309(5733), pp. 481–484. Available at: https://doi.org/10.1126/science.1112125.

Kurz, D.J. *et al.* (2000) 'Senescence-associated β-galactosidase reflects an increase in lysosomal mass during replicative ageing of human endothelial cells', *Journal of Cell Science*, 113(20), pp. 3613–3622. Available at: https://doi.org/10.1242/jcs.113.20.3613.

Kwon, G.P. *et al.* (2008) 'Contribution of Macromolecular Structure to the Retention of Low-Density Lipoprotein at Arterial Branch Points', (Ldl), pp. 2919–2927. Available at: https://doi.org/10.1161/CIRCULATIONAHA.107.754614.

Lakota, K. *et al.* (2007a) 'Serum amyloid A activation of inflammatory and adhesion molecules in human coronary artery and umbilical vein endothelial cells', *European Journal of Inflammation*, 5(2), pp. 73–81. Available at: https://doi.org/10.1177/1721727X0700500203.

Lakota, K. *et al.* (2007b) 'Serum amyloid A activation of inflammatory and adhesion molecules in human coronary artery and umbilical vein endothelial cells', *European Journal of Inflammation*, 5(2), pp. 73–81. Available at: https://doi.org/10.1177/1721727X0700500203.

Lanningham-Foster, L. *et al.* (2002) 'Overexpression of CRIP in transgenic mice alters cytokine patterns and the immune response', *American Journal of Physiology - Endocrinology and Metabolism*, 282(6 45-6), pp. 1197–1203. Available at: https://doi.org/10.1152/ajpendo.00508.2001.

Lanz, M.C. *et al.* (2022a) 'Increasing cell size remodels the proteome and promotes senescence', *Molecular Cell*, 82(17), pp. 3255-3269.e8. Available at: https://doi.org/10.1016/j.molcel.2022.07.017.

Lanz, M.C. *et al.* (2022b) 'Increasing cell size remodels the proteome and promotes senescence', *Molecular Cell*, 82(17), pp. 3255-3269.e8. Available at: https://doi.org/10.1016/j.molcel.2022.07.017.

Lashgari, A. *et al.* (2018) 'Cellular Depletion of BRD8 Causes p53-Dependent Apoptosis and Induces a DNA Damage Response in Non-Stressed Cells', *Scientific Reports*, 8(1), pp. 1–12. Available at: https://doi.org/10.1038/s41598-018-32323-3.

Lee, B.Y. *et al.* (2006) 'Senescence-associated β-galactosidase is lysosomal β-galactosidase', *Aging Cell*, 5(2), pp. 187–195. Available at: https://doi.org/10.1111/j.1474-9726.2006.00199.x.

Lee, H. *et al.* (2010) 'Targeted Expression of Catalase to Mitochondria Prevents Age-Associated Reductions in Mitochondrial Function and Insulin Resistance', *Cell Metabolism*, 12(6), pp. 668–674. Available at: https://doi.org/10.1016/j.cmet.2010.11.004.

Lee, J.H. *et al.* (2010) '53BP1 promotes ATM activity through direct interactions with the MRN complex', *EMBO Journal*, 29(3), pp. 574–585. Available at: https://doi.org/10.1038/emboj.2009.372.

Lee, S. *et al.* (2021) 'Virus-induced senescence is a driver and therapeutic target in COVID-19', *Nature*, 599(7884), pp. 283–289. Available at: https://doi.org/10.1038/s41586-021-03995-1.

Lee, Y. *et al.* (2022) 'Histone deacetylase 4 reverses cellular senescence via DDIT4 in dermal fibroblasts', *Aging*, 14(11), pp. 4653–4672. Available at: https://doi.org/10.18632/aging.204118.

Lehmann, B.D. *et al.* (2007) 'A dominant role for p53-dependent cellular senescence in radiosensitization of human prostate cancer cells', *Cell Cycle*, 6(5), pp. 595–605. Available at: https://doi.org/10.4161/cc.6.5.3901.

Lengefeld, J. *et al.* (2021) 'Cell size is a determinant of stem cell potential during aging', *Science Advances*, 7(46), pp. 1–17. Available at: https://doi.org/10.1126/sciadv.abk0271.

Leontieva, O. V. *et al.* (2012) 'Hypoxia suppresses conversion from proliferative arrest to cellular senescence', *Proceedings of the National Academy of Sciences of the United States of America*, 109(33), pp. 13314–13318. Available at: https://doi.org/10.1073/pnas.1205690109.

Leontieva, O. V. and Blagosklonny, M. V. (2016) 'Gerosuppression by pan-mTOR inhibitors', *Aging*, 8(12), pp. 3535–3551. Available at: https://doi.org/10.18632/aging.101155.

Leung-Pineda, V., Ryan, C.E. and Piwnica-Worms, H. (2006) 'Phosphorylation of Chk1 by ATR Is Antagonized by a Chk1-Regulated Protein Phosphatase 2A Circuit', *Molecular and Cellular Biology*, 26(20), pp. 7529–7538. Available at: https://doi.org/10.1128/mcb.00447-06.

Levi, N. *et al.* (2020) 'The ECM path of senescence in aging: components and modifiers', *FEBS Journal*, 287(13), pp. 2636–2646. Available at: https://doi.org/10.1111/febs.15282.

Levick, J. (2003) 'Blood vessel structure', in *Cardiovascular Physiology*, p. 9.

Levin, W.P. *et al.* (2005) 'Proton beam therapy', *British Journal of Cancer*, 93(8), pp. 849–854. Available at: https://doi.org/10.1038/sj.bjc.6602754.

Levy, M.Z. *et al.* (1992) 'Telomere end-replication problem and cell aging', *Journal of Molecular Biology*, 225(4), pp. 951–960. Available at: https://doi.org/10.1016/0022-2836(92)90096-3.

Li, R. *et al.* (2012) 'Interleukin-7 induces recruitment of monocytes/macrophages to endothelium', *European Heart Journal*, 33(24), pp. 3114–3123. Available at: https://doi.org/10.1093/eurheartj/ehr245.

Libby, P. and Theroux, P. (2005) 'Pathophysiology of coronary artery disease', *Circulation*, 111(25), pp. 3481–3488. Available at: https://doi.org/10.1161/CIRCULATIONAHA.105.537878.

Liebert, M.A. *et al.* (2006) 'Kinase Signaling Pathways', 8.

Limbad, C. *et al.* (2022) 'Senolysis induced by 25-hydroxycholesterol targets CRYAB in multiple cell types', *iScience*, 25(2), p. 103848. Available at: https://doi.org/10.1016/j.isci.2022.103848.

Lin, A.W. *et al.* (1998) 'Premature senescence involving p53 and p16 is activated in response to constitutive MEK/MAPK mitogenic signaling', *Genes and Development*, 12(19), pp. 3008–3019. Available at: https://doi.org/10.1101/gad.12.19.3008.

Lippi, G. *et al.* (2007) 'Multiple biomarkers for the prediction of first major cardiovascular events and death: Considerable costs and limited benefits', *MedGenMed Medscape General Medicine*, 9(1), pp. 2631–2639.

Little, M.P. *et al.* (2012a) 'Systematic Review and Meta-analysis of Circula tory Disease from Exposure to Low-Level Ionizing Radia tion and Estimates of Potential Popula tion Mortality Risks Mark', *Environmental Health Perspectives*, 120(11), pp. 1503–1511.

Little, M.P. *et al.* (2012b) 'Systematic Review and Meta-analysis of Circula tory Disease from Exposure to Low-Level Ionizing Radia tion and Estimates of Potential Popula tion Mortality Risks Mark', *Environmental Health Perspectives*, 120(11), pp. 1503–1511.

Little, M.P. *et al.* (2012c) 'Systematic Review and Meta-analysis of Circulatory Disease from Exposure to Low-Level Ionizing Radiation and Estimates of Potential Population Mortality Risks', *Environmental Health Perspectives*, 120(11), pp. 1503–1511. Available at: https://doi.org/10.1289/ehp.1204982.

Little, M.P. *et al.* (2012d) 'Systematic Review and Meta-analysis of Circulatory Disease from Exposure to Low-Level Ionizing Radiation and Estimates of Potential Population Mortality Risks', *Environmental Health Perspectives*, 120(11), pp. 1503–1511. Available at: https://doi.org/10.1289/ehp.1204982.

Little, M.P. *et al.* (2023) 'Ionising radiation and cardiovascular disease: systematic review and meta-analysis', *Bmj*, pp. 1–16. Available at: https://doi.org/10.1136/bmj-2022-072924.

Liu, J. *et al.* (2015) 'Impact of ER stress-regulated ATF4/p16 signaling on the premature senescence of renal tubular epithelial cells in diabetic nephropathy', *American Journal of Physiology-Cell Physiology*, 308(8), pp. C621–C630. Available at: https://doi.org/10.1152/ajpcell.00096.2014.

Liu, T. *et al.* (2017) 'NF-κB signaling in inflammation', *Signal Transduction and Targeted Therapy*, 2(March). Available at: https://doi.org/10.1038/sigtrans.2017.23.

López-Otín, C. *et al.* (2013) 'The hallmarks of aging', *Cell*, 153(6), p. 1194. Available at: https://doi.org/10.1016/j.cell.2013.05.039.

Lowe, D. and Raj, K. (2014) 'Premature aging induced by radiation exhibits pro-atherosclerotic effects mediated by epigenetic activation of CD44 expression', *Aging Cell*, 13(5), pp. 900–910. Available at: https://doi.org/10.1111/acel.12253.

Lowe, D.J. and Raj, K. (2015) 'Quantitation of endothelial cell adhesiveness in vitro', *Journal of Visualized Experiments*, 2015(100). Available at: https://doi.org/10.3791/52924.

Lu, A.T. *et al.* (2019) 'DNA methylation GrimAge strongly predicts lifespan and healthspan', *Aging*, 11(2), pp. 303–327. Available at: https://doi.org/10.18632/aging.101684.

Lupatov, A.Yu. and Yarygin, K.N. (2022) 'Telomeres and Telomerase in the Control of Stem Cells', *Biomedicines*, 10(10), p. 2335. Available at: https://doi.org/10.3390/biomedicines10102335.

Lupu, F. *et al.* (1995) 'Plasminogen Activator Expression in Human Atherosclerotic Lesions', *Arteriosclerosis, Thrombosis, and Vascular Biology*, 15(9), pp. 1444–1455. Available at: https://doi.org/10.1161/01.ATV.15.9.1444.

Lusis, A.J. (2000) 'Atherosclerosis', *Nature*, 407(6801), pp. 233–241. Available at: https://doi.org/10.1038/35025203.

Maddika, S. *et al.* (2008) 'Akt-mediated phosphorylation of CDK2 regulates its dual role in cell cycle progression and apoptosis', *Journal of Cell Science*, 121(7), pp. 979–988. Available at: https://doi.org/10.1242/jcs.009530.

Mai, S. *et al.* (2019) 'Age-related dysfunction of the autophago-lysosomal pathway in human endothelial cells', *Pflugers Archiv European Journal of Physiology*, 471(8), pp. 1065–1078. Available at: https://doi.org/10.1007/s00424-019-02288-x.

Maier, T., Güell, M. and Serrano, L. (2009) 'Correlation of mRNA and protein in complex biological samples', *FEBS Letters*, 583(24), pp. 3966–3973. Available at: https://doi.org/10.1016/j.febslet.2009.10.036.

Malkova, A. *et al.* (2021) 'Genotoxic effect of simultaneous therapeutic exposure to polycyclic aromatic hydrocarbons and UV radiation', *Journal of Applied Toxicology*, 41(6), pp. 907–914. Available at: https://doi.org/10.1002/jat.4074.

Man, J.J., Beckman, J.A. and Jaffe, I.Z. (2020) 'Sex as a Biological Variable in Atherosclerosis', *Circulation Research*, 126(9), pp. 1297–1319. Available at: https://doi.org/10.1161/CIRCRESAHA.120.315930.

Mancuso, M. *et al.* (2015a) 'Acceleration of atherogenesis in ApoE-/- mice exposed to acute or low-dose-rate ionizing radiation', *Oncotarget*, 6(31), pp. 31263–31271. Available at: https://doi.org/10.18632/oncotarget.5075.

Mancuso, M. *et al.* (2015b) 'Acceleration of atherogenesis in ApoE-/- mice exposed to acute or low-dose-rate ionizing radiation', *Oncotarget*, 6(31), pp. 31263–31271. Available at: https://doi.org/10.18632/oncotarget.5075.

Mansukhani, N.A. *et al.* (2017a) 'Sex differences in the LDL receptor knockout mouse model of atherosclerosis', *Artery Research*, 20(C), p. 8. Available at: https://doi.org/10.1016/j.artres.2017.08.002.

Mansukhani, N.A. *et al.* (2017b) 'Sex differences in the LDL receptor knockout mouse model of atherosclerosis', *Artery Research*, 20(C), p. 8. Available at: https://doi.org/10.1016/j.artres.2017.08.002.

Marcos-Jubilar, M. *et al.* (2021) 'Association of sdf1 and mmp12 with atherosclerosis and inflammation: Clinical and experimental study', *Life*, 11(5), pp. 1–14. Available at: https://doi.org/10.3390/life11050414.

Matsumoto, T. *et al.* (2016) 'Overexpression of cytotoxic T-lymphocyte-associated antigen-4 prevents atherosclerosis in mice', *Arteriosclerosis, Thrombosis, and Vascular Biology*, 36(6), pp. 1141–1151. Available at: https://doi.org/10.1161/ATVBAHA.115.306848.

Maxwell, M.M. *et al.* (2011) 'The Sirtuin 2 microtubule deacetylase is an abundant neuronal protein that accumulates in the aging CNS', *Human Molecular Genetics*, 20(20), pp. 3986–3996. Available at: https://doi.org/10.1093/hmg/ddr326.

Mazzone, A. *et al.* (1993) 'Increased expression of neutrophil and monocyte adhesion molecules in unstable coronary artery disease', *Circulation*, 88(2), pp. 358–363. Available at: https://doi.org/10.1161/01.CIR.88.2.358.

Mazzucchelli, G.D. *et al.* (2008) 'Proteome alteration induced by hTERT transfection of human fibroblast cells', *Proteome Science*, 6(1), p. 12. Available at: https://doi.org/10.1186/1477-5956-6-12.

McConnell, B.B. *et al.* (1998) 'Inhibitors of cyclin-dependent kinases induce features of replicative senescence in early passage human diploid fibroblasts', *Current Biology*, 8(6), pp. 351–354. Available at: https://doi.org/10.1016/S0960-9822(98)70137-X.

McNamara, J.J. (1971) 'Coronary Artery Disease in Combat Casualties in Vietnam', *JAMA: The Journal of the American Medical Association*, 216(7), p. 1185. Available at: https://doi.org/10.1001/jama.1971.03180330061012.

Melick, C.H., Meng, D. and Jewell, J.L. (2020) 'A-kinase anchoring protein 8L interacts with mTORC1 and promotes cell growth', *Journal of Biological Chemistry*, 295(23), pp. 8096–8105. Available at: https://doi.org/10.1074/JBC.AC120.012595.

Mendiratta, G. *et al.* (2021) 'Cancer gene mutation frequencies for the U.S. population', *Nature Communications*, 12(1), pp. 1–11. Available at: https://doi.org/10.1038/s41467-021-26213-y.

Messner, B. and Bernhard, D. (2014) 'Smoking and cardiovascular disease: Mechanisms of endothelial dysfunction and early atherogenesis', *Arteriosclerosis, Thrombosis, and Vascular Biology*, 34(3), pp. 509–515. Available at: https://doi.org/10.1161/ATVBAHA.113.300156.

Michaloglou, C. *et al.* (2005) 'BRAFE600-associated senescence-like cell cycle arrest of human naevi', *Nature*, 436(7051), pp. 720–724. Available at: https://doi.org/10.1038/nature03890.

Miller, M.J. *et al.* (2023) 'The transcription regulator ATF4 is a mediator of skeletal muscle aging', *GeroScience*, pp. 2525–2543. Available at: https://doi.org/10.1007/s11357-023-00772-y.

Miller, R.A. *et al.* (2014) 'Rapamycin-mediated lifespan increase in mice is dose and sex dependent and metabolically distinct from dietary restriction', *Aging Cell*, 13(3), pp. 468–477. Available at: https://doi.org/10.1111/acel.12194.

Miller, S.B. *et al.* (2015) 'Compartment-specific aggregases direct distinct nuclear and cytoplasmic aggregate deposition', *The EMBO Journal*, 34(6), pp. 778–797. Available at: https://doi.org/10.15252/embj.201489524.

Minamino, T. *et al.* (2002a) 'Endothelial cell senescence in human atherosclerosis: Role of telomere in endothelial dysfunction', *Circulation*, 105(13), pp. 1541–1544. Available at: https://doi.org/10.1161/01.CIR.0000013836.85741.17.

Minamino, T. *et al.* (2002b) 'Endothelial cell senescence in human atherosclerosis: Role of telomere in endothelial dysfunction', *Circulation*, 105(13), pp. 1541–1544. Available at: https://doi.org/10.1161/01.CIR.0000013836.85741.17.

Mitchell, J.D. *et al.* (2021) 'Cardiovascular Manifestations From Therapeutic Radiation: A Multidisciplinary Expert Consensus Statement From the International Cardio-Oncology Society', *JACC: CardioOncology*, 3(3), pp. 360–380. Available at: https://doi.org/10.1016/j.jaccao.2021.06.003.

Mitra, S. *et al.* (2021) 'Uchl1, a deubiquitinating enzyme, regulates lung endothelial cell permeability in vitro and in vivo', *American Journal of Physiology - Lung Cellular and Molecular Physiology*, 320(4), pp. L497–L507. Available at: https://doi.org/10.1152/AJPLUNG.00492.2020.

Mitra, S. *et al.* (2023) 'Targeting Estrogen Signaling in the Radiation-induced Neurodegeneration: A Possible Role of Phytoestrogens', *Current Neuropharmacology*, 21(2), pp. 353–379. Available at: https://doi.org/10.2174/1570159X20666220310115004.

Miwa, S. *et al.* (2022) 'Mitochondrial dysfunction in cell senescence and aging', *Journal of Clinical Investigation*, 132(13). Available at: https://doi.org/10.1172/JCI158447.

Moaddel, R. *et al.* (2022) 'Identification of gingerenone A as a novel senolytic compound.', *PloS one*, 17(3), p. e0266135. Available at: https://doi.org/10.1371/journal.pone.0266135.

Moiseeva, O. *et al.* (2009) 'Mitochondrial Dysfunction Contributes to Oncogene-Induced Senescence', *Molecular and Cellular Biology*, 29(16), pp. 4495–4507. Available at: https://doi.org/10.1128/mcb.01868-08.

Moore, J.C. *et al.* (2002) 'Cyclin D and cdk4 Are Required for Normal Development beyond the Blastula Stage in Sea Urchin Embryos', *Molecular and Cellular Biology*, 22(13), pp. 4863–4875. Available at: https://doi.org/10.1128/mcb.22.13.4863-4875.2002.

Mordes, D.A. *et al.* (2008) 'TopBP1 activates ATR through ATRIP and a PIKK regulatory domain', *Genes and Development*, 22(11), pp. 1478–1489. Available at: https://doi.org/10.1101/gad.1666208.

Moses, J.W. *et al.* (2003) 'Sirolimus-Eluting Stents versus Standard Stents in Patients with Stenosis in a Native Coronary Artery', *New England Journal of Medicine*, 349(14), pp. 1315–1323. Available at: https://doi.org/10.1056/NEJMoa035071.

Moujaber, O. *et al.* (2019) 'Cellular senescence is associated with reorganization of the microtubule cytoskeleton', *Cellular and Molecular Life Sciences*, 76(6), pp. 1169–1183. Available at: https://doi.org/10.1007/s00018-018-2999-1.

Mun, G.I. and Boo, Y.C. (2010) 'Identification of CD44 as a senescence-induced cell adhesion gene responsible for the enhanced monocyte recruitment to senescent endothelial cells', *American Journal of Physiology - Heart and Circulatory Physiology*, 298(6), pp. 2102–2111. Available at: https://doi.org/10.1152/ajpheart.00835.2009.

Mundi, S. *et al.* (2018) 'Endothelial permeability, LDL deposition, and cardiovascular risk factors—a review', *Cardiovascular Research*, 114(1), pp. 35–52. Available at: https://doi.org/10.1093/cvr/cvx226.

Murphy, K. and Weaver, C. (2016) 'Janeway's Immunobiology', in *Janeway's Immunobiology*. 9th edn. New York, New York: Garland Science, pp. 2–9.

Murshed, H. (2019) 'Radiation Biology', in *Fundamentals of Radiation Oncology*. Elsevier, pp. 57–87. Available at: https://doi.org/10.1016/B978-0-12-814128-1.00003-9.

Mykkänen, O.M. *et al.* (2001) 'Characterization of human palladin, a microfilament-associated protein', *Molecular Biology of the Cell*, 12(10), pp. 3060–3073. Available at: https://doi.org/10.1091/mbc.12.10.3060.

Nacarelli, T. and Sell, C. (2017) 'Targeting metabolism in cellular senescence, a role for intervention', *Molecular and Cellular Endocrinology*, 455, pp. 83–92. Available at: https://doi.org/10.1016/j.mce.2016.08.049.

Nakano-Kurimoto, R. *et al.* (2009) 'Replicative senescence of vascular smooth muscle cells enhances the calcification through initiating the osteoblastic transition', *American Journal of Physiology - Heart and Circulatory Physiology*, 297(5). Available at: https://doi.org/10.1152/ajpheart.00455.2009.

Napoli, C. *et al.* (1997) 'Fatty streak formation occurs in human fetal aortas and is greatly enhanced maternal, hypercholesterolemia. Intimal accumulation of low density lipoprotein and its oxidation precede monocyte recruitment into early atheroeclerotic

lesions', *Journal of Clinical Investigation*, 100(11), pp. 2680–2690. Available at: https://doi.org/10.1172/JCI119813.

Narita, Masashi *et al.* (2003) 'Rb-mediated heterochromatin formation and silencing of E2F target genes during cellular senescence', *Cell*, 113(6), pp. 703–716. Available at: https://doi.org/10.1016/S0092-8674(03)00401-X.

Nassrally, M.S. *et al.* (2019) 'Cell cycle arrest in replicative senescence is not an immediate consequence of telomere dysfunction', *Mechanisms of Ageing and Development*, 179(December 2018), pp. 11–22. Available at: https://doi.org/10.1016/j.mad.2019.01.009.

Nelson, G. *et al.* (2012) 'A senescent cell bystander effect: Senescence-induced senescence', *Aging Cell*, 11(2), pp. 345–349. Available at: https://doi.org/10.1111/j.1474-9726.2012.00795.x.

Niazi, A. and Niazi, S. (2011) 'Endocrine effects of Fukushima: Radiation-induced endocrinopathy', *Indian Journal of Endocrinology and Metabolism*, 15(2), p. 91. Available at: https://doi.org/10.4103/2230-8210.81936.

Nidadavolu, L.S. and Walston, J.D. (2021) 'Underlying vulnerabilities to the cytokine storm and adverse covid-19 outcomes in the aging immune system', *Journals of Gerontology - Series A Biological Sciences and Medical Sciences*, 76(3), pp. E13–E18. Available at: https://doi.org/10.1093/gerona/glaa209.

Nieuwkoop, T. *et al.* (2023) 'Revealing determinants of translation efficiency via whole-gene codon randomization and machine learning', *Nucleic Acids Research*, 51(5), pp. 2363–2376. Available at: https://doi.org/10.1093/nar/gkad035.

Nikitina, T. and Woodcock, C.L. (2004) 'Closed chromatin loops at the ends of chromosomes', *Journal of Cell Biology*, 166(2), pp. 161–165. Available at: https://doi.org/10.1083/jcb.200403118.

Nimonkar, A. V. *et al.* (2011) 'BLM-DNA2-RPA-MRN and EXO1-BLM-RPA-MRN constitute two DNA end resection machineries for human DNA break repair', *Genes and Development*, 25(4), pp. 350–362. Available at: https://doi.org/10.1101/gad.2003811.

Noonan, A.J. *et al.* (2019) 'A novel triple-cell two-dimensional model to study immune vascular interplay in atherosclerosis', *Frontiers in Immunology*, 10(APR). Available at: https://doi.org/10.3389/fimmu.2019.00849.

Nübel, T. *et al.* (2004) 'Lovastatin inhibits Rho-regulated expression of E-selectin by TNFalpha and attenuates tumor cell adhesion.', *The FASEB journal : official publication of the Federation of American Societies for Experimental Biology*, 18(1), pp. 140–142. Available at: https://doi.org/10.1096/fj.03-0261fje.

Ogrodnik, M. *et al.* (2017) 'Cellular senescence drives age-dependent hepatic steatosis', *Nature Communications*, 8. Available at: https://doi.org/10.1038/ncomms15691.

Ohtani, N. *et al.* (2004) 'The p16INK4a-RB pathway: Molecular link between cellular senescence and tumor suppression', *Journal of Medical Investigation*, 51(3–4), pp. 146–153. Available at: https://doi.org/10.2152/jmi.51.146.

OKUDA, K. (2002) 'Telomere Length in the Newborn', *Pediatric Research*, 52(3), pp. 377–381. Available at: https://doi.org/10.1203/01.pdr.0000022341.72856.72.

O'Sullivan, F. *et al.* (2017) 'Parallel mRNA, proteomics and miRNA expression analysis in cell line models of the intestine', *World Journal of Gastroenterology*, 23(41), pp. 7369–7386. Available at: https://doi.org/10.3748/wjg.v23.i41.7369.

Özcan, S. *et al.* (2016) 'Unbiased analysis of senescence associated secretory phenotype (SASP) to identify common components following different genotoxic stresses', *Aging*, 8(7), pp. 1316–1329. Available at: https://doi.org/10.18632/aging.100971.

Paigen, B. *et al.* (1985) 'Variation in susceptibility to atherosclerosis among inbred strains of mice', *Atherosclerosis*, 57(1), pp. 65–73. Available at: https://doi.org/10.1016/0021-9150(85)90138-8.

Palasubramaniam, J., Wang, X. and Peter, K. (2019) 'Myocardial Infarction - From Atherosclerosis to Thrombosis: Uncovering New Diagnostic and Therapeutic Approaches', *Arteriosclerosis, Thrombosis, and Vascular Biology*, 39(8), pp. E176–E185. Available at: https://doi.org/10.1161/ATVBAHA.119.312578.

Palumbo, E. *et al.* (2019) 'Individual Radiosensitivity in Oncological Patients: Linking Adverse Normal Tissue Reactions and Genetic Features', *Frontiers in Oncology*, 9(October). Available at: https://doi.org/10.3389/fonc.2019.00987.

Park, J.W. *et al.* (2022) 'Metformin alleviates ionizing radiation-induced senescence by restoring BARD1-mediated DNA repair in human aortic endothelial cells', *Experimental*

Gerontology, 160(June 2021), p. 111706. Available at: https://doi.org/10.1016/j.exger.2022.111706.

Parker, T. (2012) *Radiotherapy Services in England 2012*, *Department of Health*.

Passos, F. *et al.* (2007) 'Mitochondrial Dysfunction Accounts for the Stochastic Heterogeneity in Telomere-Dependent Senescence', 5(5). Available at: https://doi.org/10.1371/journal.pbio.0050110.

Pavletich, N.P. (1999) 'Mechanisms of cyclin-dependent kinase regulation: Structures of Cdks, their cyclin activators, and Cip and INK4 inhibitors', *Journal of Molecular Biology*, 287(5), pp. 821–828. Available at: https://doi.org/10.1006/jmbi.1999.2640.

Pederiva, C. *et al.* (2023) 'Control of protein synthesis through mRNA pseudouridylation by dyskerin', *Science Advances*, 9(30), pp. 1–18. Available at: https://doi.org/10.1126/sciadv.adg1805.

Petrocelli, J.J. *et al.* (2023) 'Disuse-induced muscle fibrosis, cellular senescence, and senescence-associated secretory phenotype in older adults are alleviated during re-ambulation with metformin pre-treatment', *Aging Cell*, (July), pp. 1–13. Available at: https://doi.org/10.1111/acel.13936.

Pettersen, A.R. *et al.* (2012) 'High On-Aspirin Platelet Reactivity and Clinical Outcome in Patients With Stable Coronary Artery Disease: Results From ASCET (Aspirin Nonresponsiveness and Clopidogrel Endpoint Trial)', *Journal of the American Heart Association*, 1(3), pp. 1–9. Available at: https://doi.org/10.1161/jaha.112.000703.

Philipot, D. *et al.* (2014) 'p16INK4a and its regulator miR-24 link senescence and chondrocyte terminal differentiation-associated matrix remodeling in osteoarthritis', *Arthritis Research & Therapy*, 16(1), p. R58. Available at: https://doi.org/10.1186/ar4494.

Philipp, J. *et al.* (2017a) 'Radiation-induced endothelial inflammation is transferred via the secretome to recipient cells in a STAT-mediated process', *Journal of Proteome Research*, 16(10), pp. 3903–3916. Available at: https://doi.org/10.1021/acs.jproteome.7b00536.

Philipp, J. *et al.* (2017b) 'Radiation-induced endothelial inflammation is transferred via the secretome to recipient cells in a STAT-mediated process', *Journal of Proteome Research*, 16(10), pp. 3903–3916. Available at: https://doi.org/10.1021/acs.jproteome.7b00536.

Pi, X., Xie, L. and Patterson, C. (2018) 'Emerging Roles of Vascular Endothelium in Metabolic Homeostasis', *Circulation Research*, 123(4), pp. 477–494. Available at: https://doi.org/10.1161/CIRCRESAHA.118.313237.

Piano, M.R. (2017) 'Alcohol's Effects on the Cardiovascular System', *Alcohol research : current reviews*, 38(2), pp. 219–241.

Piedrahita, J.A. *et al.* (1992) 'Generation of mice carrying a mutant apolipoprotein E gene inactivated by gene targeting in embryonic stem cells.', *Proceedings of the National Academy of Sciences*, 89(10), pp. 4471–4475. Available at: https://doi.org/10.1073/pnas.89.10.4471.

Pinto, M. and Moraes, C.T. (2015) 'Mechanisms linking mtDNA damage and aging', *Free Radical Biology and Medicine*, 85(5), pp. 250–258. Available at: https://doi.org/10.1016/j.freeradbiomed.2015.05.005.

Pinton, P. *et al.* (2008) 'Calcium and apoptosis: ER-mitochondria Ca2+ transfer in the control of apoptosis', *Oncogene*, 27(50), pp. 6407–6418. Available at: https://doi.org/10.1038/onc.2008.308.

Pitt, J.J. (2009) 'Principles and applications of liquid chromatography-mass spectrometry in clinical biochemistry.', *The Clinical biochemist. Reviews*, 30(1), pp. 19–34. Available at: http://www.ncbi.nlm.nih.gov/pubmed/19224008.

Plowman, P.N. *et al.* (1990) 'An instance of clinical radiation morbidity and cellular radiosensitivity, not associated with ataxia-telangiectasia', *British Journal of Radiology*, 63(752), pp. 624–628. Available at: https://doi.org/10.1259/0007-1285-63-752-624.

Pluquet, O., Pourtier, A. and Abbadie, C. (2015) 'The unfolded protein response and cellular senescence. A Review in the Theme: Cellular Mechanisms of Endoplasmic Reticulum Stress Signaling in Health and Disease', *American Journal of Physiology-Cell Physiology*, 308(6), pp. C415–C425. Available at: https://doi.org/10.1152/ajpcell.00334.2014.

Pober, J.S. and Sessa, W.C. (2007) 'Evolving functions of endothelial cells in inflammation', *Nature Reviews Immunology*, 7(10), pp. 803–815. Available at: https://doi.org/10.1038/nri2171.

Podolec, J. *et al.* (2016) 'Chemokine RANTES is increased at early stages of coronary artery disease.', *Journal of physiology and pharmacology : an official journal of the Polish Physiological Society*, 67(2), pp. 321–8. Available at: http://www.ncbi.nlm.nih.gov/pubmed/27226191.

te Poele, R.H. *et al.* (2002) 'DNA damage is able to induce senescence in tumor cells in vitro and in vivo', *Cancer Research*, 62(6), pp. 1876–1883.

Poirier, P. *et al.* (2006) 'Obesity and Cardiovascular Disease : Pathophysiology , Evaluation , and Effect of Weight Loss An Update of the 1997 American Heart Association Scientific Statement on Obesity and Heart Disease From the Obesity Committee of the Council on Nutrition , Physi', pp. 898–918. Available at: https://doi.org/10.1161/CIRCULATIONAHA.106.171016.

Prata, Larissa G.P. Langhi *et al.* (2018) 'Senescent cell clearance by the immune system: Emerging therapeutic opportunities', *Seminars in Immunology*, 40(5), p. 101275. Available at: https://doi.org/10.1016/j.smim.2019.04.003.

Prata, Larissa G.P.Langhi *et al.* (2018) 'Senescent cell clearance by the immune system: Emerging therapeutic opportunities', *Seminars in Immunology*, 40(November 2018), p. 101275. Available at: https://doi.org/10.1016/j.smim.2019.04.003.

Qi, Y. *et al.* (2015) 'IFI6 inhibits apoptosis via mitochondrial-dependent pathway in dengue virus 2 infected vascular endothelial cells', *PLoS ONE*, 10(8), pp. 1–14. Available at: https://doi.org/10.1371/journal.pone.0132743.

Qian, Z. *et al.* (2019) 'PRAF2 overexpression predicts poor prognosis and promotes tumorigenesis in esophageal squamous cell carcinoma', *BMC Cancer*, 19(1), pp. 1–8. Available at: https://doi.org/10.1186/s12885-019-5818-7.

Qin, H., Liu, P. and Lin, S. (2015) 'Effects of astragaloside IV on the SDF-1/CXCR4 expression in atherosclerosis of apoE-/- mice induced by hyperlipaemia', *Evidence-based Complementary and Alternative Medicine*, 2015. Available at: https://doi.org/10.1155/2015/385154.

Qin, Y. *et al.* (2013) 'Recombinant human CXCL8(3-72)K11R/G31P regulates smooth muscle cell proliferation and migration through blockage of interleukin-8 receptor', *IUBMB Life*, 65(1), pp. 67–75. Available at: https://doi.org/10.1002/iub.1107.

Qiu, S. and Huang, J. (2021) 'MRN complex is an essential effector of DNA damage repair', *Journal of Zhejiang University: Science B*, 22(1), pp. 31–37. Available at: https://doi.org/10.1631/jzus.B2000289.

Rabanal-Ruiz, Y. *et al.* (2021) 'mTORC1 activity is supported by spatial association with focal adhesions', *Journal of Cell Biology*, 220(5). Available at: https://doi.org/10.1083/JCB.202004010.

Rai, V. *et al.* (2012) 'Signal transduction in receptor for advanced glycation end products (RAGE): Solution structure of C-terminal rage (ctRAGE) and its binding to mDia1', *Journal of Biological Chemistry*, 287(7), pp. 5133–5144. Available at: https://doi.org/10.1074/jbc.M111.277731.

Rajaraman, P. *et al.* (2018a) 'Human individual radiation sensitivity and prospects for prediction', *Annals of the ICRP*, 47(3–4), pp. 126–141. Available at: https://doi.org/10.1177/0146645318764091.

Rajaraman, P. *et al.* (2018b) 'Human individual radiation sensitivity and prospects for prediction', *Annals of the ICRP*, 47(3–4), pp. 126–141. Available at: https://doi.org/10.1177/0146645318764091.

Ranjha, L., Howard, S.M. and Cejka, P. (2018) 'Main steps in DNA double-strand break repair: an introduction to homologous recombination and related processes', *Chromosoma*, 127(2), pp. 187–214. Available at: https://doi.org/10.1007/s00412-017-0658-1.

Ratto, E. *et al.* (2022) 'Direct control of lysosomal catabolic activity by mTORC1 through regulation of V-ATPase assembly', *Nature Communications*, 13(1), pp. 1–15. Available at: https://doi.org/10.1038/s41467-022-32515-6.

Ravi, V. *et al.* (2018) 'Systematic evaluation of the adaptability of the non-radioactive SUnSET assay to measure cardiac protein synthesis', *Scientific Reports*, 8(1), pp. 1–11. Available at: https://doi.org/10.1038/s41598-018-22903-8.

Reid, K. *et al.* (2023) 'Reducing mitochondrial ribosomal gene expression does not alter metabolic health or lifespan in mice', *Scientific Reports*, 13(1), pp. 1–15. Available at: https://doi.org/10.1038/s41598-023-35196-3.

Resnick, M.A. (1976) 'The repair of double-strand breaks in DNA: A model involving recombination', *Journal of Theoretical Biology*, 59(1), pp. 97–106. Available at: https://doi.org/10.1016/S0022-5193(76)80025-2.

Ridker, P.M. *et al.* (2017) 'Antiinflammatory therapy with canakinumab for atherosclerotic disease', *New England Journal of Medicine*, 377(12), pp. 1119–1131. Available at: https://doi.org/10.1056/NEJMoa1707914.

Ringborg, U. *et al.* (2003) 'The Swedish Council on Technology Assessment in Health Care (SBU) systematic overview of radiotherapy for cancer including a prospective survey of radiotherapy practice in Sweden 2001 - Summary and conclusions', *Acta Oncologica*, 42(5–6), pp. 357–365. Available at: https://doi.org/10.1080/02841860310010826.

Rivellini, C. *et al.* (2022) 'JAB1 deletion in oligodendrocytes causes senescence-induced inflammation and neurodegeneration in mice', *Journal of Clinical Investigation*, 132(3). Available at: https://doi.org/10.1172/JCI145071.

Rivière, T. *et al.* (2020) 'Structure and Emerging Functions of LRCH Proteins in Leukocyte Biology', *Frontiers in Cell and Developmental Biology*, 8(September), pp. 1–8. Available at: https://doi.org/10.3389/fcell.2020.584134.

Rizza, S. *et al.* (2018) 'S-nitrosylation drives cell senescence and aging in mammals by controlling mitochondrial dynamics and mitophagy', *Proceedings of the National Academy of Sciences of the United States of America*, 115(15), pp. E3388–E3397. Available at: https://doi.org/10.1073/pnas.1722452115.

Rocha, S.F. *et al.* (2014) 'Esm1 modulates endothelial tip cell behavior and vascular permeability by enhancing VEGF bioavailability', *Circulation Research*, 115(6), pp. 581–590. Available at: https://doi.org/10.1161/CIRCRESAHA.115.304718.

Rodier, F. *et al.* (2009) 'Persistent DNA damage signalling triggers senescence-associated inflammatory cytokine secretion', *Nature Cell Biology*, 11(8), pp. 973–979. Available at: https://doi.org/10.1038/ncb1909.

Rodman, S.N. *et al.* (2022) 'Sex-based differences in the severity of radiation-induced arthrofibrosis', *Journal of Orthopaedic Research*, 40(11), pp. 2586–2596. Available at: https://doi.org/10.1002/jor.25297.

Rolt, A., Nair, A. and Cox, L.S. (2019) 'Optimisation of a screening platform for determining IL-6 inflammatory signalling in the senescence-associated secretory phenotype (SASP)', *Biogerontology*, 20(3), pp. 359–371. Available at: https://doi.org/10.1007/s10522-019-09796-4.

Rönty, M. *et al.* (2007) 'Palladin interacts with SH3 domains of SPIN90 and Src and is required for Src-induced cytoskeletal remodeling', *Experimental Cell Research*, 313(12), pp. 2575–2585. Available at: https://doi.org/10.1016/j.yexcr.2007.04.030.

Roos, C.M. *et al.* (2016) 'Chronic senolytic treatment alleviates established vasomotor dysfunction in aged or atherosclerotic mice', *Aging Cell*, 15(5), pp. 973–977. Available at: https://doi.org/10.1111/acel.12458.

Ross, R. and Glomset, J.A. (1973) 'Atherosclerosis and the arterial smooth muscle cell: Proliferation of smooth muscle is a key event in the genesis of the lesions of atherosclerosis.', *Science (New York, N.Y.)*, 180(4093), pp. 1332–9.

Roth, D.B. and Wilson, J.H. (1985) 'Relative rates of homologous and nonhomologous recombination in transfected DNA', *Proceedings of the National Academy of Sciences of the United States of America*, 82(10), pp. 3355–3359. Available at: https://doi.org/10.1073/pnas.82.10.3355.

Roth, G.A. *et al.* (2018) 'Global, regional, and national age-sex-specific mortality for 282 causes of death in 195 countries and territories, 1980–2017: a systematic analysis for the Global Burden of Disease Study 2017', *The Lancet*, 392(10159), pp. 1736–1788. Available at: https://doi.org/10.1016/S0140-6736(18)32203-7.

Rousselle, A. *et al.* (2013) 'CXCL5 limits macrophage foam cell formation in atherosclerosis', *Journal of Clinical Investigation*, 123(3), pp. 1343–1347. Available at: https://doi.org/10.1172/JCI66580.

De Rozieres, S. *et al.* (2000) 'The loss of mdm2 induces p53 mediated apoptosis', *Oncogene*, 19(13), pp. 1691–1697. Available at: https://doi.org/10.1038/sj.onc.1203468.

Sabath, N. *et al.* (2020) 'Cellular proteostasis decline in human senescence', *Proceedings of the National Academy of Sciences of the United States of America*, 117(50), pp. 31902–31913. Available at: https://doi.org/10.1073/pnas.2018138117.

Sagiv, A. *et al.* (2016) 'NKG2D ligands mediate immunosurveillance of senescent cells', *Aging*, 8(2), pp. 328–344. Available at: https://doi.org/10.18632/aging.100897.

Lo Sasso, G. *et al.* (2016) 'The Apoe-/- mouse model: A suitable model to study cardiovascular and respiratory diseases in the context of cigarette smoke exposure and harm reduction', *Journal of Translational Medicine*, 14(1), pp. 1–16. Available at: https://doi.org/10.1186/s12967-016-0901-1.

Saul, D. *et al.* (2022) 'A new gene set identifies senescent cells and predicts senescence-associated pathways across tissues', *Nature Communications*, 13(1). Available at: https://doi.org/10.1038/s41467-022-32552-1.

Scandinavian Simvastatin Survival Study Group (1994) 'Randomised trial of cholesterol lowering in 4444 patients with coronary heart disease: the Scandinavian Simvastatin Survival Study (4S)', *The Lancet*, 344(8934), pp. 1383–1389. Available at: https://doi.org/10.1016/S0140-6736(94)90566-5.

Schreml, S. *et al.* (2007) 'mTOR-inhibitors simultaneously inhibit proliferation and basal IL-6 synthesis of human coronary artery endothelial cells', *International Immunopharmacology*, 7(6), pp. 781–790. Available at: https://doi.org/10.1016/j.intimp.2007.01.016.

Schröder, M. and Kaufman, R.J. (2005) 'ER stress and the unfolded protein response', *Mutation Research - Fundamental and Molecular Mechanisms of Mutagenesis*, 569(1–2), pp. 29–63. Available at: https://doi.org/10.1016/j.mrfmmm.2004.06.056.

Schulz, L. *et al.* (2023) 'Influenza Virus-Induced Paracrine Cellular Senescence of the Lung Contributes to Enhanced Viral Load', *aging and disease*, 14(4), pp. 1331–1348. Available at: https://doi.org/10.14336/AD.2023.0310.

Schwanhüusser, B. *et al.* (2011) 'Global quantification of mammalian gene expression control', *Nature*, 473(7347), pp. 337–342. Available at: https://doi.org/10.1038/nature10098.

Scott, P.H. *et al.* (2001) 'Regulation of RNA polymerase III transcription during cell cycle entry', *Journal of Biological Chemistry*, 276(2), pp. 1005–1014. Available at: https://doi.org/10.1074/jbc.M005417200.

Senatus, L.M. and Schmidt, A.M. (2017) 'The AGE-RAGE axis: Implications for age-associated arterial diseases', *Frontiers in Genetics*, 8(DEC), pp. 1–10. Available at: https://doi.org/10.3389/fgene.2017.00187.

Serra-Marques, A. *et al.* (2020) 'Concerted action of kinesins kif5b and kif13b promotes efficient secretory vesicle transport to microtubule plus ends', *eLife*, 9, pp. 1–37. Available at: https://doi.org/10.7554/eLife.61302.

Serrano, M. *et al.* (1997) 'Oncogenic ras provokes premature cell senescence associated with accumulation of p53 and p16(INK4a)', *Cell*, 88(5), pp. 593–602. Available at: https://doi.org/10.1016/S0092-8674(00)81902-9.

Shang, D., Liu, H. and Tu, Z. (2023) 'Pro-inflammatory cytokines mediating senescence of vascular endothelial cells in atherosclerosis', *Fundamental and Clinical Pharmacology*, 37(5), pp. 928–936. Available at: https://doi.org/10.1111/fcp.12915.

Sharma, V. *et al.* (2016) 'Oxidative stress at low levels can induce clustered DNA lesions leading to NHEJ mediated mutations', *Oncotarget*, 7(18), pp. 25377–25390. Available at: https://doi.org/10.18632/oncotarget.8298.

Shi, D. *et al.* (2020) 'Lysosomal polarity increases with aging as revealed by a lysosome-targetable near-infrared fluorescent probe', *Sensors and Actuators, B: Chemical*, 319(May), p. 128302. Available at: https://doi.org/10.1016/j.snb.2020.128302.

Shi, H. *et al.* (2020) 'Novel insight into the regulatory roles of diverse RNA modifications: Re-defining the bridge between transcription and translation', *Molecular Cancer*, 19(1), pp. 1–17. Available at: https://doi.org/10.1186/s12943-020-01194-6.

Shi, Y. *et al.* (2022) 'The selective NLRP3 inflammasome inhibitor MCC950 improves isoproterenol-induced cardiac dysfunction by inhibiting cardiomyocyte senescence', *European Journal of Pharmacology*, 937(November), p. 175364. Available at: https://doi.org/10.1016/j.ejphar.2022.175364.

Shimizu, Y. *et al.* (2010) 'Radiation exposure and circulatory disease risk: Hiroshima and Nagasaki atomic bomb survivor data, 1950-2003', *BMJ (Online)*, 340(7739), p. 193. Available at: https://doi.org/10.1136/bmj.b5349.

Shin, J., Nile, A. and Oh, J.W. (2021) 'Role of adaptin protein complexes in intracellular trafficking and their impact on diseases', *Bioengineered*, 12(1), pp. 8259–8278. Available at: https://doi.org/10.1080/21655979.2021.1982846.

Shindyapina, A. V. *et al.* (2022) 'Rapamycin treatment during development extends life span and health span of male mice and Daphnia magna', *Science Advances*, 8(37), pp. 1–12. Available at: https://doi.org/10.1126/sciadv.abo5482.

da Silva, R.M.F.L. (2019) 'Effects of Radiotherapy in Coronary Artery Disease', *Current Atherosclerosis Reports*, 21(12). Available at: https://doi.org/10.1007/s11883-019-0810-x.

Sima, A. V., Stancu, C.S. and Simionescu, M. (2009) 'Vascular endothelium in atherosclerosis', *Cell and Tissue Research*, 335(1), pp. 191–203. Available at: https://doi.org/10.1007/s00441-008-0678-5.

Singh, D., Rai, V. and Agrawal, D.K. (2022) 'Non-Coding RNAs in Regulating Plaque Progression and Remodeling of Extracellular Matrix in Atherosclerosis', *International Journal of Molecular Sciences*, 23(22). Available at: https://doi.org/10.3390/ijms232213731.

Siwiak, M. and Zielenkiewicz, P. (2010) 'A comprehensive, quantitative, and genome-wide model of translation', *PLoS Computational Biology*, 6(7), p. 4. Available at: https://doi.org/10.1371/journal.pcbi.1000865.

Skålén, K. *et al.* (2002a) 'Subendothelial retention of atherogenic lipoproteins in early atherosclerosis', *Nature*, 417(6890), pp. 750–754. Available at: https://doi.org/10.1038/nature00804.

Skålén, K. *et al.* (2002b) 'Subendothelial retention of atherogenic lipoproteins in early atherosclerosis', *Nature*, 417(6890), pp. 750–754. Available at: https://doi.org/10.1038/nature00804.

Skon-Hegg, C. *et al.* (2019) 'LACC1 Regulates TNF and IL-17 in Mouse Models of Arthritis and Inflammation', *The Journal of Immunology*, 202(1), pp. 183–193. Available at: https://doi.org/10.4049/jimmunol.1800636.

Smith, L.L., Coller, H.A. and Roberts, J.M. (2003) 'Telomerase modulates expression of growth-controlling genes and enhances cell proliferation', *Nature Cell Biology*, 5(5), pp. 474–479. Available at: https://doi.org/10.1038/ncb985.

Sodin-Semrl, S. *et al.* (2009) 'Increased responsiveness of human coronary artery endothelial cells in inflammation and coagulation', *Mediators of Inflammation*, 2009. Available at: https://doi.org/10.1155/2009/146872.

Solon, A.L. *et al.* (2021) 'Kinesin-binding protein remodels the kinesin motor to prevent microtubule binding', *Science Advances*, 7(47). Available at: https://doi.org/10.1126/sciadv.abj9812.

Song, P., An, J. and Zou, M.H. (2020) 'Immune Clearance of Senescent Cells to Combat Ageing and Chronic Diseases', *Cells*, 9(3). Available at: https://doi.org/10.3390/cells9030671.

de Sousa Abreu, R. *et al.* (2009) 'Global signatures of protein and mRNA expression levels', *Molecular BioSystems*, 20(4), pp. 237–244. Available at: https://doi.org/10.1039/b908315d.

Stanfel, M.N. *et al.* (2009) 'The TOR pathway comes of age', *Biochimica et Biophysica Acta (BBA) - General Subjects*, 1790(10), pp. 1067–1074. Available at: https://doi.org/10.1016/j.bbagen.2009.06.007.

Stein, K.C. *et al.* (2022) 'Ageing exacerbates ribosome pausing to disrupt cotranslational proteostasis', *Nature*, 601(7894), pp. 637–642. Available at: https://doi.org/10.1038/s41586-021-04295-4.

Steins, M.B. *et al.* (1999) 'Overexpression of tissue-type plasminogen activator in atherosclerotic human coronary arteries', *Atherosclerosis*, 145(1), pp. 173–180. Available at: https://doi.org/10.1016/S0021-9150(99)00030-1.

Stewart, F.A. *et al.* (2006) 'Ionizing radiation accelerates the development of atherosclerotic lesions in ApoE-/- mice and predisposes to an inflammatory plaque phenotype prone to hemorrhage', *American Journal of Pathology*, 168(2), pp. 649–658. Available at: https://doi.org/10.2353/ajpath.2006.050409.

Stewart, G.S. *et al.* (1999) 'The DNA double-strand break repair gene hMRE11 is mutated in individuals with an ataxia-telangiectasia-like disorder', *Cell*, 99(6), pp. 577–587. Available at: https://doi.org/10.1016/S0092-8674(00)81547-0.

Storer, M. *et al.* (2013) 'Senescence is a developmental mechanism that contributes to embryonic growth and patterning', *Cell*, 155(5), p. 1119. Available at: https://doi.org/10.1016/j.cell.2013.10.041.

Sturchler, E. *et al.* (2006) 'S100A16, a novel calcium-binding protein of the EF-hand superfamily', *Journal of Biological Chemistry*, 281(50), pp. 38905–38917. Available at: https://doi.org/10.1074/jbc.M605798200.

Su, W. *et al.* (2023) 'Clearance of senescent cells by navitoclax (ABT263) rejuvenates UHMWPE-induced osteolysis', *International Immunopharmacology*, 115(September 2022), p. 109694. Available at: https://doi.org/10.1016/j.intimp.2023.109694.

Subramanian, S. *et al.* (2014) 'Stromal cell-derived factor 1 as a biomarker of heart failure and mortality risk', *Arteriosclerosis, Thrombosis, and Vascular Biology*, 34(9), pp. 2100–2105. Available at: https://doi.org/10.1161/ATVBAHA.114.303579.

Suman, S. *et al.* (2012) 'Exposure to Ionizing Radiation Causes Long-Term Increase in Serum Estradiol and Activation of PI3K-Akt Signaling Pathway in Mouse Mammary Gland', *International Journal of Radiation Oncology*Biology*Physics*, 84(2), pp. 500–507. Available at: https://doi.org/10.1016/j.ijrobp.2011.12.033.

Sung, J.Y. *et al.* (2022) 'Metformin mitigates stress-induced premature senescence by upregulating AMPKα at Ser485 phosphorylation induced SIRT3 expression and inactivating mitochondrial oxidants', *Mechanisms of Ageing and Development*, 206(March). Available at: https://doi.org/10.1016/j.mad.2022.111708.

Suzuki, Y. *et al.* (2011) 'Surface-retained tPA is essential for effective fibrinolysis on vascular endothelial cells', *Blood*, 118(11), pp. 3182–3185. Available at: https://doi.org/10.1182/blood-2011-05-353912.

Swanson, E.C. *et al.* (2013) 'Higher-order unfolding of satellite heterochromatin is a consistent and early event in cell senescence', *Journal of Cell Biology*, 203(6), pp. 929–942. Available at: https://doi.org/10.1083/jcb.201306073.

Takagi, M. *et al.* (2005) 'Regulation of p53 translation and induction after DNA damage by ribosomal protein L26 and nucleolin', *Cell*, 123(1), pp. 49–63. Available at: https://doi.org/10.1016/j.cell.2005.07.034.

Takahashi, A. *et al.* (2012) 'DNA damage signaling triggers degradation of histone methyltransferases through APC/C Cdh1 in senescent cells', *Molecular Cell*, 45(1), pp. 123–131. Available at: https://doi.org/10.1016/j.molcel.2011.10.018.

Takasaka, N. *et al.* (2014) 'Autophagy Induction by SIRT6 through Attenuation of Insulin-like Growth Factor Signaling Is Involved in the Regulation of Human Bronchial Epithelial Cell Senescence', *The Journal of Immunology*, 192(3), pp. 958–968. Available at: https://doi.org/10.4049/jimmunol.1302341.

Tang, J.X. and Xiao, F.H. (2023) 'Editorial: The regulation of proteostasis in aging', *Frontiers in Cell and Developmental Biology*, 11(May), pp. 1–3. Available at: https://doi.org/10.3389/fcell.2023.1221510.

Terzi, M.Y., Izmirli, M. and Gogebakan, B. (2016) 'The cell fate: senescence or quiescence', *Molecular Biology Reports*, 43(11), pp. 1213–1220. Available at: https://doi.org/10.1007/s11033-016-4065-0.

Thompson, M.A. and De-Souza, E.A. (2023) 'A Year at the Forefront of Proteostasis and Aging', *Biology Open*, 12(2). Available at: https://doi.org/10.1242/bio.059750.

Thompson, M.K. *et al.* (2018) 'Practice-changing radiation therapy trials for the treatment of cancer: where are we 150 years after the birth of Marie Curie?', *British Journal of Cancer*, 119(4), pp. 389–407. Available at: https://doi.org/10.1038/s41416-018-0201-z.

Thompson, P.J. *et al.* (2019) 'Targeted Elimination of Senescent Beta Cells Prevents Type 1 Diabetes', *Cell Metabolism*, 29(5), pp. 1045-1060.e10. Available at: https://doi.org/10.1016/j.cmet.2019.01.021.

Toth, P.P. (2008) 'Subclinical atherosclerosis: What it is, what it means and what we can do about it', *International Journal of Clinical Practice*, 62(8), pp. 1246–1254. Available at: https://doi.org/10.1111/j.1742-1241.2008.01804.x.

Tribble, D.L. *et al.* (1999) *Ionizing Radiation Accelerates Aortic Lesion Formation in Fat-Fed Mice via SOD-Inhibitable Processes*, *Arterioscler Thromb Vasc Biol*. Available at: http://www.atvbaha.org.

Tsuji, S. *et al.* (2022) 'SARS-CoV-2 infection triggers paracrine senescence and leads to a sustained senescence-associated inflammatory response', *Nature Aging*, 2(2), pp. 115–124. Available at: https://doi.org/10.1038/s43587-022-00170-7.

Tuller, T., Kupiec, M. and Ruppin, E. (2007) 'Determinants of protein abundance and translation efficiency in S. cerevisiae', *PLoS Computational Biology*, 3(12), pp. 2510–2519. Available at: https://doi.org/10.1371/journal.pcbi.0030248.

Turi, Z. *et al.* (2019) 'Impaired ribosome biogenesis: Mechanisms and relevance to cancer and aging', *Aging*, 11(8), pp. 2512–2540. Available at: https://doi.org/10.18632/aging.101922.

Ueno, K. *et al.* (2017) 'Disruption of Endothelial Cell Homeostasis Plays a Key Role in the Early Pathogenesis of Coronary Artery Abnormalities in Kawasaki Disease', *Nature Publishing Group*, (March), pp. 1–11. Available at: https://doi.org/10.1038/srep43719.

Ungvari, Z. *et al.* (2008) 'Dysregulation of mitochondrial biogenesis in vascular endothelial and smooth muscle cells of aged rats', *American Journal of Physiology - Heart and Circulatory Physiology*, 294(5), pp. 2121–2128. Available at: https://doi.org/10.1152/ajpheart.00012.2008.

UNSCEAR (2008) *Sources and Effects of Ionizing Radiation*. New York.

Uzarski, J.S., Scott, E.W. and McFetridge, P.S. (2013) 'Adaptation of Endothelial Cells to Physiologically-Modeled, Variable Shear Stress', *PLoS ONE*, 8(2), pp. 17–19. Available at: https://doi.org/10.1371/journal.pone.0057004.

Vacek, T.P. *et al.* (2015) 'Matrix metalloproteinases in atherosclerosis: Role of nitric oxide, hydrogen sulfide, homocysteine, and polymorphisms', *Vascular Health and Risk Management*, 11, pp. 173–183. Available at: https://doi.org/10.2147/VHRM.S68415.

Véniant, M.M., Withycombe, S. and Young, S.G. (2001a) 'Lipoprotein Size and Atherosclerosis Susceptibility in Apoe −/− and Ldlr −/− Mice', *Arteriosclerosis, Thrombosis, and Vascular Biology*, 21(10), pp. 1567–1570. Available at: https://doi.org/10.1161/hq1001.097780.

Véniant, M.M., Withycombe, S. and Young, S.G. (2001b) 'Lipoprotein Size and Atherosclerosis Susceptibility in Apoe −/− and Ldlr −/− Mice', *Arteriosclerosis, Thrombosis, and Vascular Biology*, 21(10), pp. 1567–1570. Available at: https://doi.org/10.1161/hq1001.097780.

Vizioli, M.G. *et al.* (2020) 'Mitochondria-to-nucleus retrograde signaling drives formation of cytoplasmic chromatin and inflammation in senescence', *Genes and Development*, 34(5), pp. 428–445. Available at: https://doi.org/10.1101/gad.331272.119.

Wajapeyee, N. *et al.* (2008) 'Oncogenic BRAF Induces Senescence and Apoptosis through Pathways Mediated by the Secreted Protein IGFBP7', *Cell*, 132(3), pp. 363–374. Available at: https://doi.org/10.1016/j.cell.2007.12.032.

Walters, H.E. *et al.* (2023) 'Senescent cells enhance newt limb regeneration by promoting muscle dedifferentiation', *Aging Cell*, 22(6), pp. 1–14. Available at: https://doi.org/10.1111/acel.13826.

Walters, H.E. and Cox, L.S. (2018) 'mTORC inhibitors as broad-spectrum therapeutics for age-related diseases', *International Journal of Molecular Sciences*, 19(8), pp. 1–33. Available at: https://doi.org/10.3390/ijms19082325.

Walters, H.E., Deneka-Hannemann, S. and Cox, L.S. (2016) 'Reversal of phenotypes of cellular senescence by pan-mTOR inhibition', *Aging*, 8(2), pp. 231–244. Available at: https://doi.org/10.18632/aging.100872.

Wang, Huichen *et al.* (2003) 'Biochemical evidence for Ku-independent backup pathways of NHEJ', *Nucleic Acids Research*, 31(18), pp. 5377–5388. Available at: https://doi.org/10.1093/nar/gkg728.

Wang, L. *et al.* (2020) 'Structures of a Complete Human V-ATPase Reveal Mechanisms of Its Assembly', *Molecular Cell*, 80(3), pp. 501-511.e3. Available at: https://doi.org/10.1016/j.molcel.2020.09.029.

Wang, X. *et al.* (2016) 'CD24 promoted cancer cell angiogenesis via Hsp90-mediated STAT3/VEGF signaling pathway in colorectal cancer', *Oncotarget*, 7(34), pp. 55663–55676. Available at: https://doi.org/10.18632/oncotarget.10971.

Wang, Y. *et al.* (2022) 'PRAF2 is an oncogene acting to promote the proliferation and invasion of breast cancer cells', *Experimental and Therapeutic Medicine*, 24(6), pp. 1–11. Available at: https://doi.org/10.3892/etm.2022.11674.

Wang, Y., Boerma, M. and Zhou, D. (2016) 'Ionizing Radiation-Induced Endothelial Cell Senescence and Cardiovascular Diseases', *Radiation Research*, 186(2), pp. 153–161. Available at: https://doi.org/10.1667/RR14445.1.

Wang, Z. *et al.* (2017) 'Decreased expression of semaphorin 3D is associated with genesis and development in colorectal cancer', *World Journal of Surgical Oncology*, 15(1), pp. 1–8. Available at: https://doi.org/10.1186/s12957-017-1128-1.

Waters, S.B. *et al.* (2021) 'VEGFR2 trafficking by KIF13B is a novel therapeutic target for wet age-related macular degeneration', *Investigative Ophthalmology and Visual Science*, 62(2), pp. 20–22. Available at: https://doi.org/10.1167/IOVS.62.2.5.

Waters, S.B. *et al.* (2022) 'KIF13B-mediated VEGFR2 trafficking is essential for vascular leakage and metastasis in vivo', *Life Science Alliance*, 5(1), pp. 1–11. Available at: https://doi.org/10.26508/lsa.202101170.

Watson, S.J. *et al.* (2005) *Ionising Radiation Exposure of the UK Population: 2005 Review*.

Weber, C. and Noels, H. (2011) 'Atherosclerosis: Current pathogenesis and therapeutic options', *Nature Medicine*, pp. 1410–1422. Available at: https://doi.org/10.1038/nm.2538.

Weichhart, T. (2018) 'mTOR as regulator and lifespan, aging and cellular senescence', *Gerontology*, 64(2), pp. 127–134. Available at: https://doi.org/10.1159/000484629.mTOR.

Whittemore, K. *et al.* (2019) 'Telomere shortening rate predicts species life span', *Proceedings of the National Academy of Sciences of the United States of America*, 116(30), pp. 15122–15127. Available at: https://doi.org/10.1073/pnas.1902452116.

Wiley, C.D. *et al.* (2016) 'Mitochondrial dysfunction induces senescence with a distinct secretory phenotype', *Cell Metabolism*, 23(2), pp. 303–314. Available at: https://doi.org/10.1016/j.cmet.2015.11.011.

Williams, H.J., Fisher, E.A. and Greaves, D.R. (2012) 'Macrophage differentiation and function in atherosclerosis: Opportunities for therapeutic intervention?', *Journal of Innate Immunity*, 4(5–6), pp. 498–508. Available at: https://doi.org/10.1159/000336618.

Woldhuis, R.R. *et al.* (2020) 'Link between increased cellular senescence and extracellular matrix changes in COPD', *American Journal of Physiology - Lung Cellular and Molecular Physiology*, 319(1), pp. L48–L60. Available at: https://doi.org/10.1152/ajplung.00028.2020.

World Health Organization (2018) 'Global Health Estimates 2016: Deaths by Cause, Age, Sex, by Country and by Region, 2000- 2016'. Geneva, Switzerland.

Wu, D. *et al.* (2021) 'MZF1 mediates oncogene-induced senescence by promoting the transcription of p16INK4A', *Oncogene*, 41(3), pp. 414–426. Available at: https://doi.org/10.1038/s41388-021-02110-y.

Wu, P., Takai, H. and de Lange, T. (2012) 'Telomeric 3' Overhangs Derive from Resection by Exo1 and Apollo and Fill-In by POT1b-Associated CST', *Cell*, 150(1), pp. 39–52. Available at: https://doi.org/10.1016/j.cell.2012.05.026.

Wyld, L. *et al.* (2020) 'Senescence and cancer: A review of clinical implications of senescence and senotherapies', *Cancers*, 12(8), pp. 1–20. Available at: https://doi.org/10.3390/cancers12082134.

Xiang, Y. *et al.* (2022) 'Oxidative stress-induced premature senescence and aggravated denervated skeletal muscular atrophy by regulating progerin–p53 interaction', *Skeletal Muscle*, 12(1), pp. 1–12. Available at: https://doi.org/10.1186/s13395-022-00302-y.

Xie, J. *et al.* (2023) 'Clearance of Stress-Induced Premature Senescent Cells Alleviates the Formation of Abdominal Aortic Aneurysms', *Aging and disease*, 14(5), p. 0. Available at: https://doi.org/10.14336/ad.2023.0215.

Xie, X. *et al.* (2020) 'Low shear stress induces endothelial cell apoptosis and monocyte adhesion by upregulating PECAM-1 expression', *Molecular Medicine Reports*, 21(6), pp. 2580–2588. Available at: https://doi.org/10.3892/mmr.2020.11060.

Xu, H. *et al.* (2022) 'miR-1290 promotes IL-8-mediated vascular endothelial cell adhesion by targeting GSK-3β', *Molecular Biology Reports*, 49(3), pp. 1871–1882. Available at: https://doi.org/10.1007/s11033-021-06998-3.

Xu, M. *et al.* (2018) 'Senolytics improve physical function and increase lifespan in old age', *Nature Medicine*, 24(8), pp. 1246–1256. Available at: https://doi.org/10.1038/s41591-018-0092-9.

Yamada, K.H. *et al.* (2014) 'KIF13B regulates angiogenesis through Golgi to plasma membrane trafficking of VEGFR2', *Journal of Cell Science*, 127(20), pp. 4518–4530. Available at: https://doi.org/10.1242/jcs.156109.

Yang, D. *et al.* (2023) 'NKG2D-CAR T cells eliminate senescent cells in aged mice and nonhuman primates', 90, pp. 1–15. Available at: https://doi.org/10.1126/scitranslmed.add1951.

Yang, J. *et al.* (2004) 'Endothelial overexpression of fas ligand decreases atherosclerosis in apolipoprotein E-deficient mice', *Arteriosclerosis, Thrombosis, and Vascular Biology*, 24(8), pp. 1466–1473. Available at: https://doi.org/10.1161/01.ATV.0000134402.94963.2f.

Yang, N.C. and Hu, M.L. (2004) 'A fluorimetric method using fluorescein di-β-D-galactopyranoside for quantifying the senescence-associated β-galactosidase activity in

human foreskin fibroblast Hs68 cells', *Analytical Biochemistry*, 325(2), pp. 337–343. Available at: https://doi.org/10.1016/j.ab.2003.11.012.

Yentrapalli, R. *et al.* (2013) 'The PI3K/Akt/mTOR Pathway Is Implicated in the Premature Senescence of Primary Human Endothelial Cells Exposed to Chronic Radiation', *PLoS ONE*, 8(8). Available at: https://doi.org/10.1371/journal.pone.0070024.

Yosef, R. *et al.* (2016) 'Directed elimination of senescent cells by inhibition of BCL-W and BCL-XL', *Nature Communications*, 7. Available at: https://doi.org/10.1038/ncomms11190.

Yosef, R. *et al.* (2017) ' p21 maintains senescent cell viability under persistent DNA damage response by restraining JNK and caspase signaling ', *The EMBO Journal*, 36(15), pp. 2280–2295. Available at: https://doi.org/10.15252/embj.201695553.

Yun, M.H., Davaapil, H. and Brockes, J.P. (2015) 'Recurrent turnover of senescent cells during regeneration of a complex structure', *eLife*, 4(MAY), pp. 1–16. Available at: https://doi.org/10.7554/eLife.05505.

Zadelaar, A.S.M. *et al.* (2005) 'Increased vulnerability of pre-existing atherosclerosis in ApoE-deficient mice following adenovirus-mediated Fas ligand gene transfer', *Atherosclerosis*, 183(2), pp. 244–250. Available at: https://doi.org/10.1016/j.atherosclerosis.2005.03.044.

Zanotti, S. *et al.* (2023) 'Extracellular Matrix Disorganization and Sarcolemmal Alterations in COL6-Related Myopathy Patients with New Variants of COL6 Genes',

International Journal of Molecular Sciences, 24(6). Available at: https://doi.org/10.3390/ijms24065551.

Zecha, J. *et al.* (2022) 'Linking post-translational modifications and protein turnover by site-resolved protein turnover profiling', *Nature Communications*, 13(1), pp. 1–14. Available at: https://doi.org/10.1038/s41467-021-27639-0.

Zernecke, A., Shagdarsuren, E. and Weber, C. (2008a) 'Chemokines in atherosclerosis an update', *Arteriosclerosis, Thrombosis, and Vascular Biology*, 28(11), pp. 1897–1908. Available at: https://doi.org/10.1161/ATVBAHA.107.161174.

Zernecke, A., Shagdarsuren, E. and Weber, C. (2008b) 'Chemokines in atherosclerosis an update', *Arteriosclerosis, Thrombosis, and Vascular Biology*, 28(11), pp. 1897–1908. Available at: https://doi.org/10.1161/ATVBAHA.107.161174.

Zhan, W. *et al.* (2022) 'Pcsk6 Deficiency Promotes Cardiomyocyte Senescence by Modulating Ddit3-Mediated ER Stress', *Genes*, 13(4), p. 711. Available at: https://doi.org/10.3390/genes13040711.

Zhang, H. *et al.* (2023) 'Expression and gene regulatory network of S100A16 protein in cervical cancer cells based on data mining', *BMC Cancer*, 23(1), p. 1124. Available at: https://doi.org/10.1186/s12885-023-11574-y.

Zhang, L. *et al.* (2019) 'Cysteine-rich intestinal protein 1 suppresses apoptosis and chemosensitivity to 5-fluorouracil in colorectal cancer through ubiquitin-mediated Fas degradation', *Journal of Experimental and Clinical Cancer Research*, 38(1), pp. 1–14. Available at: https://doi.org/10.1186/s13046-019-1117-z.

Zhang, L. *et al.* (2022) *Insulin-like growth factor-binding protein-7 (IGFBP7) links senescence to heart failure*, *Nature Cardiovascular Research*. Available at: https://doi.org/10.1038/s44161-022-00181-y.

Zhang, S.H. *et al.* (1992a) 'Spontaneous hypercholesterolemia and arterial lesions in mice lacking apolipoprotein E', *Science*, 258(5081), pp. 468–471. Available at: https://doi.org/10.1126/science.1411543.

Zhang, S.H. *et al.* (1992b) 'Spontaneous hypercholesterolemia and arterial lesions in mice lacking apolipoprotein E', *Science*, 258(5081), pp. 468–471. Available at: https://doi.org/10.1126/science.1411543.

Zhang, X. *et al.* (2023) 'Over-Expression of ARID3B Suppresses Tumor Progression and Predicts Better Prognosis in Patients With Gastric Cancer', *Cancer Control*, 30, pp. 1–14. Available at: https://doi.org/10.1177/10732748231169403.

Zhao, H. and Darzynkiewicz, Z. (2013) 'Biomarkers of cell senescence assessed by imaging cytometry', *Methods in Molecular Biology*, 965, pp. 83–92. Available at: https://doi.org/10.1007/978-1-62703-239-1_5.

Zhao, L. *et al.* (2019) 'COX7A1 suppresses the viability of human non-small cell lung cancer cells via regulating autophagy', *Cancer Medicine*, 8(18), pp. 7762–7773. Available at: https://doi.org/10.1002/cam4.2659.

Zhao, L. *et al.* (2022) 'Targeted protein degradation: mechanisms, strategies and application', *Signal Transduction and Targeted Therapy*, 7(1). Available at: https://doi.org/10.1038/s41392-022-00966-4.

Zhu, Y. *et al.* (2015) 'The Achilles' heel of senescent cells: from transcriptome to senolytic drugs', *Aging cell*, 14(4), pp. 644–658. Available at: https://doi.org/10.1111/acel.12344.

Zhu, Y. *et al.* (2016) 'Identification of a novel senolytic agent, navitoclax, targeting the Bcl-2 family of anti-apoptotic factors', *Aging Cell*, 15(3), pp. 428–435. Available at: https://doi.org/10.1111/acel.12445.

Zhuang, G. *et al.* (2013) 'Phosphoproteomic analysis implicates the mTORC2-FoxO1 axis in VEGF signaling and feedback activation of receptor tyrosine kinases', *Science Signaling*, 6(271), pp. 1–12. Available at: https://doi.org/10.1126/scisignal.2003572].

Zingoni, A. *et al.* (2015) 'Genotoxic Stress Induces Senescence-Associated ADAM10-Dependent Release of NKG2D MIC Ligands in Multiple Myeloma Cells', *The Journal of Immunology*, 195(2), pp. 736–748. Available at: https://doi.org/10.4049/jimmunol.1402643.

Zou, L. and Elledge, S.J. (2003) 'Sensing DNA damage through ATRIP recognition of RPA-ssDNA complexes', *Science*, 300(5625), pp. 1542–1548. Available at: https://doi.org/10.1126/science.1083430.

10 Supplementary material

Supplementary material Table S6.1 Genes differentially expressed in HCAECs from middle-aged donors compared to young

Gene name	log2FC	PValue	FDR
UCHL1	-7.0981464	4.25E-48	6.17E-44
ERBB2	-6.7009417	1.27E-05	0.00502289
CFAP70	-6.5740465	3.59E-05	0.0115792
SFRP1	-6.3153513	0.00016892	0.040155
CRTAC1	-6.1107995	9.17E-09	8.28E-06
CD24	-5.9982168	1.21E-14	2.18E-11
IGF2	-5.024275	3.95E-08	2.86E-05
D2HGDH	-4.9704508	0.00018348	0.04223254
KIAA1522	-4.4346278	0.00016584	0.04008195
LY6K	-4.245232	4.44E-08	3.07E-05
CCNJL	-4.163307	4.07E-07	0.0002567
PALLD	-3.3255201	9.92E-06	0.00435771
ADTRP	-2.8326931	0.00018001	0.04210309
TFPI2	-2.8318808	1.10E-05	0.00469888
CNOT1	-2.5402461	2.31E-06	0.00115476
GSTM3	-2.4237721	9.71E-09	8.28E-06
CCDC190	-2.41902	8.03E-06	0.00363994
KRT19	-2.1612843	0.00014498	0.03563392
EDIL3	-2.147505	4.55E-05	0.01404641
TAGLN	-1.4871288	3.12E-05	0.01077157
RNASE1	-1.4779485	3.94E-05	0.01242182
FN1	-1.4025886	8.95E-05	0.02359246
CLU	1.3755742	0.00012374	0.0310144
PROCR	1.47641366	3.47E-05	0.01142976
BST2	1.56689747	5.79E-05	0.01713083
IL1RL1	1.56896099	1.56E-05	0.00596839
PLTP	1.6475076	0.00020286	0.04457144
HMOX1	1.85050095	1.23E-05	0.00502289
IDI1	1.99214094	6.84E-05	0.01945635
CCNA1	1.99661972	1.17E-06	0.00065493
PDGFRL	2.03882786	7.61E-05	0.02082814
DBNDD2	2.05092136	3.44E-05	0.01142976
CXCL8	2.05997881	3.17E-08	2.42E-05
MOV10L1	2.07889817	0.00019224	0.0435581
BUB3	2.17272913	2.75E-09	3.07E-06
TSC22D3	2.24192584	2.21E-06	0.00114564
MT1H	2.35937949	8.55E-05	0.02295966
CDA	2.39492896	5.33E-07	0.00030945
MT1G	2.4156662	1.15E-08	9.29E-06
MICA	2.419103	0.00019712	0.04397489
MT1F	2.47132119	4.33E-09	4.49E-06
YIPF4	2.51839656	1.33E-11	1.76E-08
MT1L	2.52115999	6.60E-11	7.98E-08
ISG15	2.68370428	5.90E-06	0.00276156
GJA4	2.73781729	1.23E-07	8.08E-05
IFI6	2.75905961	5.30E-13	7.68E-10
HRAS	3.30952891	6.51E-05	0.01887355
ARFGAP1	3.36943637	9.78E-05	0.02533312
TMEM88	3.48744705	3.03E-05	0.01072054
PLAT	3.66484831	1.54E-18	5.58E-15
COX7A1	3.79916361	1.45E-19	6.99E-16
IFITM1	3.83647394	1.14E-16	3.30E-13
AL928654.3	3.83649009	7.01E-05	0.01954753
CRIP1	3.96325426	3.91E-23	2.84E-19
MX1	4.58334154	5.06E-09	4.89E-06
GPX3	4.69236795	3.39E-15	8.20E-12
FAM3A	4.85045939	0.00012405	0.0310144
DHCR24	5.08717326	2.44E-05	0.00882765
CRYAB	6.66150479	1.25E-13	2.01E-10
ZNF433	6.74423766	4.67E-05	0.0141024
PHYHD1	6.75839627	2.36E-05	0.0087569
IFIT1	6.82786695	9.53E-15	1.97E-11
TMEM100	6.89322845	1.28E-05	0.00502289
DKK2	6.98497366	5.88E-06	0.00276156
ENOX1	7.20281686	1.58E-06	0.00084871
RELN	7.33582907	4.71E-07	0.00028474

Table S6.2 IR-induced differential gene expression in HCAECs from young donors

gene_name	logFC	PValue	FDR
PCSK7	2.37594677	2.61E-06	0.01940706
CDKN3	-4.1594426	3.35E-06	0.01940706
PGF	2.06507221	4.17E-06	0.01940706
PTTG1	-2.2366054	5.46E-06	0.01940706
CDC20	-4.1260911	7.14E-06	0.02030296
UBE2T	-2.4797821	1.85E-05	0.03595946
FAM214B	1.77912639	2.13E-05	0.03595946
DUSP1	2.37496282	2.17E-05	0.03595946
MGP	-2.0814485	2.28E-05	0.03595946
UBE2C	-4.3365427	2.66E-05	0.03776505
SPATS2L	1.86492236	3.09E-05	0.03999558
GMNN	-3.6647871	3.75E-05	0.04159709
H2AFZ	-1.4266032	4.03E-05	0.04159709
CCNB1	-3.5981228	4.10E-05	0.04159709
SULF2	2.30884344	4.39E-05	0.04159709
CTU2	4.21745993	4.94E-05	0.04166196
FAM3A	5.47393881	4.98E-05	0.04166196
PIR	-1.5214321	6.18E-05	0.04409483
DCBLD2	2.09780572	6.27E-05	0.04409483
SLC7A2	2.00357767	6.79E-05	0.04409483
FABP4	-2.6264274	7.10E-05	0.04409483
ITGB3BP	-2.6903469	7.43E-05	0.04409483
PALLD	1.97008631	7.71E-05	0.04409483
CSNK1D	1.733107	8.19E-05	0.04409483
CKS2	-1.5158109	8.19E-05	0.04409483
GJA1	1.36538176	8.26E-05	0.04409483
RAPGEF3	4.30686599	8.39E-05	0.04409483
ITGAV	1.48478577	8.68E-05	0.04409483

Table S6.3 Junctional gene set used to identify gene and proteins associated with cellular junctions

Gene
ACTN4
ACTR2
ACTR3
ARF6
ARPC1A
ARPC1B
ARPC2
ARPC3
ARPC4
ARPC5
ARPC5L
CLIP1
CTNNA1
CTNNA2
CTNNB1
CTNND1
DNM1L
DNM2
EXOC2
IQGAP1
MAPRE1
MAPRE2
RAB5A
RAB5B
RAB5C
RAB7A
RALA
SRC
TUBA1A
TUBA1C
TUBB
TUBB3
TUBB4B
TUBB6
TUBB8
TUBG1
VCL
ZYX
AFDN
CADM3
CDH13
CDH2
CDH5
CTNNA1
CTNNB1
CTNND1
DST
F11R
FBLIM1
FERMT2
FLNA
FLNC
ILK
ITGB1
JUP
NECTIN2
PALS1
PARVA
PARVB
PLEC
PVR
PXN
RSU1
VASP

Table S6.4 Adhesion gene set used for detection of gene and proteins associated with cellular adhesion

Gene
FYN
ITGA2
ITGB1
VWF
CD99
CDH5
EZR
FN1
GLG1
GNAI2
GNAI3
ICAM1
ICAM2
ITGA5
ITGB1
MMP14
MMP2
MSN
MYH10
MYH14
MYH9
MYL6
MYL6B
MYL9
MYO18A
PECAM1
PODXL
RDX
CD99
CDH5
EZR
GLG1
GNAI2
GNAI3
ICAM1
ICAM2
IL1RL1
ITGB1
MMP14
MMP2
MSN
PECAM1
RDX

Table S6.5 SenMayo gene set used to identify genes and proteins associated with senescence

Gene	Gene
ACVR1B	IGFBP6
ANG	IGFBP7
ANGPT1	IL10
ANGPTL4	IL13
AREG	IL15
AXL	IL18
BEX3	IL1A
BMP2	IL1B
BMP6	IL2
C3	IL32
CCL1	IL6
CCL13	IL6ST
CCL16	IL7
CCL2	INHA
CCL20	IQGAP2
CCL24	ITGA2
CCL26	ITPKA
CCL3	JUN
CCL3L1	KITLG
CCL4	LCP1
CCL5	MIF
CCL7	MMP1
CCL8	MMP10
CD55	MMP12
CD9	MMP13
CSF1	MMP14
CSF2	MMP2
CSF2RB	MMP3
CST4	MMP9
CTNNB1	NAP1L4
CTSB	NRG1
CXCL1	PAPPA
CXCL10	PECAM1
CXCL12	PGF
CXCL16	PIGF
CXCL2	PLAT
CXCL3	PLAU
CXCL8	PLAUR
CXCR2	PTBP1
DKK 1.00	PTGER2
EDN1	PTGES
EGF	RPS6KA5
EGFR	SCAMP4
EREG	SELPLG
ESM1	SEMA3F
ETS2	SERPINB4
FAS	SERPINE1
FGF1	SERPINE2
FGF2	SPP1
FGF7	SPX
GDF15	TIMP2
GEM	TNF
GMFG	TNFRSF10C
HGF	TNFRSF11B
HMGB1	TNFRSF1A
ICAM1	TNFRSF1B
ICAM3	TUBGCP2
IGF1	VEGFA
IGFBP1	VEGFC
IGFBP2	VGF
IGFBP3	WNT16
IGFBP4	WNT2
IGFBP5	

Table S7.1 Proteins differentially expressed in HCAECs from young and middle-aged donors.

	Young		Middle-aged	
Protein	log2FC	pvalue	log2FC	pvalue
A8K968	0.84427619	0.00286016	0.99324031	0.00031404
P3H3	0.7293105	0.02828928	1.03289788	0.00354834
A0A7P0TAQ9	0.69836626	0.03178254	0.95879768	0.00524022
KI13B	0.5930598	0.02505955	-1.4728833	0.00027026
A0A7P0Z497	0.58331473	0.015667	0.52505343	0.02706362
SC65	0.56268234	0.0330479	0.78094566	0.0051546
DLRB1	0.55376861	0.03717992	0.69470177	0.01155246
COPD	-0.4158625	0.03151981	-0.53235	0.00818842
R4GNH3	-0.4519195	0.03645348	-0.5198674	0.01834204
TCPQ	-0.5172217	0.01291846	-0.5684143	0.00726561
RUVB1	-0.5612592	0.04167387	-0.6076801	0.02906729
PSA1	-0.5781739	0.01778408	-0.7728036	0.0027795
PSMD7	-0.5849088	0.02162934	-0.9812511	0.00058719
SEPT2	-0.6268088	0.02082556	-0.6198796	0.02205354
F10A1	-0.6497787	0.03202199	-0.704949	0.02148777
SAE2	-0.723184	0.02230466	-0.6217879	0.04497872
SPS1	-0.7544421	0.0458177	-0.7490933	0.04719346
D6RGI3	-0.8088225	0.00585736	-0.8818515	0.00320075
ENOA	-0.8817436	0.00423882	-0.8384093	0.00598144
RL27	-0.8881313	0.01046586	-0.8843542	0.01073699
1433E	-0.9041313	0.00346891	-0.9662834	0.00210957
PSA7	-0.9743834	0.00010842	-0.7830868	0.00084795
G3V2S6	-0.9751186	0.03153134	-0.8163379	0.04201315
H0YN26	-1.070137	0.01557093	-1.3907699	0.00285836
LIPA1	-1.0961774	0.04039795	-1.2942945	0.0188698
A0A087WUT6	-1.102143	0.00078821	-0.6780154	0.02185333
UBL4A	-1.2390315	0.02457117	-0.9737381	0.03699051
RAN	-1.247532	0.03644527	-1.7009983	0.006698
H0YB09	-1.25418	0.0039866	-0.9653675	0.01526054
E9PFR3	-1.2683523	0.01219595	-1.6188633	0.00543481
AIMP1	-1.313095	0.00214035	-0.9403534	0.01869187
LIPB1	-1.3283529	0.00310782	-1.3130598	0.00337175
CBX3	-1.3611455	0.01180053	-1.1201346	0.03270921
SRP14	-1.4164736	0.04510299	-1.3819491	0.0499425
FEN1	-1.419063	0.02601001	-2.5917088	0.00081413
A0A8Q3SIX2	-1.4334777	0.04052337	-1.9512283	0.00790422
RLA1	-1.447727	0.00880596	-1.2928885	0.01701311
MK03	-1.4870627	0.03105574	-1.5548892	0.02504705
1433F	-1.4902642	0.01655647	-2.2030427	0.00113135
DFFA	-1.5645054	0.03469759	-1.6328925	0.02853317
ST1E1	-1.5721655	0.04486783	-2.5068847	0.03580059
PDCD5	-1.5830542	0.00156237	-2.1134653	0.00011199
E5RGN3	-1.6350088	0.02016837	-1.9878022	0.00638103
HINT1	-1.6482264	0.0194643	-2.499417	0.00291928
M0R299	-1.6500975	0.00149799	-1.0473071	0.02743212
CYBP	-1.6702334	0.00679489	-1.5106574	0.01260016
TBB8	-1.7028041	0.00402381	-1.6490737	0.00502916
ISOC1	-1.7323941	0.00714791	-2.1335146	0.00690867
TSR1	-1.7897941	0.03711969	-1.6725655	0.03360802
CHSP1	-2.6327339	3.6826E-05	-2.4829861	6.9034E-05
ITPA	-2.6657319	0.00981381	-2.5272715	0.02419019

	Young		Middle-aged	
Protein	log2FC	pvalue	log2FC	pvalue
A0A8I5KZ24	3.01711343	0.01621296	3.36597346	0.00838673
LOXL2	2.76440806	0.00435095	1.80627243	0.04558269
CO5A1	2.64363933	0.00058139	1.54934507	0.03194554
NDUS6	2.49902174	0.0082505	2.08804533	0.00596521
ATP5I	2.48614338	0.00790253	1.2950316	0.03616136
B2L13	2.46905945	0.00011895	1.10199072	0.03866409
STT3B	2.45359805	0.01539449	2.02725978	0.03959207
DPM1	2.05011154	0.01539136	1.90729765	0.02260223
ESM1	1.9510196	0.00459856	2.29278867	0.00066264
NDUA4	1.85870319	0.00020084	1.44699149	0.00175261
E9PH05	1.8496864	0.00323256	1.584648	0.00197026
U3IP2	1.79390448	0.01412014	1.89731606	0.01682548
SRPRB	1.79099899	0.00334228	1.31760311	0.02215185
FXR2	1.70629529	0.01092341	1.58330679	0.02856479
LYRIC	1.66758071	0.00154444	0.96465845	0.04125039
E7ETU9	1.6550792	0.0044613	1.22136642	0.02671431
B3GLT	1.65316417	0.03015927	2.16559497	0.00331222
A0A8V8TMA7	1.62011933	0.01756466	1.29358707	0.03093423
PABP1	1.59949179	7.2223E-05	0.81729894	0.01555452
RTN4	1.57089121	0.03241406	1.75339853	0.01877405
P4HA2	1.54153427	0.00806809	1.1826007	0.03390117
PDLI4	1.49515547	1.7679E-05	0.85181421	0.00341861
E9PGZ1	1.47960465	0.00023061	0.81388375	0.01945926
PRAF2	1.43072796	0.03383473	-1.9060908	0.00337003
DC1L2	1.42125651	7.021E-05	0.88732394	0.00436828
TMX3	1.36500496	0.00713944	1.21369405	0.01451053
SLFN5	1.3632813	0.01809388	1.35216989	0.01890153
VATF	1.30979727	0.0065249	-0.9424409	0.0219348
S10AG	1.22967725	0.01181966	-0.9355869	0.04621248
DJB11	1.21820243	0.0038695	0.92835982	0.02051432
HNRH2	1.20963972	0.00108764	1.25593667	0.00079022
NFU1	1.20897485	0.01315652	1.09877582	0.02210232
RBM4	1.16542431	0.0099794	1.15372313	0.00544778
CK5P3	1.13256991	0.04841215	1.32598758	0.02359659
PAI1	1.12902249	0.02651596	1.13217317	0.02615668
LEG1	1.10734571	0.03317225	1.20393835	0.02210251
GRN	1.10276575	0.02640608	1.40355007	0.00670059
TIGAR	1.09855883	0.00099139	0.6762456	0.02494047
GNAQ	1.07366273	0.01476077	1.0483597	0.01684164
RHEB	1.01077768	0.01486207	0.93080311	0.02305988
RL35A	0.96539672	0.03767438	1.26708677	0.00894866
WDFY1	0.9531067	0.00213554	0.65512498	0.02309211
A8MQT7	0.94124931	0.04625617	1.00563952	0.03468221
SAP	0.93407662	0.02772155	0.86652231	0.03916916
P4HA1	0.92060046	0.02647811	0.84124759	0.04014359
RCN2	0.9176411	0.01027071	0.7219717	0.03609593